MULTI-PHYSICS CO-SIMULATION OF ENGINE COMBUSTION AND EXHAUST AFTERTREATMENT SYSTEM

Development of a Multi-Physics Co-Simulation Framework of Engine Combustion and Exhaust Aftertreatment for Model-Based System Optimisation

Vasos THEMI

Submitted for the Degree of
Doctor of Philosophy

Faculty of Engineering and Informatics
University of Bradford
2017

Abstract

Vasos Themi

Multi-Physics Co-Simulation of Engine Combustion and Exhaust Aftertreatment system

Keywords: Model-Based, Multi-Physics, Co-Simulation, Engine Powertrain

The incorporation of detailed chemistry models in internal combustion engine simulations is becoming mandatory as new combustion strategies and lower global emissions limits are setting the path towards a more efficient engine cycle simulation tool. In this report, the computational capability of the stochastic-based Kinetics SRM engine suite by CMCL Innovations is evaluated in depth.

With the main objectives of this research to create a multi-physics co-simulation framework and improve the traditional engine modelling approach of individual simulation of engine system parts, the Kinetics SRM code was coupled with a GT-SUITE engine model to fill in the gap of accurate emissions predictions from one-dimensional simulation tools. The system was validated against testing points collected from the AJ133 V8 5L GDI engine running on the NEDC. The Kinetics SRM model is further advanced through a sensitivity analysis for the “unknown” internal parameters of the chemistry tool. A set of new parameters’ values has been established that gives the best overall trade-off between prediction accuracy and computational time. However, it still showed high percentage errors in modelling the emissions and it was discovered that the specific software package currently cannot simulate directed injection events.

This is the first time a Kinetics SRM/GT-SUITE coupled code is employed to model a full 8-cylinder GDI SI engine. The approach showed some limitations regarding the Kinetics SRM and that in many cases is limited to trend analysis. The coupled engine – combustion emissions model is then linked with an exhaust aftertreatment system model in MATLAB Simulink, creating a multi-physics model-based co-simulation framework of engine performance, combustion characterisation, in-cylinder emissions formation and aftertreatment efficiency.

Acknowledgement

Firstly, I would like to express my sincere gratitude to my supervisors Prof. Felician Campean and Prof Alastair Wood for the continuous support of my Ph.D. study and related research, for their patience and motivation. Their guidance helped me in all the time of research and writing of this thesis. I could not have imagined having better advisors and mentors for my Ph.D. study.

Besides my advisors, I would like to thank Dave Richardson, from Jaguar Land Rover Company, for his help, technical input and immense knowledge of internal combustion engines.

Also, special thanks to Dr. Mohammed R. Kianifar, for his insightful comments and encouragement, but also for all the fun we have had in the last four years.

Finally, I would like to thank my family, which always supported me even from thousands of miles away.

Contents

List of Figures

List of Tables

List of Acronyms

NEDC	New European Driving Cycle
GDI	Gasoline Direct Injection
SI	Spark Ignition
PDF	Probability Density Function
US	United States
CARB	California Air Resources Board
EPA	Environmental Protection Agency
EU	European Union
NMOG	Non-Methane Organic Gases
ETC	Emission Test Cycle
HC	Hydrocarbons
CO	Carbon Monoxide
CO_2	Carbon Dioxide
NO_x	Nitrogen of Oxides
PM	Particulate Matter
EPAFT	Environmental Protection Agency Federal Test
PEMS	Portable Emissions Measurement System
ECJ	European Court of Justice
EIVC	Early Inlet Valve Closing
LIVC	Late Inlet Valve Closing
BDC	Bottom Dead Centre
CAI	Combustion Auto-Ignited
HCCI	Homogeneous Charge Compression Ignition
O_2	Oxygen
H_2O	Water
N_2	Nitrogen
RSM	Response Surface Methodology
RANS	Reynolds-Averaged Navier-Stokes
LES	Large-Eddy Simulations
DNS	Direct Numerical Simulations
PCCI	Premixed Charge Compression Ignition
HiL	Hardware-in-Loop

SiL	Software-in-Loop
MiL	Model-in-Loop
ECU	Electronic Control Unit
LHS	Latin Hypercube Sampling
RPM	Revolutions Per Minute
CAD	Crankshaft Angle Degree
aTDC	after Top Dead Center
AC	Alternating Current
LMM	Localness Mixing Model
H/N+SC	Hiroyasu/Nagle Strickland-Constable
1D	One-Dimensional
EGR	Exhaust Gas Recirculation
IVO	Inlet Valve Opening
EVC	Exhaust Valve Closing
FRP	Fuel Rail Pressure
SOI	Start of Injection
PN	Particulate Number
IMEP	Indicated Mean Effective Pressure
BSFC	Brake Specific Fuel Consumption

1 Introduction

1.1 Research Motivation

Meeting the difficult and opposing emissions and efficiency goals is becoming increasingly difficult as engine and aftertreatment control complexity increases. Due to the high number of control actuators settings and design variables of the engine and aftertreatment system, real engine experiments can be extremely time consuming and costly [1]. The challenge extends more as engine and exhaust aftertreatment are optimised separately rather as one system [2]. In this regard, there is still a need to develop a coordinated operation strategy in the direction of more effective engine systems.

In the wake of efforts by the automotive industry to perform the multidisciplinary task of internal combustion engine performance, engineers have been concentrating on the use of computational modelling and optimisation [3, 4, 5]. Computational modelling is an efficient means for the process of optimising the engine, providing the ability to significantly reduce development cost and timescales. The study of complex automotive systems has been addressed with multi-domain simulation packages such as GT-SUITE, Ricardo WAVE, and AVL BOOST offering functionality, practicality and the prospect of capturing the dynamics of the system [6]. Modelling has become a vital tool to determine whether current or new designs can deliver improved fuel economy, performance and emissions reduction in addition to many other requirement improvements.

However, even though numerous combustion emissions models have been developed, the current state shows that they are limited in their ability to capture the detailed chemistry of the modern internal combustion engine [3, 4, 5]. This restricts the capability of conventional engine modelling techniques for simulating the combustion-formed gas emissions. Evidence from recent studies suggests that the probability density function-based stochastic reactor models can overcome this accuracy gap and offer detailed chemical kinetics simulation of the combustion emissions [7, 8, 9, 10, 11, 12]. Additionally, exhaust aftertreatment simulation software that combines the power of high level chemical mechanisms with fast flow and heat transfer solvers in a one-

dimensional framework is now available [13, 14, 15]. There are still some software packages which are more preferable toward the simulation of specific components in a vehicle system [16]. For instance, GT-SUITE from Gamma Technologies is extensively used for accurate engine simulation [17], Kinetics SRM engine suite by CMCL Innovations is considered able to deliver high fidelity emissions predictions [18], and Axisuite from Exothermia provides high level analysis of the physical and chemical process in exhaust aftertreatment systems [19].

Even though system models can be designed in different software, certain software packages now allow linkage through the MATLAB environment delivered by Mathworks [20]. As a result, MATLAB can be used as a universal platform for the co-simulation of various subsystem models developed in different programming languages. The work is based on the Jaguar Land Rover AJ133 V8 naturally aspirated 5-litre GDI engine. The principle of the framework is the co-simulation of multiple software packages that combine engine and combustion model outputs, evaluated based on engine test data developed from designed experiments carried out at the University of Bradford, with an exhaust aftertreatment system model, in a preliminary validation based on a part-load hot calibration of the New European Driving Cycle (NEDC). Such a simulation framework will have the potential to reduce engine development test times and provide better physical understanding of the engine and aftertreatment system.

The stochastic-based combustion modelling approach was chosen because it was derived as the best method to adopt for a fast, accurate and realistic combustion simulation framework. The work presented in this study focuses upon a stochastic-based model using the kinetics SRM suite software that has obtained increasing attention from academics and industry due to its capabilities to correlate the combustion characteristics as well as emissions concentrations with experimental data [21, 22, 23, 24, 25, 26, 27, 28]. However, from the literature review undertaken, it has been found that far too little attention has been paid to evaluating the kinetics SRM suite against experimental data from gasoline direct injection spark ignited engines. Further experimental investigations on this type of engines are required due to their

worldwide popularity and application. One of the research objectives is to investigate how well the kinetics SRM suite can predict the experimental data collected from a modern spark ignited gasoline direct injection engine.

The engine case study is based on a double overhead camshaft eight-cylinder engine with V-configuration. V8 engines are basically two inline four-cylinder engines formed together and sharing a common crankshaft. Due to their setup all reciprocating piston internal combustion engines have dynamic imbalance factors affecting their efficiency and performance. The pistons going upward facing the cylinder head are carrying more inertia compared with the pistons moving away from the cylinder head, and hence vibrations are produced. These vibrations are exponentially increased in higher engine revolutions. In a V8 engine, two pistons are always moving in synch making the inertia imbalance twice as large and more frequently occurring. Hence, the engine data from the V8 will provide a challenging assessment of a stochastic-based model which accounts for non-uniform cycles. Moreover, the engine case study covers several NEDC-based speed – load points, as well as, a control settings analysis on a single speed – load point (see Section 4.2).

The 1D fluid dynamics (GT-SUITE) and chemical reactions (Kinetics SRM suite) software packages will be used to develop engine simulations for statistical analysis of the models outputs. Each part of the global system will be evaluated individually and when an acceptable performance criterion has been achieved then the coupling processes will be carried out. Using the block diagram environment of Simulink in MATLAB the external cylinder model will be joined with the combustion analysis model. GT-SUITE will cover all the external cylinder activities such as valves opening and closing, gas exchange, thermodynamics processes, etc. The Kinetics SRM suite will deal with the in-cylinder combustion analysis including the chemical reactions using detailed chemical kinetics mechanisms for a two-zone (burned and unburned) divided combustion chamber. Completing the coupling, the exhaust aftertreatment model will receive the outputs of the cylinder and combustion models to calculate the heat, mass transfer and chemical reactions occurring in the catalytic converter.

The main drawback of this strategy is the lack of simulating ability at high accuracy levels of the detailed chemistry and complex reactions occurring in the combustion process [29]. In order to have a complete engine system simulation a one-dimensional engine model will be coupled with a chemical model, built on probability density functions. This methodology overcomes the lack of one-dimensional models to compute the combustion chemistry occurring inside the engine cylinders. Coupling such PDF-based chemical models with an already single-dimensional code has provided innovative simulation packages and new insights for the prediction of combustion [8].

1.2 Objective and Scope of Research

The main aim of the research is to develop a model-based multi-physics framework that will join engine performance, combustion emissions concentrations, together with exhaust aftertreatment analysis in a concurrent co-simulation system, setting the path towards a more efficient engine cycle simulation tool. One approach to achieving this aim is the use of different simulation codes that each target a different sub-process of the engine system, and are joined together. The objectives of the study are as follows:

- Development and validation of a stochastic-based combustion emissions model
- Design and calibration of a one-dimensional engine model
- Design of and calibration of a one-dimensional chemistry-based exhaust aftertreatment model
- Couple the engine, emissions, and aftertreatment model and perform a co-simulation of the system

1.3 List of Contributions

The main original contributions of this research can be summarised as:

- Performing a sensitivity analysis for the internal sub-models' parameters of Kinetics SRM in order to achieve a set of values that gives the highest emissions prediction accuracy while maintaining low simulation completion time

- The first full study of GT-SUITE coupled with Kinetics SRM. The engine/emissions model was calibrated and evaluated using data from a modern V8 GDI engine
- Creating a new model-based framework based on GT-SUITE for the engine performance, Kinetics SRM for engine-out emissions and Axisuite for the exhaust aftertreatment system design. Matlab Simulink was responsible for signals communication between the simulation tools

1.4 Thesis Organisation

The thesis commences by introducing a review of the gasoline direct injection engine in Chapter 2. The chapter starts by first summarising the emissions testing procedure as well as providing a brief history of the emissions standards. Next, combustion improvements and technological approaches for higher engine efficiency are given, followed by the reviewing of gasoline direct injection engine emissions, including pre- and post-treatment methods.

Chapter 3 is divided into two categories, engine simulation methodology and engine simulation technology. The first section of the chapter describes the mathematical engine modelling techniques, while the second section introduces the engine control unit, describes the engine mapping process and summarises the experimental designs.

Chapter 4 reviews the research methodology planned to satisfy the research objectives. An overview of the engine case study is given at first, followed by the theory and mathematical analysis of the models.

Chapter 5 presents the combustion emissions formation model development and validation process. The chapter gives some original work by running a parametric study of the internal parameters of the combustion model.

Chapter 6 describes the development of the multi-physics co-simulation platform, by first covering the design and calibration of the engine and exhaust aftertreatment models. The coupling method of the models and the final simulation framework build and validation processes.

Finally, Chapter 7 summarises the discussions of the research along with the conclusions and suggestions for further research developments in this area.

2 Gasoline Direct Injection Engine Review

2.1 Chapter Introduction

As shown in Table 2.1, this chapter begins by providing, in section 2.2, a review of the development of gasoline direct injection and what the real benefits are to be gained from this type of engine on automotive applications. An outline of the areas of gasoline engine combustion improvements and potential technological approaches for achieving a higher efficiency engine is described. Section 2.3 presents a brief overview of the emissions emitted by the gasoline direct injection engine, along with the treatment techniques applied inside the cylinder and through the exhaust aftertreatment system towards meeting the emissions regulations.

Table 2.1: Organisation table of the gasoline direct injection engine review chapter

2.1	Chapter Introduction
0	Emissions Testing and Legislations - Emissions testing procedure - Emissions standards
2.3	GDI Engine Combustion Review - Combustion improvements - Technological approaches
2.4	GDI Engine Emissions and Treatment methods - Combustion emissions - Emissions pre- and post-treatment
2.5	Chapter Summary

2.2 Emissions Testing and Legislations

Due to both environmental and political impacts on engine development, emissions performance standards were introduced to limit the amount of pollutants released from vehicles into the environment.

2.2.1.1 Brief History of Emissions Limits

In the mid-1950s studies in to the causes of air pollution were carried out in the United States by the U.S. Air Pollution Control Association, indicating the serious percentage of pollutant produced from automobiles [30]. However, at

that point vehicle emissions where not limited by any political or environmental boundaries. In 1967, the California Air Resources Board (CARB) confirmed the first effective emissions regulation for vehicles sold in the State of California [30]. Aiming to attain and maintain healthy air quality the CARB was managing and analysing emission records, air quality data, transportation plans, and modelling air characteristics [31].

By 1970, the federal Environmental Protection Agency (EPA) joined with the CARB to regulate emission standards for vehicles in the United States [32]. Federal "Tier 1" regulations went into effect starting in 1994, with "Tier 2" standards being phased in from 2004 to 2009 in an effort to decrease emissions. Similarly, organisations in Canada, Western Europe, Australia, and Japan were evolved to implement emission limits. Emissions standards may vary from authority to authority, like for instance the different emission standard of the European Union and the United States, or even within the same country such as the state of California compared to Texas.

The European Union (EU) has its own set of emissions legislations, defined in a series of progressively stricter steps that all new vehicles sold in EU member states must meet [33]. Table 2.2 presents the steps, typically referred to as EURO 1, 2, 3, 4, 5 and 6, taken by the EU for reducing gasoline passenger vehicle emissions. The standards for gasoline passenger vehicles are different from diesel vehicles which have a lower value of carbon monoxide but higher nitrogen oxides emissions. Up to EURO 4, particulate emissions for gasoline direct injection and generally for gasoline engines were not regulated, but from the introduction of EURO 5 the particulate matter emission for the gasoline direct injection engine is limited to 0.005 grams for every kilometre.

Table 2.2: European emission standards for gasoline passenger vehicles

	EURO 1	EURO 2	EURO 3	EURO 4	EURO 5	EURO 6
Year introduced	1992	1996	2000	2005	2009	2015
Carbon monoxide [g/km]	2.72	2.2	2.3	1.0	1.0	1.0
Total hydrocarbons [g/km]	-	-	0.2	0.1	0.1	0.1
Nitrogen oxides [g/km]	-	-	0.15	0.08	0.06	0.06
Hydrocarbons + Nitrogen oxides [g/km]	0.97	0.5	-	-	-	-
Particulate matter [g/km]	-	-	-	-	0.005 for GDI	0.005 for GDI
Particulate number [#/km]	-	-	-	-	-	$6x10^{11}$ for GDI

Due to the very fast growth in China's prosperity, the number of road vehicles has increased rapidly, forcing the state environmental protection administration of China to introduce emission legislations [34]. The People's Republic of China adopted the European standards and introduced them at the same time with the EU. In the meantime, India was regulating the emission limits with the first effective in 1989 and continued every few years to slowly tighten up the limits, until their introduction of the EU standards from the year 2000 [35]. From the 2000s Australia likewise, started coordinating the motor vehicle emissions based on the EU standards and introduction dates [36].

The Japanese air pollution control act began regulating air pollutants in 1968 and announced the first set of vehicle emissions legislations in 1973. Provisional standards were generated in 1975 and 1976, until the "mean emissions" legislation taking place in 1978 [37]. The 1978 standard was adopted from the US but adjusted to the Japanese slower driving cycle giving maximum limits for carbon monoxide of 2.7g/km, 0.39g/km for hydrocarbons and 0.48g/km for nitrogen oxides [38]. Stronger regulations for all vehicle categories were submitted in 1992 with the proposition of the motor vehicle nitrogen oxides law, established to limit the high concentration of the pollutant from vehicles in cities.

Japan is one of the biggest automotive manufacturers worldwide producing in 2001, 8.1 million passenger cars [39] and more than 9.9 million in 2008 [40]. To deal with this massive pollutant concentration the exhaust emission regulation of 2000 limited the average value of gasoline passenger cars to 0.67 grams of carbon monoxide per kilometre, and hydrocarbons and nitrogen oxides to 0.08 gram per kilometre. In 2005 a new long-term regulation was announced with the goal of dropping the limits of carbon monoxide to 1.15 and 0.05 for both hydrocarbons and nitrogen oxides. In 2009, a particulate matter restriction for gasoline passenger vehicles was introduced limiting the gasoline vehicles to 0.005g/km [41].

Moreover, the latest emissions legislation, EURO 6, follows the same restrictions as the previous emissions regulation; however, it also imposes a particulate number limit for gasoline direct injection engines only. There is a huge concern related to the regulation of the particle number from gasoline direct injection engines due to their particles size distribution. While regulating the particulate emissions in terms of total mass of particulate matter produced per kilometre is a practical method of controlling the large size particles, it is however a very ineffective approach for the smaller particle ranges. Growing health issues from more toxic smaller size particles have developed a particle mass and number measuring technique, with integrated size categories applied to the particulates [42]. Derived from the particulate number standard of diesel vehicles a legislation particle number limit for solid particles larger than 23nm is set [43]. Moreover, investigations on the size of the particulate matter revealed that a significant percentage of the total emitted solid particles from gasoline direct injection engines belong to the small range class with diameter below 23 nm [44]. Due to their nano-size these particles can penetrate lung tissue and pass into the bloodstream.

New emission standards introduced in the coming years will focus on proper functioning of pollutants control and requirement for treatment devices to last for a distance of 100,000 miles [33]. On-board diagnostic systems monitor the performance of the emissions treatment equipment during the normal operation of the vehicle; including emissions management at idling speed and at cold-starting conditions [45, 46]. The on-board diagnostic will warn the

driver of faults in the engine or the emissions control system, obliging the driver to have the vehicle checked. Analysis regarding the cost of new emission control technologies required has contributed to the EURO 6 proposal to ensure that the new standard provides a cost-effective mean for emissions control and does not adversely affect the affordability of vehicles [47].

Furthermore, the EURO 6 standard is still significantly weaker than the correspondingly standards currently in force in the US [32]. The addition of the Tier 3 program will set new emissions standards from 2017. As with EURO 6 the new US legislation will cover emissions from the tailpipe as well as the evaporative emissions [48]. Sulphur in gasoline will be limited to no more than 10ppm and the emission control equipment durability will increase to 150,000 miles, an additional 150% increase over the European legislation mileage. The sum of non-methane organic gases (NMOG) with NO_x will also be limited to a stringent maximum of 86 mg per mile for 2017, gradually dropping to 30mg/mile in 2025. In addition, the United States Environmental Protection Agency suggested a particulate matter maximum of 0.01 gram per mile and 5mg/mile for formaldehyde [48]. Moreover, the evaporative emissions are going to be measured through a 3-day test procedure and on-board diagnostic systems will cover all new vehicles.

2.2.1.2 Emissions sampling and testing

Emissions testing performed in laboratories is vital for the type approval procedure of vehicles. Following a combination of a specified driving cycle in conjunction with predetermined test conditions, vehicles are tested on a chassis dynamometer [46]. The emission standards are derived from emission test cycles; the repeatable procedure that allows the comparison of exhaust emissions between different vehicles. During a test the vehicle is set in a controlled laboratory environment that replicates specifics settings of the vehicle's actual operation [49]. Parameters such as the intake air temperature and mass flow, and vehicle' speed and load are included in the process to imitate the vehicle running in actual road-use situations [1]. The emission test cycles (ETC) are commonly categorised into their hardware layout, and so they are divided into engine and chassis ETC [50].

The engine testing platform measures steady-state values such as the air fuel ratio, temperatures, pressures and pollutant concentrations in the exhaust gas through various sensors placed in important areas of the engine [49]. All input values are recorded by a data acquisition unit, and the engine running mode (engine torque and speed) is controlled by actuators such as throttle opening [1]. The engine ETC can only examine a single engine, whereas the chassis ETC assesses the whole vehicle (with the engine).

The vehicle's driving wheels run on big rollers where the dynamometer replicates the vehicle's inertia weight, air drag, and road friction. Due to the fact that the entire vehicle is tested rather than just its engine, the chassis ETC increases the accuracy of actual driving emissions [51]. Improved valuation of the technologies applied to counteract the emissions and the final tailpipe pollutant concentrations are gained. Without getting too much into the hardware details, each emission test cell is fitted with a constant volume sampling system, reliable conventional analysers and systems for sampling exhaust pollutants into separate bags [52]. Total quantities of HC, CO, NO_x and PM are measured at the end of the process by the emissions analyser, as seen in Figure 2.1.

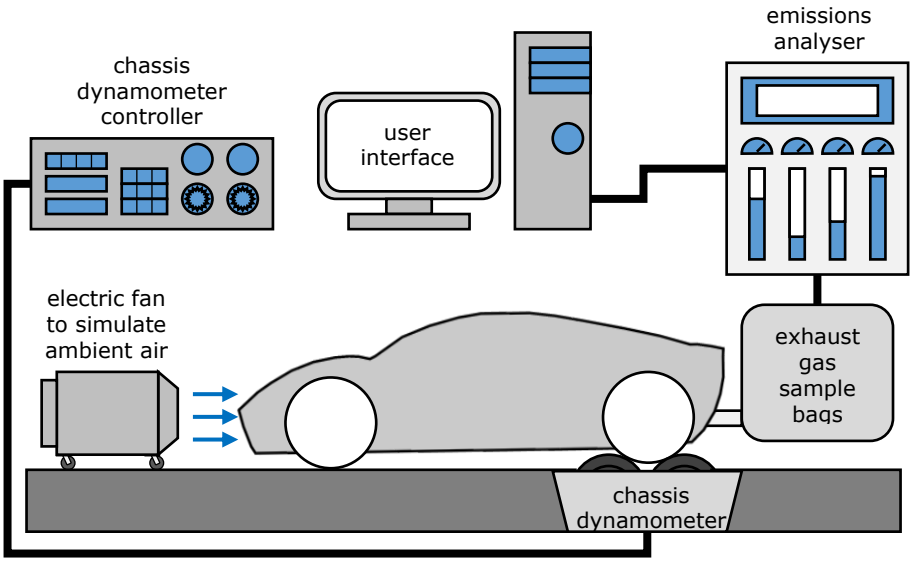

Figure 2.1: Chassis emission test cycle

Emissions standards are based on the reliability of the tests, but testing the vehicle or just its engine has to reflect real-world driving with the highest possible quality [53]. Since testing a vehicle/engine under every possible combination of speed and load is unrealistic and requires extremely high effort, emission tests have as a reference a time dependent driving cycle, a series of vehicle speed points against the time in seconds [33, 32]. As a result of the drive cycle usage, the cost, time and effort of emissions tests is diminished. Different drive cycles have been created by various countries and organisations to weigh the pollutant concentrations of vehicles, with the most common cycles to be the new European driving cycle (NEDC) [33], the US environmental protection agency federal test (EPAFT) [32] and the JC08 from Japan [54].

As shown in Figure 2.2, the NEDC total duration is 1180 seconds and involves two parts; the urban driving part which takes place for the first 780 seconds, and the extra urban part then occurring to the end of the cycle [33]. The test procedure is initiated with the engine starting at 25 degrees Celsius, referred to as cold-starting, and pausing there for 11 seconds. Afterwards, the urban driving cycle can be divided into 4 identical parts that are basically repeated until the 780th second. Next, the extra urban part is a single section that represents high speed driving, with a maximum speed of 120 km/h [55].

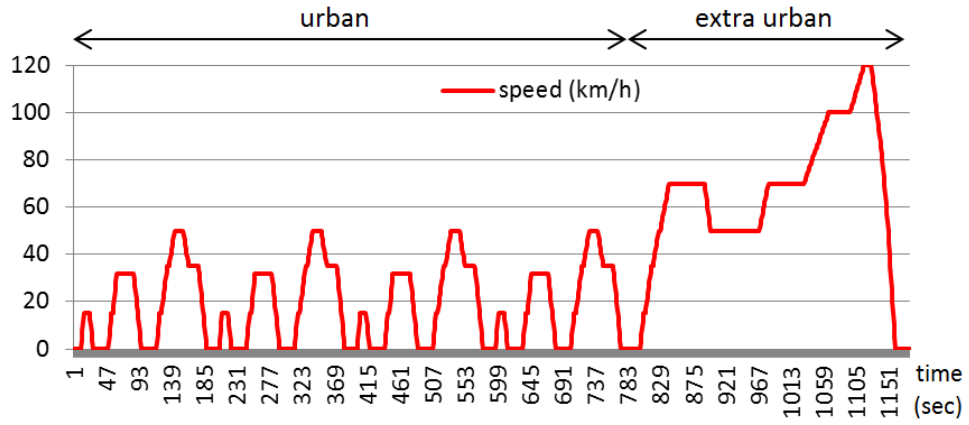

Figure 2.2: New European Drive Cycle

Furthermore, the US driving cycle consists of 3 phases; cold-start, transient and hot-start [32]. The vehicle is kept for 8 hours at an ambient temperature of 25 °C before the initiation of the first phase. The “cold start” phase has a

duration of 505 seconds with average speed of 41.2 km/h and fundamentally represents the starting of the vehicle under cold conditions. Followed by the second stage, that involves more transient accelerations and decelerations for 864 seconds, the “transient” phase aims to represent a city driving course with frequent stops/starts until the vehicle is driven onto the highway [30]. Next the vehicle’s engine is shut down for 10 minutes, representing the vehicle parked for a short period of time, and finally the “hot start” phase is executed, which is a repeat of the cold phase speed points but having the vehicle hot starting (Figure 2.3).

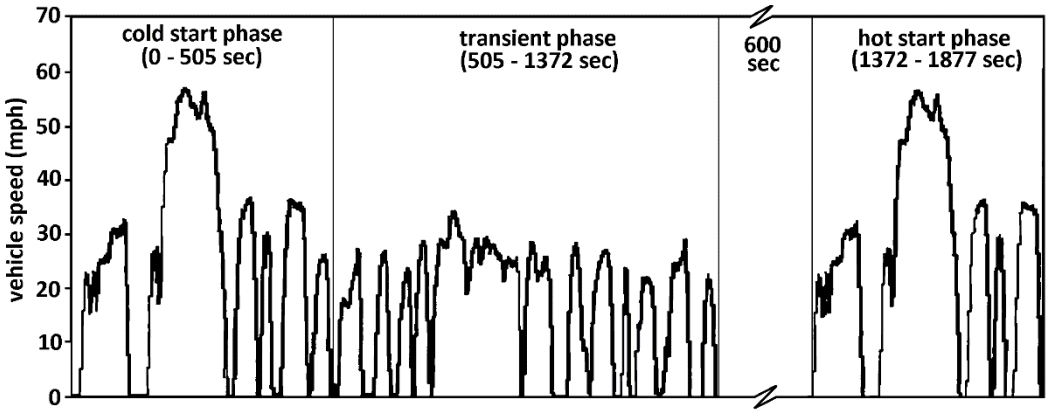

Figure 2.3: United States drive cycle

The JC08 test in Japan exposes a vehicle to a 1200 seconds cycle with both cold and warm starts (Figure 2.4). With a top speed of 82 km/h, the JC08 represents city driving with stationary traffic, idling periods, and transient starts and stops [56]. The drive cycle test is initiated with the vehicle cold starting and is then repeated with a hot start. The total emissions are determined with the warm start counting towards 75%, and the cold start counting for the remaining 25% [54].

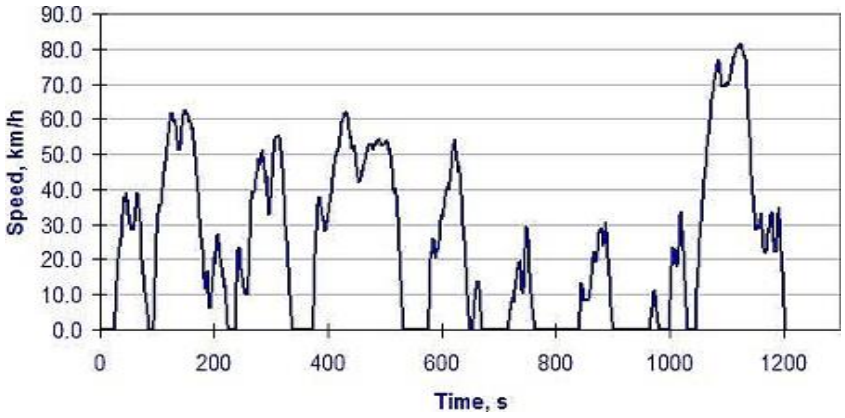

Figure 2.4: Japanese driving cycle [54]

Even though emission limits have become more stringent in the past decade, road transport is still the key source of pollutant emissions. In 2008 NO_x and CO were contributing 41% and 34%, respectively, to the entire pollutant outputs within the EU [57]. Prompted by the continuing air quality issue, the European Council determined that the current applied “New European Driving Cycle” will have to be replaced by a harmonized global driving cycle [58].

Constructed based on data sets from the EU, India, Japan, Korea, China and the US this global harmonized drive cycle will use appropriate weight factors to represent typical driving conditions [59]. Strict guidance in terms of gear selection, total vehicle weight, with or without passengers and cargo, fuel quality, ambient temperature, type of tyres and tyre pressure will be set. Moreover, the future drive cycle will involve three different tests, depending on the engine power to vehicle’ kerb weight ratio (kW/Ton).

Vehicles with a power to weight ratio above 34:1 will be tested in a cycle of 1800 seconds that involves four parts; low, medium, high, and extra high speed (above 130 km/h). Vehicles with a ratio between 22 and 34 will be tested with the same cycle, of the high ratio vehicles, but without the extra high-speed part. Vehicles with a ratio below 22:1 will be tested with a cycle that has only the low and medium parts [60].

Moreover, under investigation for future additional measures of pollutant emissions are the use of portable emissions measurement systems (PEMS). Basically, a PEMS is a mobile laboratory for assessing the vehicle’s real-world emissions. Initially introduced for heavy duty trucks and buses in early 2000

the PEMS identifies the actual emissions of the vehicles during their daily operation [61]. The ECJ (2011) analysed the on-road emissions from 12 gasoline and diesel light duty vehicles using PEMS on a test route of 4 phases; rural, city, up and down a hill, and motorway driving. To conclude, their findings showed a great difference between on-road driving measurements and the data collected from a laboratory driving cycle.

Future measures added to the standard laboratory tests will be the monitoring of emissions in driving modes that cannot be simulated in a test bed, such as high-speed driving of more than 130 km/h and checking the vehicle and aftertreatment system in a greater range of temperatures. The reliability and accuracy of the PEMS equipment is promoting this mobile tool for the identification and review of the emission factors for the future. Currently the main constraints of the PEMS are its dimensions and weight, but with the technological improvements it is expected that these limitations will be overcome [62].

2.3 GDI Engine Combustion Review

This section presents a review of some of the advancements made in gasoline direct injection engines to increase of the combustion process efficiency.

2.3.1 Compression Ratio

The ratio of the maximum cylinder volume to the minimum compressed volume that a piston can reach is called the compression ratio. A gasoline engine operating at a higher compression ratio will increase its thermal efficiency by the added heat density in the combustion chamber, resulting in higher cylinder pressures and hence more mechanical energy that will be converted to net power output from a given mass of air fuel mixture [63]. However, gasoline engines are typically operating on a limited compression ratio to prevent knock from occurring and disturbing the combustion stability and performance, as well as damaging the components of the engine. Nonetheless, the knocking phenomenon occurs only when the engine is running at full load, giving the opportunity of higher compression ratios at part load conditions. Variable compression ratios-based gasoline engine is a

possible design for running a high compression ratio on part load and a low compression ratio on full load operations [64, 65].

2.3.2 Intake Valves Timing

In addition to variable compression through new methods, the actual compression ratio of an engine can be altered by controlling the closing time of the intake valves [63]. The two strategies for controlling the intake trapped mass are early inlet valve closing (EIVC) and late inlet valve closing (LIVC). EIVC works by limiting the amount of air drawn into the cylinders. The valve period is short with the valve closing well before bottom dead centre (BDC). The charge is expanded with compression only starting when the piston reaches the same position after BDC as the valve closed before BDC. The effective compression ratio is less than the geometric compression ratio because compression only starts part-way up the compression stroke [66, 67].

LIVC closes the valve after BDC and controls the charge volume by the piston pushing air out of the cylinder as it goes beyond BDC (on the compression stroke). The compression starts when the valve closes so the effective compression ratio is lower than the geometric compression ratio. Either advancing or retarding the closing of the intake valves will force the engine in some way to operate at a different compression ratio, however such an engine requires additional pressure charging by a forced induction system to recover the pressure loss due to the changes in the intake process and thereby retain its full load performance.

2.3.3 Fuel Octane

Because knocking is highly sensitive to the temperature of the mixture while it’s being compressed, a gasoline direct injection engine is directly spraying fuel into the cylinder allowing this way the surrounding air to cool, decreasing knock tendency. However, the knock limit is dictated by the octane number of the gasoline. In general, a higher octane number fuel can endure higher compression rates, permitting the engine to use higher compression ratios. The direct injection of a gasoline and alcohol fuel blend is another alternative to allow the gasoline engine to operate with higher compression ratios if a higher-octane fuel is formed [68]. However, there are some problems with the

application of alcohol – gasoline fuel, such as the costly production of alcohol and use, the increase of certain types of emission pollutants formed by the engine, as well as toxic waste generated by synthesizing the mixture.

2.3.4 Engine Displacement

Frictional loss is proportional to the surface area of the mechanical component, therefore in practice a smaller displacement engine will in general have less friction in comparison with a larger engine. Furthermore, a smaller engine weighs less, has lower installation requirements and provides more frequent shifts at higher load and wide-open throttle conditions. This is known as engine downsizing and is achieved usually by reducing the capacity of the engine and perhaps the number of cylinders [69].

Despite having a lower displacement, the performance of a downsized engine is maintained by forced air induction via a turbocharger or a supercharger [70]. This configuration provides the engine with the needed air mass, ensuring that power and performance are not compromised, plus helps the engine to achieve carbon dioxide emissions targets and good fuel economy [71, 72]. Nonetheless, a common problem that occurs in real-world conditions when turbocharging downsized engines is low air flow conditions at low engine speeds that result in low torque. A possible solution to this problem is by better control of the response of the turbine by systems such as regulated two-stage [73] or twin-entry turbochargers [74]. These systems can, however, be complex and with costly manufacturing process.

2.3.5 Alternative Combustion Architecture

While engine downsizing shifts the engine operation points to higher efficiency regions, the pumping loss at part load is still present. As illustrated in Figure 2.5, alternative combustion strategies like lean-burn and Homogeneous Charge Compression Ignition have been developed. The lean-burn method uses an excess of air in the mixture combustion thus reducing heat transfer and pumping losses due to less throttling. Such an engine is able to operate at higher compression ratio and thus provide better performance and fuel economy. The main weakness of this method is that the combustion forms higher nitrogen oxide concentrations, hence a more complicated

aftertreatment system is required to either directly reduce the pollutant or implement nitrogen oxide storage and conversion technologies [75, 76]. Controlled auto-ignited combustion (CAI) or homogeneous charge compression ignition (HCCI) is an alternative combustion method that works by compressing a well-mixed mixture to the point of auto-ignition.

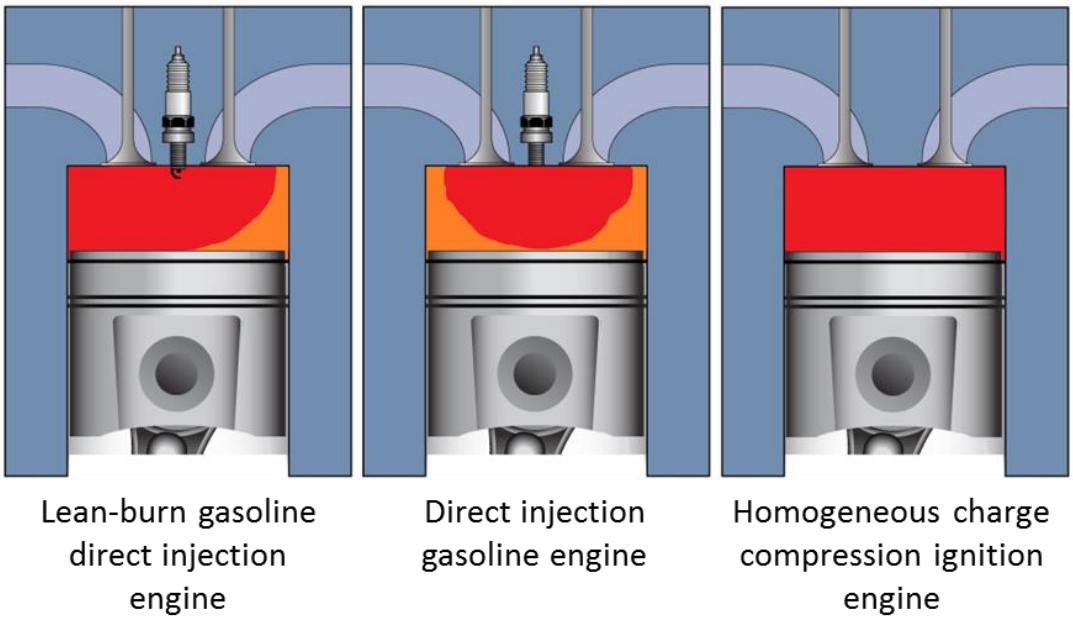

Figure 2.5: Alternative combustion engines

Rather than igniting the mixture via a spark plug, the HCCI combustion works more like the diesel cycle where the ignition is initiated by the high levels of temperature and density during the compression stroke. Unlike the lean-burn combustion, this alternative strategy achieves low levels of nitrogen oxide emissions due to the much leaner and cooler combustion conditions. The entire mixture is simultaneously combusted in the combustion chamber producing equivalent power, but with less fuel used the process releases fewer emissions.

Although there are advantages over typical gasoline direct injection engines in thermal efficiency and nitrogen oxide emissions, the main challenge of the HCCI combustion is controlling the process itself. With a spark ignited engine the combustion timing is essentially controlled by the spark ignition timing. However, in the homogeneous charge the ignition is determined by the charge mixture composition, pressure and temperature [77]. Controlling and

monitoring the mixture to auto-ignite is a very difficult task which involves sufficient pressure and temperature levels, as a result the engine cannot instantly maintain proper combustion timing over the full range of speeds and loads. Additionally, an important issue is cold-starting an HCCI engine since a spark ignition is needed to get the engine going and hot before switching to HCCI combustion [78]. Also, the transition between normal spark ignition (SI) to HCCI model or HCCI to SI is very difficult while maintaining control of emissions and avoiding misfires.

2.3.6 Fuel Injection

The fuel injection system is a crucial component of the gasoline direct injection engine. Its structure comprises a high-pressure fuel pump supplying pressurised fuel through a fuel line into high pressure electronic fuel injectors mounted into the cylinders of the engine [79]. The injectors are designed in such a way that the fuel is sprayed out of an orifice in a swirling motion forming a cone shape that allows the fuel to be dispersed inside the cylinder and burned more efficiently. However due to the typical inward opening of the injector, the structure of the fuel spray is affected by changes in injection pressure, ambient pressure, and the operating temperature of the injector [80]. This results in significant changes over the in-cylinder density causing problems in the optimisation of the fuel injection timing. As illustrated in Figure 2.6 the in-cylinder charge dynamics can be improved by tumble and swirl motion induced in the cylinder [81]. However, if too much turbulence is generated through swirl or tumble motion it will disturb and deregulate the flame propagation.

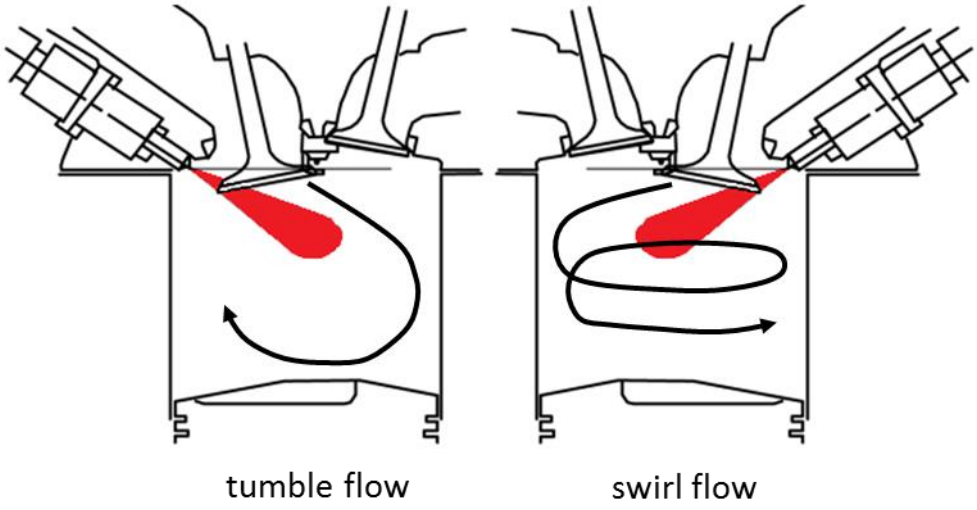

Figure 2.6: Schematic of the tumble and swirl flow motion inside the cylinder

In order to achieve a well spray-guided combustion, multi-hole nozzle and piezoelectric injectors are being continuously developed and used. Multi-hole injectors can break up the fuel spray in very small drops resulting in a larger fuel surface area. The injector distribution pattern can be formed in principle by the number of holes in the design along with angled spray arrangements. Yet the multi-hole injector application relies on higher than usual injection pressure in order to get a good fuel atomisation [82]. In addition, the smaller nozzle hole' diameter of the multi-hole injector increases the tendency for the orifices to be concealed with soot.

A potential solution to this deposit problem is by placing the injector in a lower temperature region inside the combustion chamber, ensuring that fuel does not get deposited back onto the injector tip. The options for the injector position in the cylinder however are very limited due to the valves and the spark plug. The injector position is important to ensure fuel is not sprayed onto the piston or the cylinder walls, as well as avoiding fuel spraying onto the inlet valves if they are open during injection. An important method of reducing injector tip coking is the design of the injector orifice [83, 84].

Moreover, piezoelectric injectors make use of their material electric charge to rapidly activate and deactivate fuel injection, thereby allowing highly accurate additions to be delivered and so significantly improving the dynamic range and operational flow rate of the injector [79]. Another advantage of this injector

type is that because of their greater flow rate and multiple injections per cycle capability, piezoelectric actuated injectors can operate with both gasoline and alcohol fuels. However, piezoelectric materials have a particular operating limit for temperature and stress. If the material is operating outside its temperature limitations or is mechanically overstressed, it will cause partial or even total loss of its piezoelectric properties.

2.4 GDI Engine Emissions and Treatment methods

A brief overview of the exhaust gas emissions is given this section, followed by the in-cylinder and finally engine-out gas emissions treatment techniques.

2.4.1 Introduction to Emissions Pollutants

Hydrocarbon fuels are the primary energy source for internal combustion engine based passenger vehicles and the main contributor to the formation of pollutant emissions from passenger vehicles [85]. As the fuel burns during the combustion process hydrogen reacts with the oxygen in the air charge resulting in water formation [86]. Due to insufficient amounts of oxygen in the cylinders the hydrogen atoms do not burn or they partially burn. As for the carbon atoms of the injected hydrocarbon fuel, due again to lack of oxygen and in-homogeneity in the combustion chamber, i.e. locally slightly rich areas, they are converted to carbon monoxide.

As it shown in Figure 2.7 in an ideal combustion with the ambient air having a satisfactory quantity of oxygen concentration [air = around 78% Nitrogen (N_2) + 21% Oxygen (O_2)], then all the hydrogen atoms would transform to water [Hydrogen (H) + Oxygen (O_2) = Water (H_2O)] and the carbon would fully convert to carbon dioxide [Carbon (C) + Oxygen (O_2) = Carbon dioxide (C_2O)]. In the same perfect conditions, the nitrogen would not be affected by the combustion process [87].

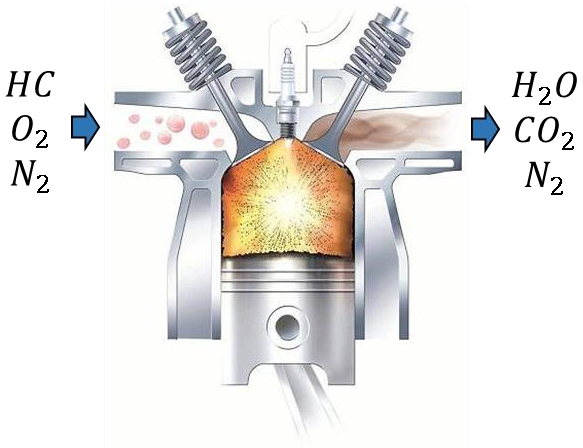

Figure 2.7: Ideal combustion emissions

Stone [88] reported measurement of combustion temperatures exceeding 1800°C for a typical gasoline engine. Hillier [89] suggested that at combustion temperatures above 1300°C the nitrogen in the intake air will react with the oxygen to form nitrogen oxides. The term nitrogen oxides cover the main group of two oxides; nitric oxide and nitrogen dioxide [Nitrogen (N2) + Oxygen (O2) = Nitric oxide (NO) and Nitrogen dioxide (NO2)].

Another pollutant investigated is particulate emissions. New emission legislations, such as EURO 6, are focusing on introducing a limit on particulate matter from gasoline engines. With a range of 0.01 up to 10,000 nm these chemically complex microscopic particles are made up of soot, ash, aerosols and carbon compounds [90].

2.4.2 In-Cylinder Emissions Pre-Treatment Techniques

2.4.2.1 Hydrocarbons

The origin of hydrocarbon emissions is the incomplete or partial combustion of fuel. A mixture richer in fuel will produce more hydrocarbons due to limited oxygen atoms reducing oxidation of the hydrogen and carbon atoms. In contrast, a leaner mixture will force the hydrocarbon formation to drop due to a higher amount of pressurised air. Also, as shown in Figure 2.8, hydrocarbons will increase with more extreme lean mixtures because the flame is quenching due to the low temperatures and the mixture is left unburned. Generally, any drop in the efficiency of the combustion process will have, as an outcome, a higher level of hydrocarbons [90].

Advancing the ignition timing causes higher in-cylinder peak pressure which pushes even more of the mixture into the crevices of the combustion chamber, were the fuel is left unburned and hence increasing hydrocarbons concentration [63]. The lower HC emission at retarded ignition timings is due to the combustion being hotter and not being complete when the exhaust valves opens. However, this combustion is less efficient than with the ignition advanced because it does not position peak pressure at the correct crank angle to have the maximum efficiency on driving the piston/crank mechanism.

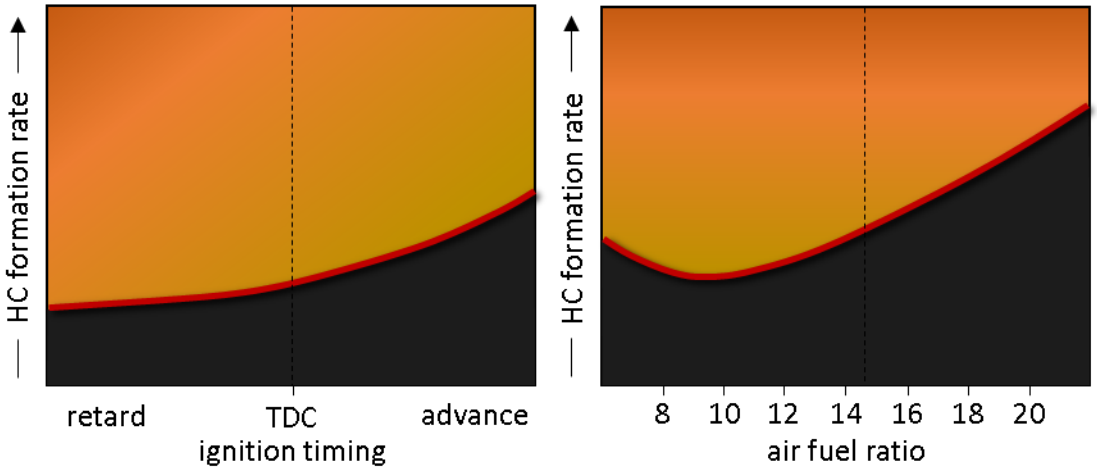

Figure 2.8: Effect of ignition timing and air fuel ratio on hydrocarbons

Igniting the mixture before the piston reaches the top of the cylinder will initiate the combustion earlier, hence providing the mixture more time to fully burn before the piston rise to top dead centre. Additionally, advancing the ignition timing will raise the peak pressure of the cylinder allowing more power production. Optimising the ignition timing is crucial in the performance and efficiency of the engine since too soon or too late mixture ignition may cause excessive vibrations and potential engine damage. Advancing the mixture ignition is controlled mainly when the engine speed is high so it will give efficient combustion time for the mixture. Delayed ignition timing is more suitable when the engine load is high, such as at a wide opening of the throttle, since the flame propagates at a slower rate but its longer duration reduces hydrocarbon formation. Furthermore, under cold-starting conditions, with the exhaust gases temperature increasing, the engine emits fewer hydrocarbons with a retarded ignition [91].

Using highly accurate electronic control of the fuel injection and the ignition timing, the engine's ECU can alter the actuator settings to maximise the overall efficiency under all engine operating conditions [92]. Nevertheless, even with a properly calibrated engine through transient operation regions any lack of oxygen into the combustion chamber will cause a drop of the ignition flame temperature and hence will promote unburned hydrocarbons[63]. Unburned hydrocarbons can be absorbed by the oil that the engine uses to lubricate its components and use it as a shield against the flame. Any fuel lost during the combustion will subsequently re-enter the next step of the cycle, meaning additional unburned hydrocarbons.

2.4.2.2 Carbon Monoxide

Use of accurate fuel and ignition systems can also reduce the formation of carbon monoxide pollutant [89]. Generated even under ideal pressure and temperatures, carbon monoxide emissions are almost completely linked to the air fuel ratio. The lack of oxygen in the combustion process leads to unburnt fuel, so partial reaction products are produced. Hubbard (1995) proposed that through the primary charge of oxygen on hydrocarbons, carbon monoxide is formed by a rapid reaction; $C + ½ O_2 = CO$ [93]. Under suitable conditions of temperature and oxygen concentration, combustion gases, which are formed in the initial zone accommodating high carbon dioxide, will be affected by the interaction of the gases with the segments of unburnt fuel [94]. The reduction reaction is endothermic; heat is absorbed by the surrounding fuel regions causing the temperature of the gases to drop. While heat is absorbed from the gases, the carbon monoxide emission will freeze when the temperature drops below 700°C [95].

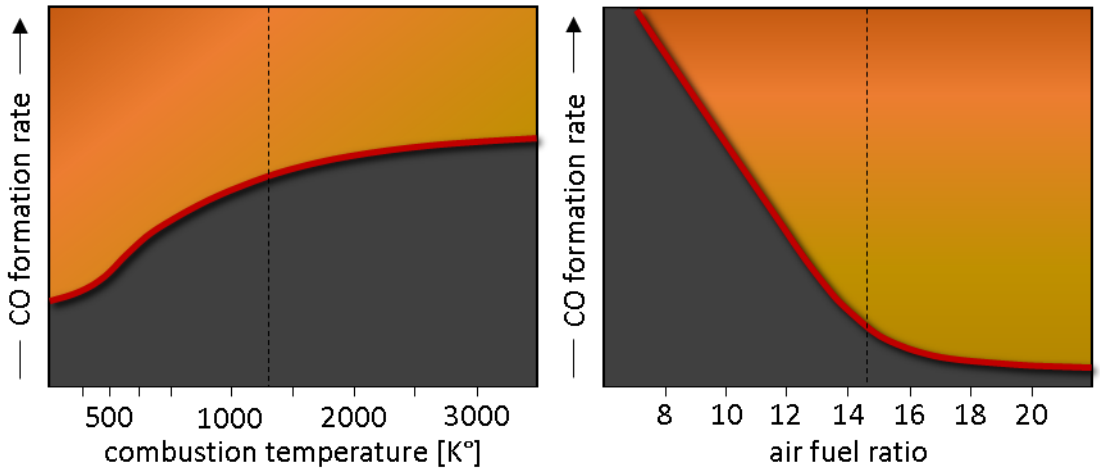

Figure 2.9: Effect of combustion temperature and air fuel ratio on carbon monoxide

Diesel engines generally generate less carbon monoxide emissions than gasoline engines due to richer air charge. On the contrary, gasoline engines run under homogeneous charge for the complete combustion of the air fuel mixture. In real world conditions, this ideal design does not exist. A delayed fuel injection or poor fuel vaporisation, typically when the engine is cold starting or it's running under high load, create an insufficient oxygen condition. Carbon monoxide quantities at very fuel rich mixtures (ex. 10 grams of air for every 1 gram of fuel) are extremely high, but it drops dramatically as the mixture strength moves towards the stoichiometric ratio Unlike hydrocarbon behaviour, carbon monoxide will not rise again after it passes the stoichiometric quantity and it will keep dropping, but with a much slower rate (see Figure 2.9). A small amount of CO is always present due to the water/gas equilibrium.

2.4.2.3 Nitrogen oxides

As explained in detail by Heywood the formation of nitrogen oxides has its source in the burned region of the ignited mixture [63]. As the temperature level reaches the proper combustion temperature (higher than 1600°C) the mixture starts to burn through a chain of detonations, see Figure 2.10. The nitrogen oxides though are not produced by the initial ignition of the mixture, but with the resulting unburned regions. Nitrogen oxide behaviour is different from that of hydrocarbon and carbon monoxide in that oxides of nitrogen are

almost zero at very rich mixtures (of 12:1 to 9:1 air fuel ratio). Nitrogen oxides increase along with the decrease of the mixture strength in fuel until a peak point between 15.5 and 16.5:1 is achieved. If the engine is operating on leaner mixture (beyond the peak) nitrogen oxides fall, though a leaner mixture will generate driveability issues [96]. Mainly NOx formation is dependent on 2 control parameters, oxygen availability and combustion temperature. As oxygen availability increase from very rich mixtures NOx levels increase. NOx formation starts to reduce as the combustion temperature starts to drop with lean combustion.

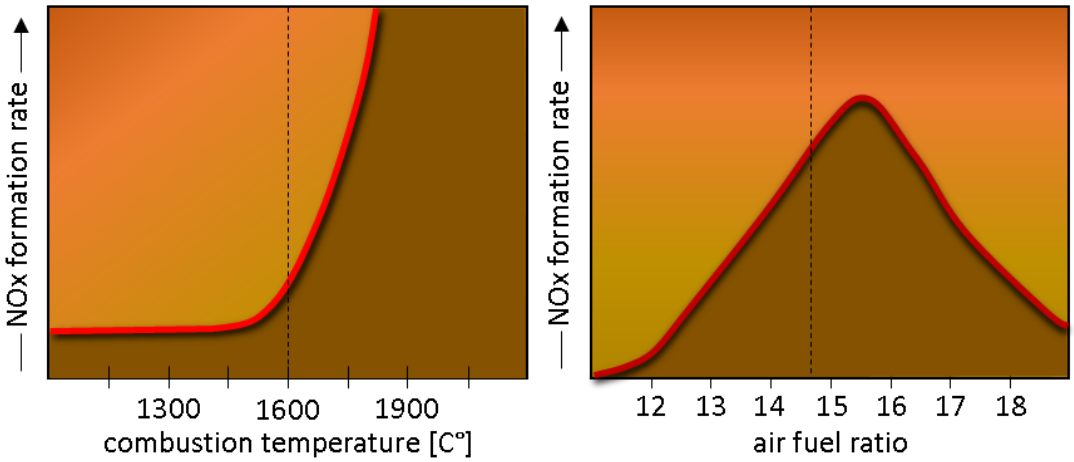

Figure 2.10: Effect of combustion temperature and air fuel ratio on nitrogen oxides

2.4.2.4 Particulate Matter

Generally, particulate matter pollutant generated by an engine is formed through and after the combustion of the high hydrocarbon fuel. The formation and size of particulate matter varies according to the fuel composition, the combustion temperature and pressure, as well as the combustion flame propagation [97]. An engine with rich air fuel ratio will end having higher particulate matter formation compared to an engine running lean. A mixture richer in fuel normally occurs during cold-starting since more fuel is added for combustion to warm up the engine. Also, the engine usually runs on richer mixtures when it is under high demand; for instance, when the vehicle is going uphill.

In addition to richer air fuel ratios, the lubricant of the engine may enter the cylinders through tiny gaps between the piston ring and the piston. Several components like the valves, valve seals, and piston rings tend to wear creating enough space for oil to pass through. Also, while the engine is sucking air in for the combustion process, oil can also be drawn into the cylinder contributing to the particulate matter production [98].

2.4.3 Exhaust Aftertreatment System

2.4.3.1 Positive Crankcase Ventilation

Introduced in 1961, the first means to treat exhaust emissions, and more specifically the hydrocarbons, was the positive crankcase ventilation system [99]. While the piston is moving inside the cylinder of the engine, a small amount of gas escapes from the combustion chamber through the piston rings and ends up in the crankcase [100]. As illustrated in Figure 2.11, rather than allowing the combustion gases to escape to the atmosphere, the ventilation system returns the gases through a controllable valve from the crankcase back to the intake manifold, so they can return to the combustion chamber.

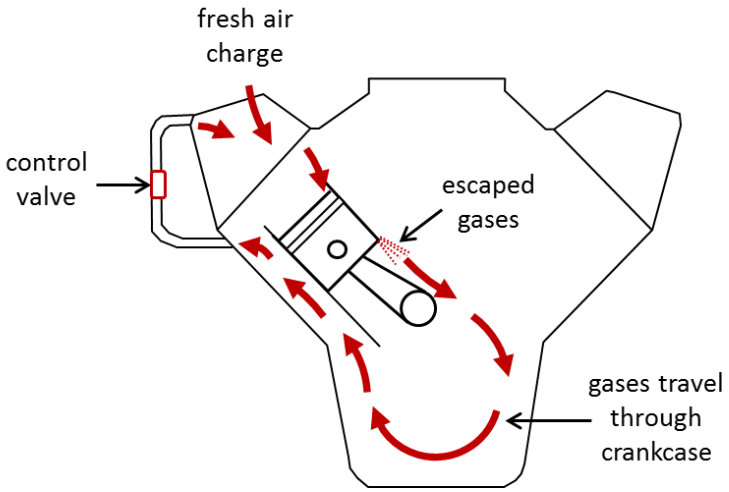

Figure 2.11: Schematic of the gas flow through the positive crankcase ventilation system

2.4.3.2 Exhaust Gas Recirculation

In 1973 the first exhaust gas recirculation system was fitted to the intake manifold of the engine to reduce nitrogen oxides emissions [101]. Through a controlled actuator valve, a percentage of the exhaust gases are recirculated

back to the intake manifold and re-introduced into the engine cylinders along with the fresh air charge. With the introduction of the exhaust gases into the mixture of air and fuel, the recirculation system lowers the peak cylinder temperature and since nitrogen oxides are mainly produced from very high temperatures inside the cylinder, the approach helps the engine to reduce the pollutant concentration at low loads and speeds [102].

Exhaust gas recirculation is widely used mainly to reduce nitrogen oxides, but due to the reduced cylinder temperatures caused by the addition of the cooler exhaust gases the thermal efficiency of the engine and engine life are also improved [104]. Additionally, the system has the potential of cutting down pumping losses on spark ignition engines at part load. This method however, may lead to significant reductions in engine performance, as well as causing the combustion process to produce more particulate matter. Due to the working principle of the exhaust gas recirculation system, less oxygen is available for combustion in the cylinder, increasing the formation of particulates, and since the recirculated gases lower the peak cylinder temperature, the result is lower peak cylinder pressures that generally result in less engine power. However, injecting the combustion by-products back into the cylinder may cause cycle-by-cycle combustion instability in light load operation.

2.4.3.3 Three-Way Catalytic Converter

Three-way catalytic converter technology is extensively implemented to reduce nitrogen oxides, unburned hydrocarbons and carbon monoxide emissions simultaneously. The catalytic converter was introduced in 1974 to deal with the emissions problem and deliver an effective combustion process [99]. This device is located in the exhaust system, after the exhaust manifold, and converts pollutants from the exhaust gas coming out of the engine cylinders into significantly less toxic by-products [103].

The quantity of fuel mixed with the intake air is the foundation block of an engine' aftertreatment structure. The air fuel ratio is responsible not only for the performance (in respect to power, efficiency and drivability) of an engine, but also for the chemical composition of the exhaust gas [104]. Although the

dynamics of the exhaust gas are affected by numerous other factors, the core of the exhaust gas aftertreatment system is the air-fuel ratio. The stoichiometric ratio is the ideal air-fuel ratio at which, in theory, no oxygen or fuel will remain in the exhaust gas composition [105]. For gasoline engines, the stoichiometric ratio is approximately 14.7 grams of air for every 1 gram of fuel injected [88].

As seen in Figure 2.12 the stoichiometric air fuel ratio is used because it allows the catalytic converter to deal with the hydrocarbons, carbon monoxide and nitrogen oxides [63]. The catalyst is oxidising the hydrocarbons and carbon monoxide, while the nitrogen oxides reduction is done by removing oxygen from the exhaust gas. If the exhaust gas is from rich combustion (less than $\lambda = 1$), then it is a reducing atmosphere and oxygen can be taken away from the nitrogen oxides, however, there is no sufficient oxygen to oxidise the hydrocarbons and carbon monoxide. If the exhaust gas is from a leaner combustion (greater than $\lambda = 1$), then it is an oxidising atmosphere and there is enough oxygen to oxidise the hydrocarbons and carbon monoxide, but the nitrogen oxide chemical reaction will not work [106]. The Cerium and ceramic honeycomb structure of the catalyst acts an oxygen medium [107]. When it is very slightly lean, the stored oxygen will be used to remove the nitrogen oxide. When it is slightly rich the oxygen is given out by the Cerium so the carbon monoxide and hydrocarbons oxidation reaction can still work.

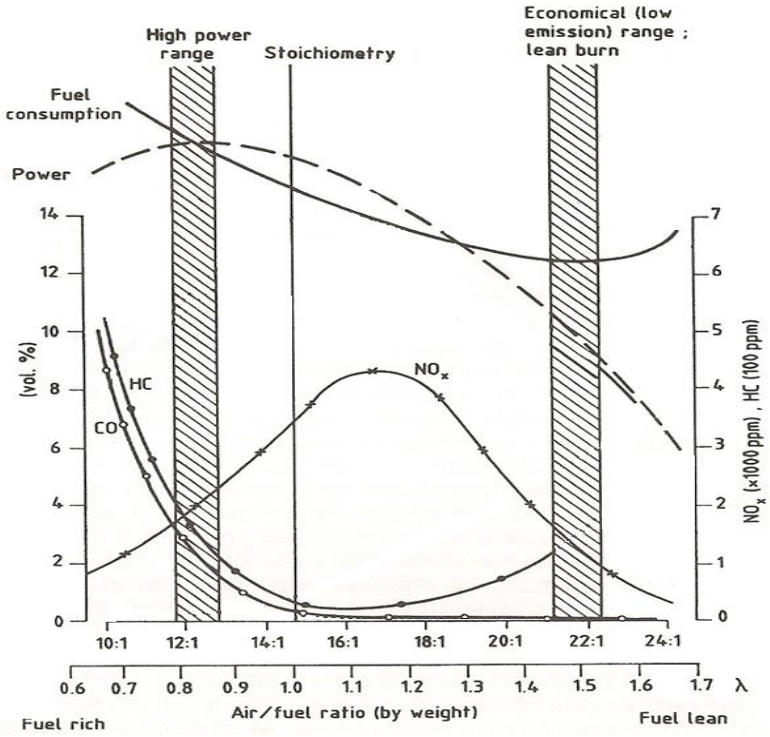

Figure 2.12: Typical quantity of emissions plotted against air fuel ratio [104]

It is clear that the goal of a stoichiometric fuelling is not for the engine to reach its maximum power/torque point, but to enhance the efficient operation of the aftertreatment system. The engine management system, the computer that controls all the functions of the engine, reads input signals from various sensors placed at vital points in the engine and its components [92]. The opening of the throttle mechanism that controls the available air passing into the combustion chamber, the intake air flow rate, and the instantaneous engine running speed are some of the crucial input signals fed to the engine management system for determining the next transition in the engine. The system controls the engine by sending output signals to electro hydraulic actuators such as the fuel injector, the spark plugs and the camshaft for the valve timing. Moreover, additional sensors are employed to monitor the combustion products, to back up the engine management system's calculations [92].

Even though the engine performs an imperfect combustion, at least in terms of power output, the exhaust gas reactions are being treated by the catalytic converter. A catalyst is a chemical element that causes a chemical reaction goes faster. For this reason, as the combusted gases from the cylinders pass

through the catalytic converter, chemical reactions arise on the catalyst surface that break apart the emissions and convert them into less harmful gases. Typically for a gasoline engine a three-way catalytic converter is fitted to the exhaust system to reduce the level of nitrogen oxides to nitrogen and oxygen, as well as oxidising the unburned hydrocarbons and carbon monoxide emissions to form water and carbon dioxide [108]. The “three-way” term is given to the catalytic converter due to the fact that is able to treat the all three pollutants simultaneously.

The catalytic converter system has to be running under stoichiometric ratio in order to gain its maximum conversion efficiency [109]. The catalyst is formed by a washcoat of precious metals, surrounded by a honeycomb structure core. The honeycomb core of the catalyst, made by either ceramic or metallic foil monoliths, provides a large surface area in order to assist the wash-coat. The washcoat is responsible for supporting the precious metals and hence its surface area maximises the catalyst active available surface to the exhaust emissions. The most common valuable metals used for the catalytic converter are rhodium as a reduction agent, palladium for oxidation and platinum, acting both as a reduction and oxidation catalyst [110].

2.4.3.4 Particulate Filter

In the mid-1980s special filters were designed to remove the particulate matter from the exhaust gas of the engine [111]. The particulate filters were initially introduced for the diesel aftertreatment system only, however, nowadays they are also engaged in modern gasoline engines due to high requirements applied on this type of engine [112]. Given the available space under a vehicle’s floor, the available space close to the engine and the filter’s volume, the gasoline particulate filter can be added to the aftertreatment system separately to the catalytic converter, along or under the catalyst [47].

The main differences between the particulate filters used for diesel and gasoline fuelled engines are that gasoline engines requires a filter with smaller dimensions and that the exhaust gas of a gasoline engine is able to achieve high temperatures (up to 700°C) for a continuously and efficiently automated passive regeneration of the filter [113]. Furthermore, the particulate filter has

to be characterised by high robustness and durability. The system has to ensure the quality of its emission control operation during a vehicle's lifetime and hence eliminate the need for replacing or servicing the filter [114]. Moreover, the filter has to deal with the challenge of reducing the nitrogen oxides emissions along with the particulate emissions control. The filter has to fully function through a car's operation and at the same time decrease the concentration of particulates in the exhaust gases.

The particulate filter is designed in such a way that the exhaust gas will be forced to go through the filter. There are two basic designs type of particulate filters; the wall and the fibre flowing filters [115]. As seen in Figure 2.13 for the wall-flow filter a honeycomb structure with channels blocked at alternated ends traps the particulate emissions while the exhaust gas is forced to flow through its walls. The wall-flow particulate filter has excellent particle removal efficiency since it can block more than 95% in mass and 99% in number for particulates of up to 100 nm in diameter [116]. The walls of the filter are made from cordierite or silicon carbide with the main difference between them being their melting points. Cordierite filters are made from magnesium iron aluminum cyclosilicate, a type of ceramic material, which in comparison to other particulate filters are fairly cheaper but have a low melting point about 1200°C, while the silicon carbide wall flow filter has a melting point around 2700°C, more than twice the temperature of ceramic wall flowing filters [117, 118].

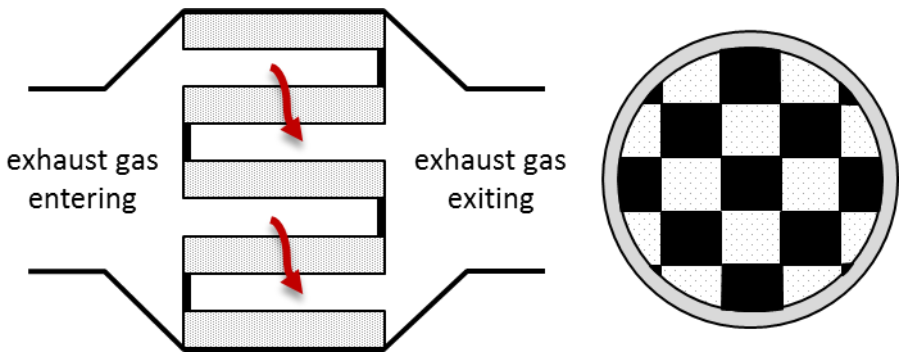

Figure 2.13: Exhaust gas flow through a wall-flow particulate filter

The second type of particulate filter design is the fibrous filters; fibres made from ceramic are mixed together to form a spongy barrier. This type of filter

has the advantages over the wall flow design of taking any custom size or shape, plus they can generate lower back pressure [119]. Due to their structure, they will require a layout that provides them with more regeneration properties [120]. Metal fibres intertwined together can be used, having the benefit of using electrical current to regenerate the filter [121], but with this material comes the most expensive particulate filter arrangement.

2.5 Chapter Summary

This literature chapter has highlighted the main developments of the technology on gasoline direct injection engines towards efficiency increase and performance enhancement for this type of engine. Followed by a brief history of the emissions legislations for gasoline engines, as well as how the pollutants sampling and testing procedure are performed. There are several technologies which offer the potential of lower emissions, however, this chapter focuses only on the fundamental approaches of treating the pollutants during and after combustion (compression ratio, ignition timing, exhaust gas recirculation, three-way catalyst, particulate filter, etc.).

3 Overview of Engine Modelling and Calibration

3.1 Chapter Introduction

The chapter is mainly divided into two parts; engine simulation methodology in Section 3.2 and the engine simulation technology in Section 3.3. Section 3.2 introduces the engine mathematical modelling methodology, and also concludes with a description of stochastic engine models and how the Kinetics SRM suite, which is based on the stochastic simulation technique is suited for the aim of the present research. Section 3.3 reviews engine mapping methodology by first introducing the engine control unit and its complex role in engine control. The process of developing an empirical analysis of engine performance, the engine mapping procedure, is broadly presented. Additionally, an outline of the different experimental designs for the engine mapping process is given.

3.2 Engine Simulation Methodology

Engine mathematical modelling is generally considered as the procedure of describing the physical and chemical phenomena occurring in an engine system with the aid of mathematical equations and computational simulation codes. Computer aided simulation of automotive systems has contributed enormously to the automotive research and engine development community [122, 123]. Encouraged by enhanced production when compared to the traditional prototype development processes and by the continuous increase in computational power, computer aided simulation allows fast and compact analysis of complex vehicle systems. However, increasingly demands for performance and efficiency requires advancing the level of accuracy, complexity and quality in the computational models developed.

Current and future emissions legislations will require cleaner and more efficient engine powertrain systems. This challenge requires multidisciplinary effort at all stages of engine research and development, and the rapid development of computer technology has encouraged the use of multi-platform simulation approaches to compute the nature of the essential process responses in engine systems [124].

In general, mathematical engine models can be classified into two main categories; behaviour and physical models. Behaviour engine modelling or black-box engine modelling, only shows the interactions between inputs and outputs, without any knowledge of the mathematical relationships involved (see Figure 3.1). Multiple inputs and outputs can be adopted into the box structure. In the second category of engine models, the inputs, outputs and the internal dynamics of the system are known, a so-called physical or grey-box model, in which all the necessary information is available for simulating the system.

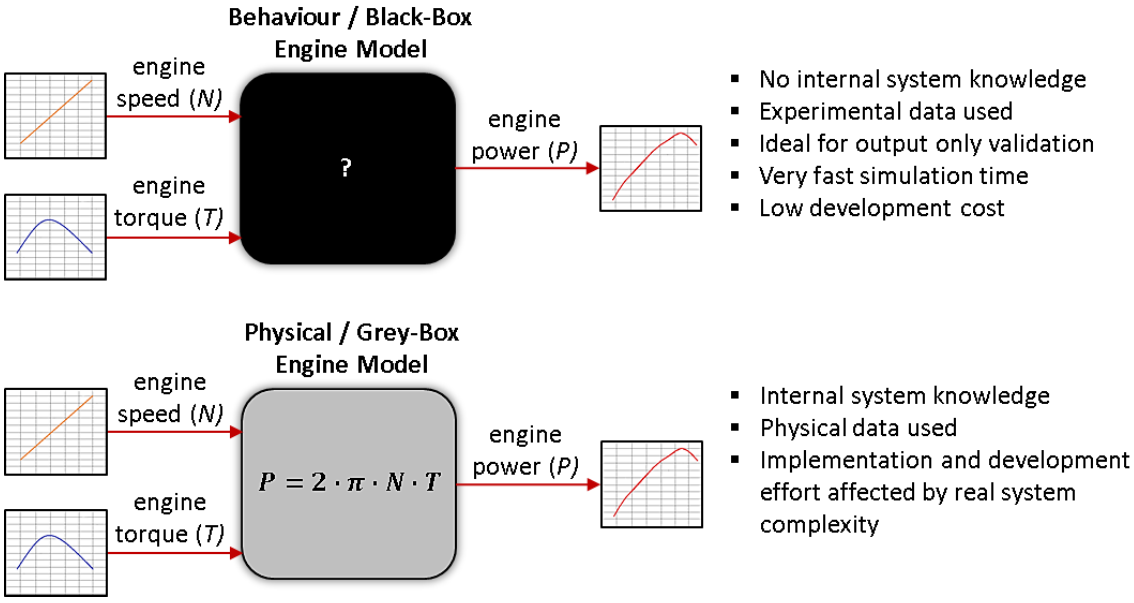

Figure 3.1: Simple example of black- and grey-box engine models

Behaviour engine models' structure is ideal when the validation of the output is the main concern, rather than knowing how that output was produced [125]. This type of modelling approach represents the engine system by an empirical description or set of transfer parameters that do not describe any internal physics. Because of this, the behaviour models are usually very fast with low implementation costs. However, these models lack flexibility and are not appropriate for any form of sensitivity analysis [126].

On the other hand, in physical engine models the internal knowledge of the item under consideration needs to be validated along with the output, and so the complexity of a real system will strongly affect the complexity of a physical model along with simulation times and implementation efforts [127]. A major

disadvantage of this modelling strategy is the use of approximations and averaged values for physical details, however, physical models provide flexibility and enable design sensitivity analysis and optimisation of the engine system [128]. A very common approach in engine models' application is the division of the system into sub-models represented by different modelling techniques [129].

3.2.1 Behaviour-Based Engine Models

The increase of control demanding technologies, like variable valve timing, advance ignition management, variable exhaust gas recirculation, variable geometry turbine, and many more, has a great impact on the complexity of the engine control process. However, behaviour-based engine models can neglect the complexity of a system by simply hiding the relation of inputs and outputs within their structure. Look-up tables, response surface methodology, and artificial neural networks are contained within this modelling technique.

3.2.1.1 Look-up Tables

Several inputs of the internal combustion engine can be represented in multidimensional look-up tables or maps. The main drawback of look-up tables in engine modelling is the exponential growth of the data points with increasing number of inputs. Therefore, in terms of practicality, a look-up table engine model usually uses one- or two-dimensional input space [127]. As illustrated in Figure 3.2, a one-dimensional look-up table includes one output that is depended on one input, whereas a two-dimensional table will consist of a set of data points within its grid with each data point having two inputs. An estimation parameter is employed to link the data points together. The accuracy of the model strongly depends on the number of points on the grid.

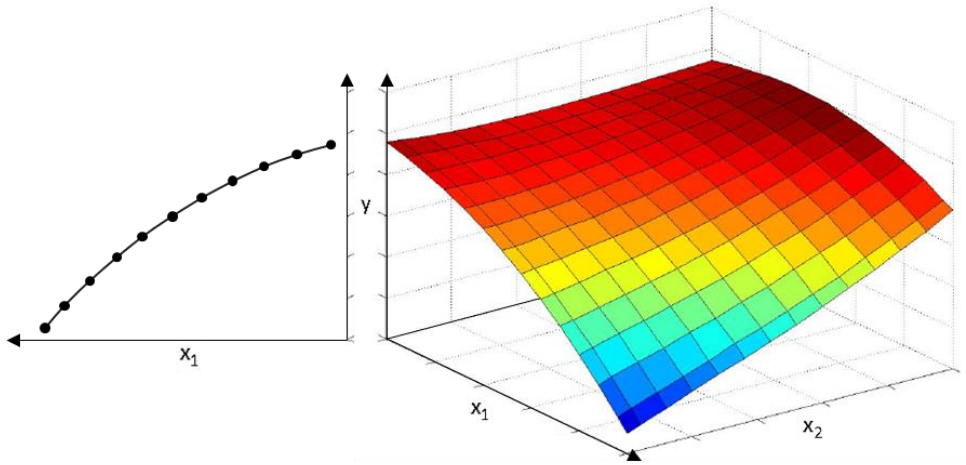

Figure 3.2: One-dimensional look-up table for one input at the left and two-dimensional look-up table for two inputs at the right

3.2.1.2 Response Surface Methodology

Response Surface Methodology (RSM) is a set of statistical techniques developed for solving black-box-based optimisation problems [130]. Design of experiments are created to determine the relationship between the design variables (inputs) and the responses (outputs) of the simulation. The method relies on the fit of empirical equations to identify the key inputs of the design and analyse the effect of the inputs on the objective function to optimise an output or a set of outputs [131]. The choice of efficient experimental designs can make the application of RSM reduce the cost of expensive analysis methods, such as finite element or computational fluid dynamics simulation [132].

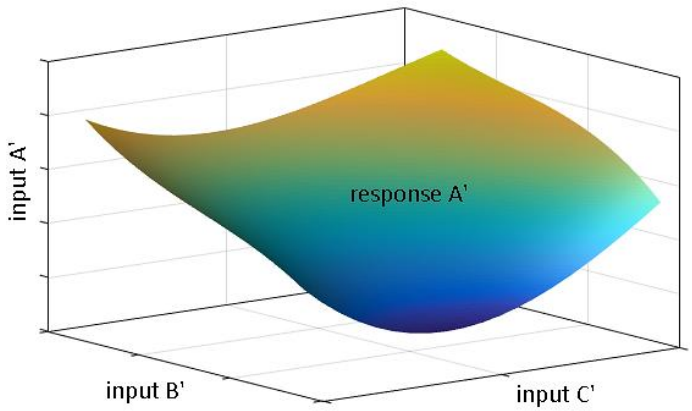

Figure 3.3: Profile example of surface response generated from a RBF-model with three variables (input A', B', C') in the optimisation of response A'

Due to the huge advantage over the classical one-factor-a-time optimisation analysis, the RSM is largely used for generating a large amount of information from a small number of experiments. However, because of the relatively few data sets required, the real global optimum might be missed in the search if the experiment is not able to capture a sufficient design space [133]. It might be the case that the response surface developed is invalid for regions other than the studied ranges of factors. It should also be noted that the main limitation of the method is that RSM is a black-box approach, hence it is very difficult to estimate the accuracy of the approximation [134].

3.2.1.3 Artificial Neural Network

A very powerful method among behaviour-based engine modelling is the artificial neural network technique. Inspired by the organisation of neurons in the brain, the major feature of this type of engine model is its ability to learn how to perform a particular task [135, 136]. The artificial neural networks will then extrapolate the frame between input and output data [137]. This method can be used to distinguish engine data that is similar to the examples given during the training stage. Figure 3.4 illustrates the simplified architecture of an artificial neural network engine model. Within the black-box there are layers of neurons, which are basically the data computational elements of the system. Typically, there is one input layer and one output layer of neurons; however intermediate layers can be introduced.

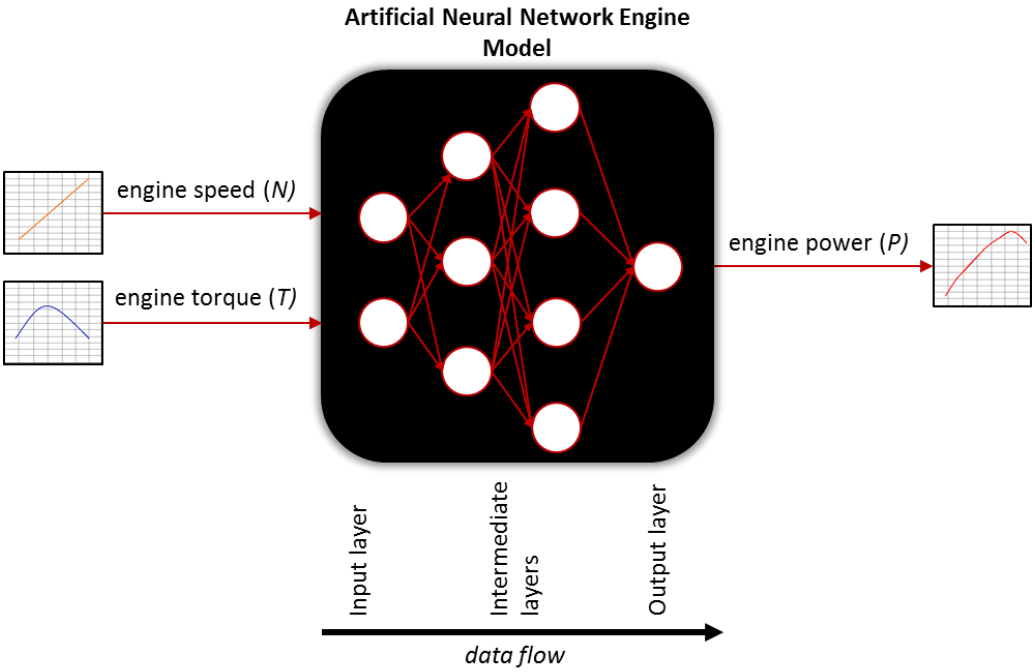

Figure 3.4: General architecture of an artificial neural network engine model

Generally, neurons receive inputs, and process them to obtain an output. Hence, the neurons in the output layer will gather information from all the neurons in the intermediate layer or directly from the input layer of neurons if there are only two layers. Each data sent to the neurons in the following layer have an individual weight factor that will determine the outcome being transferred to the next set of neurons. The data flow inside the network follows only one feed-forward direction; input data are processed in the input layer's neurons and the results of the operation are passed to the neurons of the intermediate or output layer.

The simplicity of an artificial neural network has been used for predicting engine performance, such as torque, power and specific fuel consumption [138, 139, 140, 141]. Wu and Gisca [142, 143] adopted artificial neural network models for defining the functioning parameters of the internal combustion engine such as in-cylinder pressure and mixture strength. A neural network based solution is efficient in terms of time; however, great knowledge in the design selection of the network is needed. Furthermore, because of its black-box nature, artificial neural networks are prone to over-fitting data with several consequences, such as becoming excessively

complex and with poor predictive performance. Additionally, the training outcome of the network will depend crucially on the choice of the inputs.

3.2.2 Physical-Based Engine Models

Based on combination of empirical data and fundamental knowledge of the system, the physical modelling technique refers to full or partial interpretation of the system in physical terms. Furthermore, these type of engine models can be categorised based on their dimensional information, as:

- Thermodynamics-based;
- Fluid-dynamics-based;
- Stochastic-based.

3.2.2.1 Thermodynamic Modelling

In thermodynamic modelling, most of the characteristics are averaged through the engine cylinder and no three-dimensional information (x,y,z) is available [144, 145, 146]. Thermodynamic internal combustion engine models are also known as zero-dimensional because they have no spatial resolution, quantities are independent of space, and therefore they do not contain any information on the internal fluid mechanics [147, 148]. Thermodynamic models can be categorised into single and multi-zone models.

3.2.2.1.1 Single-zone thermodynamic

Single-zone thermodynamic engine models are based on the conservation of mass and energy through the first law of thermodynamics and have no spatial resolution, because all the thermodynamic properties are considered as uniform and one single control volume is taken (see Figure 3.5). In these models the only independent variable is time and all the thermodynamic properties are homogeneous. The first law of thermodynamics states that the internal energy of the combustion is considered to be stable and evenly transformed from one form to another form with no losses [149]. A uniform mixture composition, temperature and pressure is used for the combustion process, to calculate the internal energy of the system, and hence to determine the enthalpy alteration.

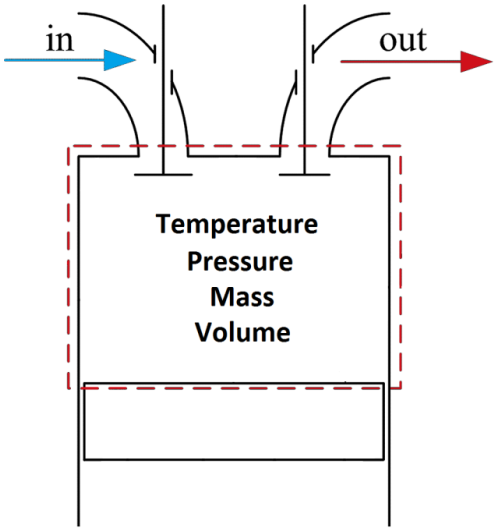

Figure 3.5: Single-zone thermodynamic engine models assume the cylinder as one single control volume with homogeneous properties

Single-zone models are useful as a prognostic tool when the heat release or the fuel mass burning rate are being determined [150]. A single-zone model may produce a system of ordinary differential equations for air fuel ratio pressure, temperature and quantity but it neglects the combustion chamber geometry, fuel evaporation, as well as the spatial difference of the mixture configuration and temperature [122]. By adopting a homogeneous mixture of ideal gases at all times the fuel is burned immediately when it is injected into the cylinder thus any unburned fuel vapour, fuel ignition delay, and even late combustion, are being disregarded [123]. Single-zone thermodynamics engine modelling does not take flow into account; the fluid is modelled as a perfectly mixed system with homogenous reactions, hence any mixing details and inhomogeneity of the mixture are not captured [151, 152].

3.2.2.1.2 Multi-zone thermodynamic

In multi-zone thermodynamic internal combustion engine models, the combustion chamber is divided into several zones, with each zone possessing uniform thermodynamic properties. As with single-zone models, the first law of thermodynamics is applied to each of these control volumes with appropriate boundary conditions. Multi-zone thermodynamics models take into consideration the geometry of the combustion chamber and the existence of burnt and unburnt gases [153, 154, 155, 156, 157, 158, 159].

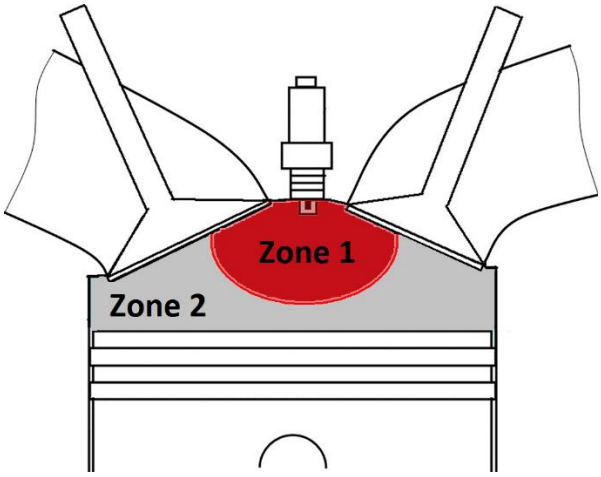

Figure 3.6: Multi-zone thermodynamic models is dividing the cylinder into a number of zone with uniform properties

As seen in Figure 3.6, multi-zone thermodynamic modelling divides the combustion chamber into at least two zones, unburnt and burnt, but any number of zones can be applied based on the results of a sensitivity analysis for convergence of simulation outputs [160]. By splitting the fuel into portions these models can describe the temporal and spatial distributions of both temperature and concentration [161]. The combustion process in each individual fuel partition is investigated as an air fuel mix procedure, resulting in separate thermodynamics systems having a burnt and an unburned zone with a homogeneous temperature for each zone and no heat transfer between them [144, 153, 162].

The approach of dividing the combustion chamber into zones with uniform thermodynamic properties (i.e. temperature, composition, etc.) allows a more accurate prediction of combustion characteristics (i.e. pressure, duration, exhaust emissions, etc.) since temperature and species stratification are analysed in more detail. Furthermore, combustion in thermodynamic modelling is not occurring instantaneously and it can be described by the use of a Wiebe function [88].

$$x(\theta) = 1 - exp\left(-a \cdot \left(\frac{\theta - \theta_0}{\Delta\theta_b}\right)^{m+1}\right) \qquad \text{Equation 3.1}$$

$x(\theta)$ is the mass fraction burnt at crank angle θ, θ_0 is the crank angle at the start of combustion and $\Delta\theta_b$ is the combustion duration. Constants a and m are adjustable parameters which their values can be defined based on experimental engine data of the cylinder pressure (see Figure 3.7).

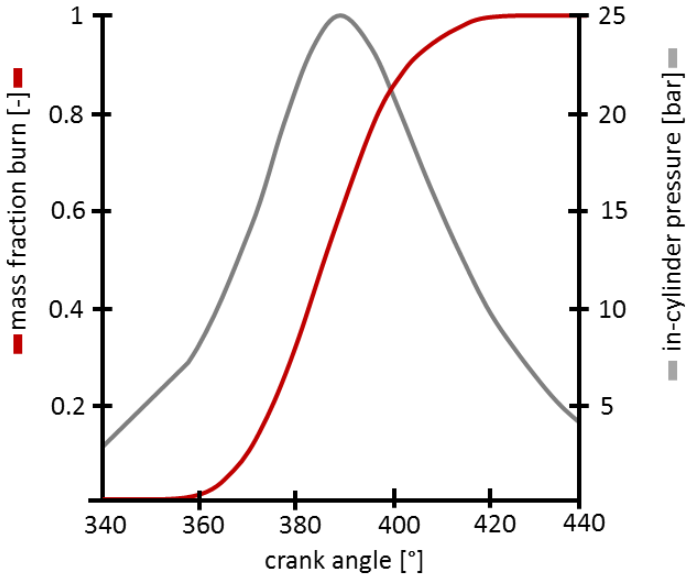

Figure 3.7: In-cylinder pressure profile and mass fraction burned

3.2.2.2 Fluid Dynamics Modelling

Whereas thermodynamic models lack an ability to analyse spatial flow variations, local velocity and temperature fields, fluid dynamic models, known as dimensional or computational fluid dynamics models, can examine time-based variations of velocity, temperature and pressure fields in one, two, or three dimensions [161]. For instance, case studies for flow analysis (i.e. flows through valves, fuel injection flow, in-cylinder flow, etc.) are linked with highly detailed dimensional resolution, where multi-zone modelling cannot be applied [163, 160]. Overall, dimensional engine models are divided into two main groups; one-dimensional and multi-dimensional.

3.2.2.2.1 General Fluid Dynamics Laws

The fluid dynamics modelling approach relies on the solution of the conservation equations of mass [164], momentum [165], species and energy [166]. A system is divided into smaller components that have volumes with constant fluid properties (pressure, temperature, density, and internal energy). In addition to the fluid properties each volume has a mass flux and

fluid velocity that can only be transferred across the volume boundaries. A fluid dynamics simulation simultaneously solves the equations for conservation of mass, momentum and energy for each volume using the volumes' fluid properties [167].

Conservation of mass simply states that the mass in a fixed control volume cannot be decreased or increased, but it can be conserved and changed into a different form, as illustrated in Figure 3.8. Applying mathematical logic, the conservation of mass equation is developed by adding up the flow rate of the mass entering and leaving the control volume, and hence determining the net mass flow rate within the volume. The principle of the conservation of momentum states that the total momentum of the control volume remains unchanged through time [165]. In a moving fluid element there are two kinds of forces that an element can experience; surface force like pressure and stress, and body forces, which can be simplified as gravity force.

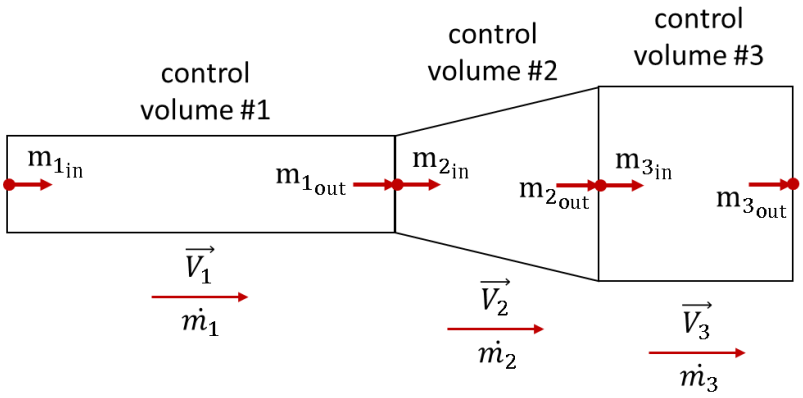

Figure 3.8: Conservation of mass through control volumes

Since we have a mass flow rate, we have the fluid mass. We also have a change of velocity between the starting and ending points of the control volume, hence we have the acceleration of the fluid. Newton's second law states that if there is an acceleration going on and there is a mass associated with it, then there must be a force [168]. It can be stated that the force acting on the fluid is the mass flow rate multiplied by the change in velocity. Newton's third law states that for every force there is an equal and opposite reaction, hence the force acting on an object by the fluid is going to be equal and negative. The rate of change of the momentum of the volume is the sum of all

forces acting on it. In a control volume the conservation of momentum is used to determine the resulting forces from the momentum change and the acting pressure on the entry and exit of the volume.

Finally, conservation of energy states that the sum of kinetic and gravitational energy is constant. A given flow field will contain thermal and kinetic energy. Energy conservation can be defined as the rate of change of energy, which is the sum of energy transfer of the system, hence work plus heat. In a control volume the net rate of energy transfer by heat and works transfers is equal to the difference between the rates of outgoing and incoming energy by mass flow [169].

3.2.2.2.2 One-Dimensional Fluid Dynamics

As seen in Figure 3.9, in a one-dimensional simulation the complete engine system is discretised into smaller volumes; the entire intake and exhaust system are modelled by many volumes, where the junctions are represented by a single volume and the pipes are divided into several sections [170]. Physical parameters, such as temperature, pressure, density, etc. are uniformly simulated for each volume; nevertheless, a finer discretisation increases the accuracy of a simulation [171].

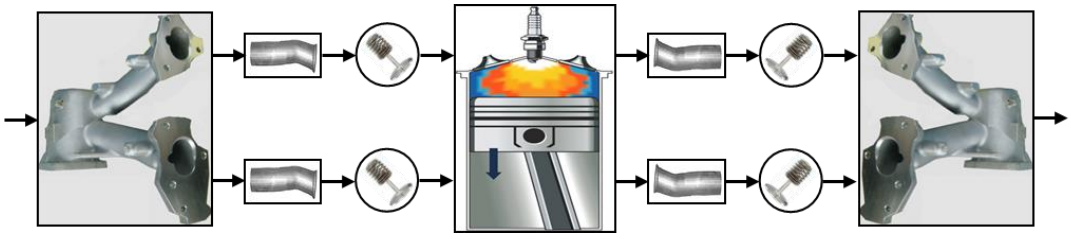

Figure 3.9: Example of discretization of the engine system into smaller volumes

One-dimensional codes are developed to simulate engine flow throughout the whole engine system. Important procedures of the system are defined by means of mathematical expressions in a way that the physical conditions, such as pressures, temperatures and mass flows, will be determined through all the computational segments at all time. One-dimensional calculation is highly adjustable and can be adapted for the simulation of transient engine

operations; however, considering that they consist of numerous empirical parameters, they need to be fitted with experimental data [172].

Engine-oriented one-dimensional programs have gradually been utilised to support the engine design stage [173, 174]. Generally, their application initiates from the calibration of a base engine model of experimental data to simulate the influence of various engine configurations on the performance output. At that point input variables, such as the inlet and exhaust pipe geometry and valve timing and lifting, can be adjusted in terms of the prediction ability of the model [175, 176, 177, 178].

3.2.2.2.3 Multi-Dimensional Fluid Dynamics

One-dimensional engine modelling can also be used to set initial and boundary conditions needed by a multi-dimensional simulation. Utilising discretisation methods and turbulence models to analyse the flow through the cylinders of the engine [129, 179], multi-dimensional modelling is best for determining the optimum design characteristics for individual components, where one-dimensional models are best-suited for optimising the design of an entire flow system. For instance, a multi-dimensional simulation can be used to design and optimize the cooling system of the engine; pump, coolers [180, 181], etc., but a one-dimensional approach can take the performance characteristics of the components and use them to simulate the system [182, 183, 184, 185].

Based on the general laws at any location within the engine cylinder, computational fluid dynamics models constitute a system of partial differential equations founded on Navier-Stokes equations [186, 187]. Despite the evolution of modern computer capabilities and more efficient numerical algorithms, multi-dimensional fluid dynamics is the most computational demanding method applied to internal combustion engine simulation [188]. The combustion chamber or generally the region of interest (i.e. intake and exhaust ports might be included) is replaced by a mesh of cells (see Figure 3.10). For each cell of the defined geometry, partial differential equations for conservation of mass, momentum (Navier-Strokes equations), energy, and species concentrations is solved. How accurate and how computationally

costly the simulation will be depending on the defined geometry, as well as, the quality of the formed mesh and the fluid properties [129].

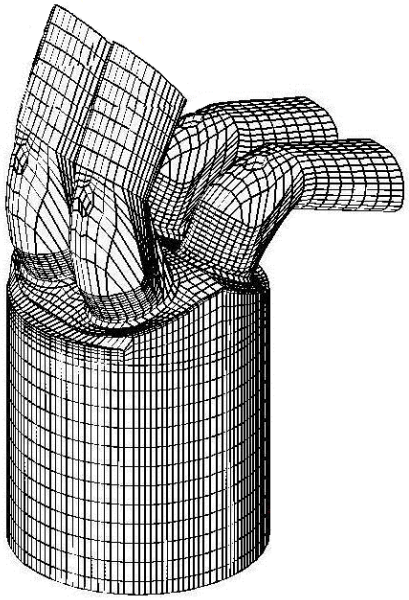

Figure 3.10: Meshed engine cylinder and valves ports in multi-dimensional simulation

To sum up, multi-dimensional codes helps to design components while one-dimensional codes enables us to determine the effects of various design changes and operating conditions across an entire system. A number of previous studies have applied the multi-dimensional modelling method to analyse the air flow within a combustion chamber and correlated the simulation results with experimental measurements [189, 190, 191, 192, 193, 194, 195].

Additionally, three-dimensional combustion models have been engaged for the evolution of a downsized gasoline engine with power and efficiency increase [196, 197, 198]. The multi-dimensional approach has also been used for the optimisation of engine geometry and injection strategy, as well as, inspection of multiple direct fuel injections with advanced flexible valve timings [199, 200, 201, 202]. Belal et al (2013) chose a multi-dimensional code to model the turbulence and combustion processes with sufficient detail to include fuel injection and spray formation [203]. With a computational grid of 200,000 mixed cells types and a time step of 0.5 crank angle, the fuel jet was

divided into a single segment for each crankshaft angle. Attempts to reduce the unrealistic computational effort needed by multi-dimensional simulations involve the introduction of multi-zone sub-models to simulate the burning mixture zone and the unburned sector surrounding it [204]. This simulation scheme runs faster but at the expense of prediction accuracy.

It is well known that turbulence flow inside an engine cylinder plays a very important role in the combustion process [205]. Turbulent flow is irregular and chaotic, consisting of a spectrum of different scales or eddy sizes. The most important characteristic of turbulent flow is the fact that velocity and pressure at a point, fluctuate with time in a random manner. Turbulent motions in the engine cylinder occur at various length and very short timescales. The variation in length and timescales are responsible for the difficulty of numerically analysing turbulent flow. A full detailed numerical solution of the combustion turbulent flow is impossible and cannot be predicted exactly, thus the general approach is to use methods to provide approximated information about the flow.

As illustrated in Figure 3.11, there are four main approaches for turbulence flow simulation [206, 207, 208, 209]; Reynolds-averaged Navier-Stokes equations (RANS), Large-Eddy simulations (LES), direct numerical simulations (DNS) and stochastic turbulence modelling using probability density functions (PDFs). Without going into too much detail of the different levels of numerical solutions for turbulent combustion, RANS computes only the averaged motion and models the effect of fluctuations [210]. Next, LES neglects small scales of the flow and focuses on the large scales of the turbulence to be fully resolved. LES provides better prediction of the turbulence flow but the computational cost of this approach is extremely large [211]. DNS also requires huge computational resources since it is resolving every length and time scale of the turbulent flow [212]. Finally, the stochastic PDF-based method defines the relative probability of the variable in a given interval [213, 214].

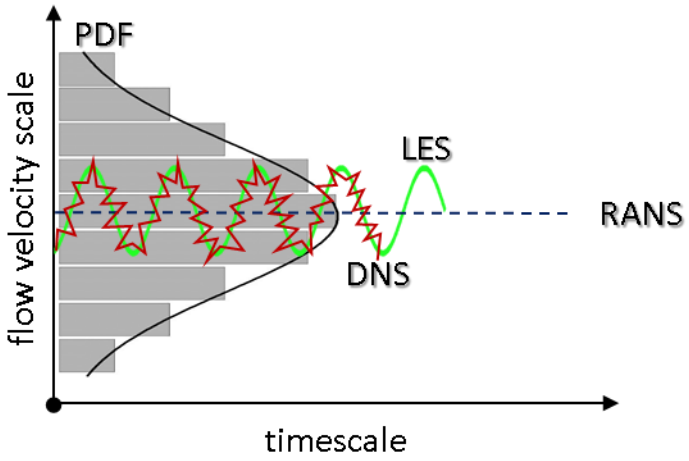

Figure 3.11: The four main approaches for turbulence flow simulation

3.2.2.3 Stochastic-Based Engine Modelling

Due to the random motion of turbulent flow statistical methods are therefore helpful to describe a turbulent flow field. The aim of the method in turbulence modelling is the description of the fluctuating velocity and scalar fields in terms of their statistical distributions. Characterised as “one of the most promising and powerful approaches” for turbulent fluctuations studies [215], the stochastic approach is able to model mixing and chemical reaction in turbulent reacting flows for multi-dimensional fluid dynamics and multi-zone thermodynamics combustion models. The first stochastic PDF-based model was established by Dopazo and O'Brien [216], where the statistical method was used to model mixing and chemical reaction in turbulent reacting flows.

Stochastic modelling simulates the turbulence processes happening in combustion by the use of global and local quantities in the computational space of the cylinder [217]. Global quantities (mass, volume, density and pressure) remain constant, while local thermochemical quantities such as mixture mass density, molecular weight, specific heats, temperature and exhaust gases are being divided, arranged and categorised into levels within the computational space [218]. Both types of quantities, global and local, are evolved with reference to time and they alter with the variation of the combustion chamber volume as the piston moves up and down.

The mass within the cylinder of the engine is divided into a number of elements called particles, which have a chemical composition, temperature

and species concentration and are statistically described by a probability density function (PDF). The variations of chemical reactions and turbulence flows may be analysed by both the PDF and particle model approaches. The PDF approach uses the joint probability density function of the species concentrations and the particle model represents the turbulent mixture using equal sized particles with uniform composition. At a certain rate, two particles at a time, are mixed together exchanging chemical reactions. Rather than applying a specified rate for the particles interactions, a PDF evolution of the particle compositions was implemented by Pope [219] making the first step to link the probability approach with particle models and enabling the advantages of each method to be exploited. This method has become the dominant approach for modelling and solving PDF equations.

The stochastic particles employed by the PDF technique move through the computational domain with unique instantaneous velocities. The state of a stochastic particle is described by its position and velocity, as well as by the values of the reactive scalar that it represents as a function of time. The probability density function is computed as, basically, the ratio of the number of times an event occurs to the number of times that all event occurs [220].

Let Φ express the value of a design variable, for example the mass fraction of oxygen, at a specific location and time in the flow. The flow is measured in units of time and hence for each time step there is a different value of the oxygen mass fraction, Φ. Thus, Φ can be described as a random variable. The development of the probability density function is determined through particle mixing and detailed chemistry. The particles are randomly selected to interact with each other exchanging in this way heat and chemical composition [8]. How often these mixing events occur is set by a turbulent mixing time [21]. Turbulence is essential for the combustion process in engines since it prepares and mixes the fuel before combustion. Particularly in the case of direct injection engines the combustion of the mixture is strongly affected by the mixing process [221].

A stochastic PDF-based model can compute results with similar accuracy compared to a typical multi-dimensional engine model but within minutes instead of days achieving accurate results [222, 223, 11]. Stochastic models are gradually dominating in the area of engine combustion modelling as they offer the analysis of a mixture's detailed combustion chemistry along with fast simulation times at low computational cost.

Employing chemical reactions and gases dynamics into modern engine simulation technologies offers the prospective of developing a more powerful and superior simulation tool. In the simulation of combustion, by use of chemical reactions and kinetics, the results are strongly affected by the quality of the chemical model. The fuel and oxidizer are the foundation base of an internal combustion engine chemical model. The complexity of the model depends on the complexity of the fuel. For example, small fuel species like hydrogen haves a chemical model density under 10 species, while more complex fuel species such as iso-octane can have hundreds of species in the chemical model. In addition, features such as soot emission calculations need a chemical model that includes those specific species and reactions.

Despite the evolution of detailed chemistry fuel models, the challenge to practically implement them into standard engine simulation codes remains. The increase of computational time and power associated with resolving detailed chemistry along with dynamic mathematical functions has historically limited the possibility of the implementation of such models. While there is a large volume of published studies describing the important role of multi-dimensional computational fluid dynamics models and their ability to provide detailed simulations [224, 225, 226, 227, 228, 229, 230, 231, 232, 233], it has been conclusively shown [198] that this kind of modelling requires huge simulation times and computational power in addition to their very complex setup, run, and post process requirements.

Including large detailed chemistry models into multi-dimensional codes results in unrealistic computational timescales. This has been demonstrated [234] by running a multi-dimensional fluid dynamic model with a detailed kinetic mechanism composed of 872 reactions and 188 species. For a single engine

cycle the simulation took 28 days to complete the task. The computational time can be reduced by replacing the multi-dimensional model with lower quality, but still sufficient, modelling approaches. The simulation times for thermodynamics or single-dimensional based engine cycles, which are universally employed in engine design and development, is mostly in the order of seconds per cycle. However, even with the combination of a different modelling scheme with detailed chemistry, they will still result in large solution times.

Even so, recent experimental and computational investigations in chemical kinetics modelling have provided more robust fuel models that are able to compute the combustion characteristics of the higher molecular weight hydrocarbon fuel used in internal combustion engines [235, 236, 237, 238, 239, 240]. These latest surrogate fuel models include thousands of species and elementary reaction steps, increasing the understanding of fuel combustion and soot formation origins, in addition to providing improved accurately predictions of emissions pollutants [241].

As mentioned above, an alternative to computational fluid dynamics is the PDF modelling technique. In a computational fluid dynamics model the chemical composition, temperature, and mass, are spatially resolved, whereas a PDF-based combustion model belongs to the zero-dimensional thermodynamics model category where there is no spatial resolution and therefore don't contain any information on the fluid mechanics. Introducing the latest robust detailed chemistry model to a PDF-based combustion code will increase the system benefits since of emissions prediction ability, it will be capable of faster turbulence processes simulations [7, 27]. PDF-based models have been demonstrated to be a productive modelling tool due to the integration of detailed chemistry whilst managing relatively low computational cost [242]. The empirical findings of a number of previous studies supporting the above approach [21, 22, 23, 24, 25, 26, 27].

Essentially with every run of a PDF-based combustion model, different outputs will be produced due to built-in random processes. The advantage of this modelling technique is that the simulation takes into account, in its

computation, the inhomogeneity and turbulence within the combustion process by using physical quantities described by probability density function distributions [218]. Hence the model can account for variations of the quantities modelled by PDF-based variables, like cylinder mass, within the combustion chamber making it perfect for cycle-to-cycle variations studies. The best approach to model a real phenomenon as realistically as possible relies on the simulation study to analyse it. Previous research has shown that PDF-based models are advantageous tools for representation of the real world [243].

Cycle-to-cycle variations in spark ignition engine combustion tend to reduce performance and efficiency [244, 245]. Detailed investigation of the cycle-to-cycle variations is difficult because of the problem of controlling and measuring the changes of all the influencing factors [246]. In-cylinder charge motion can vary between cycles, changing both rate at which unburned air fuel mixture is entrained and the profile of the turbulent flame front.

Variations in local turbulence during ignition time may move the flame kernel, thereby altering the interactions between the flame and the piston cylinder walls [247 – 250]. Consequently, it is not clear which factor has the largest effect on the combustion variations and therefore how to reduce these variations [251]. One solution to this problem is through the use of computer simulation [252]. However, running many engine cycles on a multi-dimensional model with detailed chemistry would be extremely expensive in terms of computational time and power. It has been concluded [253] that the initial flame growth rate is controlled by the laminar flame speed at the spark plug and the initial eddy burn size. If the fuel is well mixed with the air flow and the engine is operating at a high load, the dominant cause of variations in the early combustion is the flow situation in the area of the spark plug [254]. Control and reduction of combustion cyclic variations can help, to some extent, to move towards improved fuel economy and reduced emissions levels [255].

3.2.2.4 Evaluation of Engine Simulation Methodology

In conclusion, multi-dimensional computational engine simulations are the best current technique for determining the optimum design characteristics for individual components and new engine concepts, whereas single-dimensional models are suitable for optimising the various design changes and operating conditions across the engine system. Widely spread throughout the engine development industry, the single-dimensional modelling approach is able to determine how the engine will operate without the need of powerful processing and time-costly computation [256].

The approach of stochastic PDF-based engine modelling has been concluded as the best method to adopt for a fast, accurate and realistic combustion simulation framework. The presented study focuses upon a stochastic PDF-based model using the kinetics SRM suite, an application that has obtained increasing attention from academics and industry alike due to its capabilities to correlate combustion characteristics and emissions concentrations with experimental data [21 – 28]. The model is solved by theoretically breaking down the combustion into a user-defined number of stochastic particles that statistically represent the probability distribution function of the in-cylinder mixture. Hence, each particle has its own mass, temperature, and species concentrations. For each stochastic particle the software solves the fuel injection, the chemical kinetics, turbulent mixing, piston movement, and heat transfer processes. Generally, it can be said that increasing the number of stochastic particles, increases the resolution of the solution, but also the computational time needed for the tasks.

The kinetics SRM suite is a stochastic PDF-based closed volume engine cycle, meaning that the PDF initiates from the closing of the intake valves and terminates at the opening of the exhaust valves. The closed engine volume is divided into an equally size timescale. The code follows the thermodynamic modelling analysis, where the energy equation progresses with every time step. There are two zones, burnt and unburnt, each modelled based on a PDF with the number of stochastic particles set by the user. A Monte Carlo technique with second-order operator splitting solves the system equations for every time step, moving the properties of the stochastic particles from the

unburnt gas zone to the burnt gas zone according to the progression of the PDF.

The cylinder pressure is calculated based on the ideal gas law where the instant pressure equals the product of the gas molecules number, gas universal constant, and temperature over the cylinder instant volume. One can visualise it as the pressure of the gas inside the cylinder pushing the piston downwards, hence increasing the volume of the cylinder. Work is defined as force multiplied by displacement. Work is done by the gas signifying a change in energy. As the gas energy is increase, the amount of work on the cylinder increases. In an ideal gas all the internal energy of its molecules is in the form of motion, kinetic energy, and hence any alteration causes a change in temperature. To sum up:

- pressure is inversely proportional to the cylinder volume, meaning that higher volume equals lower pressure;
- pressure is directly proportional to the temperature, or higher temperature equals higher pressure;
- volume is directly proportional to temperature, hence a higher volume will give higher temperature.

The cylinder pressure is assumed to be homogeneous and the local quantities of mass fractions, temperatures, etc. are dealt with as random variables of the probability density function. The position of the piston alters the cylinder volume resulting in compression or expansion of the gas and the change of pressure.

The flame ignition process is modelled using a Wiebe function [146, 63]. As the flame propagates along the combustion chamber, chemical reactions and heat release processes occurring between the particles of the unburned and burned zones. Due to the stochastic particles within the two gas zones having different properties, a pressure correction procedure is also needed to equalise the particles' pressure. This is done by performing an isentropic compression or expansion to a value. The total volume of all particles has to be equal the total cylinder volume. With every pressure correction, temperature and density of all the particles are updated.

Furthermore, the default iso-octane n-heptane mechanism is used. The properties of the specific mechanism are registered to CMCL Innovation and is not disclosed [18, 257]. The chemistry mechanism describes the complex interaction between the chemical species, promoting critical combustion related processes to be analysed. Such studies may be focusing on combustion profiling, ignition, flame propagation, knocking, multiple direct injection, or emissions formation [22, 24, 25, 27, 258, 223, 259].

As mention before, the kinetics SRM suite has been successfully employed in a number of earlier studies with the engine experimental data collected from port fuel injected HCCI [260], single early direct injection HCCI [22] and dual injection HCCI engines [21]. In addition, analysis of natural gas fuelled [23], hydrogen-rich gas [25], and different fuel blends [24] on HCCI engines have been examined using the software. The kinetics SRM suite has also been coupled to the computational fluid dynamics code KIVA for studying the influence of direct injection on a PCCI engine [11] and implemented with a single-dimensional fluid dynamics tool for the in-cylinder stratification investigation of a direct injection diesel engine [28].

However, through the literature review completed, it has been found that far too little attention has been paid to evaluate the kinetics SRM suite against experimental data from gasoline direct injection spark ignited engines. Further experimental investigations on this type of engines are needed due to their worldwide popularity and application. One of the research objectives is to investigate how well the kinetics SRM suite can predict the experimental data collected from a modern spark ignited gasoline direct injection engine.

3.3 Engine Simulation Technology

3.3.1 Introduction to Engine Control and Mapping

The engine control unit is designed to monitor, through sensors, and manage, through actuators, the operating state of the engine. The unit operates in a closed continuous loop, as seen in Figure 3.12:

- Input signals are received from various sensors placed in the engine powertrain;

- Information is processed and based on a program (more commonly known as engine map) saved on its internal memory the unit switches to the appropriate operating conditions algorithm;
- With reference the operating setup mode, for example, hard acceleration, signals are provided to the actuators to change their settings accordingly;
- Process is repeated.

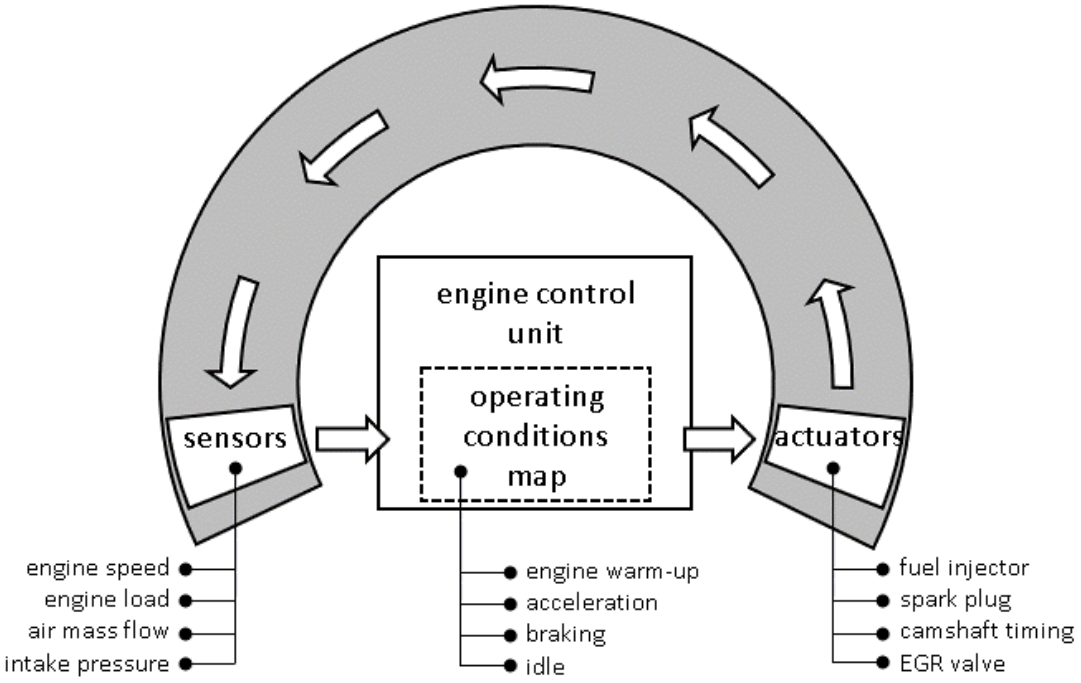

Figure 3.12: Engine control unit closed loop operation

The manufacturer needs to constantly satisfy the emissions limits and at the same time to meet customer requirements for performance, drivability and efficiency [261]. Moreover, to the fact that the engine is controlled by intelligent actuator modules makes the whole process produce non-linear and variable responses [262]. For instance, such actuator modules are the valve timing/lifting, the multi-tasked injection system and the exhaust aftertreatment set up. An engineer simply cannot advance one actuator setting without adjusting one (or a range of) the remaining actuators.

Taking for example the injection system; if the engine is supplied with a rich mixture the output is better performance, but also fuel consumption and exhaust emissions become higher [63]. The extra fuel causes instability to the

operation of the after treatment system and also more unwanted noise is produced from the engine. Another case is valve timing; having the exhaust valves open before bottom dead centre and close just after top dead centre causes the engine to lose a small percentage of power, but at the same time this timing helps the piston to clean the cylinder from the by-product gas [88]. Ultimately as more and more factors are involved into the engine tuning process, so the engine optimisation gets more complicated. The optimisation complexity of the system is combined with the need for shorter development times to produce an exceedingly demanding challenge [128].

In order to increase the practicality and efficiency of engine testing, powerful software tools are constantly being developed to assist with the task of mapping the engine. Engine mapping is defined as the process carried out with the aim of deriving an empirical model of how an engine powertrain with certain characteristics behaves [1]. Once a viable engine model is developed there are three in-loop testing techniques that can be applied; hardware- [263, 264], software- [265, 266, 267] and model-in- loop.

In-loop testing is basically the representation of an engine's subsystem, such as the combustion chamber, in a simulated environment. This testing scheme is essentially a loop constructed by the inputs, the system under test and the outputs. The simulation supplies the system under testing with the inputs, and it then processes the signals and produce the outputs [268]. Hardware-in-Loop (HiL) aids the evaluation of control strategies implemented on a real electronic control unit for testing and validation phases. Software-in-Loop (SiL) allows testing of the control strategies through the use of a software model in a virtual real-time environment. Model-in-Loop (MiL) simulates the entire engine system environment [269], like for instance by using an engine model and an ECU model with its control strategy [270, 271].

3.3.2 Outline of Experimental Design Techniques

With increasing engine complexity, the number of controllable variables and test time are growing exponentially [272]. To a great extent, engine mapping and testing are constructed on statistical experimental design and flexible hierarchical modelling techniques. Experimental Design or Design of

Experiments (DoE) in general is defined as the strategy of planning how controlled measurements are going to be recorded during an experimental process [273].

DoE is an answer to the question of how the optimum combination of actuator settings can be reached, in order to get the best fuel economy, lowest emissions, and maximum engine performance with the fewer experiments as possible [274]. This strategy combines test designs and methods for measuring a predetermined part of the experiment to create a statistical model that matches the experimental measurements as closely as possible [275]. By identifying the most effective points for testing the actuators of the engine DoE significantly reduces the experimental effort, time, and cost. The approach is mainly divided into three design categories that the experiment is based on; classical, optimal and space filling [276]. Essentially how the experiment design is set up depends on the objectives of the system and the number of factors to be investigated.

3.3.2.1 Classical Designs

The standard way of mapping the engine is by applying the single factor optimisation technique [277]. The method starts with all factors kept to a constant, except one that is allowed to move from its minimum to its maximum, presenting in this way its optimum value. This method may appear a straight forward process, but causes a geometric growth in the number of experiments [278]. Moreover, due to the principle that this technique follows, altering and optimising one factor at a time, the path to find the optimum solution is bypassed by the different starting points of the “optimum” factor values. An alternative to single factorisation is the full factorial optimisation technique [279]. The experimental process is carried on by examining both the influence of each factor on the output and also the influence generated between each factor [280]. Again, this is not suitable for engine mapping, the reason being is the huge number of experimental measurements needed to achieve a full test grid [281].

Another classical design option is the Box-Behnken layout (Figure 3.13), which spreads the testing points equally, following a spherical path with one point at the centre of each edge of the space and a single point at its core [282]. This layout can only deal with variables that have three levels – high, centre and low – for reaching the optimum. Up to three factors, the design requires relatively few numbers of runs, but if the number of factors increases more, then a Box-Bahnken design becomes unsuitable [283].

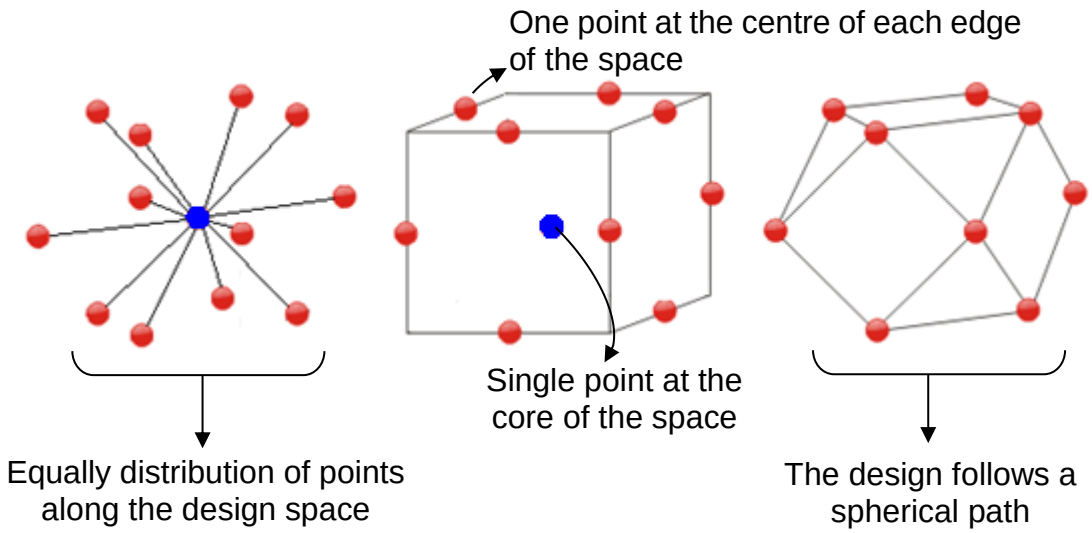

Figure 3.13: Box-Behnken design

Presented by Raymond and Montgomery (2002) a more advanced design layout is the central composite (Figure 3.14) that uses corner points and either faces points (three-level factors) or extended points (five-level factors). This design requires variables to be set out of their range and as the number of factors increase, so its efficiency drops.

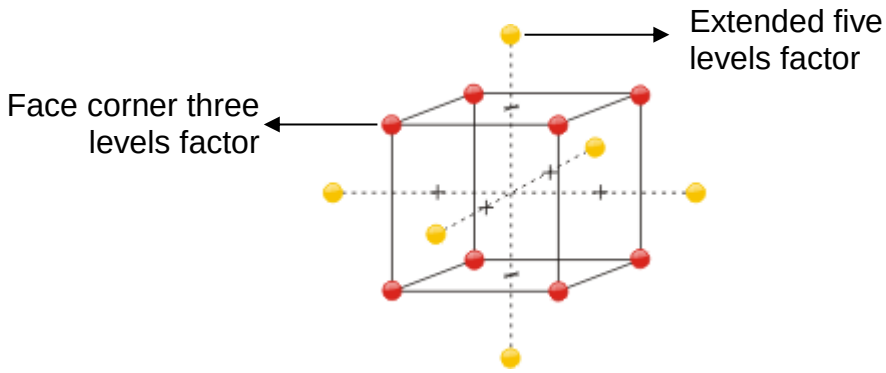

Figure 3.14: Central composite design

Plackett and Burman constructed a design that is useful for identification of the important factors that influence a model with the fewest possible runs [284]. For instance, a Plackett-Burman design for up to 11 factors requires 12 runs. The weakness of this design is that it cannot define the relation between the factors interactions. Regular Simplex (Figure 3.15) is a different layout that takes the highest point derived from a triangular shape [285]. The shape of the simplex design is generated by the number of factors; for two factors a simplex is a triangle, for three factors it is a tetrahedron, for four factors it is a pentachoron, and so on. This design is able to determine which process variables (or factors) influence some characteristics of the product. Simplex designs take as granted that no interactions exist between the factors of interest [286].

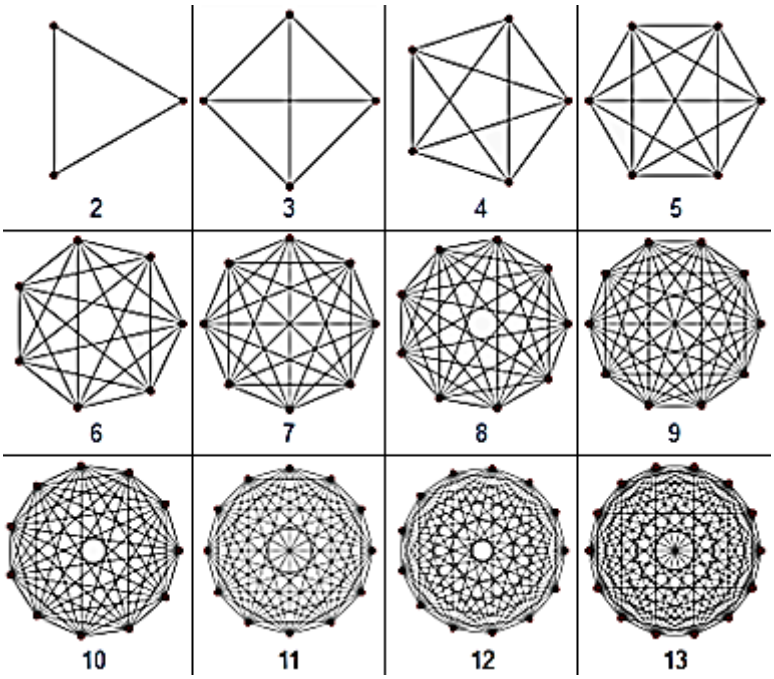

Figure 3.15: Regular simplex design with different number of factors [287]

3.3.2.2 Optimal Designs

Some classical designs may reach the desirable objective, but only with a much higher quantity of test runs than an optimal design [288]. Moreover, optimal designs counteract the disability of non-optimal to handle multiple types (primary and secondary influence on the output) and number of factors

[289]. The optimality of such a layout is based on an “information matrix” approximation within a constrained design space. Thus, the limitation of the experiment must be identified in order to continue with an optimal design. There are several optimal designs with the most significant for this case study to be A, D and V-Optimality [290]. As mention above the optimality type has as its foundation a statistical matrix and how the information of that matrix will be manipulated. As is illustrated in Figure 3.16, A-Optimal design finds the inverse of the information matrix and based on that is reducing the sum of the diagonal terms. The outcome is the decrease of the mean difference between the estimations of the design’s coefficients.

$$information\ matrix\ inverse = \begin{bmatrix} -2 & 2 & -4 \\ -1 & 1 & 3 \\ 2 & 0 & -1 \end{bmatrix}$$

$$sum\ of\ diagonal\ terms = (-2) + (1) + (-1) = -2$$

Figure 3.16: A-Optimal design statistical matrix calculations

Alternatively, D-Optimality uses the determinant of the matrix to increase the estimation and V-Optimal designs are trying to find the minimum of the mean difference of a number of particular points [291]. As Figure 3.17 shows, D and V optimal designs can be straightforward compared in terms of how their points are scattered in the design space. The test points for D-Optimality are placed in most of the time on the limits of the space, whereas V-Optimality points are commonly surrounded by the boundaries of the design space.

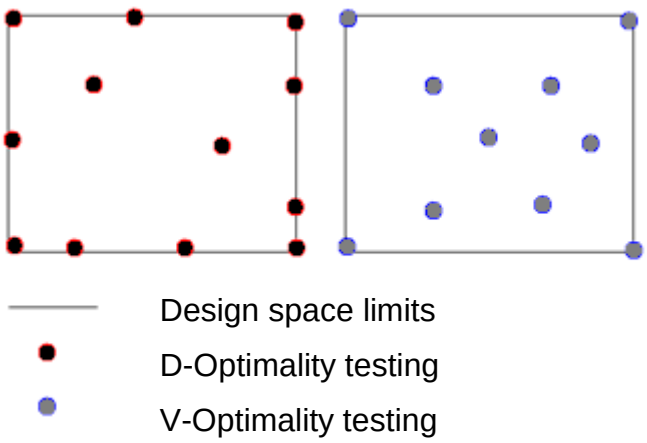

Figure 3.17: D and V Optimal designs

3.3.2.3 Space-filling designs

Space-filling designs are scattering the testing points equally throughout the experimental space [292]. A Latin square can be described as an a×a array packed with non-similar figures in each row and in each column. An example is a 3×3 square with the figures 1, 2 and 3. Hence the first row will be 1-2-3, the second row 3-1-2, and lastly 2-3-1 as the third row (see Figure 3.18).

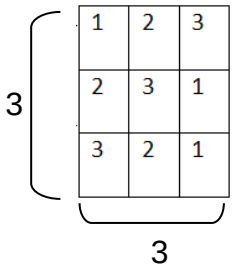

Figure 3.18: Latin cube with unique figures in each row and column

First described by McKay (1979) Latin Hypercube sampling (LHS) is developed by an equal number of Latin squares on each dimension, but with each integer to be unique on each column of the hypercube. Figure 3.19 gives an idea of how a LHS is constructed. By showing the Hypercube as a two-dimensional side projection it is obvious that each point is unique in the vertical axis. The size of the interval section of the hypercube determines how many experiments will take place [293].

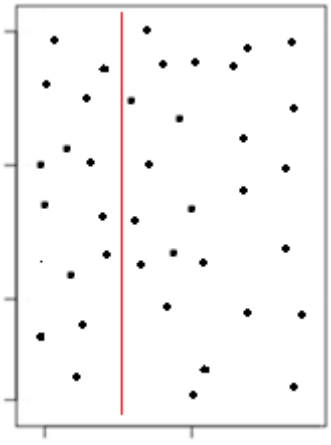

Figure 3.19: Each point is unique in the vertical axis of the Latin Hypercube

Halton (1964) generated a sequence to place the testing points in deterministic positions. Prime numbers (ex. 2,3,7,9,11,13,17,19, etc.) act as the base of the sequence and divides the unit interval (from 0 to 1). For

example, if the base is the prime number 3 then the interval splits up into 3 equivalent spaced parts (see Figure 3.20).

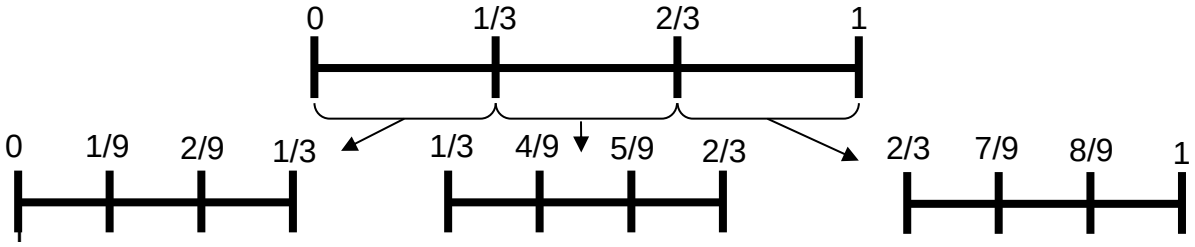

Figure 3.20: Halton sequence divides the interval in terms of the base number

The first two figures of the Halton sequence are therefore 1/3 and 2/3. The procedure continues by breaking each part of the previous interval into 3 equal spaced parts and so on [294]. Hence, the Halton sequence for number 3 becomes: 1/3, 2/3, 1/9, 4/9, 7/9, 2/9, 5/9, 8/9, etc. In low dimensional problems Halton sequences are excellent for handling the design, but problems are introduced when the number of primes increases [297]. A sample of a Halton sequences design is presented in Figure 3.21.

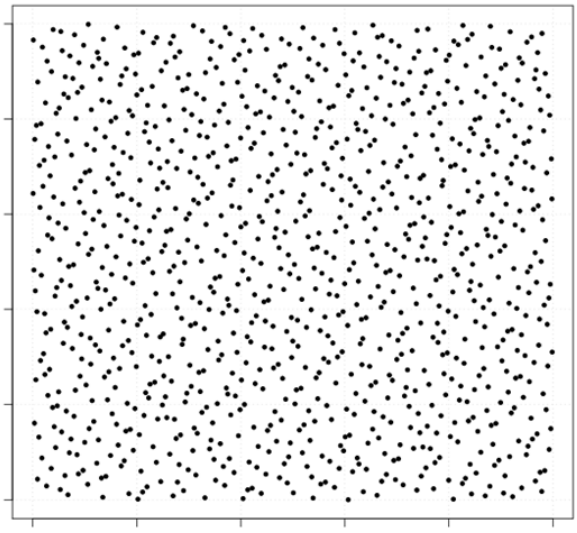

Figure 3.21: Halton sequences design [295]

Nevertheless, originally introduced by Yates (1936), Lattice designs are equally coordinating the points in the space between the intervals (0 to 1) in a triangular grid [296]. For 3 factors (m=3) the Lattice design splits the interval up as 0, 1/m, 2/m and 1 or in this case; 0, ⅓, ⅔ and 1. Then all possible arrangements of the coordinates are used and a 3×3 design will be

constructed, resulting in 10 design runs. As the factor's level increases the complexity of the design grows and the estimation fades [297]. Figure 3.22 demonstrates a Lattice design with three factors and starting from the left the experiment runs on 3 levels, then 4 levels and finally 5 levels.

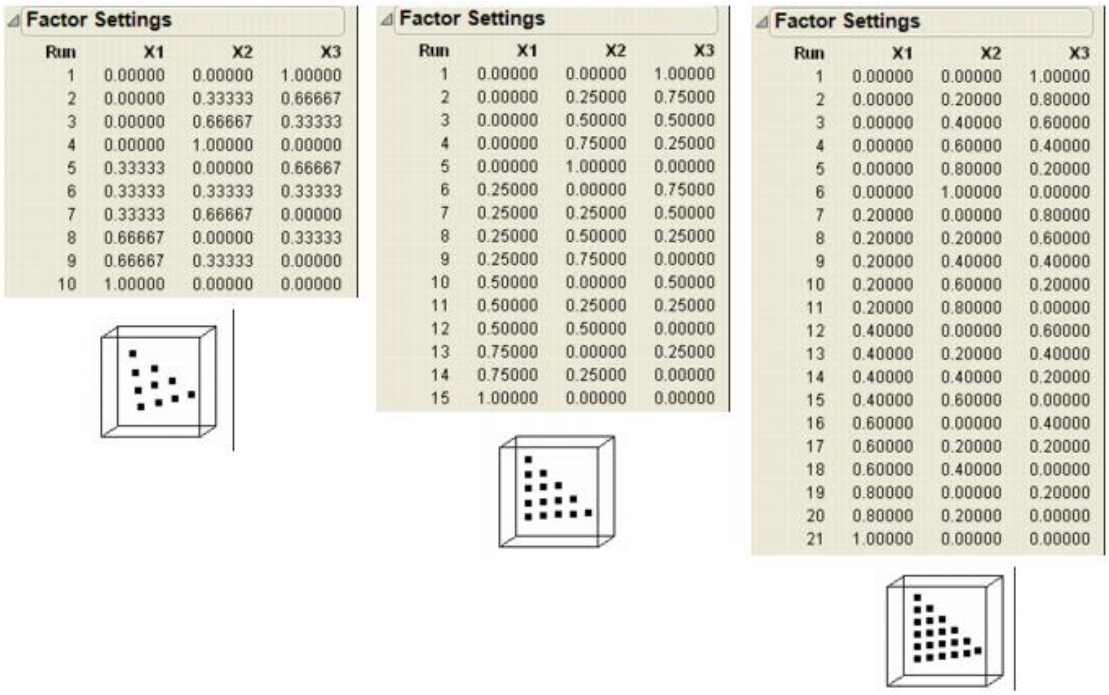

Factor Settings

Run	X1	X2	X3
1	0.00000	0.00000	1.00000
2	0.00000	0.33333	0.66667
3	0.00000	0.66667	0.33333
4	0.00000	1.00000	0.00000
5	0.33333	0.00000	0.66667
6	0.33333	0.33333	0.33333
7	0.33333	0.66667	0.00000
8	0.66667	0.00000	0.33333
9	0.66667	0.33333	0.00000
10	1.00000	0.00000	0.00000

Factor Settings

Run	X1	X2	X3
1	0.00000	0.00000	1.00000
2	0.00000	0.25000	0.75000
3	0.00000	0.50000	0.50000
4	0.00000	0.75000	0.25000
5	0.00000	1.00000	0.00000
6	0.25000	0.00000	0.75000
7	0.25000	0.25000	0.50000
8	0.25000	0.50000	0.25000
9	0.25000	0.75000	0.00000
10	0.50000	0.00000	0.50000
11	0.50000	0.25000	0.25000
12	0.50000	0.50000	0.00000
13	0.75000	0.00000	0.25000
14	0.75000	0.25000	0.00000
15	1.00000	0.00000	0.00000

Factor Settings

Run	X1	X2	X3
1	0.00000	0.00000	1.00000
2	0.00000	0.20000	0.80000
3	0.00000	0.40000	0.60000
4	0.00000	0.60000	0.40000
5	0.00000	0.80000	0.20000
6	0.00000	1.00000	0.00000
7	0.20000	0.00000	0.80000
8	0.20000	0.20000	0.60000
9	0.20000	0.40000	0.40000
10	0.20000	0.60000	0.20000
11	0.20000	0.80000	0.00000
12	0.40000	0.00000	0.60000
13	0.40000	0.20000	0.40000
14	0.40000	0.40000	0.20000
15	0.40000	0.60000	0.00000
16	0.60000	0.00000	0.40000
17	0.60000	0.20000	0.20000
18	0.60000	0.40000	0.00000
19	0.80000	0.00000	0.20000
20	0.80000	0.20000	0.00000
21	1.00000	0.00000	0.00000

Figure 3.22: Lattice design with three factors and three (left), four (middle) and five (right) levels [298]

Additionally, there is the Sobolov space-filling design (Figure 3.23) which is based on an algorithm for uniformly creating an ordered list of points [299]. The points of a Sobolov design have a unique position by avoiding each other. This design expands as the number of the input variables gets bigger. A maximum of 6 input factors is suited in order for this layout to be effective.

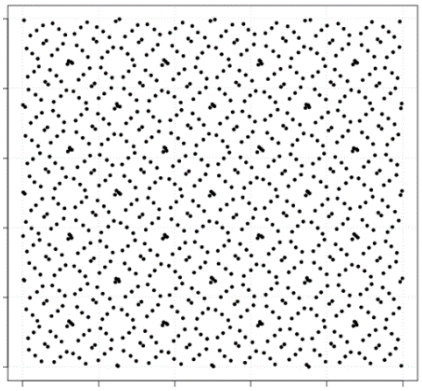

Figure 3.23: Sobolov design example [295]

3.3.2.4 DoE Summary

Discarding the classical design types due to their impracticality for modern engine applications there are space filling and optimal designs. The main difference between these two types is that space filling doesn't require any knowledge about how the input factors of the model affect the outcome [300]. This design layout can be applied for new engines to investigate their limitations and how they will behave. In contrast, optimal designs are an efficient layout when there is at least some knowledge of the operating system.

Moreover, a mix and match approach can be utilised. Starting with one design style and continuing to an entirely different style. For instance, an engineer could start with space filling to examine a new type of engine. As long as the relationship between inputs and outputs is established, an optimal design may come into play to test in detail the constrained space. Each type of design, either optimal or space filling is strongly dependent on the type of model to be used [283]. While an optimal design is best for polynomial models, a space filling is most suitable for radial basis function. Therefore, the type of the design not only relies on the number of factors but also on the model type.

3.4 Chapter Summary

Because of its availability of analysing internal components and logic, physical-based modelling provides a deep insight into a real system. Additionally, this type of mathematical modelling technique can be easily revised to simulate similar systems by means of changing the model structure or parameters [301]. In contrast, a behaviour-based model depends only on the system that is being trained as well as the operating range over which it has been identified. Even if such a model changes to simulate similar systems a considerable amount of trial and error testing is required.

The internal combustion engine system involves a combination of thermodynamics, kinematics and fluid dynamics processes occurring at the same time, and producing an accurate physical-based model to simulate such a system can be very time consuming. Nevertheless, it is still considered to

be an effective approach for engine modelling, especially when an analysis is performed to identify and validate the internal parameters of the system.

Moreover, due to the increase number of engine control variables, appropriate experimental designs aid the engine mapping procedure through efficient testing strategies.

4 Research Methodology

4.1 Introduction

The research aims to develop a model-based multi-physics framework of engine, emissions and aftertreatment. The work discussed in this thesis focuses in three aspects:

- Improving the current stochastic-based GDI combustion modelling process in kinetics SRM engine suite, in a way to deliver accurate engine-out emissions concentrations with the minimum possible simulation time
- Applying the kinetics SRM within the solver of GT-SUITE, aiming to advance even more the 1D code prediction capabilities
- Joining the engine – combustion model with a chemical reaction-based 1D exhaust aftertreatment model developed in Axisuite, aiming to construct a co-simulation framework covering the engine performance, combustion-formed emissions, and exhaust aftertreatment system efficiency

Moreover, the chapter is divided in two main sections:

- Section 4.2 presents a revision of the AJ133 V8 GDI engine case study, and
- Section 4.3 covers the mathematical theory behind the models as well as the simulation execution plan.

4.2 Engine Case Study

The engine system's parameters (e.g. valve timing, spark ignition, etc.), and outputs (e.g. in-cylinder pressure, temperatures, etc.) are based on the hot steady state data set of the AJ133 V8 GDI engine case study. Consisting the case study are two engine data sets. The first one, shown in Table 4.1: Engine speed – load points, involves a total of 6 engine speed (RPM) – load (Nm) points selected by the sponsoring company to represent the engine operating under the NEDC part load conditions. The second engine data set consists of 60 testing points at a single engine operating condition at 1250RPM and 125Nm with various control settings.

Table 4.1: Engine speed – load points

Speed [RPM] – Load [Nm] point	Number of testing points	Ignition timing range [CAD bTDC]	Injection timing range [CAD]	Inlet valves opening range [CAD aTDC]	Exhaust valves closing range [CAD aTDC]
700 – 28	8	37.5 – 51	290 – 335	32 – 50	15 – 50
1250 – 125	9	36 – 49.5	305 – 337	1.5 – 50	34 – 43
1500 – 41	7	47.25 – 60	305 – 313	24.5 – 49.75	8 – 30.5
1500 – 105	9	39.75 – 57	276 – 345	1.5 – 49.75	33 – 37.5
2000 – 81	10	37.5 – 63.75	289 – 347	1.75 – 49.75	10 – 41.5
2000 – 199	17	27 - 36	281 – 360	1.5 - 50	8 – 43.25

The engine case study starts by examining for each of the engine speed – load points, the engine control parameters, such as the ignition and valves timing, along with observations of the engine responses of interest (typically; emissions and fuel consumption). After the analysis of the engine control parameters and key responses, an experimental design is formed for steady state engine data collection on the engine dynamometer. Figure 4.1 summarises the model calibration process based on the engine case study.

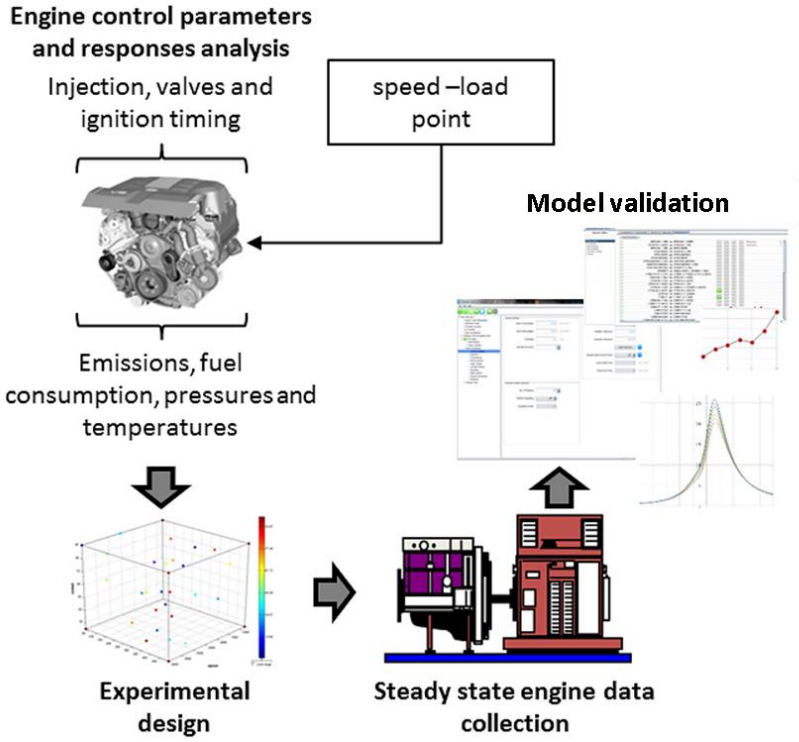

Figure 4.1: Methodology adopted for the steady state model based calibration process for the engine case study

As illustrated in Figure 4.2, the AJ133 V8 engine was coupled to a transient AC dynamometer at the powertrain testing facility located at the University of Bradford. The test type chosen was the “speed – torque” setup, meaning that the engine speed is controlled by adjusting the engine load through the throttle position. Ambient conditions of the engine were monitored but not controlled. Furthermore, the engine coolant was controlled at 90°C, while the fuel was supplied to the engine at 3 bar constant rate with its temperature maintained at 20°C. Fuel consumption was recorded using a Coriolis fuel mass flow meter sensor. A sampling rate of 1Hz was used for the engine test and data was recorded for 60 seconds for each testing point. The engine control unit was coupled with an ETAS-INCAS interface allowing the control of the engine parameters. In-cylinder pressures were gained via an AVL Indi-Smart system with cylinder pressure sensors. Exhaust emissions were sampled pre-catalyst from both banks and analysed using a HORIBA MEXA-9100 emissions bench. At the exhaust tailpipe a particulate sample line was placed allowing particulate sampling by an AVL condensation particle counter.

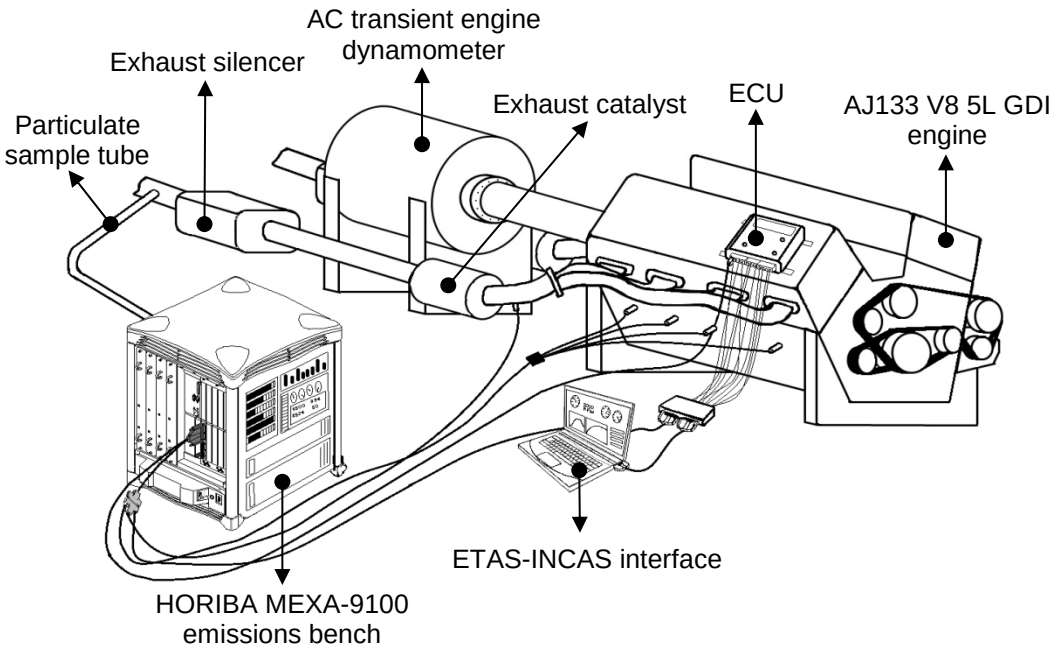

Figure 4.2: Schematic of the engine coupled to the dynamometer at the powertrain testing facility at the University of Bradford

4.3 Multi-Physics Simulation Platform Analysis

4.3.1 Kinetics SRM Emissions Model

The combustion and emissions analysis is carried out by the kinetics SRM Suite from CMCL Innovations, a software chosen by the sponsor company. There are a few software tools for emissions simulation and they can generally be divided into multi-dimensional fluid dynamics-based, such as KIVA [302] and AVL Fire [303], and detailed chemical kinetics-based, like CHEMKIN [304]. Although fluid dynamics-based tools can simulate the combustion products within the internal combustion engine in great detail, they need extremely computational power. Kinetics SRM suite significantly reduces the computational effort and simulation times compared to the multi-dimensional computational fluid dynamics approach, while delivering results of target accuracy [8]. Additionally, the kinetics SRM suite has the advantage over other detailed chemical kinetics-based tools due to its use of stochastic engine modelling techniques for more realistic combustion characteristics.

The software package is derived from a stable stochastic reactor model used for engine simulations [21, 26, 242]. Here, the term reactor describes the close engine cycle; the cylinder-related process happening from the closing of the intake valves until the opening of the exhaust valves. kinetics SRM suite is using a multidimensional probability density function and stochastic particles that move randomly through physical space due to particle convection and also through composition space due molecular mixing and reaction. The stochastic reactor model is applied to the closed volume of the engine cycle; from the opening of the inlet valves till the closing of the exhaust valves.

The model assumes statistical homogeneity, meaning that the probability density function is assumed to be the same throughout the engine cycle. The model calculates the evolution of the chemical species' mass fractions and the temperature as a function of time. The random scalar variables are combined into a single vector "ψ" whose distribution is given by the probability density function "$\mathrm{P}(\psi)$". The following sections describe the application of the stochastic reactor model for direct injection engine combustion and its solution for the closed volume in-cylinder mixing, crevice flow, heat transfer, pressure, fuel injection, flame propagation, and emissions formation.

4.3.1.1 Turbulent Mixing

A Localness Mixing Model (LMM) is applied in the kinetics SRM Suite to model the effect of turbulent flow mixing in the engine stochastic reactor. The mixing model is parameterised by a scalar mixing rate, defined in terms of a mixing time (τ_m). The mechanical-to-scalar timescale ratio, C_φ, is assigned as a user-defined input [305].

$$\tau_m = \frac{2\tau}{C_\varphi} \qquad \text{Equation 4.1}$$

The turbulence timescale (τ) is specified using an empirical k-ε turbulence model. Detailed k-ε turbulence models, as well as a user-defined turbulence models are additional options in kinetics SRM suite. The user-defined turbulence model requires turbulent mixing timescales during injection events using experimental or multi-dimensional numerical techniques. The detailed k-ε model simulates the evolution of the turbulent kinetic energy, including turbulence generation effects such as swirl and tumble.

However, for the current stage of the research, an empirical k-ε turbulence model is applied [63] in which the turbulence timescale is calculated as the turbulent kinetic energy (k) over the turbulence dissipation rate (ε). The turbulence dissipation rate is defined as the rate at which the turbulence kinetic energy is converted into thermal energy. The turbulent kinetic energy is approximated using the turbulence intensity along the length of the engine cylinder stroke (S) at a given engine speed (N).

$$k \approx \left[\frac{S \cdot N}{30}\right]^2 \qquad \text{Equation 4.2}$$

The cylinder stroke length is also used in the empirical calculation of the turbulence dissipation rate, along with the turbulence kinetic energy as:

$$\varepsilon \approx \frac{k^3}{0.1 \cdot S} \qquad \text{Equation 4.3}$$

Moreover, in order to be able to account for the physical proximity of the material that is being mixed, the LMM works by identifying neighbouring particles based on their proximity in composition space. The model is constrained such that mixing can only occur between neighbours, but an

intermittency is introduced to overcome the problem of particles remaining neighbours throughout the mixing process. The particles are designated as being in either a mixing or a non-mixing state, and are moved between states depending on a non-dimensional age property. Only particles in the mixing state are considered when identifying neighbouring particles. This causes the identities of the neighbouring particles to change discontinuously in time.

4.3.1.2 Crevice Flow

The model assumes that the pressure in the crevice volume equalises with the pressure in the cylinder during each time step by exchanging mass (Δm) between crevice and cylinder. The crevice gas is assumed to be homogeneous and its temperature is assumed to be the same as the wall temperature, which is kept constant throughout the simulation. The symbols m, n, P, R, T, and V denote the molecular mass, number of moles, pressure, ideal gas constant, temperature and volume respectively.

$$\Delta m = \frac{P_{cylinder} - P_{crevice}}{\frac{R \cdot T_{cylinder}}{V_{cylinder} \cdot m_{cylinder}} + \frac{R \cdot T_{crevice}}{V_{crevice} \cdot m_{crevice}}} \qquad \text{Equation 4.4}$$

After the exchange mass is calculated, the particle and crevice compositions, pressure, temperature, and mass are updated. Mass is only transferred between the crevice and some of the existing particles, the exchange particles, their number and the time they remain exchange particles are determined by a crevice time factor and mass factor. The mass factor is the fraction of the total cylinder mass that may exchange mass with the crevice at any one time. Exchange particles are selected randomly with a uniform distribution, until their total mass equals or exceeds the mass required. New exchange particles are chosen after a time that is determined by the crevice time factor and the mixing time.

4.3.1.3 Piston Movement

As illustrated in Figure 4.3, the effect of the piston reciprocating motion on the PDF is given in terms of crank angle degree, θ as [63]:

$$V(t) = V_c + \frac{\pi}{\alpha} b^2 \left(l + \alpha - \alpha cos(\theta) - \sqrt{l^2 - \alpha^2 cos^2(\theta)} \right) \qquad \text{Equation 4.5}$$

V_c is the clearance volume, b the engine bore, l the connecting rod length and α the ratio of l to the crank radius, r.

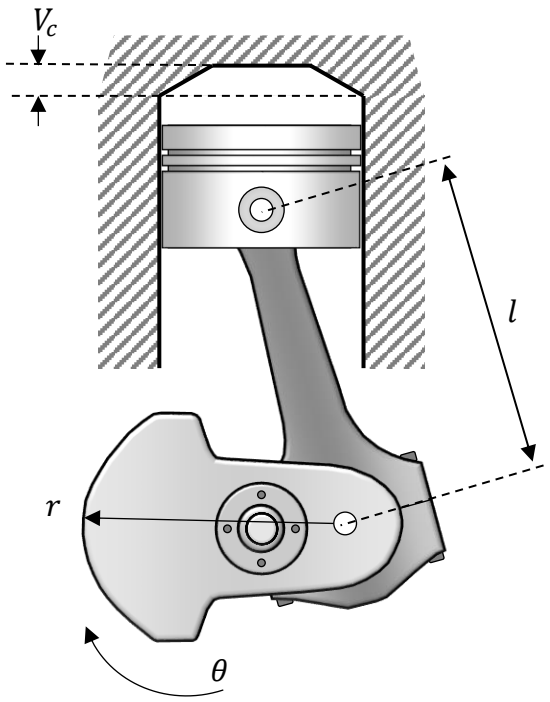

Figure 4.3: Simplified geometric layout of the piston position in terms of crank angle degree

4.3.1.4 Convective Heat Transfer

Heat transfer in the engine, between the cylinder charge and the walls, affects the combustion process. This results in a lower temperature boundary layer surrounding the hotter core. This temperature stratification alters the combustion phasing and duration. The heat transfer between the solid walls of the cylinder and the mass fluid motion is known as convection and is modelled by the finite difference method [306]. Additionally, a stochastic jump process is used [23] causing inhomogeneity in the temperature distribution, improving emissions and combustion duration predictions. Fluctuation is induced by parameter h^i and C_h is an input parameter in the model which changes the magnitude of the fluctuation over an exponentially distributed time step.

$$h^i = \left| \frac{T^i - T_w}{C_h} \right| \qquad \text{Equation 4.6}$$

The amount of heat transferred between the cylinder charge and the cylinder walls during each time step is modelled by the function $U(T)$.

$$U(T) = -\frac{C_{HT} \cdot h_c \cdot A}{c_v \cdot m}(T - T_w) \qquad \text{Equation 4.7}$$

h_c is the convective heat transfer coefficient of the process, A is the available heat transfer area and C_{HT} is the user defined heat transfer multiplier.

4.3.1.5 Pressure Equalisation

A change in pressure occurs in each stochastic particle, due to chemical reactions and heat transfer. Expansion and compression of fluid parcels will occur in the cylinder due to the equilibration of the pressure fluctuations. This is especially important in spark ignition combustion, as the hotter burned gases expand and compress the cooler unburned gases [307]. In Kinetics SRM engine suite it is assumed that a quasi-instantaneous pressure equilibration occurs through isentropic compression and expansion of the particles.

The specific heat capacity ratio, γ, is used to relate the pressure and volume of an ideal gas that undergoes an isentropic compression or expansion [63].

$$p_1^{(i)} \cdot {V_1^{(i)}}^{\gamma^{(i)}} = p_2^{(i)} \cdot {V_2^{(i)}}^{\gamma^{(i)}} \qquad \text{Equation 4.8}$$

$p_1^{(i)}$ and $V_1^{(i)}$ denote the pressure and volume of the i^{th} particle, respectively. The composition and temperature of each particle is used to calculate each particle's γ. The subscripts 1 and 2 denote the values before and after the equilibrium. There is no particle index on p_2 as all particles have the same pressure after equilibration. As the sum of the particle volumes must equal the total cylinder volume, V, the above equation can be manipulated to [305].

$$V = \sum_{i=1}^{N_{par}} V_1^{(i)} \left(\frac{p_1^{(i)}}{p_2}\right)^{1/\gamma^{(i)}} \qquad \text{Equation 4.9}$$

p_2 is the only unknown. The above equilibrated pressure is calculated using Newton's method [308]. The particle temperatures, T^i, are then updated by

$$T_2^{(i)} = T_1^{(i)} \left(\frac{p_1^{(i)}}{p_2} \right)^{1/\gamma^{(i)}-1}$$ Equation 4.10

The specific heat capacity ratio of each particle is determined by its composition and temperature before and after the equilibrium, with the sum of the particle volumes equal to the total cylinder volume [308].

4.3.1.6 Direct Fuel Injection

A physical model for direct injection with pre-defined parameters for droplet diameter, injection velocity, cone angle, effective evaporation rate, liquid temperature and the latent heat of evaporation can be used in the Kinetics SRM engine suite. For faster computational time the fuel for all the engine cases is assumed to be fully premixed at intake valve closing. Hence an equivalence ratio, Φ, for the complete oxidation of the hydrocarbon fuel is introduced to the engine simulations [305].

$$\Phi = \frac{4[C] + [H]}{2[O]}$$ Equation 4.11

C, H, and O denote the total molar concentrations of carbon, hydrogen, and oxygen respectively. The equivalence ratio is a passive scalar and hence is not affected by chemical reaction. This makes it suitable for studying exclusively the effects of mixing in a reacting flow.

4.3.1.7 Flame Propagation

The flame propagation simulation in Kinetics SRM suite can be modelled by the use of a multi-zone spark ignition sub-model. Since the combustion and heat release rates were known for this engine case study, a two-zone empirical Wiebe model was applied to represent in a functional form the mass fraction burned versus crank angle [146].

$$x_b = 1 - exp\left(-\alpha \left(\frac{\theta - \theta_o}{\Delta\theta} \right)^m \right)$$ Equation 4.12

θ is the crank angle, θ_o is the start of combustion set as the spark timing, $\Delta\theta$ is the total combustion duration (x_b = 0 to x_b = 1), and α and m are user adjustable parameters known as the anchor angle and Wiebe exponent, respectively. For this study a modified empirical Wiebe is used based on anchor angles, making the process of parameterising the Wiebe model easier.

Basically, the modified Wiebe model introduces the burned mass fuel fractions at anchor angle, start of combustion duration and end of combustion duration [63].

4.3.1.8 Gas-Phase Emissions

The chemical species and their corresponding thermochemistry data and reaction rates used in the simulation are defined by the adopted chemical kinetic mechanism or fuel model. The evolution of each chemical species is reported at each time-step for a global mass fraction, molar and mole fraction composition. In order to simulate gas-phase emissions it is important that the adopted chemical kinetic mechanism includes chemical species containing the specific gas-phase emissions atoms and a sufficiently accurate description of the emissions formation chemistry.

The mechanism applied in this project is the CMCL kinetics & SRM Engine Suite detailed chemical kinetics mechanism. It includes chemistry for the oxidation of n-heptane and iso-octane blends including detailed NO_x and soot formation pathways. It has been calibrated with engine applications in mind and has proven effective in simulating engine combustion in all operating modes for dozens of engines over hundreds of operating points [305]. Due to commercial sensitivity it cannot be viewed.

4.3.1.9 Particulate Matter Emissions

The mass within the cylinder is divided into a number of particles, which have a unique chemical composition, temperature and species concentration based on probability density functions. Figure 4.4**Error! Reference source not found.** presents a simple illustration of the cylinder mass distributed along a number of stochastic particles with properties defined by a probability density function. Again this part of the investigation is done by keeping all the parameters constant and only changing one variable at a time, for this case the number of stochastic particles.

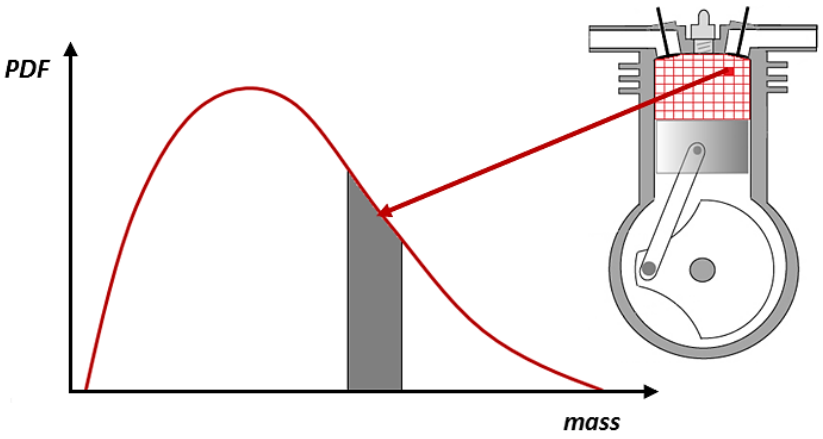

Figure 4.4: Cylinder mass divided into a number of stochastic particles with properties described by a probability density function

The Hiroyasu/Nagle and Strickland-Constable (H/N+SC) soot model is employed here as an empirical soot model. Soot is formed in the rich unburned-fuel regions of the injected fuel spray where the fuel vapours are heated by the combustion hot gases. Soot is then oxidised when it comes in contact with the unburned oxygen. Hence the concentration of soot is governed by the difference of the formation and oxidation of soot during the engine cycle [97]. The soot formation is determined based on the Hiroyasu model [309], whereas the oxidation of soot is computed using a Nagle and Strickland-Constable method [257].

The soot formation rate, m_{form}, is computed by assuming a first order reaction of vaporised fuel, m_{vf}. C_1 and C_2 are the user defined pre-exponential and exponential soot formation factors.

$$\frac{dm_{form}}{dt} = 150 \cdot C_1 \cdot m_{vf} \cdot exp\frac{-6290 \cdot C_2}{R \cdot T} \qquad \text{Equation 4.13}$$

The soot oxidation rate, $\mathrm{m_{oxid}}$, is predicted by assuming a reaction between soot and oxygen.

$$\frac{dm_{oxid}}{dt} = C_3 \cdot m_s \cdot w \cdot \frac{M_c}{\rho_s \cdot d_s} \qquad \text{Equation 4.14}$$

$\mathrm{C_3}$ is a user defined pre-exponential soot oxidation factor, M_c is the carbon molecular weight of 12 grams per mole for gasoline, ρ_s and d_s are the soot density and soot diameter defined as 2.0 g/cm^3 and 4.5E-7 cm [257]. The term

“w” is the net reaction rate of the following set of reactions, where the term C_4 is the user defined exponential soot oxidation factor and P_{ox} is the oxygen partial pressure in atmospheric pressure.

$$w = \frac{k_a \cdot P_{ox}}{1 + K_z \cdot P_{ox}} \cdot x + k_b \cdot P_{ox} \cdot (1 - x) \quad \text{Equation 4.15}$$

$$k_a = 20 \cdot \exp\left(\frac{-15100 \cdot C_4}{T}\right) \quad \text{Equation 4.16}$$

$$k_b = 4.46 \text{ x } 10^3 \cdot \exp\left(\frac{-7640 \cdot C_4}{T}\right) \quad \text{Equation 4.17}$$

$$k_t = 1.51 \text{ x } 10^5 \cdot \exp\left(\frac{-48800 \cdot C_4}{T}\right) \quad \text{Equation 4.18}$$

$$k_z = 20 \cdot \exp\left(\frac{-15100 \cdot C_4}{T}\right) \quad \text{Equation 4.19}$$

4.3.1.10 Numerical Solution

The probability density function transport equation is the sum of the chemical reaction, turbulent mixing, crevice flow, fuel injection, piston movement, and heat transfer process, and is solved using a Monte Carlo stochastic particle method [310]. An ensemble of stochastic particles makes up a statistical representation of the probability density function. To solve the probability density function equation, an operator splitting technique is employed so that each term can be treated separately [311].

The simulation starts at inlet valves closing with time equal to zero. Here the simulation time is defined in crank angle degrees, hence by the addition of every time-step the simulation moves a crank angle degree value away from the inlet valve closing event. Temperature, composition, and mass are regulated among the number of stochastic particles. The algorithm progress in time (or crank angle degree duration) by adding one time-step at a time, until it reaches the end of the simulation time (given by the opening of the exhaust valves). So, for example, if the simulation starts at -120 crank angle degrees after top dead center, with a time-step of 1 crank angle degree, then the system equation will be solved for -120, -119, -118, and so on, until reaching the crank angle degree at which the exhaust valves open.

With every time-step the algorithm also performs a cylinder volume change, due to the piston movement [63], as well as gas exchange between the cylinder bulk volume and the cylinder crevice volume. The operator then solves for the turbulent mixing, followed by the stochastic heat transfer and the chemistry step. A change in pressure occurs in each stochastic particle, due to chemical reactions and heat transfer, thus a pressure equilibration step adjusts the cylinder pressure. Finally, the direct injection even is performed and then the algorithm progress in time by the addition of another time-step and continues the loop.

4.3.2 GT-SUITE Engine Performance Model

GT-SUITE is the leading engine and vehicle simulation tool used by engine developers [312]. Even though the software is suitable for analysis of a wide range of issues related to the engine powertrain, this section presents only the engine performance simulation and the theory behind this specific module.

4.3.2.1 General Flow Solution

The solution of GT-SUITE is based on one-dimensional fluid dynamics, representing the flow and heat transfer in the piping and manifolds of the engine system. The flow dynamics involves the simultaneously solution of the conservation equations (3.2.2.2.1 General Fluid Dynamics Laws) in one dimension, which means that all quantities are average across the flow direction. The whole engine system is separated in components with each one being discretised in smaller volumes with constant fluid properties. As illustrated in Figure 4.5, each volume carries scalar variables like pressure, temperature, density, energy, etc. and the volumes are linked together by boundaries with vector variables (mass flux, velocity, etc.) calculated respectively.

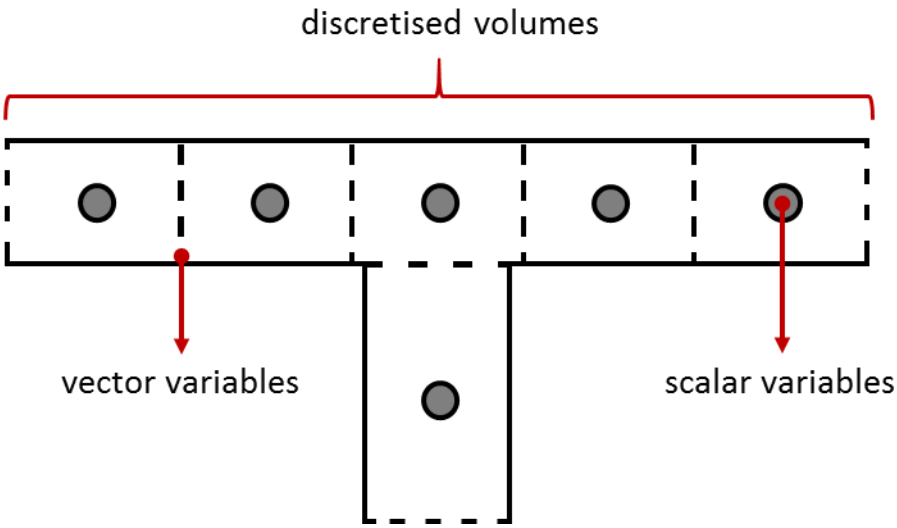

Figure 4.5: Schematic of the discretised volumes with scalars quantities at centroid and vector quantities at boundaries

The conservation equations solved by GT-SUITE are being given below. The equations of mass (Equation 4.20) and momentum (Equation 4.21) conservation are used to calculate the trapped air and residual masses of the system, as well as to determine the fuel dynamics and mass flow rates. Also using the implicit solution of the equation of energy (Equation 4.22), GT-SUITE ensures that energy is conserved through the whole system and computes the heat transfer from a volume to the walls or another volume.

$$\frac{dm}{dt} = \sum_{boundaries} \dot{m} \qquad \text{Equation 4.20}$$

$$\frac{d\dot{m}}{dt} = \frac{d\rho \cdot A + \sum_{boundaries}(\dot{m} \cdot u) - 4 \cdot C_f \cdot \frac{\rho \cdot u^2}{2} \cdot \frac{dx \cdot A}{D} - C_p \cdot \left(\frac{1}{2}\rho \cdot u^2\right) \cdot A}{dx} \qquad \text{Equation 4.21}$$

$$\frac{d(pHV)}{dt} = \sum_{boundaries}(\dot{m} \cdot H) + V \cdot \frac{dp}{dt} - h \cdot A_s \cdot \left(T_{fluid} - T_{wall}\right) \qquad \text{Equation 4.22}$$

Where:

$\dot{m}$	boundary mass flux into volume
V	Volume
p	Pressure

ρ	Density
A	cross section flow area
A_s	heat transfer surface area
H	total enthalpy
h	heat transfer coefficient
T_{fluid}	fluid temperature
T_{wall}	wall temperature
u	velocity at the boundary
C_f	skin friction coefficient
C_p	pressure loss coefficient
D	equivalent diameter
dp	pressure differential acting across the length of mass element in the flow direction

4.3.2.2 Engine Model Layout

The engine system is constructed based on objects in GT-SUITE that represents the actual components of the engine; like the air filter, throttle body, manifolds, piping, valves, fuel injectors, cylinders, etc. All the components of the model are linked together using connection lines to mirror the flow path. After the engine system is assembled each object needs to be discretised into small volumes. Figure 4.6 below shows the complete AJ133 V8 GDI engine performance model in GT-SUITE.

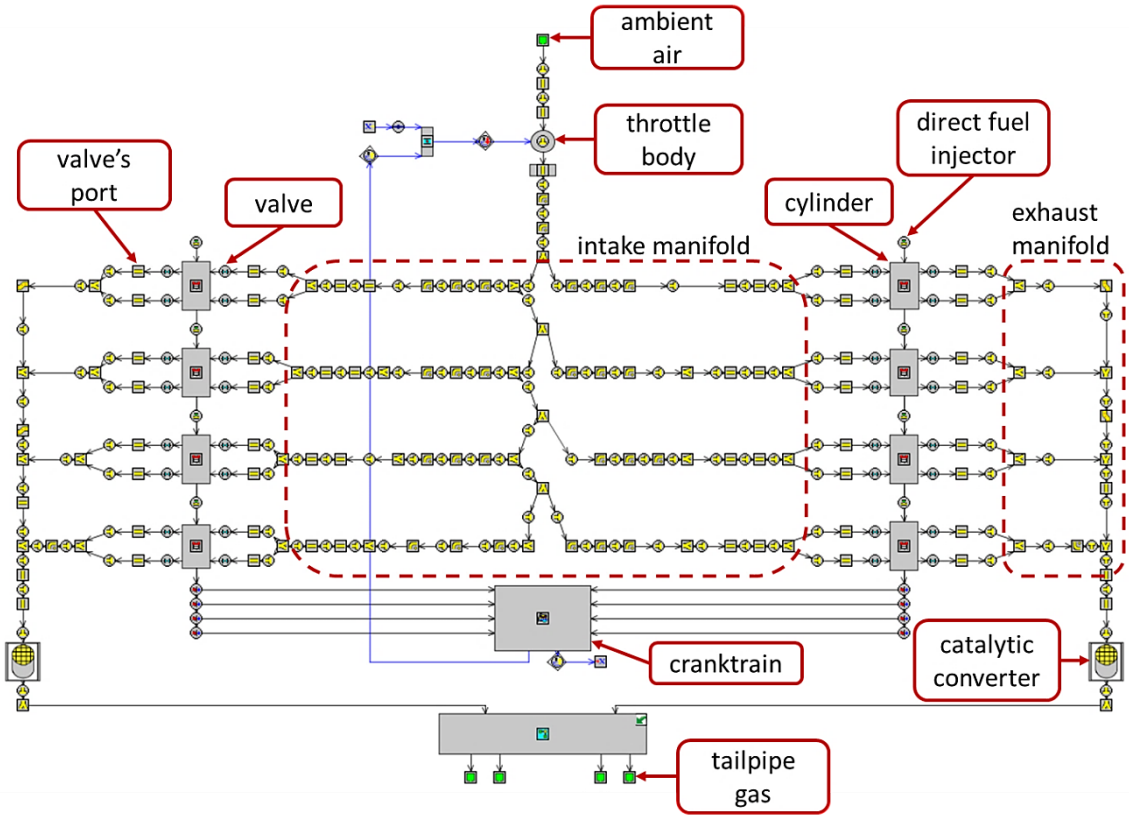

Figure 4.6: AJ133 V8 5Lt GDI naturally aspirated engine system in GT-SUITE

4.3.2.3 Ambient Air and Air Filter

The ambient air of the model is composed of 76.7% nitrogen and 23.3% oxygen, a standard air composition, with atmospheric pressure and temperature at 1 bar and 300K. This set of ambient conditions was applied to all the simulation cases. Moreover, the air filter has a substantial influence on intake system pressure drop and is therefore a vital part of the engine performance model. However, the levels of detail for the air filter sub-model needs to match the objectives of the simulation. Since the model will not be applied for intake acoustic analysis, a fairly simple but effective representation of the air filter was used. A single pipe object was applied to model the air filter volume with two orifices objects to represent the entering and exiting openings.

4.3.2.4 Throttle controller

The air passes through the air filter and through a set of piping its eventually going through the throttle blade. An orifice object was used to simulate the throttle blade with its geometry being controlled by the engine brake torque

and the engine speed signals provided by the engine cranktrain object. GT-SUITE determines the performance of the engine by calculating the brake torque for a user-defined speed. This is called speed mode and is suitable for steady state simulation. Experimentally it was found that the simulation times were significantly reduced using this approach because of the elimination of the relatively long period of time that is required for the crankshaft speed to reach steady state.

4.3.2.5 Intake and Exhaust Manifolds

The manifold systems are divided into numerous straight pipes, curved pipes, flow splits and orifices objects. The length of the pipes, inlet and outlet diameter, as well as surface roughness and wall temperature were defined. For the curved pipes the radius of curvature and curvature angle were additionally needed. Flow splits were characterised by a volume, surface roughness and temperature of the wall. When a pipe's diameter needed to change an orifice element was placed defined by a discharge coefficient and a diameter.

4.3.2.6 Cylinder Valves and Ports

The cylinder valves of the engine are being modelled using the "ValveCamConn" element with a user-defined valve lift profile as a function of crank angle, a valve reference diameter and the analogous flow characteristics (discharge coefficients). Based on these values the software determines the volumetric flow rate of the cylinder and any losses because of friction generate from the valves shape. The flow coefficient of the valve takes into account also any pressure losses caused by the port. The intake and exhaust ports of the engine's cylinder are being represented geometrically using a pipe element with a diameter the same as the valve's diameter.

4.3.2.7 Direct Fuel Injectors

An "InjConn" part is used to model direct injection into the cylinder. Specified by an injector delivery rate, air fuel ratio, injected fuel temperature, injection timing and a fuel properties set (heat of vaporisation, density, etc.) the injectors are connected directly to the engine's cylinders.

4.3.2.8 In-Cylinder Flow Combustion and Heat Transfer

The in-cylinder flow is modelled by several regions; the central core, the squish, the head recess, and the piston cup. Taking into consideration the cylinder geometry, piston motion and valves' flow rates, the simulation calculates for each of the flow regions its radial, axial and swirl velocities at each time step to determine the cylinder heat transfer properties. The heat transfer in the cylinder is defined by combining the in-cylinder heat transfer coefficients with the wall temperature of the cylinder head, cylinder walls and piston. A "flow" convective heat transfer coefficient model is applied for each combustion chamber surface including any spatial variation [313].

$$h_{c,surface} = \frac{1}{2} \cdot C_f \cdot \rho \cdot u_{eff,surface} \cdot C_p \cdot Pr^{-2/3} \qquad \text{Equation 4.23}$$

Where:

$h_{c,surface}$	convective heat transfer coefficient for each surface
C_f	skin friction coefficient
C_p	Gas specific heat capacity
Pr	Prandtl number
ρ	gas density
A_s	heat transfer surface area
$u_{eff,surface}$	effective velocity outside the boundary layer for each surface

Furthermore, the appropriate management of combustion within the engine model is critical to achieve a well calibrated model that is suitable for the simulation of engine performance. The most common approach is using the mass fraction burned, the ratio of the cumulative heat release to the total heat release. When the mass fraction burned is plotted against crank angle degrees, as seen in Figure 4.7, the curve can be described using a Wiebe function.

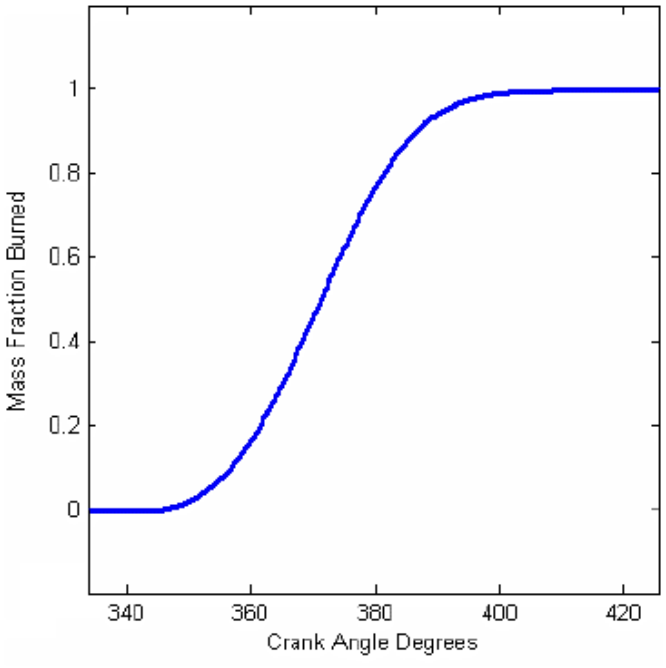

Figure 4.7: Representative Wiebe curve determined by the burned mass fraction across crank angle

Conventional engines are running on stable combustion characteristics; therefore, the coefficients of the Wiebe function could be assumed to be constant for all operating conditions. Even if the engine is running at high speeds the combustion process will take place more rapidly, but maintaining the constant burn rate with respect to crank angle. Suppose the engine load is increased then a larger quantity of air fuel mixture will be introduced to the cylinders, but the ratio of the mixture will be kept stoichiometric. Therefore, for a stable combustion with no auto-ignition or misfire, the properties of the mass fraction burn rate will remain the same. However, if the engine is equipped with a variable camshaft phasing, like the AJ133 engine under study, then the rate of the mass fraction burn will significantly be altered. The reason for this is that the flow patterns will change due to heavy valve overlap and residual exhaust gases combined with the fresh mixture charge, requiring a more complex set of coefficients for the Wiebe function. But then again the current testing stage of the AJ133 engine is running operating conditions at relatively low engine speeds (maximum engine speed at 2000 RPM) with the variable camshaft phasing mechanism not engaging.

4.3.3 Axisuite Exhaust Aftertreatment Model

The current development practise involves virtual testing using a detailed physical-chemical exhaust aftertreatment model developed in Axisuite. The software is based on a modular simulation platform covering the whole range of engine exhaust components, however only the main module used for the simulation of the catalyst, called Axicat, will be described below [314].

4.3.3.1 Channel Geometry

Axicat can perform multi-dimensional simulations, and including axisymmetric meshes. As shown in Figure 4.8 in a 1D mesh (axial coordinates) the catalytic converter geometry is divided into slices whereas in the 2D simulation (axial and radial coordinates) the front of the converter is also divided into ring-shaped sectors. The 3D mesh (axial, horizontal and vertical coordinates) is the most computationally costly but is able to model irregular geometries, making it ideal for concept designs. However, a 1D mesh was selected as a sufficient setup for the current stage of the research.

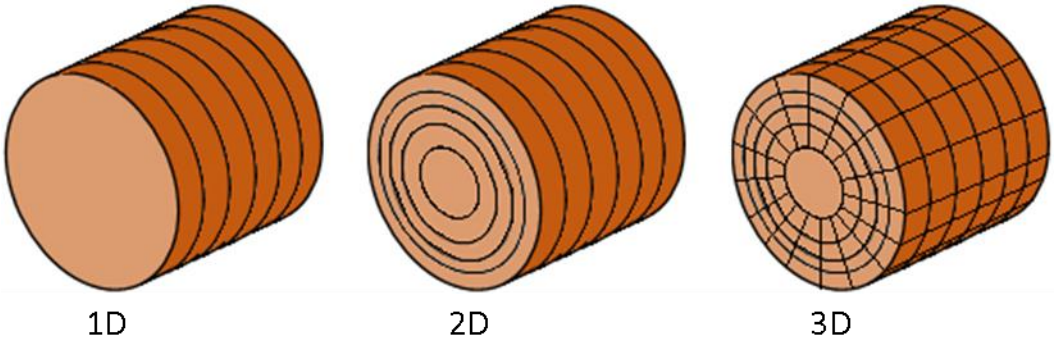

Figure 4.8: Examples of catalytic converter mesh design in Axitrap

As illustrated in Figure 4.9 the washcoat of the catalyst is assumed to be uniformly placed on the channel walls and based on the user-defined cell density, substrate thickness and washcoat thickness, the module will determine the basic geometrical properties of the channels [315]. The cell density and the wall thickness (w_w) will determine the uncoated channel diameter (d) of the channel, while its internal diameter (d_h) includes the washcoat thickness (w_c).

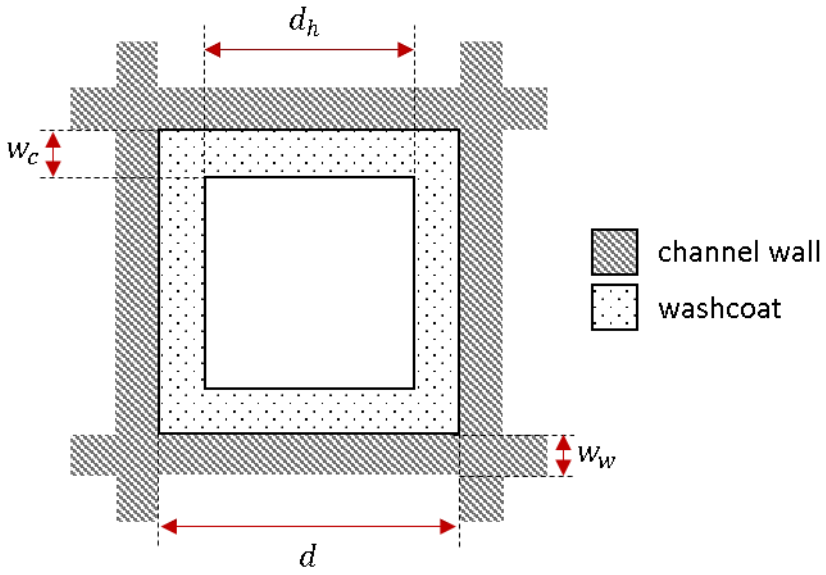

Figure 4.9: Basic geometrical properties of the catalyst's channel

4.3.3.2 Pressure-Drop

Axicat uses the conservation equations of mass and momentum to calculate the pressure drop of the flow through the catalyst (z direction). The pressure drop inside the channels $\left(\frac{dp}{dz}\right)$ is determined based on the correlation of Hagen-Poiseuille for laminar flow [316].

$$\frac{dp}{dz} = -\frac{28.5 \cdot \mu \cdot \dot{m}/\rho_g \cdot A_{monolith} \cdot \varepsilon}{{d_h}^2} \qquad \text{Equation 4.24}$$

Where

ε	void fraction of the coated monolith
$\dot{m}$	mass flow rate [kg/s]
μ	dynamic viscosity [Pa·S]
ρ_g	gas density [kg/m^3]
$A_{monolith}$	surface area of the monolith [m^2]
d_h	internal diameter of the channel [m]

Because of the smaller in diameter ends of the catalyst, a sudden contraction of the flow occurs at the inlet and a sudden expansion at the outlet. These pressure drop rates are modelled using the following formulas [317]

$$\Delta P_{contraction} = C_{exp}\left(1.1 - 0.4 \cdot \frac{{d_h}^2}{(d + w_w)^2}\right) \cdot \rho_g \cdot \left({\dot{m}}/{\rho_g \cdot A_{monolith} \cdot \varepsilon}\right)^2$$

Equation 4.25

$$\Delta P_{expansion} = C_{exp}\left(1 - \frac{{d_h}^2}{(d+w_w)^2}\right)^2 \cdot \frac{\rho_g \cdot \left({\dot{m}}/{\rho_g \cdot A_{monolith} \cdot \varepsilon}\right)^2}{2}$$

Equation 4.26

Where C_{exp} is a pressure drop multiplier adjusted by the user. Moreover, the pressure drop occurring inside the diffuser is calculated by the following formula. A diffuser coefficient (ζ) is introduced for the diffuser pressure drop rate, as well as, the inlet (A_{in}) and outlet (A_{out}) areas.

$$\Delta P_{diffuser} = \frac{\zeta}{2}\left(1 - \frac{A_{in}}{A_{out}}\right)^2 \cdot \frac{\dot{m}^2}{\rho_{in} \cdot A^2}$$

Equation 4.27

Acting as flow resistances, these pressure drop equations are modelling the path of the flow through the catalyst and the total pressure drop between the inlet and the outlet of the component (Figure 4.10).

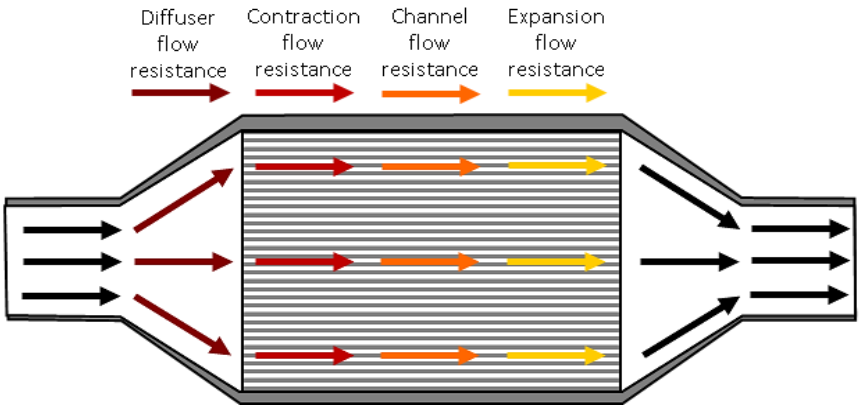

Figure 4.10: Flow distribution through the catalyst

4.3.3.3 Species balance

Axicat assumes the rate of species diffusion to be equal to the rate of chemical reaction; therefore, the species number is kept constant. Even though this assumption can represent steady-state operations, for transient conditions the module uses oxygen storage reaction schemes to account for the dynamic change of temperature and composition.

$$\dot{n_{i,j}} \cdot \left(y_{g,i,j}, y_{s,i,j}, T_{g,i}\right) = R_{i,j}\left(y_{S,i}, T_{S,i}\right) \qquad \text{Equation 4.28}$$

Where

$\dot{n}$	molecular flux [mol/m^{3}s]
y	molar fraction
T	temperature [K]
R	reaction rate [mol/m^{3}s]
i	spatial element index
j	species index
S	Solid
g	exhaust gas

The coupling between reaction and diffusion rates involved in the above equation is achieved by the intralayer reaction/mass transfer model; which simulates the mass transfer both in the gas phase and in the substrates/washcoat pores [318]. This model works by first determining the external mass transfer of the reactants from the channel flow to the channel surface. For the species in the washcoat and wall a coupled mass conservation and reaction equation is used [319].

$$-D_{w,j}\frac{d}{dw}\left(f_w\frac{dy_j}{dw}\right) = \frac{f_w}{c_m}\sum_k c_{j,k}R_k \qquad \text{Equation 4.29}$$

Where

$D_{w,j}$	effective diffusivity of species j in wall/washcoat pores [m^2/s]
f_w	geometric parameter (ratio of layer thickness to channel diameter)
c_m	molecular density of gas [mol/m^3]
R	reaction rate [mol/m^{3}s]
k	reaction index

The effective diffusivity is calculated based on the parallel pore model [320], as following.

$$\frac{1}{D_{w,j}} = \frac{\tau}{\varepsilon_{pore}}\left(\frac{1}{D_{mol}} - \frac{1}{D_{knud,j}}\right) \quad \text{Equation 4.30}$$

With the Knudsen diffusivity;

$$D_{knud,j} = \frac{d_{pore}}{3}\sqrt{\frac{8 \cdot Rc \cdot T}{\pi M_j}} \quad \text{Equation 4.31}$$

Where

d_{pore}	mean pore size [m]
M_j	molecular mass of species j [kg/mol]
τ	Tortuosity
ε_{pore}	Porosity
D_{mol}	molecular diffusivity of species j [m^2/s]
Rc	gas constant [j/mol K]

The convective mass transfer from the bulk gas to the washcoat/wall surface is computed based on the “film” approach with mass transfer coefficients $k_{i,j}$ corresponding to laminar channel flow.

$$\frac{d\left(v_g y_{g,j}\right)}{dz} = -k_j\left(\frac{S_F}{\varepsilon_{pore}}\right)\left(y_{g,j} - y_{S,j}\right) \quad \text{Equation 4.32}$$

$$\frac{d\left(v_g y_{1,j}\right)}{dz} = \frac{1}{d_h f_{-w}} k_{1,j}\left(y_{1s,j} - y_{1,j}\right) \quad \text{Equation 4.33}$$

Where

v_g	exhaust gas velocity [m/s]
k_j	mass transfer coefficient of species [m/s]

f_w	ratio of layer thickness to channel diameter
S_F	shape factor for heat conduction
subscript 1	conditions in the channel
subscript $1s$	conditions at gas/solid interface of the channel

The channel mass transfer coefficient for each species is given by;

$$k_j = \frac{Sh \cdot D_{mol,j}}{d_h} \qquad \text{Equation 4.34}$$

The molecular flow at the surface of the gas/solid interface in the channel is expressed as;

$$-D_j f_{-w_c} \frac{dy_i}{dw} \Big|_{1s} = -df_{-w_c}{}^2 \frac{d}{dz}\left(\nu_g y_{1,j}\right) \qquad \text{Equation 4.35}$$

4.3.3.4 Cone modelling

Axicat simulates the inlet and outlet cone of the catalyst as a 1D pipe with variable diameter along its length and constant thickness. As the exhaust gas is entering the cone, it exchanges heat with the cone wall by convection and the cone wall exchanges heat with its surroundings by convection and radiation. The convective heat transfer between the exhaust gas and the cone walls is calculated as;

$$H_{conv,in} = h \cdot \pi \cdot d_h \cdot d_z \cdot \left(T_g - T_s\right) \qquad \text{Equation 4.36}$$

Based on the Nusselt number, Axitrap computes the convection coefficient inside the cone.

$$h = \frac{Nu \cdot \lambda_g}{d_h}$$

As for the external convective heat transfer to ambient (h_{amb}) is given as;

$$H_{conv,out} = h_{amb} \cdot \pi \cdot (d_h + 2w_c) \cdot d_z \cdot (T_s - T_{amb}) \qquad \text{Equation 4.37}$$

The radiation heat losses ($H_{rad,losses}$) are determined by;

$$H_{rad,losses} = C_{rad} \cdot \varepsilon_{rad} \cdot \sigma \cdot \pi \cdot (d_h + 2w_c) \cdot d_z \cdot (T_s^4 - T_{amb}^4) \quad \text{Equation 4.38}$$

The energy balance equation for the exhaust gas is given by the following equation.

$$H_{conv,out} = h_{amb} \cdot \pi \cdot (d_h + 2w_c) \cdot d_z \cdot (T_s - T_{amb}) \quad \text{Equation 4.39}$$

Whereas a 1D heat conduction equation is describing the energy balance of the solid phase of the cone.

$$\rho_s \cdot C_{p,S} \cdot \frac{dT_s}{dT} = \lambda_{S,z} \cdot \frac{d^2T_s}{dz^2} + H_{conv,in} - H_{conv,out} - H_{rad,losses} \quad \text{Equation 4.40}$$

4.3.4 Simulation Framework Implementation Plan

MATLAB Simulink will be the fundamental environment for integrating the models and developing the optimisation co-simulation framework. The combustion and emissions formation model, designed in Kinetics SRM engine suite, will be implemented through a combustion template created in GT-SUITE. The template allows the engine performance model to be linked with the Kinetics SRM code. The engine performance model, with the build-in combustion and emissions model will be extracted as an S-Function block to the Simulink interface. Input signals for the main engine settings (like engine speed, ignition timing, etc.) will be connected to the GT-SUITE/kinetics SRM coupled model. The signals connected to the input port of the coupled model block will be transmitted to the GT-SUITE simulation.

During that period the Kinetics SRM code will take over for the combustion and compression strokes, generating the combustion characteristics and emissions concentrations. After that, GT-SUITE will complete the engine cycle and it will provide the output signals to the output port of the S-Function block. Moreover, the exhaust aftertreatment designed in Axisuite will be converted into Simulink S-Function and parameters blocks. Finally, the output signals of the GT-SUITE/Kinetics SRM part will be connected as input signals

of the Axisuite exhaust aftertreatment section completing the multi-physics co-simulation framework (Figure 4.11).

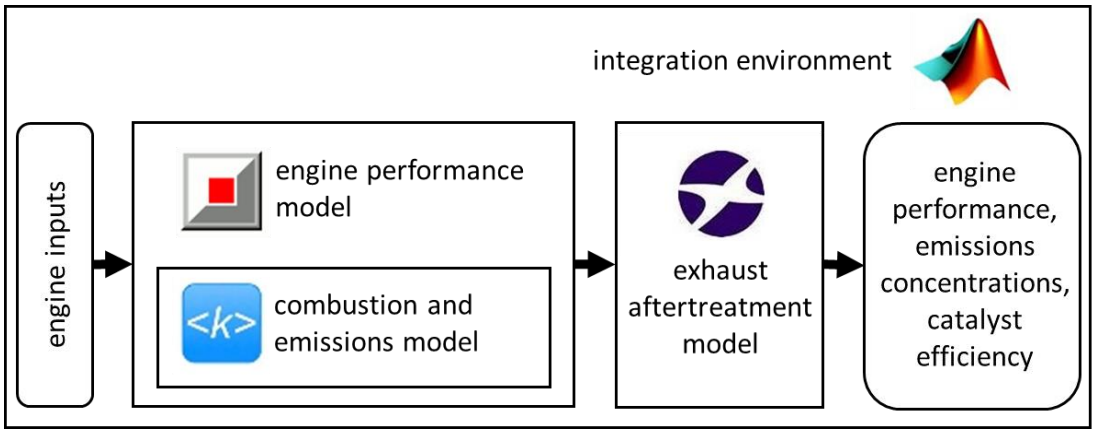

Figure 4.11: Multi-physics co-simulation framework schematic view

4.4 Chapter Summary

The chapter started by presenting the AJ133 V8 GDI engine case study, which is based on key steady-state engine speed – load points for a NEDC analysis. A summary of the engine testing setup and experimental methodology are also given. Next, the chapter gives the mathematical theory behind each individual model and finally provides the implementation plan for the co-simulation framework.

5 Development of Chemical Kinetics Emissions Formation Model

5.1 Chapter Introduction

This chapter presents a detailed study of the emissions formation model development and validation process. The structure of the chapter is given in Table 5.1. Section 5.2 discusses the preliminary setup of the model, which includes the chemical mechanism chosen for the simulation, numerical solver, fuel composition, engine geometrical parameters, and simulation settings. An investigation of the emissions model initial setup parameters is given in section 5.3, while in section 5.4 a sensitivity analysis for the internal parameters of the heat transfer and turbulent mixing sub-models is performed to evaluate in detail the emissions formation model. After calibrating the model, a global validation based on the engine case study is done and described in section 5.5. Finally, in 5.6 a prediction capability test for one engine speed – load operating point is testing how well the emissions formation model can pick up the changes of the engine parameters.

Table 5.1: Organisation table of the chemical kinetics emissions formation model chapter

5.2	Preliminary Setup of the Model
5.3	Initial Conditions Analysis
5.4	Heat Transfer and Turbulent Mixing Analysis
5.5	Global Results and Validation
5.6	Evaluation of Simulation Prediction

5.2 Preliminary Setup of the Model

The parameterisation of the model involved the calibration of the predicted in-cylinder pressure profiles. The model was implemented to simulate 60 different test points run on the GDI engine, described in 4.2. The reaction mechanism selected was the internal CMCL mechanism n-Heptane/Iso-

Octane with detailed NOx and soot formation pathways, appropriated for gasoline spark ignition engine simulation. Table 5.2 shows a list of the available chemistry mechanisms in the Kinetics SRM engine suite software package.

Table 5.2: Internal chemistry mechanisms in Kinetics SRM engine suite

Kinetics SRM suite Internal Mechanisms
Reduced Diesel with NOx
h-Heptane/Iso-Octane with NOx & Soot
Dual-Fuel (natural gas/diesel) oxidation with NOx
Toluene/i-octane/n-heptane/ethanol inc. soot/NOx
Detailed gasoline mechanism
Dual NG Diesel mechanism
Ethanol mechanism
H2 mechanism
Methane mechanism
Multi-Fuel mechanism
N Heptane mechanism
Propane mechanism
Toluene mechanism
TRF mechanism

Once the chemistry mechanism was defined, the simulation timing was set based on the valves timing. The intake valves closing time, in terms of crank angle degrees after top dead centre, initialises the simulation, while, the end of simulation is specified as the opening of the exhaust valves in crank angle degrees after top dead centre. A single engine simulation cycle was chosen to be sufficient for the current stage of the research. Kinetics SRM engine suite offers the choice of two numerical solvers, which are used to integrate the equations that describe the processes occurring on each stochastic particle. The chemistry solver-2 is used here due to the fact that the spark ignition engine setup has a number of species greater than 750. The chemistry solver-1 is usually used for simpler surrogate fuels. The number of stochastic particles was initially set to 100, as recommended [305].

Next, in the geometry branch the engine geometric settings [321] were set as given in Table 5.3. Engine speed changes according to the engine operating conditions of each testing case. Moreover, initial conditions like pressure and temperature at inlet valves closing were set to be exactly the same as with

the engine experiment for a more real-world simulation. The fuel is modelled as being composed of 95% iso-octane I-C8H18 and 5% h-heptane N-C7H16, which corresponds to an octane number of 95. The oxidiser is composed by N_2 and O_2 with mass fraction 0.7676 and 0.2324 respectively.

Table 5.3: Engine geometric settings [321]

Parameter	Value	Units
No. of cylinders	8	-
Bore	92.5	Mm
Stroke	93	Mm
Connection rod length	151.75	Mm
Wrist pin offset	1.1	Mm
Compression ratio	11.5	Mm
Crevice volume	4.5	%
Pent roof angle	148.1	deg
Piston bowl radius	40.875	mm
Piston bowl depth	-2.39	mm
Location of spark	2.94	mm
Total intake valve area	907.92	mm^2
Max inlet valve lift	5.5	mm
Blowby ring gap	-0.02	mm

Even though the software is able to simulate single and multiple injection events, it has been verified after closer examination of the software that any direct injection event before the closing of the intake valves cannot be taken into account in the calculations. Since all the available engine data have the direct injection occurring during the intake stroke, the current investigation is being limited and the system will not be able to directly investigate the influence of the direct injection on the combustion. A quick comparison between a Kinetics SRM simulation of a spark ignition engine example with and without direct injection showed an average of 230% reduction in computational time in minutes when the model is running with direct injection off. Despite the fact of not having a direct fuel injection in the system, an equivalence fuel/air ratio has been set to 1.0, meaning that the air fuel mixture is fully premixed during the intake stroke.

Average surface temperature for piston top, cylinder head and cylinder liner were all set to a typical 400K [148] since their effect on the simulation outputs was minimal and further investigation was unnecessary. In the spark ignition

sub-model an empirical modified two-zone Wiebe was chosen for calibration of the in-cylinder pressure profile. Burned mass fuel fraction at anchor angle, start of combustion and at end of combustion duration where set to 0.5, 0.1 and 0.9 correspondingly. For the different operating conditions between each engine test, spark timing, anchor angle and combustion duration were set accordingly. In order to accelerate the calibration of the in-cylinder pressure profile of the model, the heat transfer, turbulent mixing and soot formation sub-models where switched off temporarily. Additionally, a low number of stochastic particles were used for the preliminary setup of the model.

5.3 Initial Conditions Analysis

An investigation of the Kinetics SRM engine suite's initial parameters was carried out to confirm the effect of the parameters on engine performance outputs and emission concentrations, as well as the variability of the stochastic-based model. The analysis is based on a single testing point at 2000RPM – 199Nm. This engine case was chosen because its got the highest speed and load value, in addition to the highest number of testing points from all the engine cases. By averaging all the parameters of this speed – load case, a single operating point with settings matching the average values was chosen. The model was set to run one engine cycle, with the engineering common sense conditions in Table 5.4 under investigation, while keeping all the parameters constant and only changing one variable at a time.

Table 5.4: Kinetics SRM engine suite initial conditions under investigation

Initial conditions	Minimum value	Maximum value	Step value
Initial pressure [bar]	0.35	1	0.05
Initial temperature [K]	300	400	5
Compression ratio [-]	9.5	12.5	0.5
Cylinder crevice volume [%]	3	5.5	0.5
Exhaust gas recirculation [-]	0	1.4	0.2
Combustion profile: ➢ a parameter [-] ➢ Wiebe duration [-] ➢ m parameter [-]	 ➢ 1 ➢ 2 ➢ 1	 ➢ 30 ➢ 40 ➢ 15	 ➢ 1 ➢ 2 ➢ 1
Number of stochastic particles [-]	10, 15, 20, 25, 30, 50, 75, 100, 125, 150		

5.3.1 In-Cylinder Pressure

It is well known that the performance of the internal combustion engine is influenced by the intake charge conditions. The most important intake conditions affecting gas engine performance are the intake pressure and temperature [109]. Figure 5.1 shows the effect of intake charge pressure variation on the in-cylinder pressure profile. It can be seen that the pressure inside the cylinder increases with the increase of the inlet pressure for the intake charge.

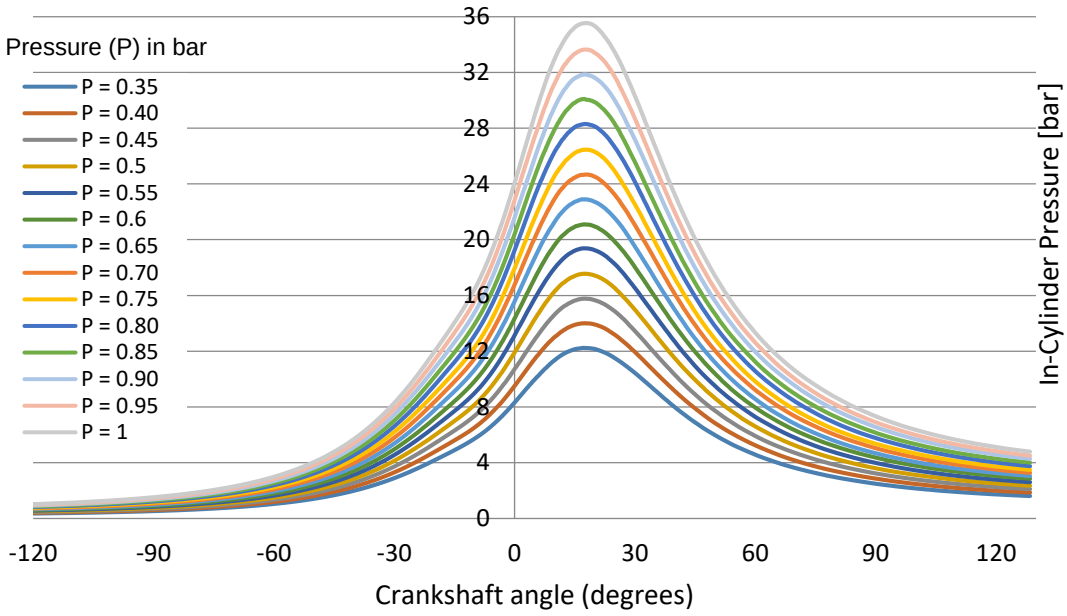

Figure 5.1: Influence of initial pressure on in-cylinder pressure profiles

5.3.2 Cylinder Temperature

While increasing the intake charge pressure increases the cylinder pressure, reducing the temperature of the initial charge, also showed an increase on the in-cylinder pressure along with a trend of moving the peak pressure further away top dead centre, see Figure 5.2. Overall, higher initial temperature gives a steeper rate of pressure rise. Peak pressures for higher initial temperatures are lower because of the decrease in trapped cylinder mass with the increase initial temperature. In order to have a more representative and real-word realistic model, for the present study the initial conditions are assumed identical to that observed in the engine test data set during intake valve closing.

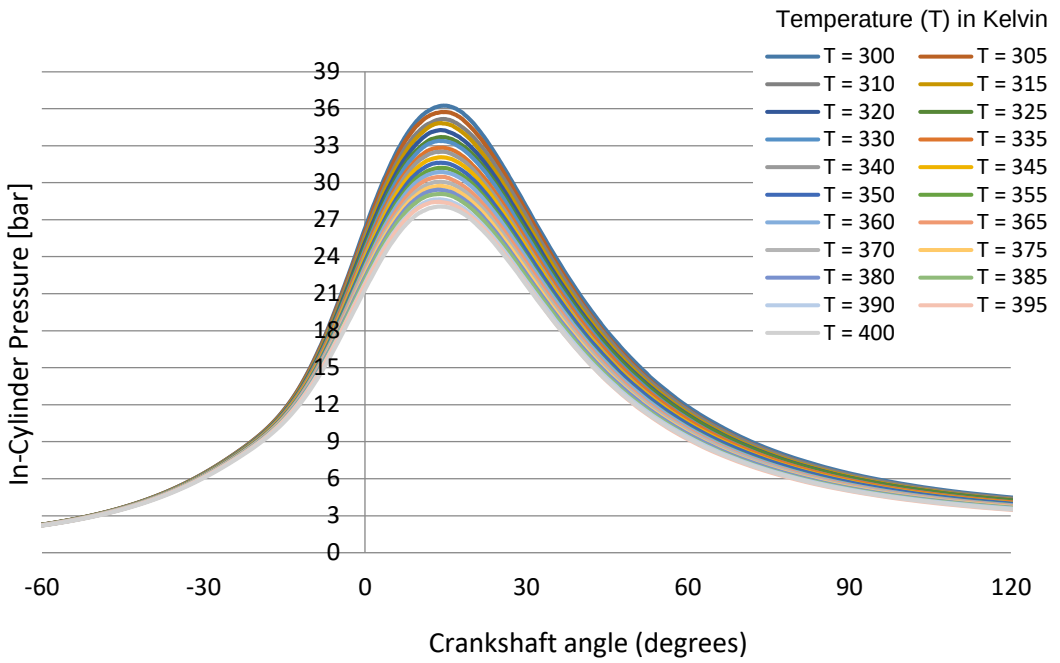

Figure 5.2: Influence of initial temperature on in-cylinder pressure profiles

Changes to the cylinder wall and liner temperatures as well as piston top temperature, which are set constant throughout the final run, showed very little effect on global pressure and heat release profiles. Changes to fuel temperature and density were examined as well and showed not significant effects on global results.

5.3.3 Compression Ratio

Higher compression ratios lead to higher combustion efficiency due to higher in-cylinder peak pressures, as shown in Figure 5.3. Additionally, carbon monoxide formation decreased with increasing the compression ratio, illustrated in Figure 5.4. With higher compression ratio, the compression temperature is higher causing the combustion to initialise faster with peak pressure occurring earlier as the ignition timing was constant for the simulations. Furthermore, almost no effect was observed on the carbon dioxide emissions with the increase of the compression ratio. This is because carbon dioxide is linked to the amount of total fuel used and since the mass of fuel injected was kept the same; the compression ratio had no effect on this pollutant.

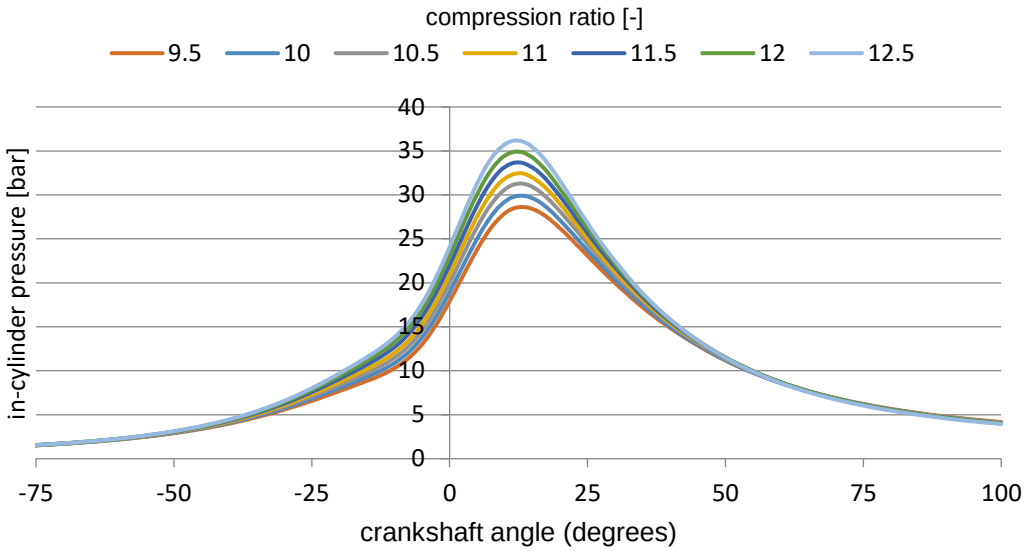

Figure 5.3: Effect of compression ratio on in-cylinder pressure profiles

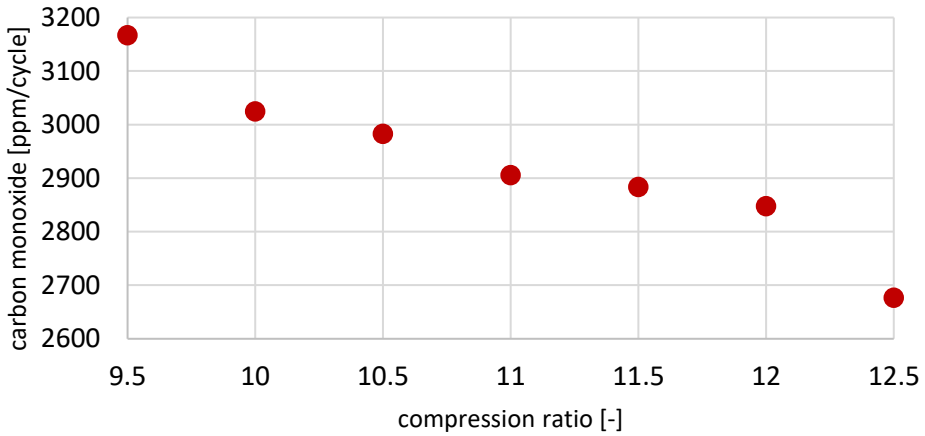

Figure 5.4: Effect of compression ratio on carbon monoxide emissions

The combustion peak temperature is directly proportional to the formation of nitrogen oxides; a higher compression ratio generates higher temperatures, hence as illustrated in Figure 5.5, producing higher nitrogen oxide emissions from the combustion process [322]. As mentioned before, with the increase of the compression ratio the duration of the combustion process is limited and the air fuel mixture has less time inside the cylinder to fully combust. The incomplete combustion of the mixture is associated to the hydrocarbon formation inside the combustion chamber [109].

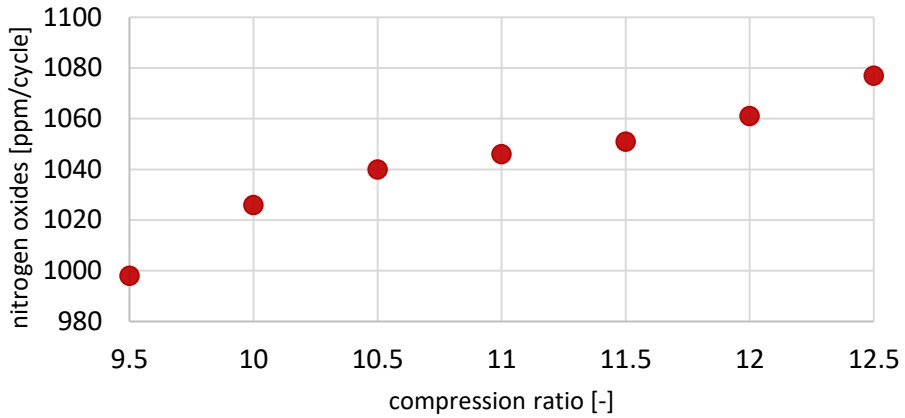

Figure 5.5: Effect of compression ratio on nitrogen oxides emissions

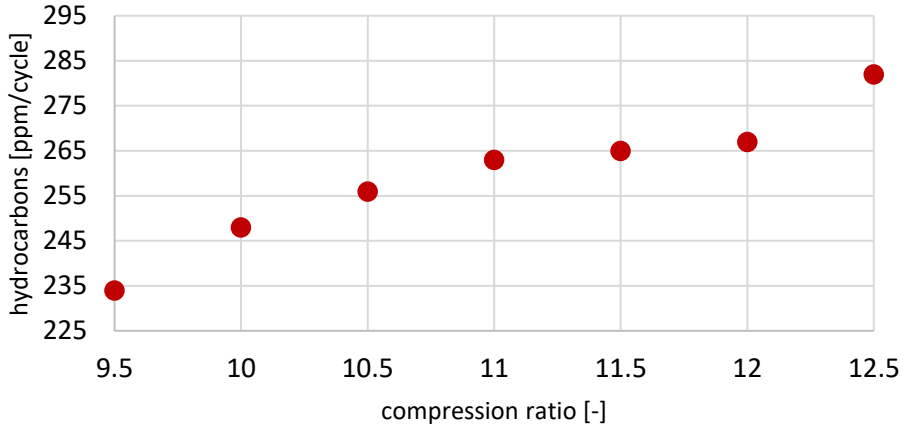

Figure 5.6: Effect of compression ratio on hydrocarbons emissions

5.3.4 Piston crevice volume

The piston crevice volume is composed of the gap between the piston rings and the cylinder walls and is the largest crevice within the combustion chamber. The effect of different percentage of crevice volume is shown in Figure 5.7. As was expected with a smaller percentage of crevice volume the available capacity of the combustion chamber increases, hence the peak pressure increases. The piston crevice volume for the AJ133 engine is 25cc in 625cc cylinder volume, which would only be a 4% of course, but when the burn is happening that small volume reduces the peak pressure of the cylinder and cuts down potential power. Figure 5.8 presents the extended combustion duration with the increase of the crevice volume for the 2000RPM-199Nm engine cycle.

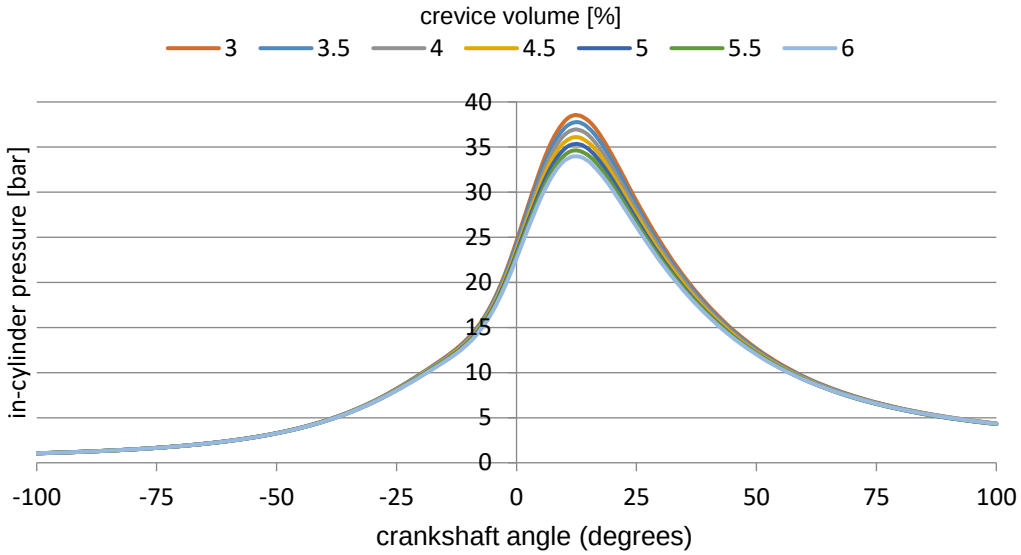

Figure 5.7: Effect of crevice volume percentage on the in-cylinder pressure profile

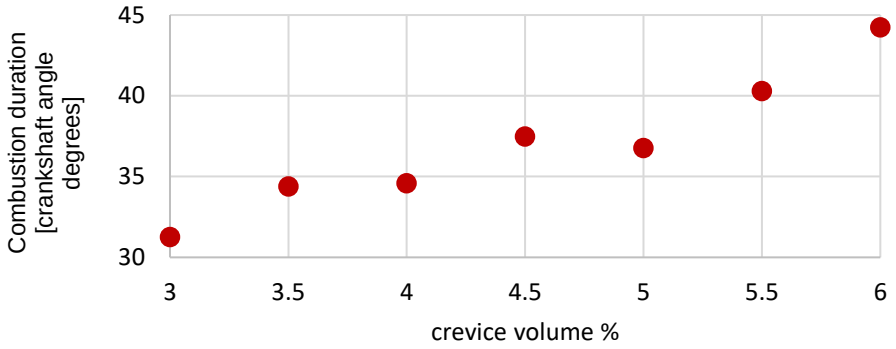

Figure 5.8: Effect of crevice volume percentage on the combustion duration in crankshaft angle (degrees)

Further investigation on engine-out emissions showed that the piston crevice volume is one of the main contributors to carbon monoxide, nitrogen oxides and hydrocarbons emissions. General observations, with every interval increase of the crevice volume:

- A very small quantity of carbon dioxide is linearly reduced
- Carbon monoxide increases linearly by an average of 3%
- Hydrocarbons concentration increases by an average of 6%
- Nitrogen oxides decrease linearly by an average of 11%

In general, the sensitivity of the emissions to the combustion-chamber crevices is influenced strongly by the in-cylinder flow field and combustion, which influence the concentration of burned gases in the crevice gases.

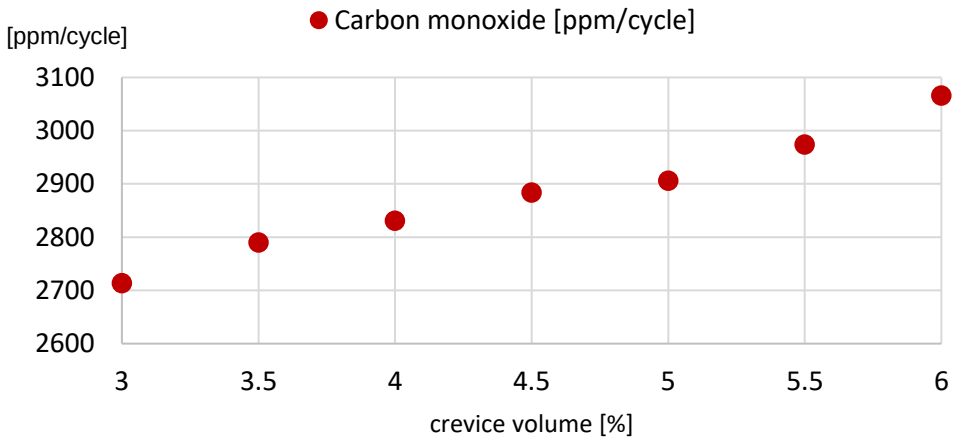

Figure 5.9: Effect of crevice volume percentage on predicted CO emissions

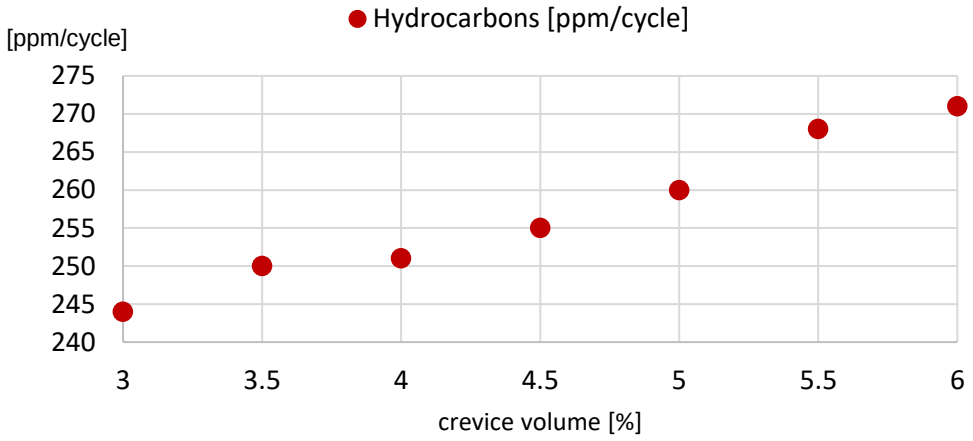

Figure 5.10: Effect of crevice volume percentage on predicted HC emissions

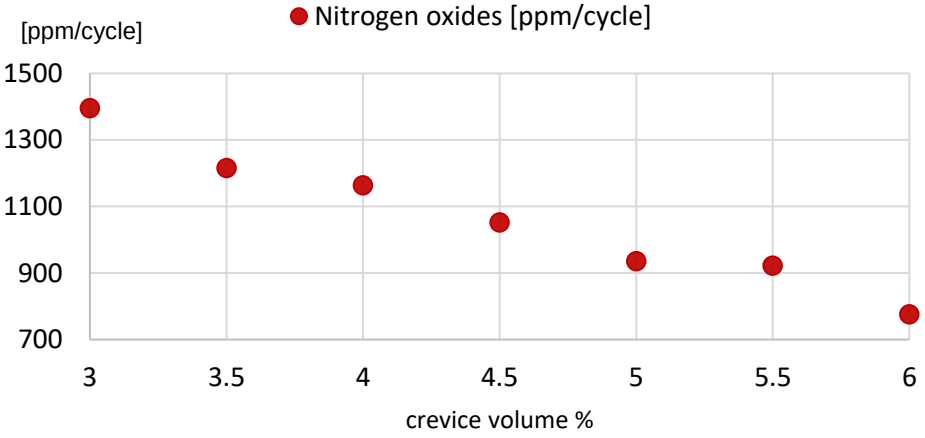

Figure 5.11: Effect of crevice volume percentage on predicted NOx emissions

5.3.5 Exhaust gas recirculation

Additional analysis was done on the exhaust gas recirculation (EGR) mass fraction. The EGR mass fraction parameter of the model showed little effect on cylinder pressure, combustion duration and ignition time, but as expected the increase of EGR was reducing the nitrogen emissions [63, 323], see Figure 5.12. With a larger proportion of exhaust gas recirculated back to the cylinder, less available oxygen concentration is in the fresh charge increasing hydrocarbons and carbon monoxide. However, the last two are post-treated through the use of the three-way catalytic converter [79, 324].

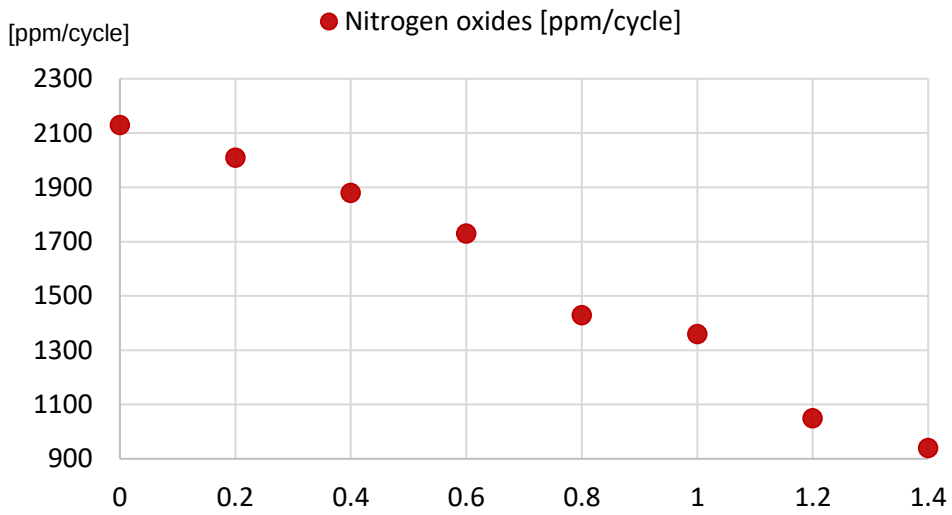

Figure 5.12: Effect of EGR mass fraction on predicted nitrogen oxides

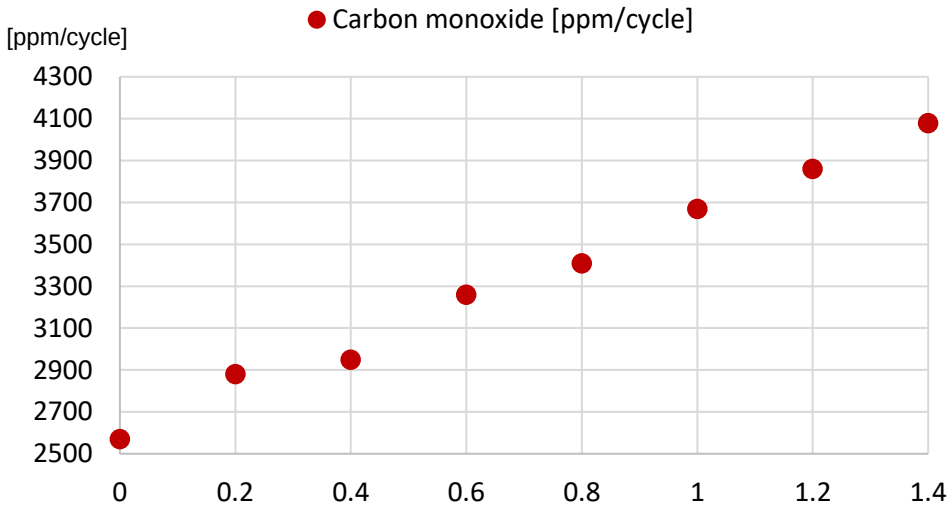

Figure 5.13: Effect of EGR mass fraction on predicted carbon monoxide

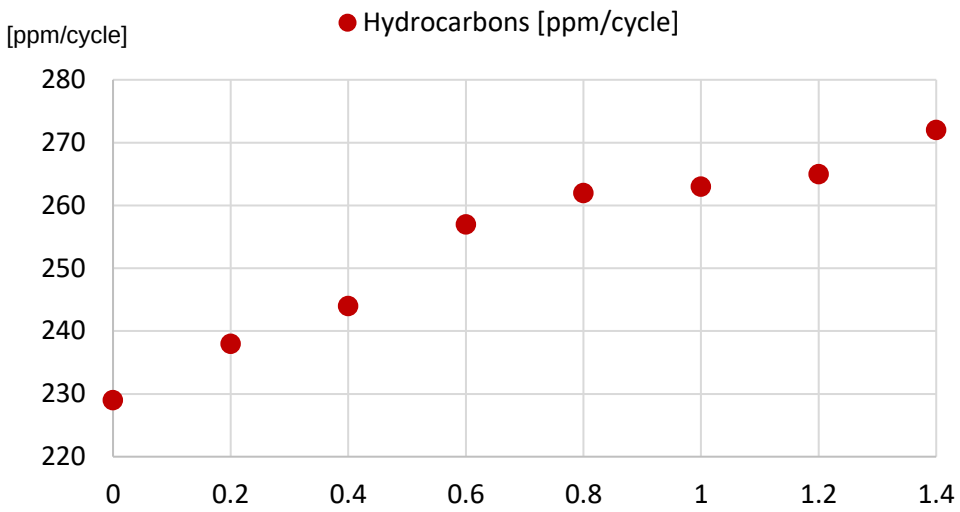

Figure 5.14: Effect of EGR mass fraction on predicted hydrocarbons

5.3.6 Combustion profile

The flame propagation event is modelled using a modified Wiebe function. During the flame spread one new particle is added at each time step in the burned-gas zone accounting for the amount of fresh gas burned during this time step. The behaviour of the Wiebe function, as seen in Figure 5.15, is strongly affected by parameter α or anchor angle, as it is called in Kinetics SRM; as the anchor angle increases the peak pressure of the cylinder drops and at the same time moves away from top dead centre. In Figure 5.16 the cylinder peak pressure follows a linear descent, which for this case is reduced by an average of 0.77 bar, and the crankshaft angle that peak pressure occurs at rises by an average of 0.89 degree with every increment.

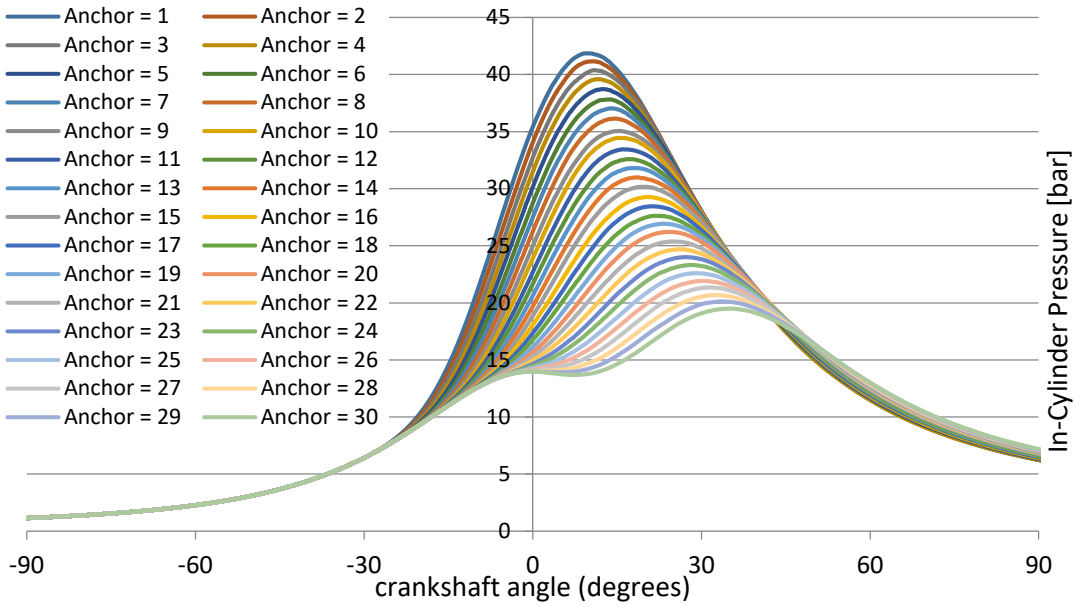

Figure 5.15: Effect of Wiebe function anchor angle parameter on in-cylinder pressure profile

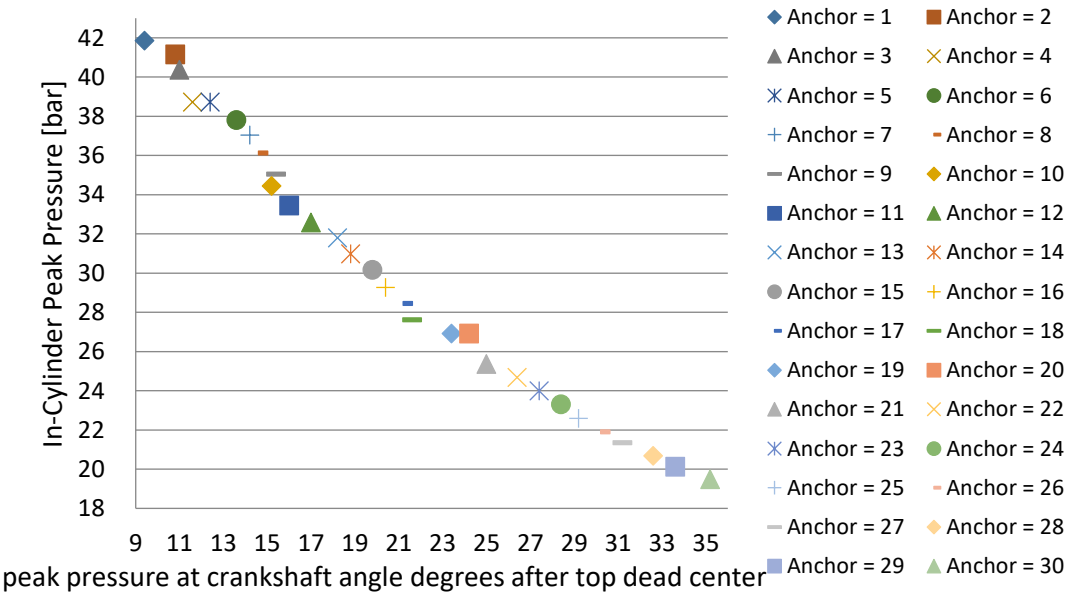

Figure 5.16: Effect of Wiebe function duration parameter on in-cylinder peak pressure

As illustrated in Figure 5.17, the “m” parameter of the Wiebe function appears to smooth up the pressure curve producing a more even profile, while at the same time reduces peak pressure.

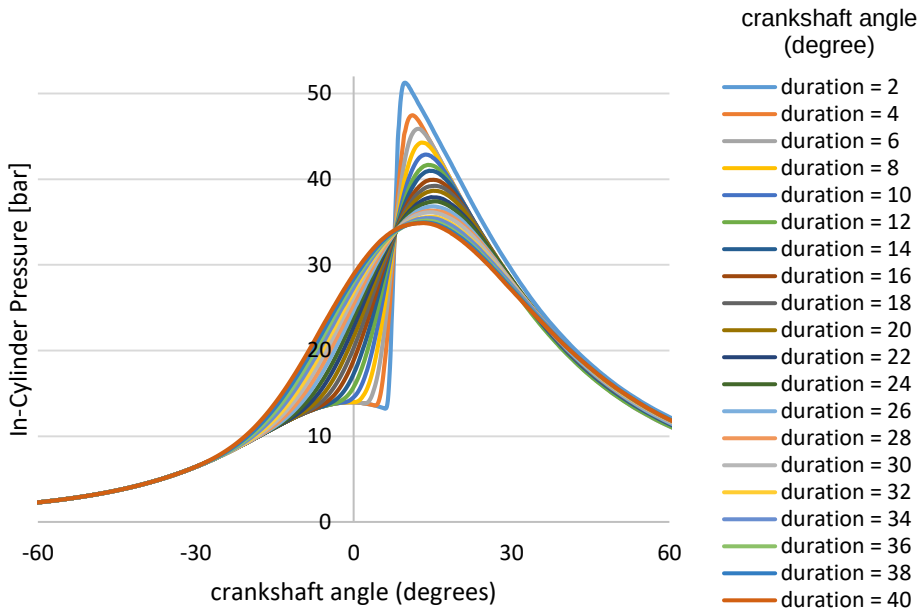

Figure 5.17: Effect of Wiebe function duration parameter on in-cylinder pressure profile

5.3.7 Number of Stochastic Particles

An investigation of the influence of the number of stochastic particles on the simulation results has been studied. Simulation computational time needed was recorded on a 3.4GHz single-core desktop computer with 16GB memory available, employing the same detailed kinetic mechanism with soot formation used for the work in this report. Due to the difficultly of simulating particulate matter, just for this part of the investigation three engine speed load cases with different operating conditions were used to evaluate the model's predictions. The outputs of the engine cases were averaged in order to have one global value for comparison.

Computational time can be said that is rising as the number of particles increase, but it is clearly revealed in Figure 5.18 that the below 30 stochastic particles the simulation runs much faster compared to a higher number of particles case. Numerous previous studies used a common 100-particles setup [23, 21, 25, 24, 26, 27], however the spark ignition gasoline direct injection setup has not been fully evaluated in the Kinetics SRM engine suite [18, 257]. Emphasis is given for the model to run fast, as well as, accurate simulations. Hence the engine cases were repeated starting from a small number of particles, where on average the computational times is between 11

and 22 minutes for the 10- and 25-particles setup, and up to 150-particles, which needed 232 minutes to complete.

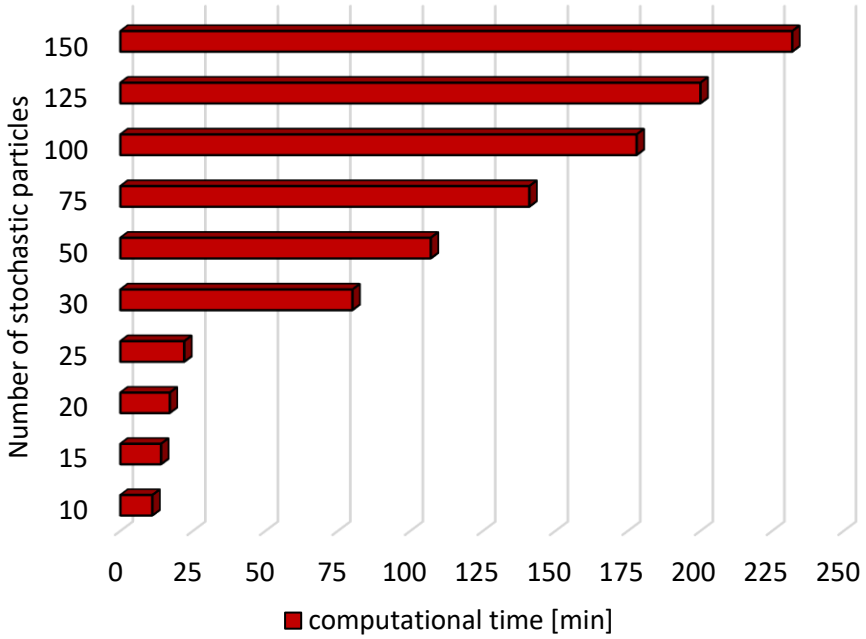

Figure 5.18: Influence of stochastic particles number on computational time [min]

Through the literature it can be said that in general the increase of the stochastic particles defining the cylinder mass, increases the resolution and the quality prediction of the simulation [223]. This is somehow true but the number of stochastic particles must be chosen based on the convergent outputs and not on the computational space resolution. As the number of stochastic particles increases, expensively large number of calculations must be solved with every time step of the code resulting in impractical computation times. Achieving simulation results that are sufficiently accurate compared to the experimental data, while keeping the computational time at a minimum is the objective of this study.

For this number of stochastic particles analysis, very little sensitivity was observed on the cylinder pressure, cylinder temperature, mass fraction burn, and ignition time. This was expected due to the setup of the stochastic reactor model;

- global quantities such a total mass, volume, mean density and pressure are not varying within the in-cylinder compositional space, plus
- the pressure in the cylinder is assumed to be spatially homogeneous and is calculated from the ideal gas law.

However local quantities such as chemical species mass fraction are assumed to be stratified within the in-cylinder compositional space. Both global and local quantities are allowed to evolve with respect to time by allowing these scalars to be influenced by the process of changing the cylinder volume with respect to crank angle and solving chemical kinetic reaction schemes. Across the sensitivity analysis of the number of stochastic particles, emissions and heat loss proved the most sensitive model outputs.

The number of stochastic particles showed almost no effect on the carbon dioxide. However, for the carbon monoxide emissions, the predicted values are at an error level above 20% for the low number of particles runs (below 20 stochastic particles). The lowest error is obtained at 25 stochastic particles, and as the number of particles increases the error percentage increases almost linearly till the 100-particle run. As seen in Figure 5.19, from the 125-particle the predicted carbon monoxide value gets closer to the experimental value but with the expense of simulation cost. The prediction accuracy was determined based on the percentage error formula with the experimental and simulated values given by V_{exp} and V_{sim}.

$$\left|\frac{V_{exp} - V_{sim}}{V_{exp}}\right| x100 \qquad \text{Equation 5.1}$$

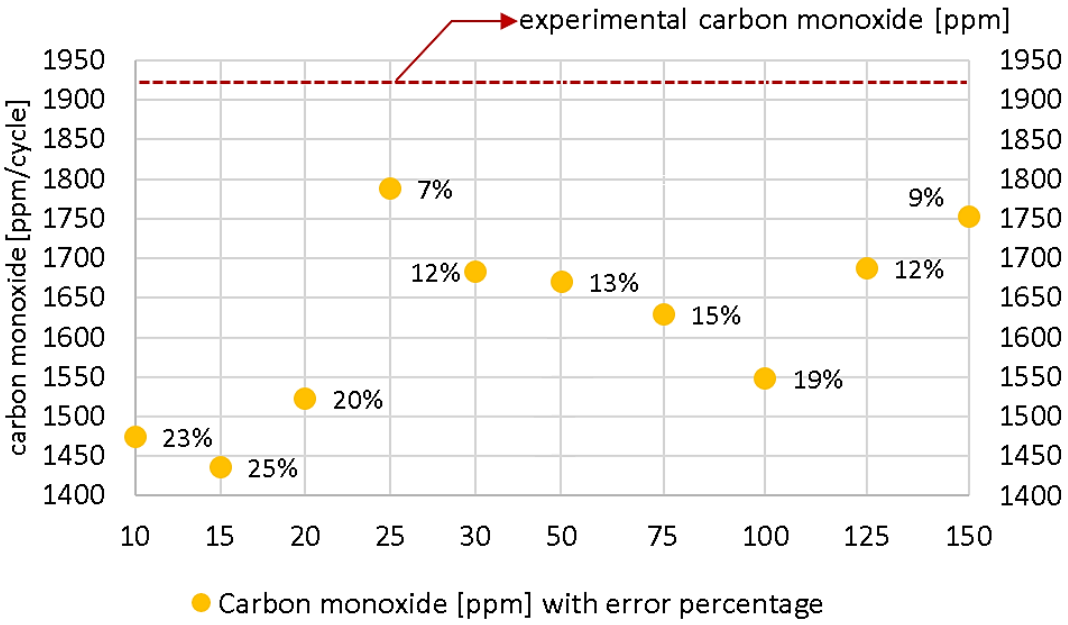

Figure 5.19: Effect of number of stochastic particles on CO prediction

Moreover, as illustrated in Figure 5.20, its found that the simulation hydrocarbons value was linearly reduced as the number of stochastic particles increases. However, with the increase of the number of particles, the model was able to better predict the experimental hydrocarbons value producing less estimation error.

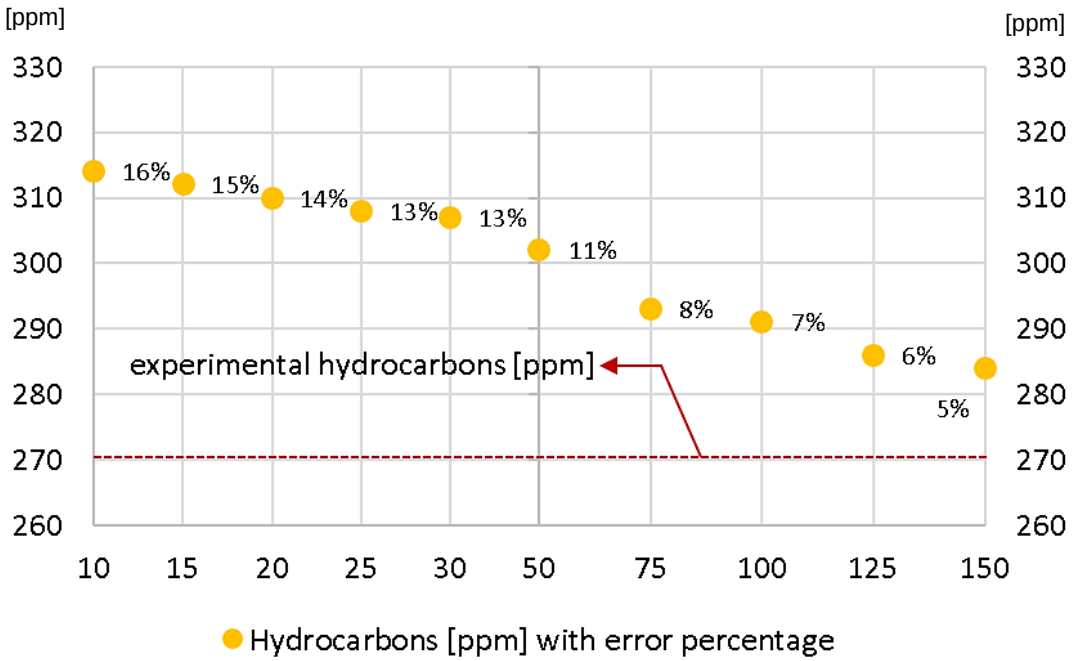

Figure 5.20: Effect of number of stochastic particles on HC prediction

Next, the concentration of nitrogen oxides starts to reduce with a low number of stochastic particles, but after the 25-particles case it can be seen in Figure 5.21 that more nitrogen is formed as more stochastic particles are introduced into the cylinder description. Unfortunately, due to the lack of experimental nitrogen oxides data, a comparison between the engine and the simulated nitrogen concentrations is not currently possible.

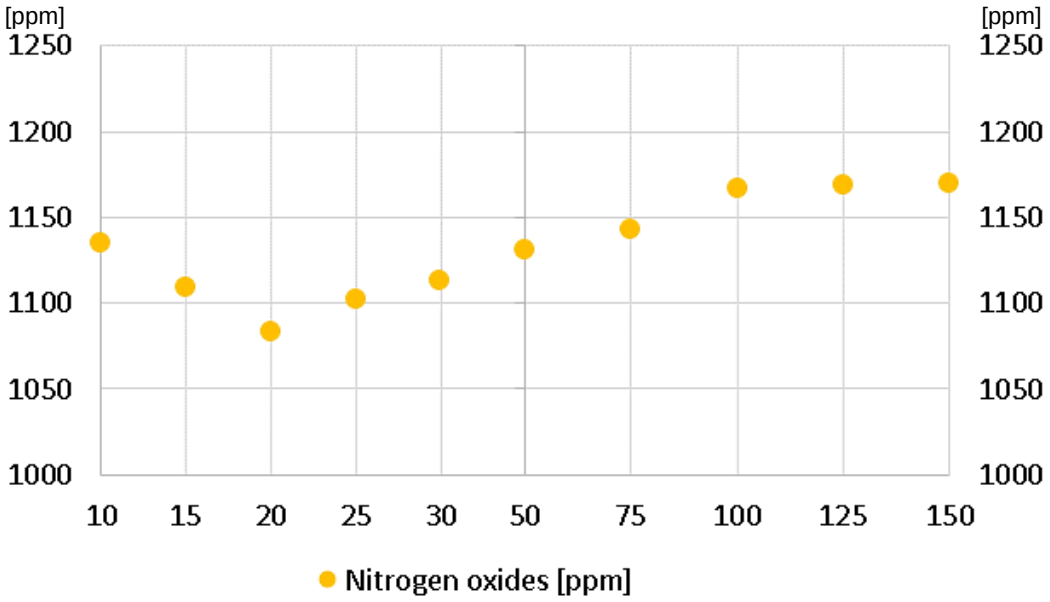

Figure 5.21: Effect of number of stochastic particles on nitrogen oxides

Finally, when the analysis was focused on the particulate number it was discovered that the model was unable to produce any number of particulates for simulation runs that had a number of stochastic particles lower than 25. In terms of prediction accuracy, as it can be seen from Figure 5.22, the medium values of stochastic particles were estimating the formation of particulate number much more accurate than setups with higher stochastic particles number.

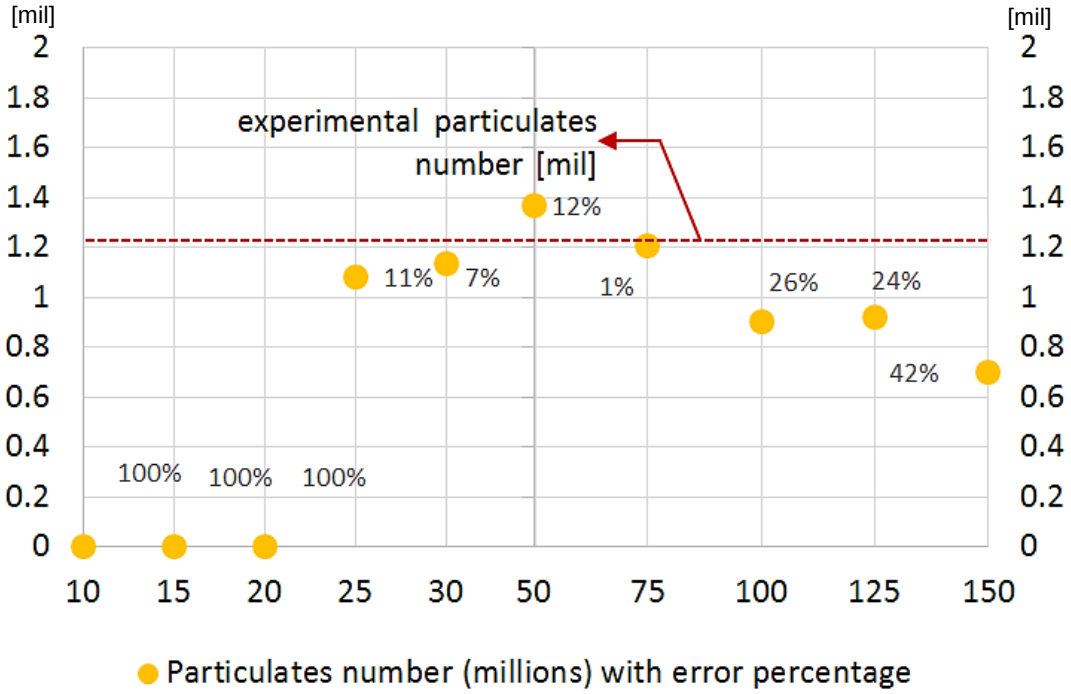

Figure 5.22: Effect of number of stochastic particles on particulates number

5.3.8 Stochastic Variability

As stated in 3.2.2.3, the Kinetics SRM is based on a stochastic reactor engine model. Due to its stochastic nature the model should produce different results with every run. 10 identical runs of the same engine test point where executed verifying that randomness is present. As it is shown in Figure 5.23, the expected outputs affected by the stochasticity of the PDF-based model were the emissions concentrations and number of soot particles. A reference line in red shows the experimental value for each pollutant and an absolute error percentage (see Equation 5.1) is calculated comparing each simulation run with the experimental value corresponding to the selected testing point.

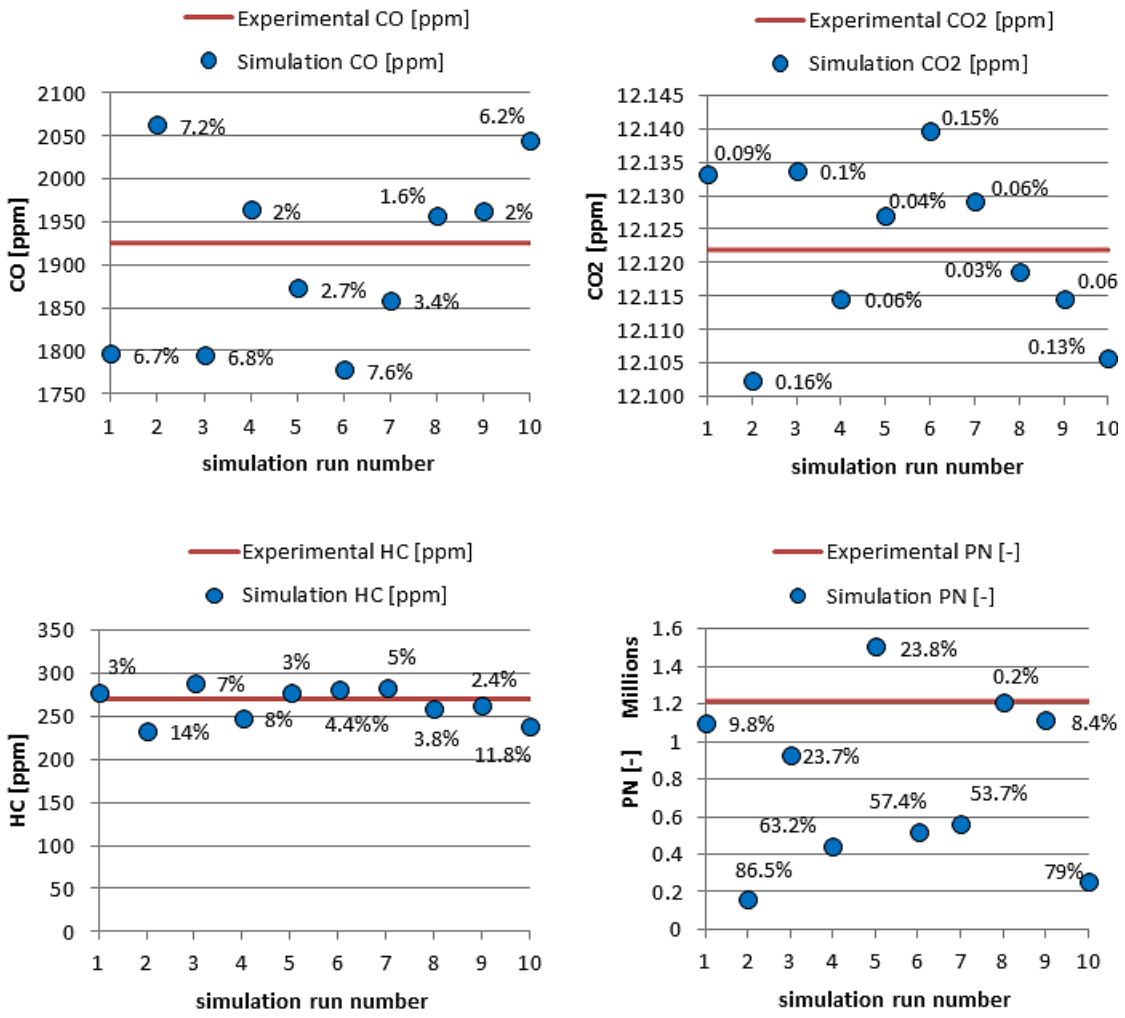

Figure 5.23: Stochastic variability test for emissions

5.3.9 Analysis Summary

An investigation was carried out examining the main initial conditions of the model. The initial settings are found to have a great effect on the in-cylinder pressure propagation. The study has shown that even small changes in the modelling parameters, like initial pressure or the compression ratio, will alter the combustion profile, therefore the exact pressure, temperature, exhaust gas recirculation mass fraction, etc. measured from the engine experiment at inlet valves closing (start of Kinetics SRM simulation) should be used for a more realistic setup.

Furthermore, these variables are classified as global quantities in the stochastic reactor, in other words they are not affected by the randomness of the model. A variability test was performed verifying the stochasticity of

Kinetics SRM on the emissions concentrations. Even with all the initial conditions kept constant the model will still predict different emissions with each run thanks to its heat transfer and turbulent mixing sub-models and their stochastic setup.

5.4 Heat Transfer and Turbulent Mixing Analysis

In order to fully examine the emissions formation model, the heat transfer and turbulent mixing parameters needed to be investigated. A two-phase sensitivity analysis of the Kinetics SRM engine suite “unknown” parameters has been completed based on the global results of one testing point for each of the 6 speed – load case given in Table 4.1. The analysis is focused on two sub-models of kinetics SRM suite; heat transfer and turbulent mixing. For the heat transfer sub-model the parameters under investigation are the heat transfer constant and the heat transfer exchange factor. As for the turbulent mixing sub-model the key parameters examined are the turbulent mixing timescale and the mechanical-to-scalar timescale ratio. The range of the 4 parameters is given in Table 5.5.

5.4.1 Methodology

For the first phase of the investigation, the one-factor-at-a-time analysis, focuses for both on simulation accuracy and computational time, whereas the second phase, the sensitivity analysis based on the experimental design technique, takes into consideration only the prediction accuracy of the simulation. This is due to the much larger number of testing points that the simulation must run, making it almost impossible for the investigation of prediction quality together and computational time.

Table 5.5: Heat transfer and mixing sub-models parameters and their range

Factor	Minimum	Maximum	Step
Heat transfer constant [-]	500	3000	500
Heat transfer exchange factor [-]	0.05	0.3	0.05
Turbulent mixing time [s]	0.005	0.2	0.005
Mechanical-to-scalar timescale ratio [-]	0.5	3	0.5

The parameterisation of the model is a crucial process that aims to;

- study the general behaviour of the model with the changes of parameters,
- test the robustness of the results,
- identify model inputs that cause significant change in the output and should therefore be the focus of attention for the calibration procedure,
- search for errors in the model structure by encountering unexpected input outputs relationships, and
- reduce the model's calibration procedure by recognizing the sensitivity of parameters

All the simulation runs are based on a 25-stochastic particles setup since this number of stochastic particles gives the best trade-off between computational time and emissions prediction accuracy. The first phase of the "unknown" internal parameterisation analysis is based on the one-factor-at-a-time method, where the value for only one factor is allowed to gradually increase while keeping the rest of the parameters values constant and at their typical settings [325]. However, statistically designed experiments that vary several factors simultaneously are more efficient when studying multiple factors [326, 327].

Hence, the second phase of the analysis is performed based on a space-filling Latin hypercube design in a one-stage test plan created using Matlab Model-Based Calibration (MBC) toolbox. For the current work, the benefit of the one-factor-at-a-time investigation is that computational time along with the prediction errors can be taken into consideration when searching for the optimal settings. Whereas, the high number of simulation tests (600 in total) of the experimental design will prolong the investigation significantly if computational time was considered. Nonetheless, the advantage of the experimental design analysis is that it can identify and study any possible interactions between the factors.

5.4.2 One-Factor-at-a-Time Analysis

5.4.2.1 Heat Transfer Sub-Model

The heat transfer process in the model is generally applied by allowing individual stochastic particles, selected on the basis of having similar composition, to interact by exchanging gas composition (fuel, chemical species, etc.) as well as heat or heat to the wall. Any heat transferred from the charge to the walls of the cylinder will affect not only the thermal efficiency of the engine, but engine performance and combustion emissions as well.

The heat transfer in Kinetics SRM suite is determined by the product of the cylinder wall – gas temperature difference and the relation of the user-defined heat transfer constant and the available heat transfer area over the specific heat capacity and the total mass in the cylinder. The heat transfer constant introduces a stochastic jump process in the model, resulting in random inhomogenities in the temperature. The heat transfer constant had the most effect on the hydrocarbon emissions and particulate number. The simulation demanded more time as the heat transfer constant increased, but in general the best combination of prediction accuracy (based on Equation 5.1) and computational time was achieved at a heat transfer constant with value of 1000, see Figure 5.24.

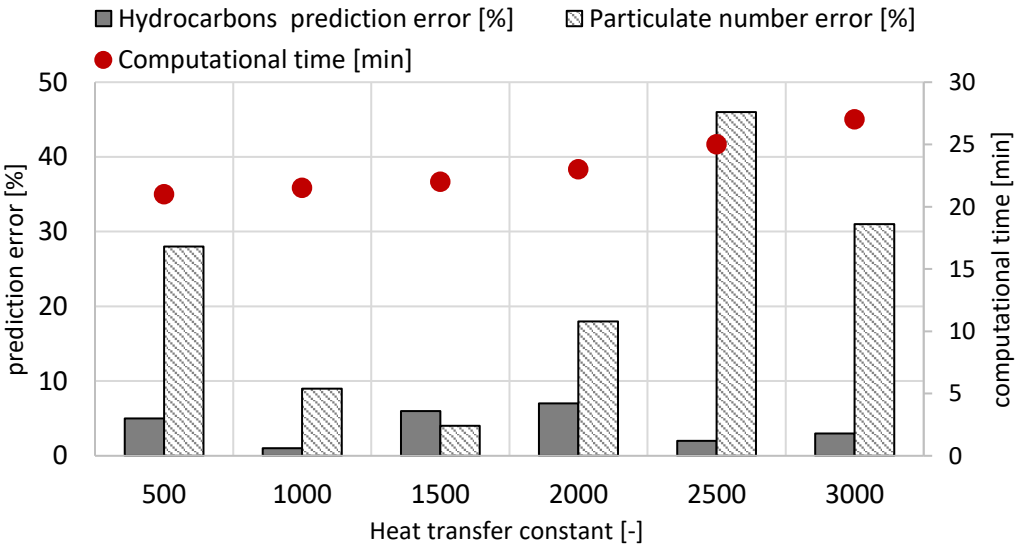

Figure 5.24: Computational time and error comparison between experimental and simulation hydrocarbons and particulate number against the heat transfer constant

It was found that the stochastic particle heat transfer exchange factor had the greatest effect on hydrocarbons, nitrogen oxides and particulate number. As the particle heat transfer exchange factor rises it was observed that it reduces both the concentration of hydrocarbons and nitrogen oxides (Figure 5.25). It was observed that at values smaller than 0.1 for the heat transfer exchange factor, the model wasn't producing any particulates. Also from an exchange factor of 0.1 and above the computational time needed for the model to complete the run was reduced. As is shown in Figure 5.26, the optimal value for the heat transfer exchange factor was found to be at 0.2, which gives the best prediction accuracy for both hydrocarbon concentration and particulate number with relatively fast simulation run time.

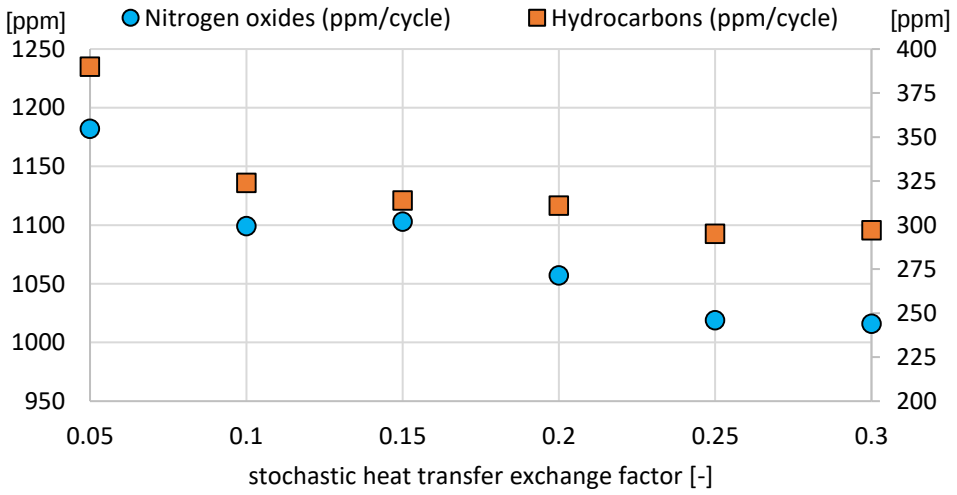

Figure 5.25: Effect of stochastic heat transfer exchange factor on hydrocarbons and nitrogen oxides

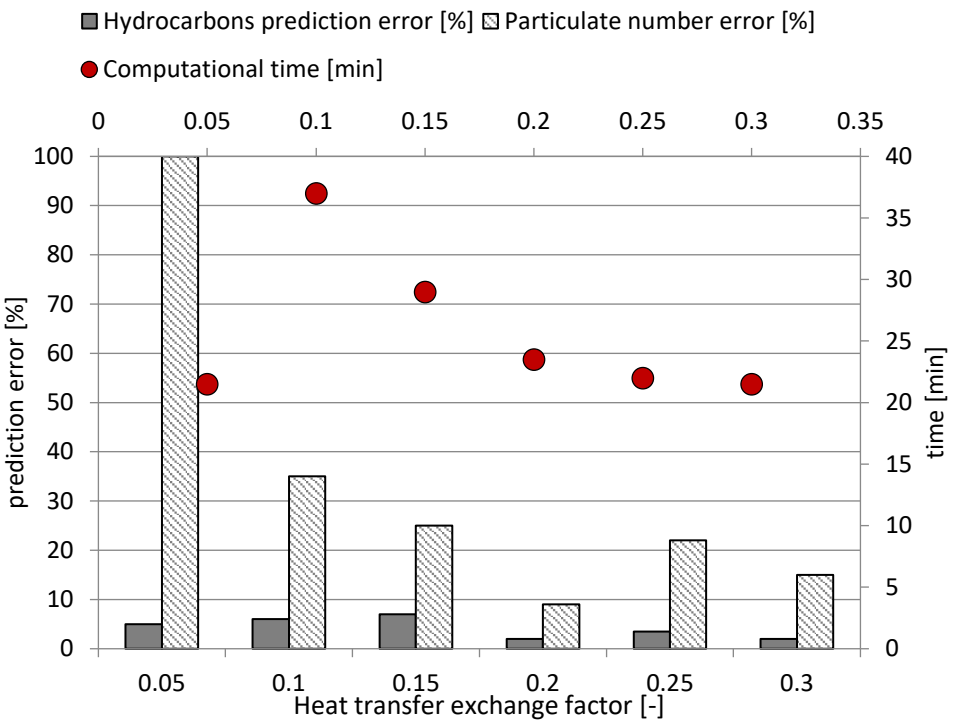

Figure 5.26: Computational time and error comparison between experimental and simulated hydrocarbons and particulate number against the heat transfer exchange factor

5.4.2.2 Turbulent mixing

In the Kinetics SRM engine suite how often the stochastic particles will interact with each other is mainly determined by the turbulent mixing timescale [257]. From the turbulent mixing timescale, the largest effect observed was on hydrocarbons, carbon monoxide and particulate number, because these pollutant emissions are a result of the cumulative effects of the proceeding combustion event itself. It can be seen in Figure 5.27 that the best trade-off between model accuracy and simulation time needed was at 0.005 seconds turbulent mixing time.

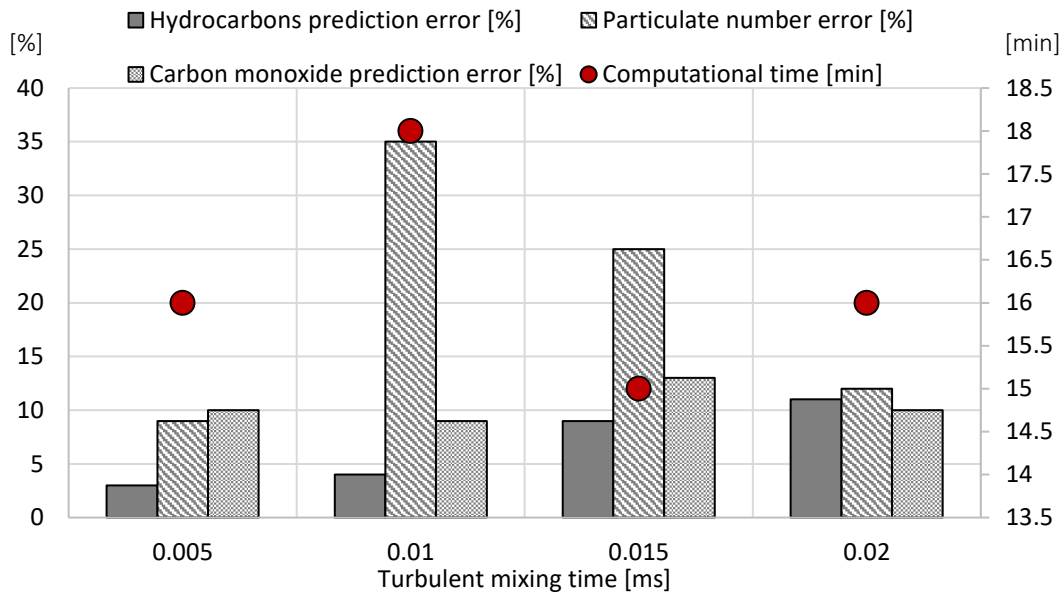

Figure 5.27: Computational time and error comparison between experimental and simulation hydrocarbons and particulate number against the turbulent mixing time

Moreover, the mechanical-to-scalar timescale ratio is a coefficient that defines the ratio between the hydrodynamic turbulence timescale to a scalar timescale. The sensitivity of global emissions and computational time to this coefficient was found to be insignificant. The largest effect observed was on carbon monoxide and nitrogen oxides; however, the linear drop on concentration was too small to take into account, as seen in Figure 5.28.

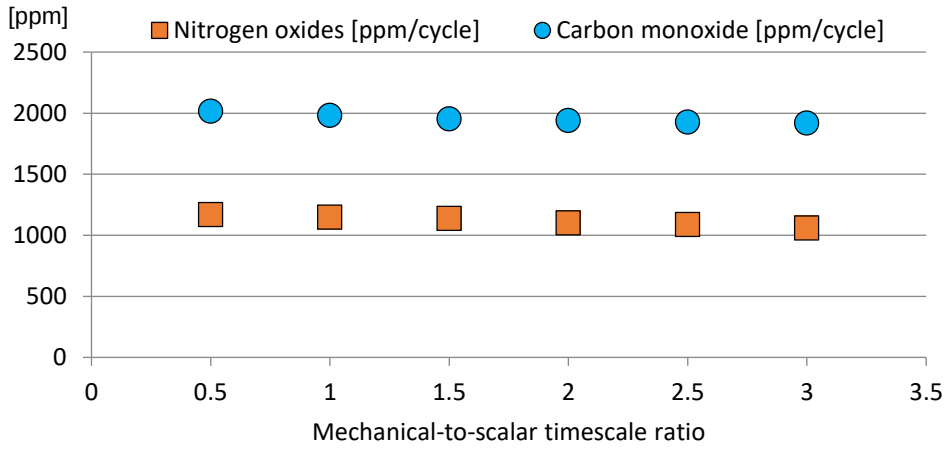

Figure 5.28: Mechanical-to-scalar timescale ratio effect on carbon monoxide and nitrogen oxides

5.4.2.3 Analysis Summary

Based on the averaged results of 6 testing points, one from each speed –load engine case, the key parameters of the heat transfer and turbulent mixing sub-models of the Kinetics SRM engine suite were investigated in a one-factor-at-a-time sensitivity analysis. The results of the investigation are summarised as follows:

- Heat transfer constant had the greatest effect on hydrocarbons and particulate number. With the increase of the heat transfer constant value, more time was needed to complete the simulation. The best trade-off between prediction accuracy and computational time was found to be at a heat transfer constant value of 1000
- Heat transfer exchange factor mainly affects hydrocarbons, nitrogen oxides and particulates number. It was observed that with a value less than 0.1, the model was not producing any particulates. Moreover, increasing the heat transfer exchange factor value allows the simulation to run faster. The lower prediction error – time needed was established at 0.2
- Turbulent mixing timescale had the largest effect on hydrocarbons, carbon monoxide and particulate number, with its optimal value confirmed at 0.005 seconds
- Mechanical-to-scalar timescale ratio mostly influenced carbon monoxide and nitrogen oxides concentrations, however the effect was too small to take into account. The value for this parameter was set to 2.0, a value recommended by Pope (1985) for stochastic engine simulations [257, 311]

5.4.3 Experimental design investigation

So far the sensitivity analysis was performed by altering one parameter at a time while keeping the rest of the parameters constant. In order to fully examine the behaviour of the model in a more efficiently way, the analysis was extended to include the simultaneously variation of the four internal model parameters inspected previously. The model-based calibration toolbox in MATLAB was used to define the optimal test plan based on a design of

experiments method, and generate the calibration for the 6 operating points at different engine speed and engine load.

The toolbox offers a full range of proven experimental designs (classical, optimal and space-filling), but due to the low knowledge about the variables under investigation a space-filling experiment with Latin hypercube design style was selected. A total of 600 testing points; 100 points for each of the 6 engine operating points, was used to create the design space. The sample size of 100 points per engine case assures that the maximum amount of important information will be extracted from the output data. As with the one-factor-at-a-time analysis, the parameters value and range were set based on Table 5.5. A sample of the Latin hypercube design is given in Table 5.6, whereas Figure 5.29 displays the full design matrix with all four parameters across the predetermined design space.

Table 5.6: Example of the Latin hypercube experimental design for one engine speed load point

Point	Heat Transfer Constant [-]	Heat Transfer Exchange [-]	Mechanical-to-Scalar Timescale [-]	Turbulent Mixing Timescale [s]
1	2874	0.173	1.914	0.0017
2	2495	0.043	1.939	0.0059
3	904	0.010	0.652	0.0050
4	2672	0.137	2.015	0.0087
5	2116	0.117	1.182	0.0028
6	727	0.066	1.005	0.0072
7	2722	0.029	1.889	0.0015
8	1157	0.175	0.500	0.0067
⋮	⋮	⋮	⋮	⋮
99	1005	0.167	1.561	0.0051
100	626	0.037	1.586	0.0093

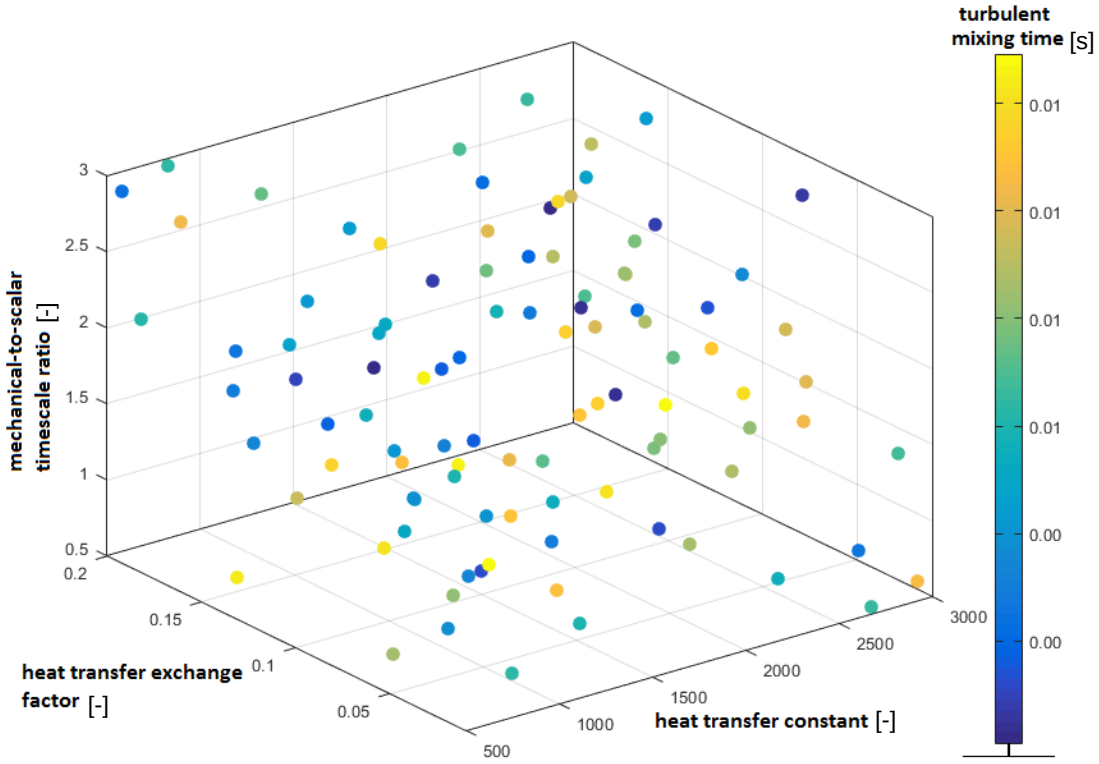

Figure 5.29: 4D scatter view of the experimental design matrix showing the parameter values in the computational space

A model for each of the 6 engine speed load points was created in Kinetics SRM engine suite with the heat transfer and turbulent mixing sub-models based on the values from the space-filling experimental design. With an average of 22 minutes per test point, the analysis needed almost 10 days to complete. The key outputs interested from the analysis were the carbon monoxide, hydrocarbons and particulate number. The three responses were fed back to the MATLAB toolbox for a surface analysis. In Figure 5.30 the test plan of the experimental design model can be viewed in terms of its inputs and responses.

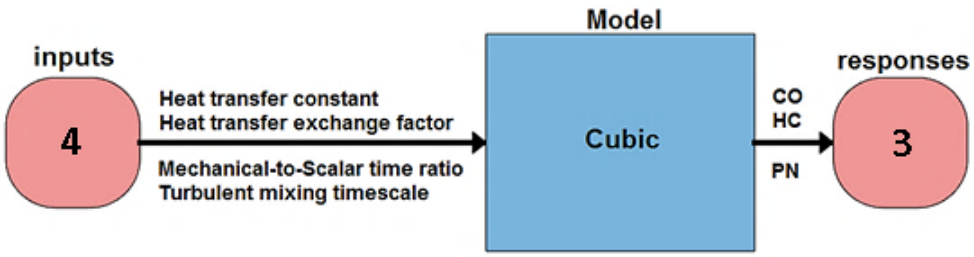

Figure 5.30: Single-stage test plan of the experimental design in MATLAB model-based calibration toolbox

A 3rd order (cubic) polynomial-based response surface model was employed to model the responses [328]. In order not to over-fit the data a Minimize PRESS stepwise algorithm was used, where at each step the term that will improve the PRESS statistic (or more commonly known as predicted sum of squares error) the most is removed, hence improving the predictive quality of the model [329]. This analysis was focusing on just the prediction accuracy, whereas before both simulation accuracy and computational time were taken into consideration. A cross section view sample of the parameters across their range is presented in Figure 5.31. As with the one-at-a-time factor analysis, one factor can be altered at different values while the other factors are fixed at a constant position. By comparing the responses of the plots, in this case the experimental against simulated value prediction error, it was seen that the trend analysis in general agrees with the one-factor-at-a-time investigation performed in 5.4.2.

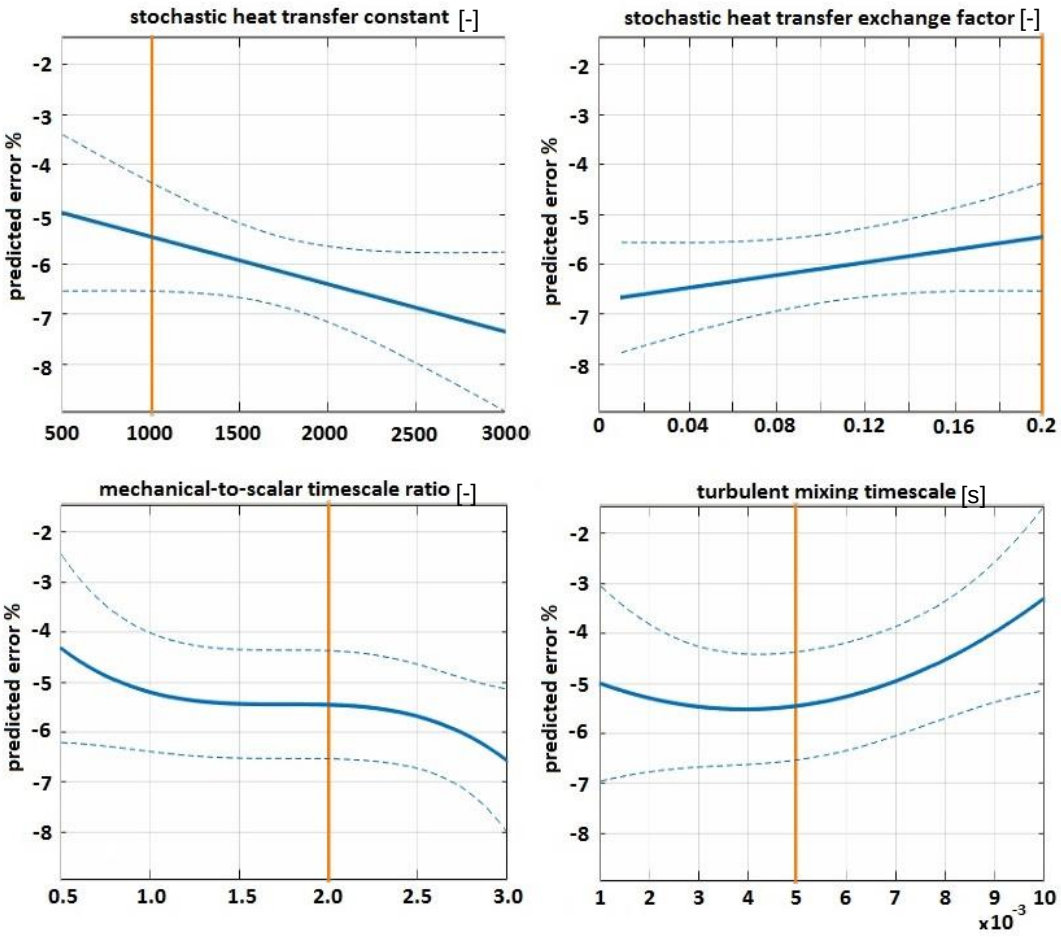

Figure 5.31: For one engine speed-load point a cross section view of all inputs across their range against the predicted error for carbon monoxide concentration

Moreover, Figure 5.32 shows the carbon monoxide response surface analysis. Contour plots of the response surfaces were used to explore the effect of changing factor levels on the response. As a general rule, if there is an interaction between the factors the model will show a twist in the response surface. For all the 6 engine cases under investigation only one surface plot for one of the responses (carbon monoxide) was showing a small twist between the heat transfer exchange factor with the heat transfer constant, as well as, the turbulent mixing time with the heat transfer exchange factor. Since this was observed in only one out of 6 speed – load cases and for only one response, it was neglected.

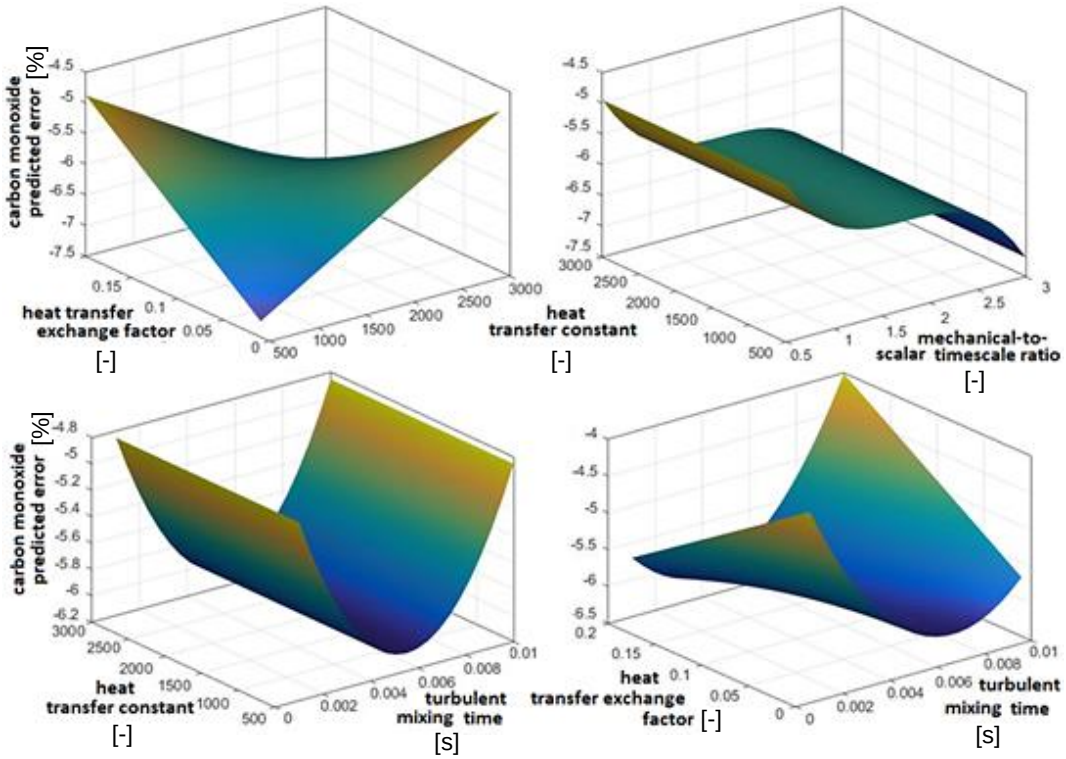

Figure 5.32: Surface plots of the 4 parameters against the carbon monoxide predicted error

5.4.3.1 Summary of analysis

The experimental design sensitivity analysis was performed based on a 600-testing points space-filling Latin hypercube plan. As with the single factor analysis, the parameter value and range was set based on Table 5.5. The trend analysis of the responses for the cross section view plots supports the choice of the optimal parameters values chosen in Section 5.4.2.3.

Furthermore, the study of the surface plots showed no significant relationship among the factors due to the limited interaction between them.

5.5 Global Results and Validation

Once the internal parameters of the model had been examined and the performance of the model in the calibration phases was considered satisfactory, the next step was to carry out the parameterisation of the model with respect to all the engine operating points. Rather than applying a unique calibration for each engine operating point, the objective was to apply a global set of parameters for all the points. For all the engine cases the model was parameterised by fixing the stochastic heat transfer constant to 1000 and particle heat transfer exchange factor to 0.2. The localness mixing model was fixed with a mechanical-to-scalar timescale ratio at 2.0, a value recommended by Pope (1985) for stochastic engine simulations, and with a turbulence timescale of 0.005 seconds, derived from the sensitivity analysis. A 25-stochastic particles setup was set for the simulation.

5.5.1 In-Cylinder Pressure

In-cylinder pressure profile was examined first. The agreement between simulated in-cylinder pressure and experimental pressure was acceptable, and the model correspond well to the variations in operating conditions. Figure 5.33 presents the in-cylinder pressure profile evaluation for one engine case for each of the engine speed – load points. The most noticeable differences between the engine experiment pressure profiles and the simulation pressure profiles were observed just after the mixture ignition, causing a lower build-up of the simulated pressure. A very small pressure difference (for approximately 10 out of 60 engine cases tested) was observed through the variation examination between the two profiles during mixture compression. However, close to top dead centre the simulation pressure progresses and matches the experimental pressure till expansion.

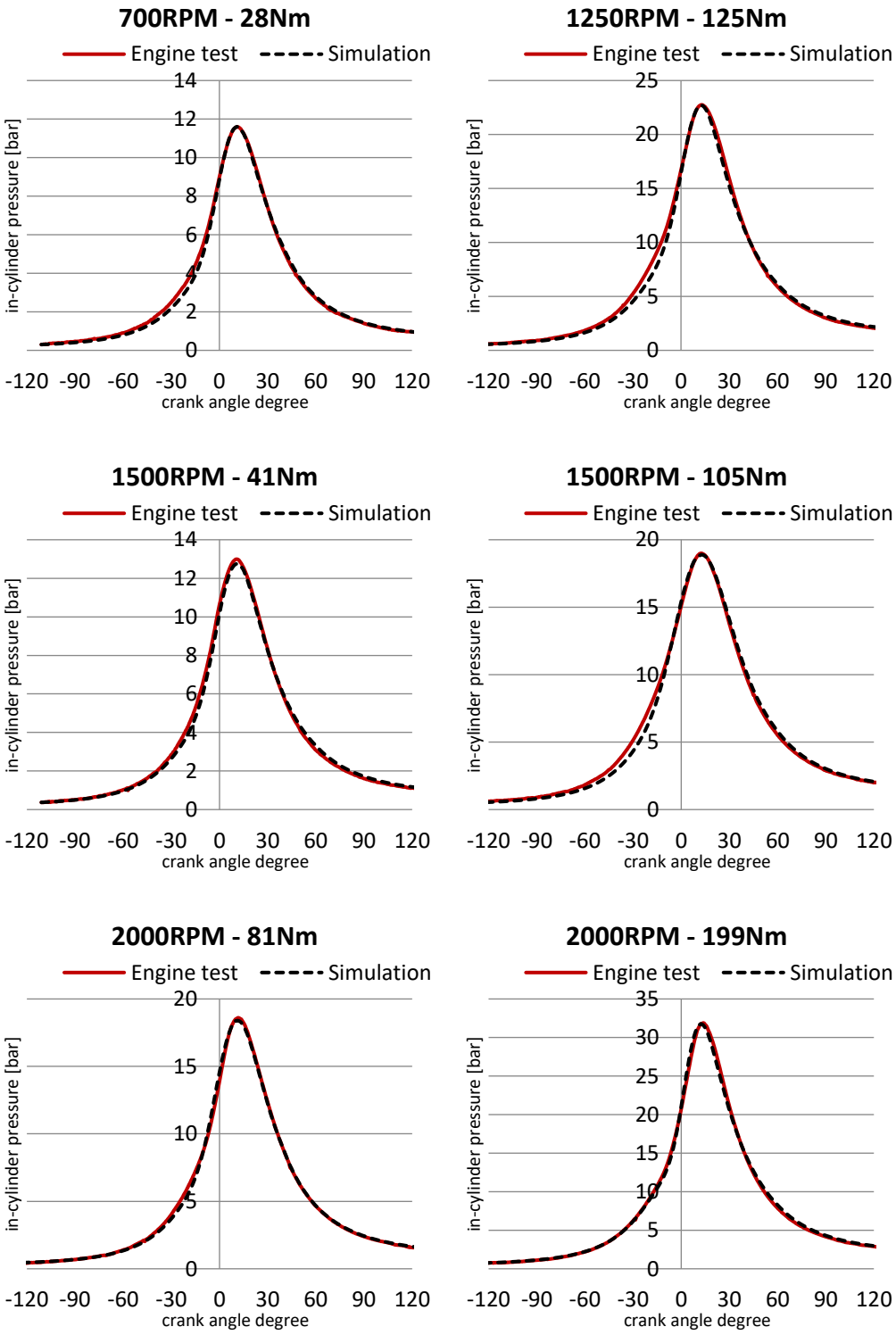

Figure 5.33: In-cylinder pressure profile evaluation

5.5.2 Combustion Emissions

Next, emissions results are discussed per engine speed – load point. In this way the trends of Kinetics SRM can be better examined with the variation in operating conditions (see Section 4.2).

5.5.2.1 Hydrocarbons

It can be seen in Figure 5.34 that the model under-predicts the hydrocarbons emissions for the 2000RPM-81Nm engine speed – engine load case, with an average absolute error of 24%.

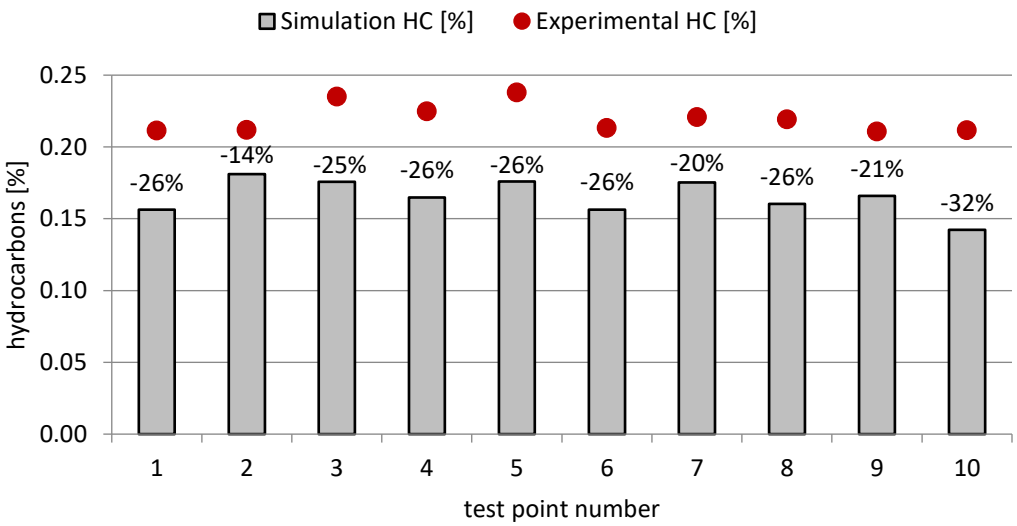

Figure 5.34: Hydrocarbons evaluation for the 2000RPM – 81Nm engine speed – engine load case

The 1250RPM-125Nm speed – load engine case seems to behave the same, with an absolute error percentage between experimental and simulated hydrocarbons value of 20%.

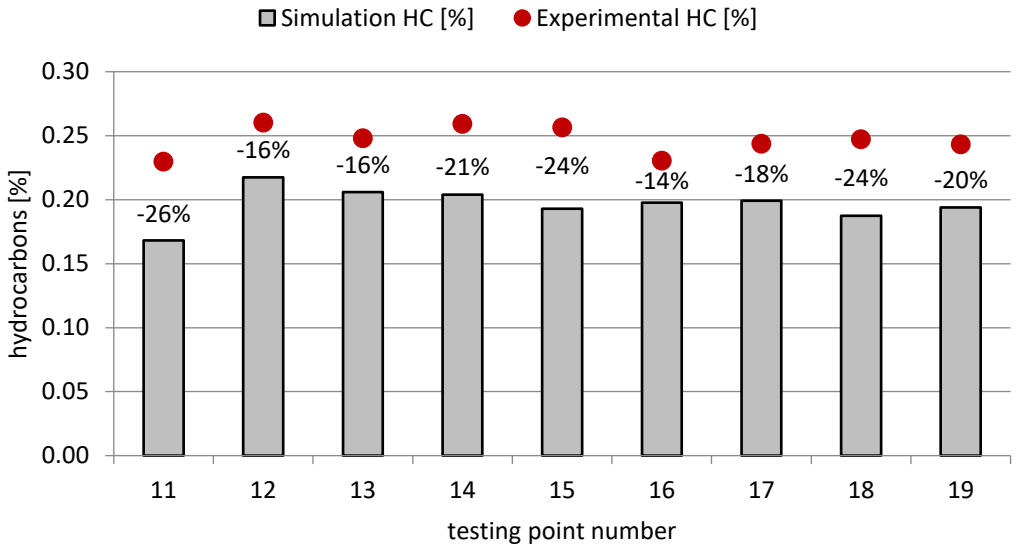

Figure 5.35: Hydrocarbons evaluation for the 1250RPM – 125Nm engine speed – engine load case

Hydrocarbons concentrations for the 2000RPM – 199Nm engine case as seen in Figure 5.36 below, are over-predicted by the model with an average error of 30%.

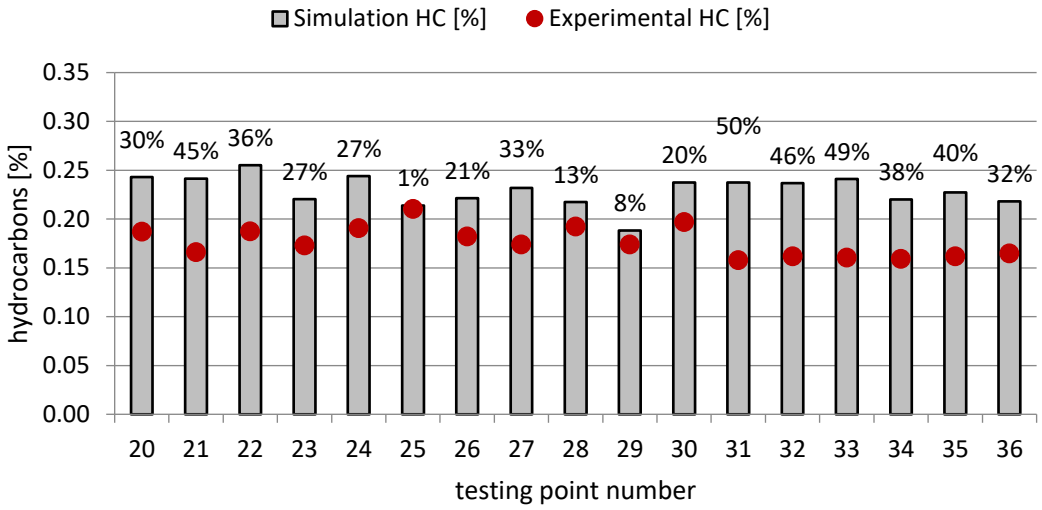

Figure 5.36: Hydrocarbons evaluation for the 2000RPM – 199Nm engine speed – engine load case

The emissions model seems to produce good hydrocarbons predictions for the 1500RPM – 105Nm engine case with an average error prediction between simulation and experiment of 7% and a highest error value at 17 % (Figure 5.37)

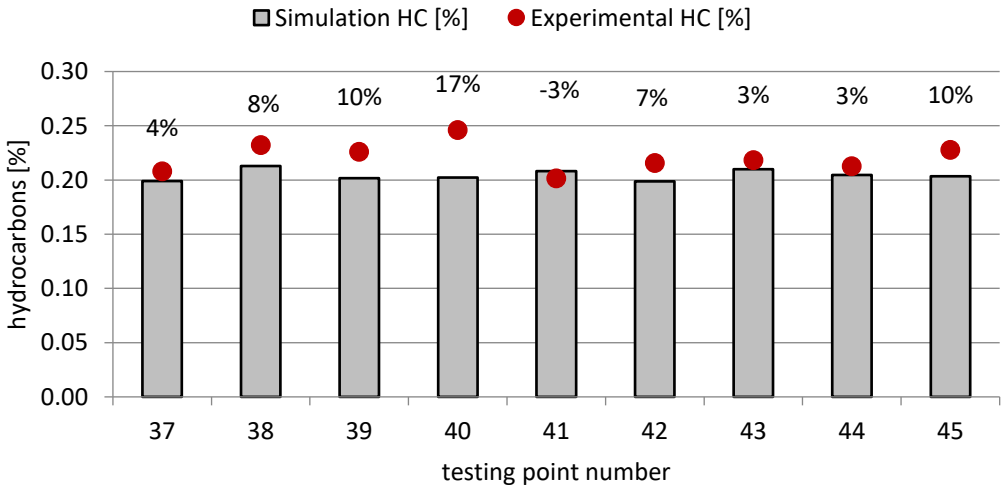

Figure 5.37: Hydrocarbons evaluation for the 1500RPM – 105Nm engine speed – engine load case

Furthermore, for both the 1500RPM-41Nm (Figure 5.38) and 700RPM-28Nm (Figure 5.39) engine cases the Kinetics SRM engine suite is highly under-predicted, with an absolute prediction error of 54% and 79% respectively.

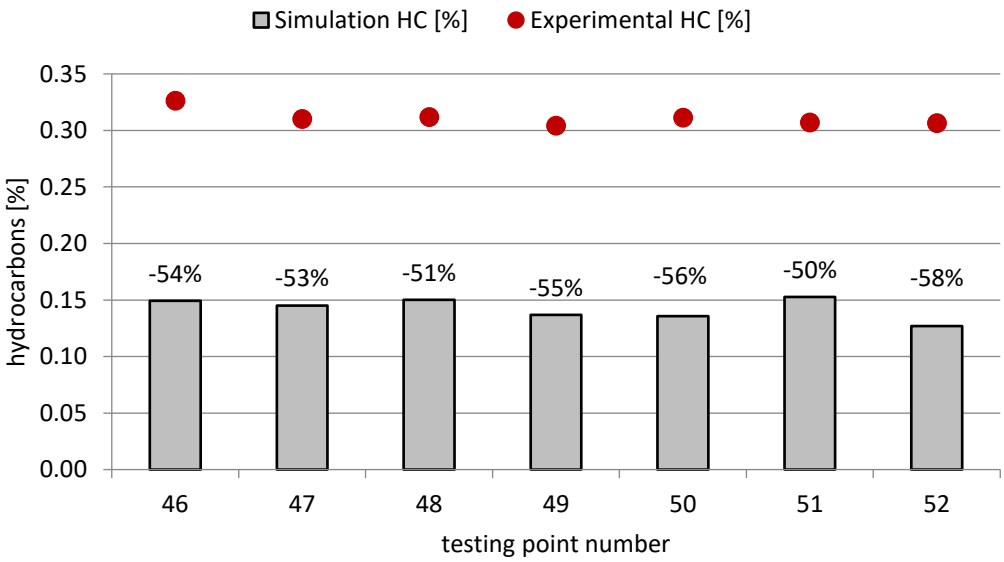

Figure 5.38: Hydrocarbons evaluation for the 1500RPM – 41Nm engine speed – engine load case

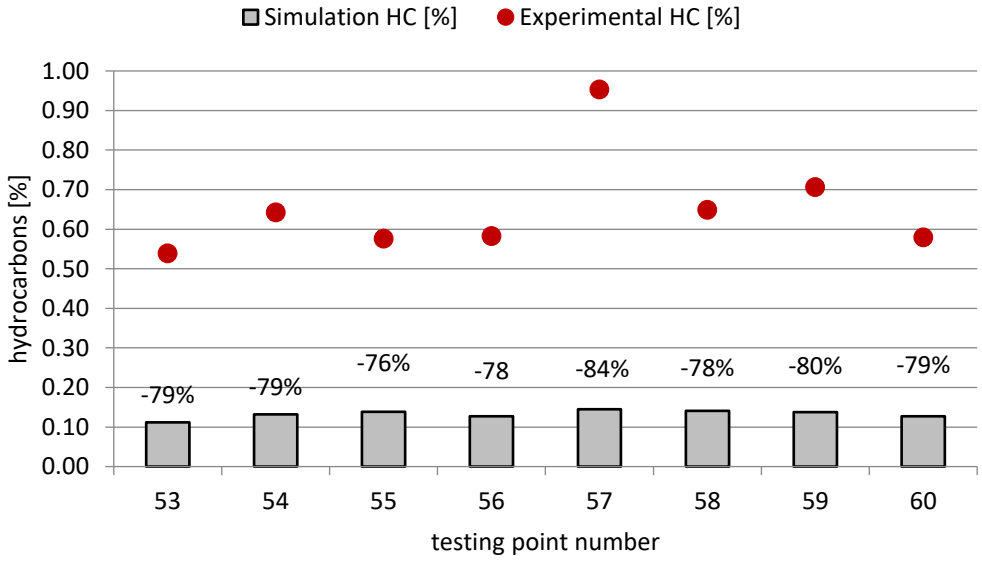

Figure 5.39: Hydrocarbons evaluation for the 700RPM – 28Nm engine speed – engine load case

5.5.2.2 Carbon Monoxide

Moving to the carbon monoxide evaluation, Figure 5.40 shows the over-predicted simulated carbon monoxide concentration for the 2000RPM - 81Nm case.

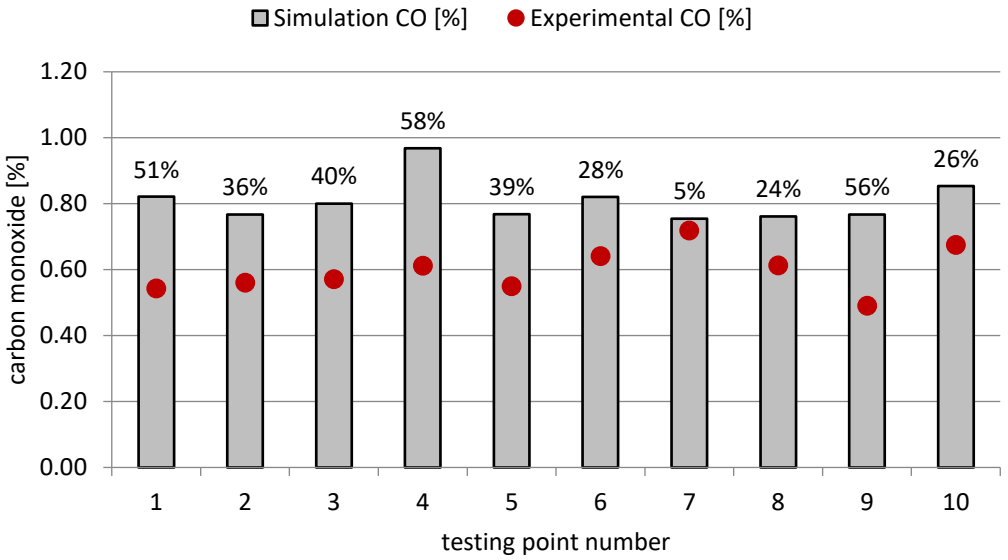

Figure 5.40: Carbon monoxide evaluation for the 2000RPM – 81Nm engine speed – engine load case

As shown in Figure 5.41 below, almost half the concentrations for the 1250RPM - 125Nm engine case were under-predicted but the rest of the testing points agreeing well with the engine test.

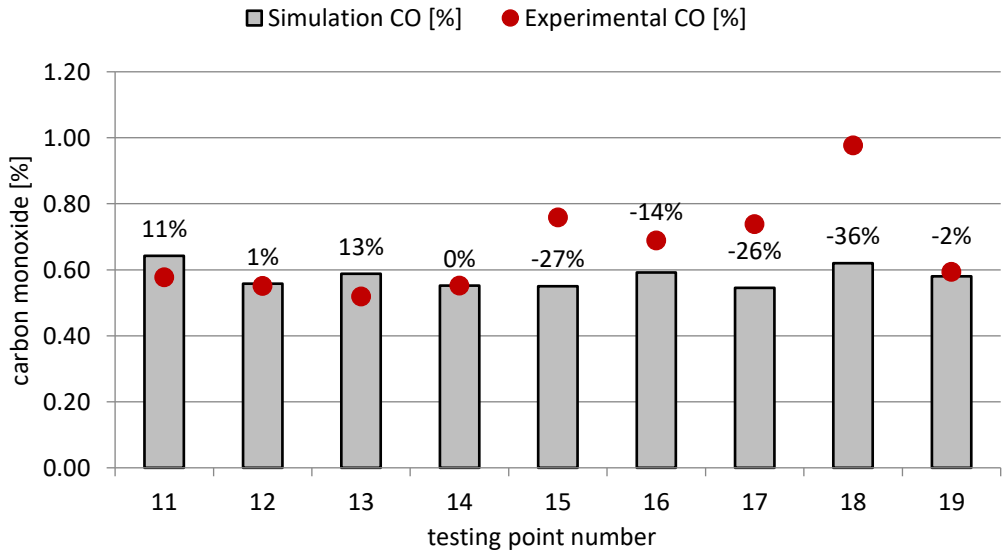

Figure 5.41: Carbon monoxide evaluation for the 1250RPM – 125Nm engine speed – engine load case

Figure 5.43 shows some mixed accuracy levels for the 2000RPM – 199Nm speed – load case, with the carbon monoxide for most of the testing points under predicted and a couple over-predicted simulated values. For this engine case the model managed to get an average prediction value of 10%.

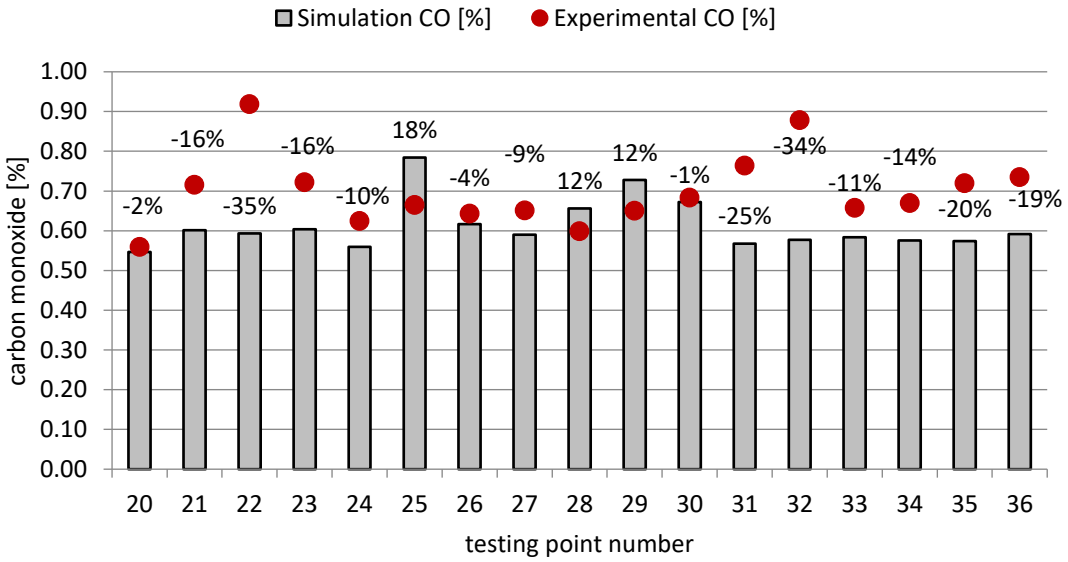

Figure 5.42: Carbon monoxide evaluation for the 2000RPM – 199Nm engine speed – engine load case

In the 1500RPM-105Nm case (see Figure 5.43), carbon monoxide concentration for 4 out of 9 testing points were fairly accurately predicted, whereas for the rest of points the model under-predicts.

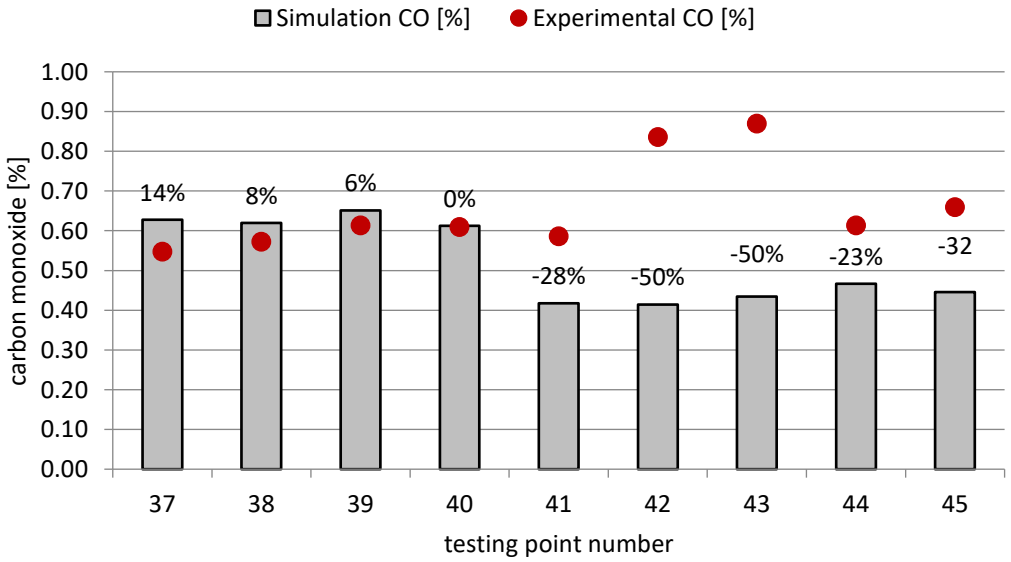

Figure 5.43: Carbon monoxide evaluation for the 1500RPM – 105Nm engine speed – engine load case

Very good prediction accuracy was gained from the simulation results of the 1500RPM – 41Nm case with an average prediction error of 4%. However, as before the model under-predicts the formation of the pollutant for the idle 700RPM-28Nm case, resulting in an average error of 24% (Figure 5.44).

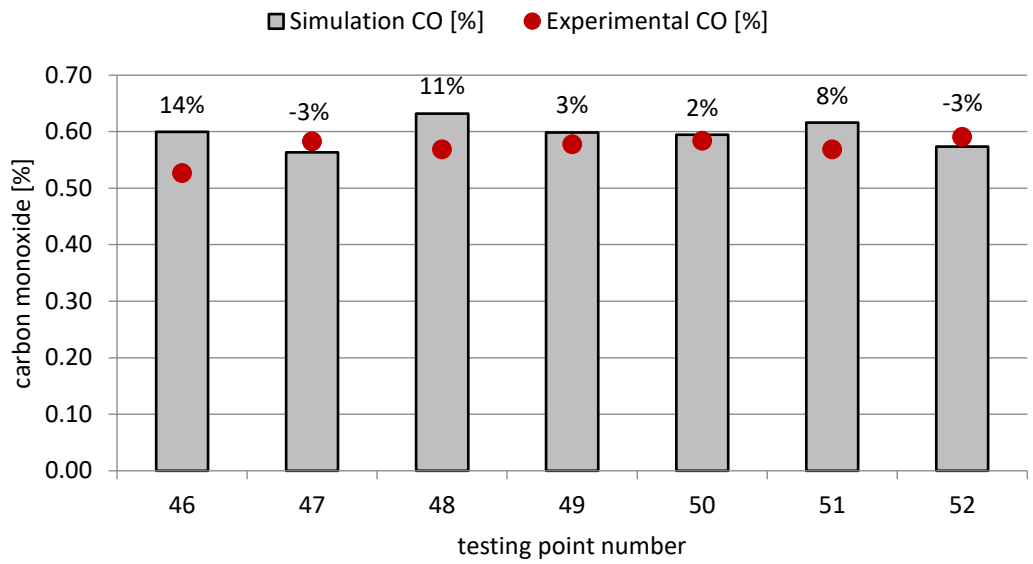

Figure 5.44: Carbon monoxide evaluation for the 1500RPM – 41Nm engine speed – engine load case

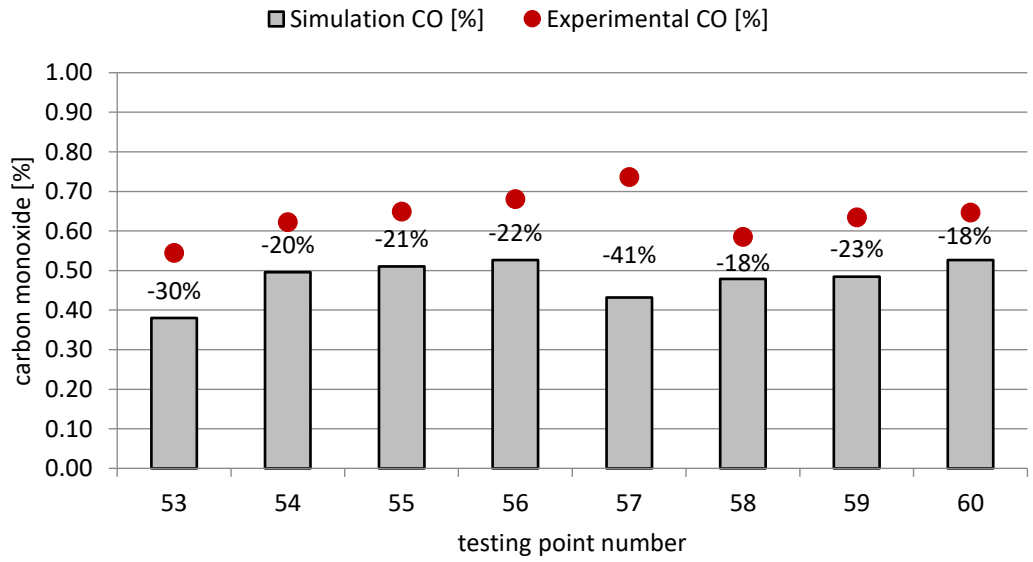

Figure 5.45: Carbon monoxide evaluation for the 700RPM – 28Nm engine speed – engine load case

5.5.2.3 Carbon Dioxide

Continuing with the carbon dioxide simulation results, the Kinetics SRM engine suite was able to accurately predict this emission concentration for all the engine speed – load cases and all the testing points with only an average 1.1% prediction error compared with the experimental values. Figure 5.46 presents the error percentage between the simulated carbon dioxide value and the experimental value, with the highest error levels observed for the 700RPM – 28Nm engine case.

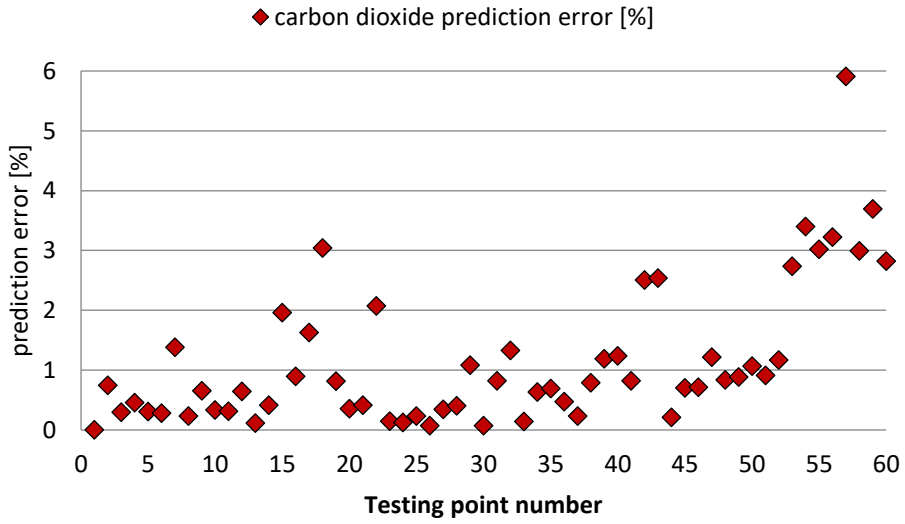

Figure 5.46: Carbon dioxide prediction error percentage for the 60 testing points

5.5.2.4 Particulate Number

Finally, as seen in Figure 5.47 for the particulate number the model had mixed prediction error levels for the testing points of the 2000RPM-81Nm case, over-predicted the 1250RPM-125N and 1500RPM-105Nm, but under-predicted the 2000RPM-199Nm, 1500RPM-41Nm and 700RPM-28Nm runs.

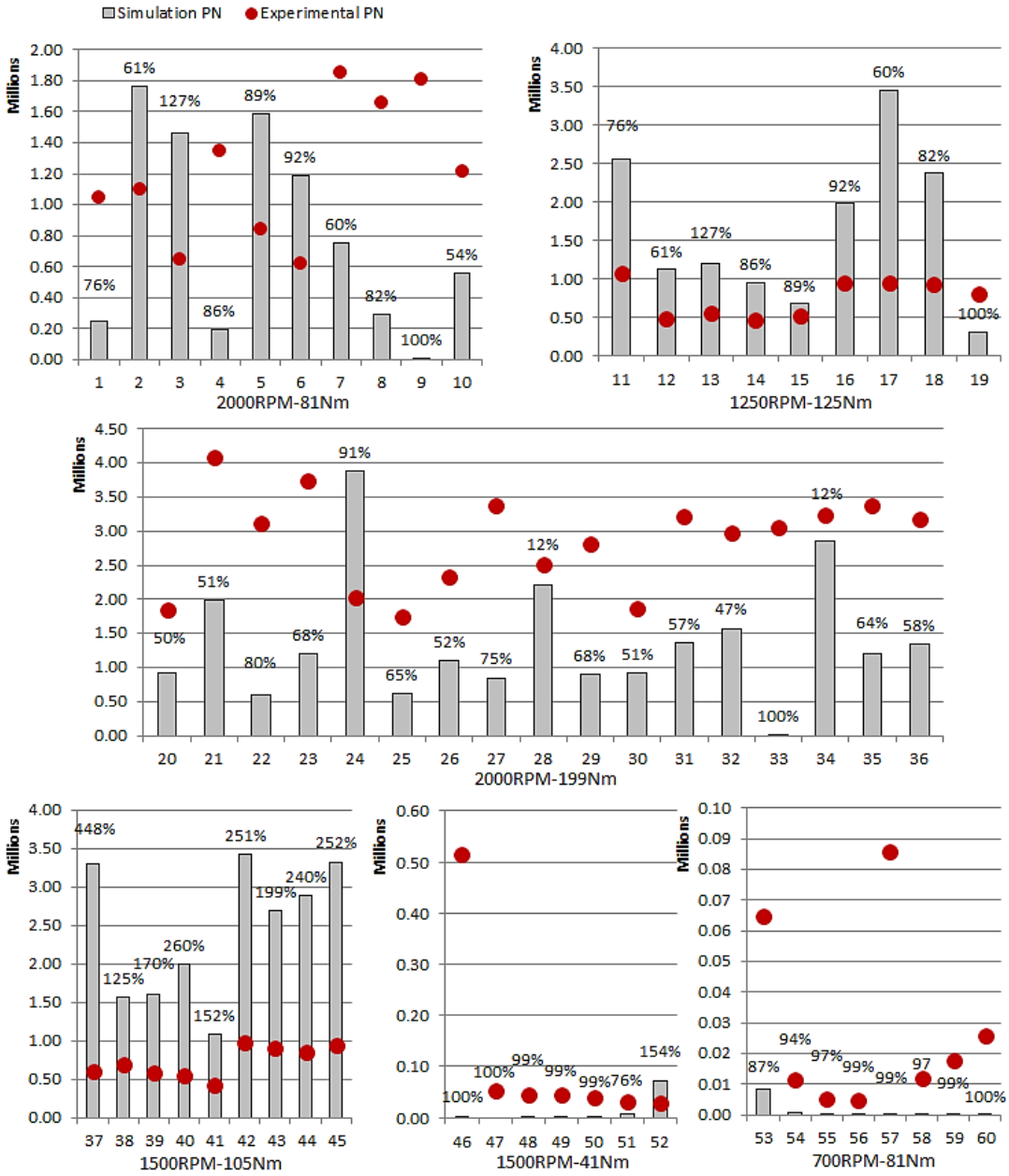

Figure 5.47: Particulate number prediction and error percentage for the 60 testing points

5.6 Evaluation of Simulation Prediction

It is crucial to check how capable the emissions model is at predicting the pollutants while the actuator settings of the engine changes. A single case with the engine running at 1250RPM and 125Nm load was available. This engine case involved 60 testing points distributed along a space-filling design with the following parameters; inlet valves opening (IVO), exhaust valve closing (EVC), fuel rail pressure (FRP) and start of fuel injection (SOI).

For the reason that the emissions model was limited to simulating the closed engine volume, from the closing of the intake valves until the opening of the exhaust valves, hence any direct fuel injection events before the intake valve closing time was disregarded. In order to execute this prediction capability analysis with the available engine data, the in-cylinder pressure profile for each of the 60 points was calibrated separately using the mass fraction burned in each individual engine cycle, along with the model involving a fuel air equivalence ratio parameter.

The analysis was carried out in Matlab MBC toolbox using an RBF Gaussian statistical model to correlate the factors (IVO, EVC, FRP, SOI) with the responses (HC, CO, CO2, PN). The FRP and SOI values were fixed at a relatively standard value and the analysis was focused on how sensitive the emissions model was to changes of IVO and EVC timing. In general, the model responds well with the variations of the valves timing. Prediction accuracy was not the main focus of this investigation, instead the analysis is based on the comparison of the trends between the simulation and the experimental data.

For the hydrocarbons it can be seen in Figure 5.48 that there is a clear trend between the simulation predictions and the measurements for the IVO timing. For the same pollutant the model is able to provide good correlation between simulation and experiment for a shorter combustion, whereas the EVC timing gets farther away from top dead centre and as the duration of the combustion increases the model loses its trend correlation.

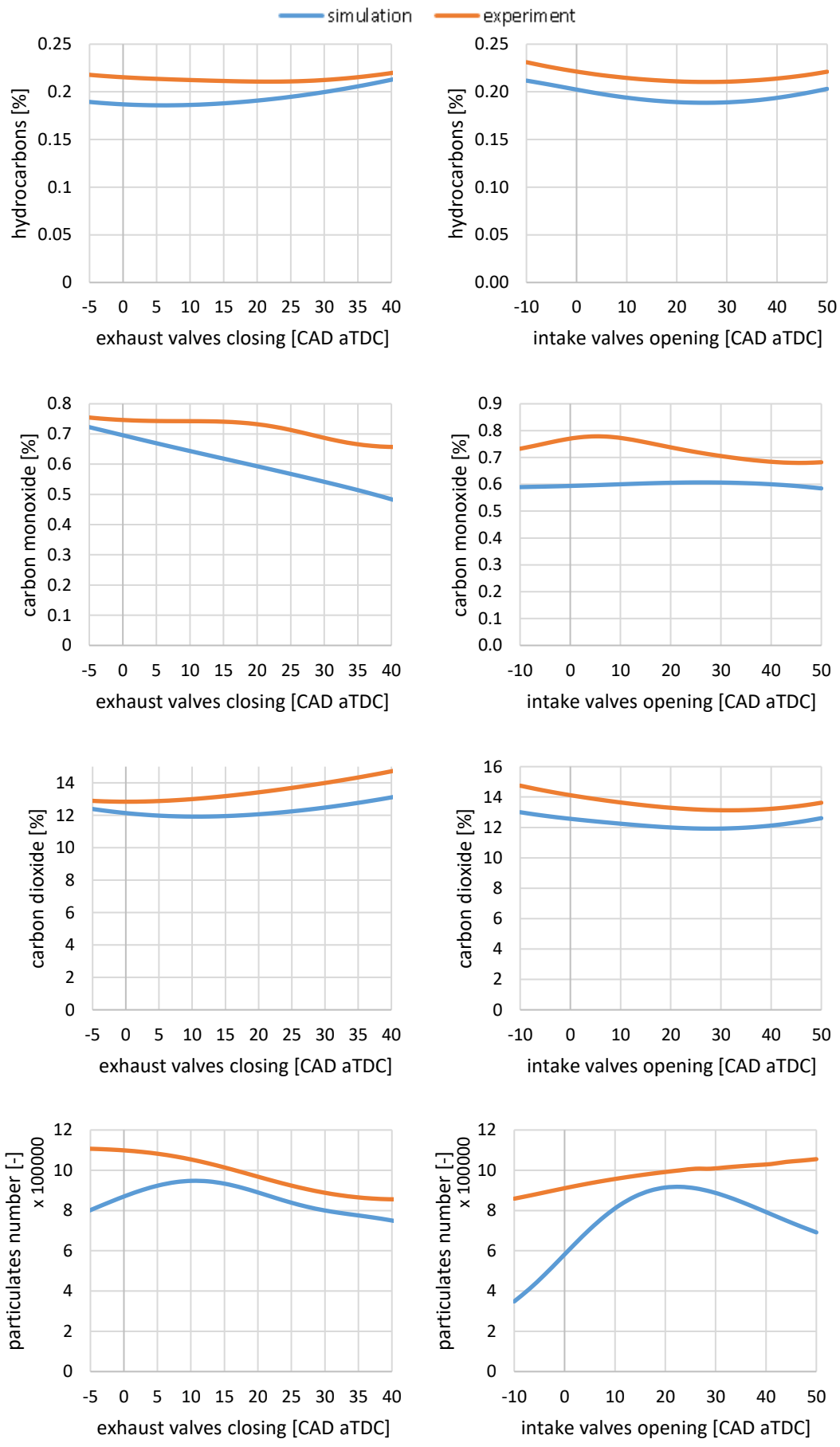

Figure 5.48: Emissions model prediction analysis against valve timing

Similar effect is observed for the carbon monoxide percentage, as the EVC was delayed the simulation cannot sustain a good trend. For the carbon monoxide values against IVO, there was a clear inability of the emissions model to accurately predict the specific pollutant formation around top dead centre. Furthermore, other than a small delay of the simulation to follow the experiment's trend just before EVC at top dead centre, the emissions model gives excellent predictions along the different valves timings for carbon dioxide.

Finally, when comparing the trends for the particulate number, the simulation gives the best prediction after 10 crankshaft angle degree after top dead centre for EVC but only a small section in the middle values of IVO timing agree with the engine measurements for soot. Testing reliability and equipment efficiency must be taken into consideration when measuring soot particles, as well as, the complexity and inability of even modern simulation codes to accurately predict the particulates number. In addition, the emissions model did not involve any direct injection event calculations which would have a different effect on the mixture and consequently the particulates number.

Jarvis et al. (2006) highlights the large spatial variation of the flow inside the cylinder during the intake stroke, which are linked to variations in the compression phase till the opening of the exhaust valves. Even at constant speed, due to the engine instantaneous geometry high cyclic variations are present in the region around the valve jet. In light of all these issues it can be set that overall the simulated predictions of the emissions model are following some trend when compared with the experimental results, however, the predicted results show large errors.

5.7 Chapter Summary

This chapter outlines the development of an emissions formation model based on the Kinetics SRM engine suite. The model was further advanced through sensitivity analyses of the turbulent mixing and heat transfer sub-model. The results of the investigation showed new parameter values that enhance the ability of the model to predict the emissions more accurately as well as more efficiently in terms of simulation time.

6 Multi-physics Simulation Platform Development

6.1 Chapter Introduction

The chapter is divided into three main sections as follows.

- Section 6.2: The development of the engine performance model in GT-SUITE is given, along with the calibration method carried out to match the experimental engine data with the simulation outputs
- Section 6.3: Presents the exhaust aftertreatment system design process in Axisuite
- Section 6.4: Provides the method of structuring and validating the simulation framework. First the coupling between the engine and the combustion model is given in 6.4.1, along with the conversion of the coupled model into a MATLAB Simulink block. Similarly, in 6.4.2 the exhaust aftertreatment model is transferred into the environment of Simulink to finally be linked together with the rest of the system in 6.4.3. A simulation time reduction procedure is introduced into 6.4.4.

6.2 Engine Performance Model

6.2.1 GT-SUITE Model Development

GT-SUITE uses one dimensional gas dynamics to represent the flow and heat transfer in the components of the engine model. These components are linked together with connection objects. Within the components the properties must be defined by the user. A solver module calculates the mass and energy flow through the different components and the results of the calculations are shown in a post-processor module, GT-POST. Furthermore, a model of the AJ133 V8 naturally aspirated GDI engine was built within GT-SUITE. The model is build up from several parts that represent the different components of the engine. Starting from the engine cylinder part, the settings for the cylinder geometry must be defined; bore, stroke, connecting rod length, wrist pin to crank offset, compression ratio, and clearance height, as shown in Figure 6.1.

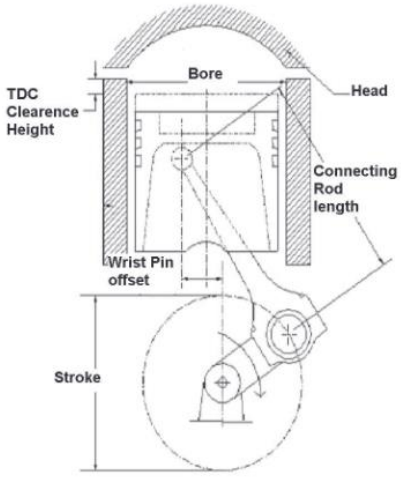

Figure 6.1: Engine cylinder schematic showing the setup of the engine cylinder part in GT-SUITE [330]

These parameters are collected and correspond with the data shown in Table 6.1. The reference state for volumetric efficiency is used strictly as a reference to calculate volumetric efficiency. This object usually corresponds to the ambient conditions. The cylinder combustion mode allows the combustion rate that is calculated in one cylinder by the direct injection jet combustion model to be imposed on upon other cylinders. When cylinder to cylinder variations are not of interest, the use of slave cylinders can reduce computation time compared to independently calculating combustion in each cylinder. Within the cylinder part several models can be used to calculate the conditions in the cylinder. The engine cooling system is heated by the cooling fluid and the compressed air, then because the piston is not directly cooled by the cooling liquid its temperature is always higher than the cylinder head and wall temperature.

Table 6.1: Engine cylinder parameters

Parameter	Value	Units
Bore	92.5	mm
Stroke	93	mm
Connecting rod length	151.75	mm
Compression ratio	11.5	-
TDC clearance height	0.001	mm
Wrist pin to crank offset	1.1	mm

The cylinder parts are connected together via the engine cranktrain part, which also models the crankshaft of the engine and translates the force acting on each piston into the crankshaft output brake power. For this part of the model the engine type, number and configuration of the cylinders, engine speed, engine load, engine friction and start of cycle must be determined. For the engine type a 4-stroke is chosen and the firing order configuration for the V8 banks (defined as A and B) of the engine is given as 1A, 1B, 4A, 2A, 2B, 3A, 3B and 4B. The engine speed, load and friction are set as desired input factors in the case setup where several user-applied parameters can be defined. The start of the cycle value is set to be equal to the intake valve closing time of the first cylinder. This value is specifying the starting angle within a calculated cycle and has no effect on the simulation predictions.

Next, four sets of valves cam parts are attached to each cylinder of the engine model representing the two intake and two exhaust valves of the AJ133. The valve cam object defines the characteristics of a cam-driven valve including its geometry, lift profile, and flow characteristics. Moreover, all the flow channels of the engine, like the manifold pipes, are modelled using the straight pipe and bend pipe objects. The main pipe settings are diameter at inlet and outlet end, length, surface roughness, wall temperature and heat conduction object. As shown in Figure 6.2, the discretization length determines in how many volumes the pipe elements are divided for iteration calculation purposes. Generally, smaller discretization length results in better accuracy and frequency resolution, but at the expense of execution time. The next

parameter is the discretization length. Because only relatively short straight pipes are used, the discretization length is set to the length of the pipes. Since all the pipes used on the AJ133 engine are of the same material (galvanized iron), a surface roughness of 0.02 applies for all the pipes.

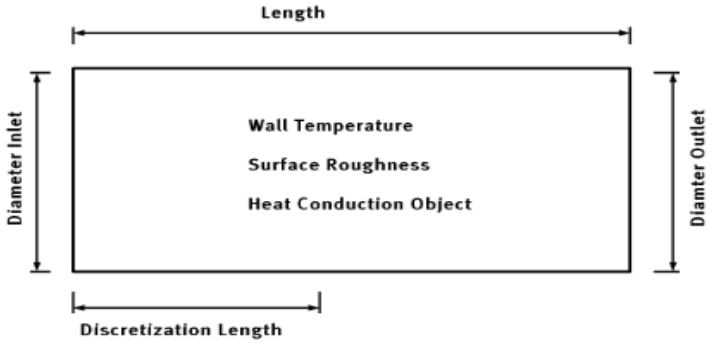

Figure 6.2: Schematic of the straight pipe in GT-SUITE

6.2.2 Calibration Method

The model was calibrated and validated against the engine data from the case study, given in section 4.2. The following data were available through the several engine speeds and engine load points:

- Power, brake torque
- Motoring friction power
- Air flow, fuel flow, air-fuel ratio
- IMEP, BSFC, volumetric efficiency
- Intake and exhaust ports and manifolds pressure and temperature
- Cylinder pressure and combustion rate

The calibration method of the engine model was mainly focused on the highest engine speed case which makes it easier to see the effect of any change at this speed. After tuning the simulation case with the highest speed within the calibration error, then a comparison over the whole range of engine cases is made;

1. Matching the intake manifold. Calibration error within 2%.
2. Calibration of the volumetric efficiency by eliminating any flow loss and heat transfer problems between the intake and manifold measuring point and between manifold measuring point and the cylinder. Also, the

most influential factors on the volumetric efficiency of the engine are the valves, ports, runners, and manifolds plenums; hence adjustment of valve events and matching tuned speeds is required.

3. Matching the cylinder pressure profile during combustion by imposing burn rate fractions
4. Matching the exhaust temperatures with heat transfer parameters for the exhaust ports and tuning the wall temperature solver
5. Calibrating the friction mean effective pressure from measured engine torque data

The volumetric efficiency curve was achieved by comparison of the discharge coefficients of the corresponding intake and exhaust components (valves, manifolds, runners, etc.). The discharge coefficients were provided by the sponsor company from experimental measurements of the flow characteristics through the intake and exhaust manifolds systems. Figure 6.3 demonstrates the change of the volumetric efficiency for two different values for the discharge coefficient of the intake runner.

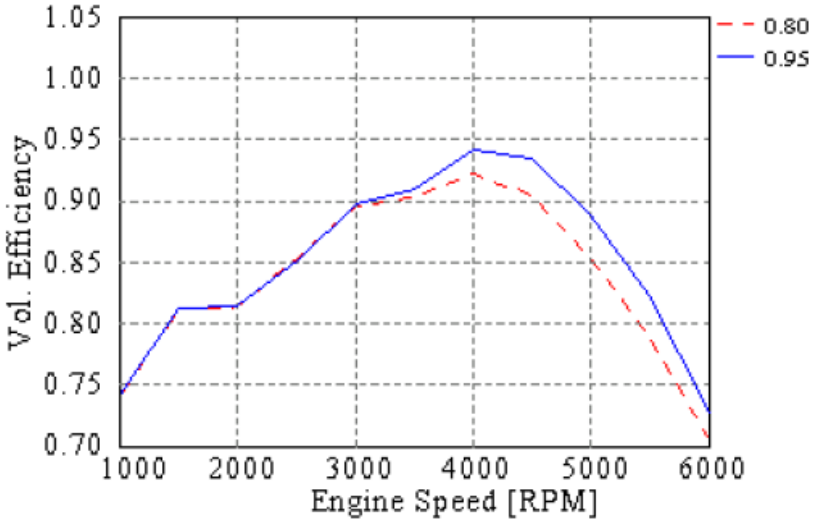

Figure 6.3: Volumetric efficiency curves for different intake runner discharge coefficients [312]

Another crucial factor affecting the volumetric efficiency of the engine is the heat transfer effect, as illustrated in Figure 6.4. Actual experimental measurements were used to describe the thermal properties of the system's

components, as well as to determine the value for the friction mean effective pressure.

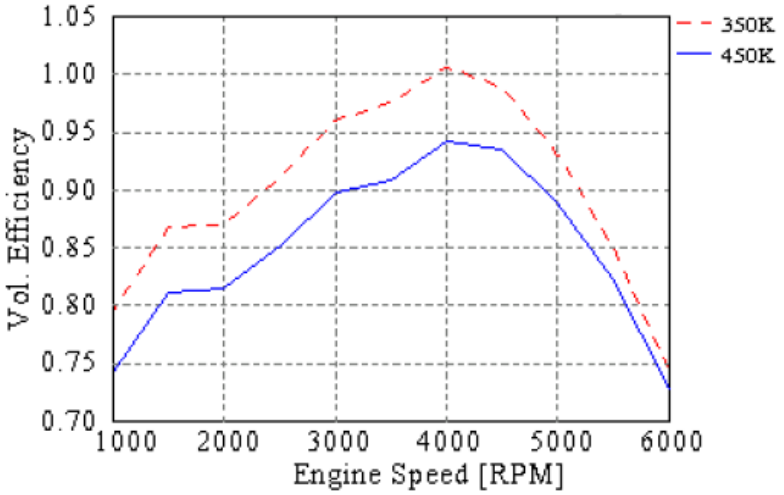

Figure 6.4: Volumetric efficiency curves for different intake port wall temperatures [312]

Once the volumetric efficiency of the engine is calibrated, the next step is matching the in-cylinder pressure profile using the measured mass fraction burn at the start of combustion, during combustion, and finally at the end of the combustion, see Figure 6.5 below. Finally, the brake torque (Figure 6.6), engine power and engine friction were matched with the measured motoring torque data.

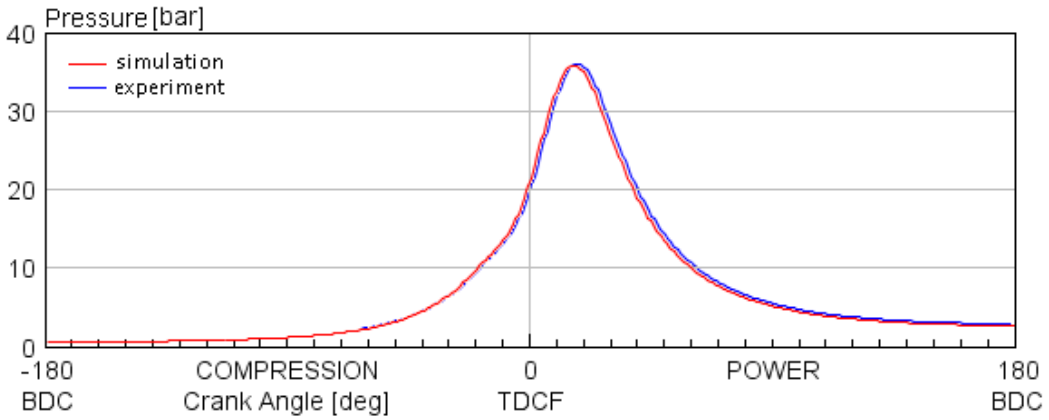

Figure 6.5: In-cylinder pressure profile validation

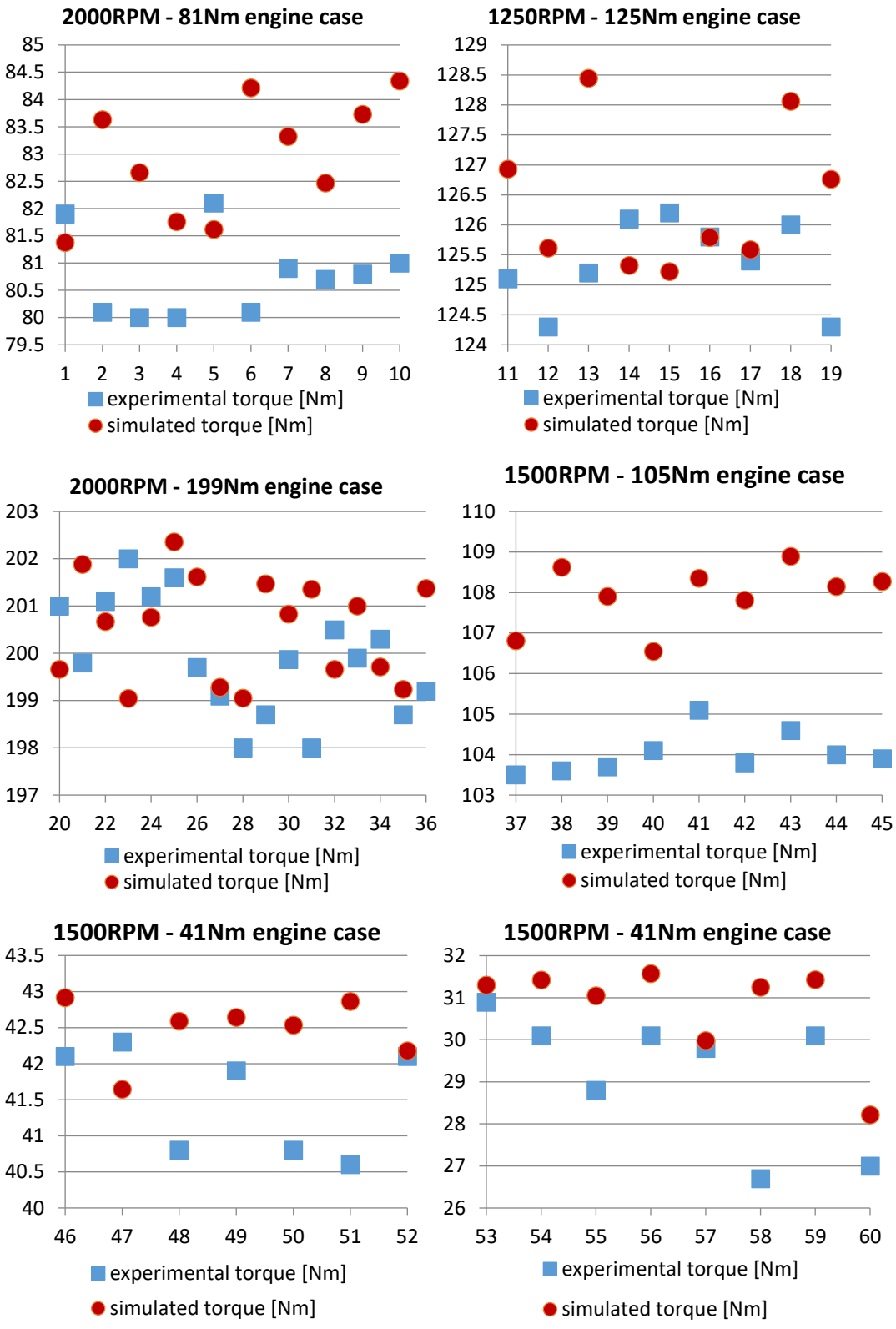

Figure 6.6: Brake engine torque validation

6.3 Exhaust Aftertreatment Model

6.3.1 Design Process

Axicat includes an extensive set of reaction kinetics from Pontikakis and Stamatelos, calibrated to experimental data using a genetic algorithm approach, that can be applied to model any type of catalytic coating [331]. The kinetic rate parameters included in the rate expressions were calibrated for the specific washcoat and catalyst formulation by the sponsor company through transient operation testing and were provided as an encrypted parameters library.

The three-way catalytic converter of the exhaust aftertreatment system was configured based on all the variables that describe the geometrical, thermophysical and chemical properties of the component, as well as initial state, ambient conditions and simulation parameters. The converter initial state was defined by the exhaust gas temperature, mass flow rate and emissions concentrations of the AJ133 V8 GDI engine operating through the EURO 5 NEDC. The simulation time was to equal the NEDC duration with a time step of 1 second. A 1D discretization for both the monolith geometry and washcoat was applied. Moreover, the washcoat consisting of 70% Al_2O_3 and 30% CeO_2 has a substrate length and diameter of 0.152 m and 0.1184 respectively. A cell density of 400 cells per in^2 and substrate thickness of 1.14 x 10^{-4} m defines the channel cross-section, as seen in Figure 6.7 below.

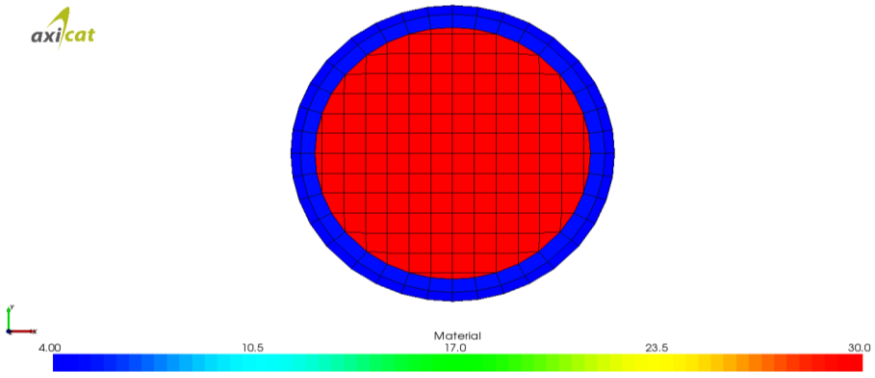

Figure 6.7: Catalyst geometry view in Axisuite

As shown in Figure 6.8, exhaust pipes before and after the catalyst are represented by the pre- and post-catalyst single-wall pipe components. The

exhaust system pipes are configured with a length of 0.2 m and an internal diameter of 0.063 m. Furthermore, the inlet block represents the engine-out gas entering into the exhaust aftertreatment system. All the post-simulation data are stored in the outlet block, which symbolises the exhaust tailpipe.

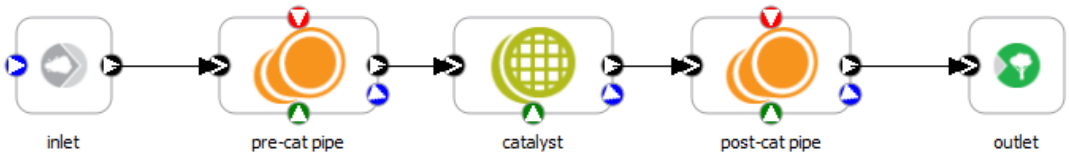

Figure 6.8: AJ133 V8 GDI exhaust aftertreatment system setup in Axisuite

6.4 Simulation Framework Build and Validation

6.4.1 Engine and Combustion Simulink Model

Standalone versions of the GT-SUITE engine performance model and the Kinetics SRM combustion and emissions model have been calibrated and validated against experimental engine data. Furthermore, coupling of the stochastic-based combustion-emissions model with the 1D engine model contributes directly to achieving the goals motivating this work. As seen in Figure 6.9, a combustion template was created in GT-SUITE allowing the external cylinder model object to be linked with the Kinetics SRM code. The template allows the definition and control of all the aspects of the combustion modelling between IVC and EVO, including burn rate, species composition, heat transfer, turbulent mixing, and emissions.

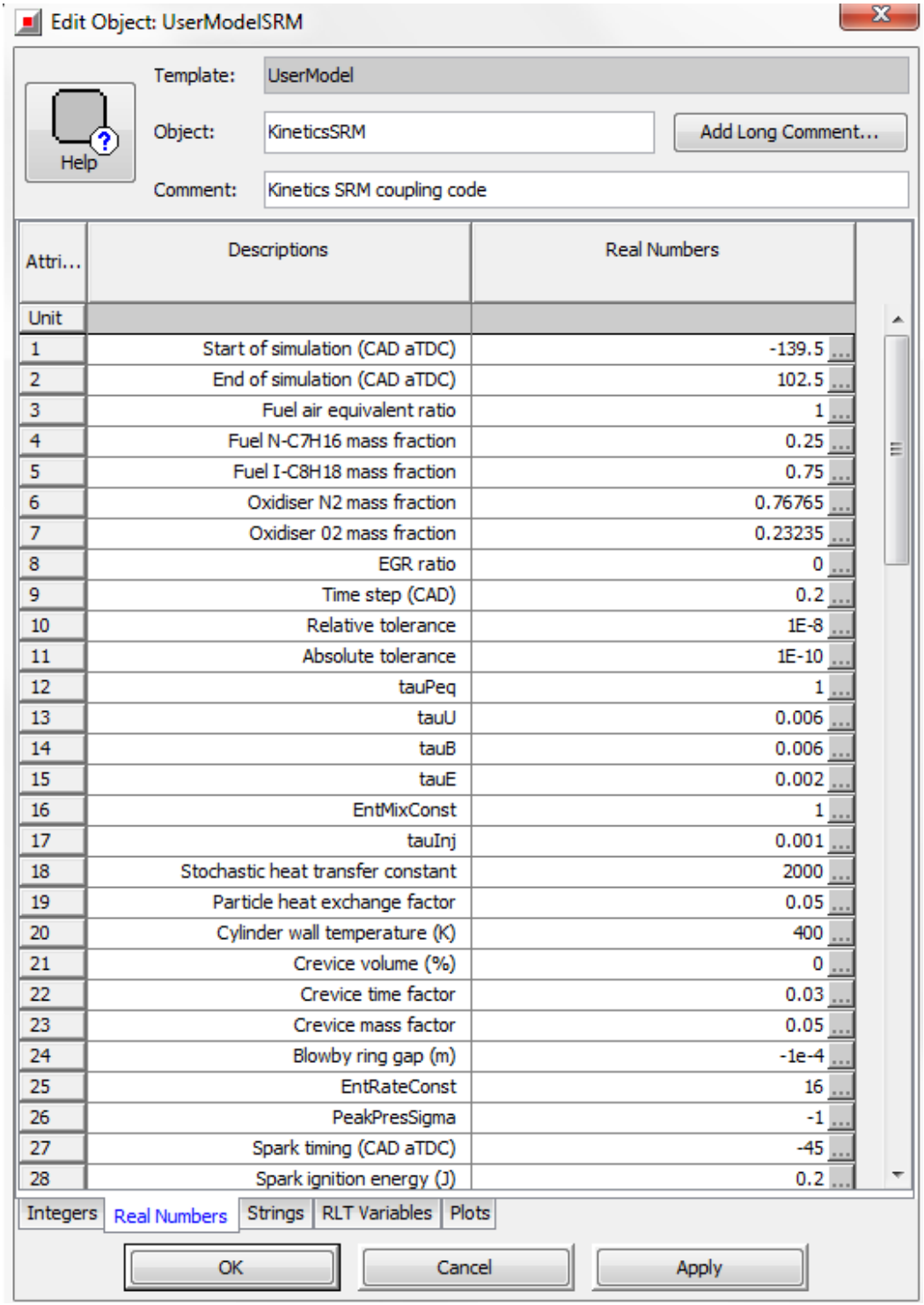

Figure 6.9: Combustion template in GT-SUITE engine model

The combustion is set to initiate the Kinetics SRM code at the 10th cycle of the engine model, allowing this way the engine model to reach steady state conditions. All the internal parameters (number of stochastic particles, turbulent mixing parameters, heat transfer coefficients, etc.) of the Kinetics SRM code are derived from the sensitivity analysis performed in Chapter 5

and used for the combustion template. Any physical parameters like for example cylinder geometry, crevice volume, or wall temperatures were provided by the engine model directly to the combustion template at the imposed starting angle (IVC).

During this phase it was important that the engine performance model was well calibrated to provide the combustion and emissions model with the correct initial conditions set. The results from a preliminary run of 6 engine testing points, one at each engine speed – engine load case, with the co-simulation system were acceptable in terms of engine performance (torque, fuel consumption, etc.) as well as engine-out emissions concentrations.

After the combustion model was implemented into engine performance model, the next step was converting the GT-SUITE model into a S-Function block in the environment of MATLAB Simulink, as shown in Figure 6.10. Engine parameter values were provided to the system using a lookup table block in Simulink, while a bus signal selector was extracting the 4 main signals; brake mean effective pressure, torque, fuel consumption and emissions. The last one was fed to a subsystem for units' conversion and for generating the plots for NOx, CO2, CO, HC and PN.

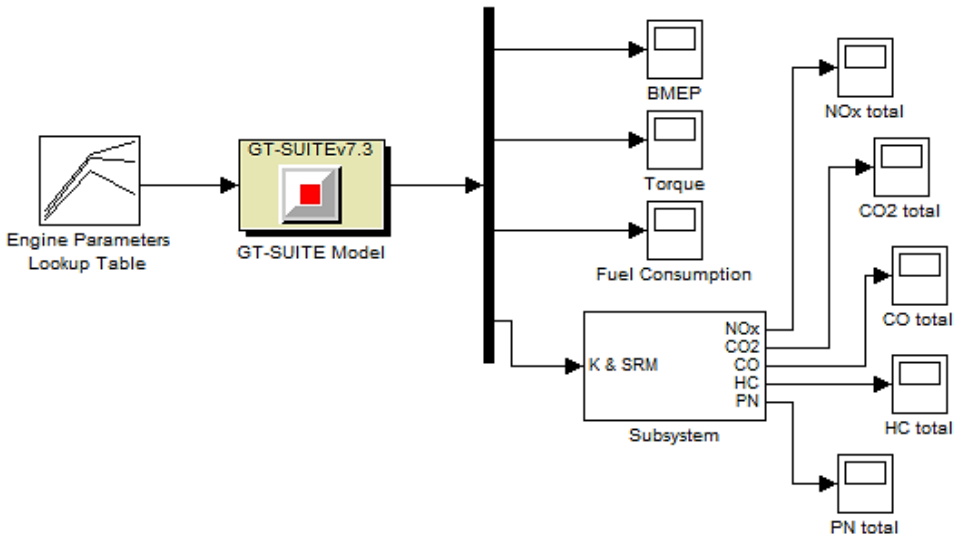

Figure 6.10: GT-SUITE model in the environment of MATLAB Simulink

6.4.2 Exhaust Aftertreatment Simulink Model

Next the exhaust aftertreatment model designed in Axisuite, needed to also be transformed into Simulink blocks so it would eventually link with the engine and combustion part. Axisuite consist of a Fortran-based solver that enables the export of the current model in Simulink S-functions. A limitation of this feature is that the main components of the aftertreatment, e.g. exhaust pipes, catalytic converter, etc. cannot be edited after their transfer to Simulink. Moreover, the exhaust gas and inlet flow streams are bus signals containing the mass flow rate in [kg/s], the gas temperature [K] and the gaseous species concentrations going through the aftertreatment system. As shown in Figure 6.11, the signals are travelling through the blocks representing the exhaust pipe before the catalyst, the catalytic converter itself and the exhaust pipe after the catalyst.

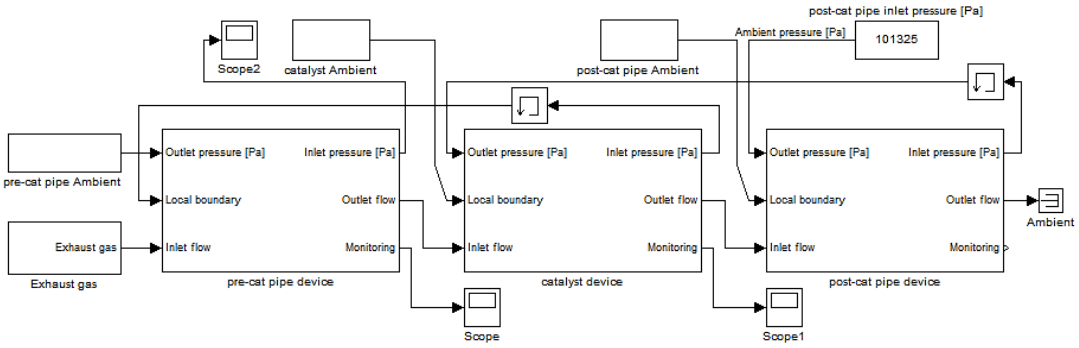

Figure 6.11: Exhaust aftertreatment model in the environment of MATLAB Simulink

6.4.3 Global Simulink Co-Simulation System

With all parts of the multi-domain system re-designed using the graphical user interface of MATLAB Simulink, they were then combined together completing the model-based framework. A single look-up table with all the inputs of the system configures each part of the framework. Key outputs of the engine performance, emissions concentrations and aftertreatment efficiency are stored at the end of each case run in a MATLAB file. As shown in Figure 6.12, the input parameters (e.g. spark timing, valves timing, etc.) are provided to the Engine-Combustion block which is basically the GT-SUITE engine model with the built-in Kinetics SRM code. Simulink monitors the data of the GT-

SUITE engine model through sensor blocks, while actuator blocks control the parameters of GT-SUITE.

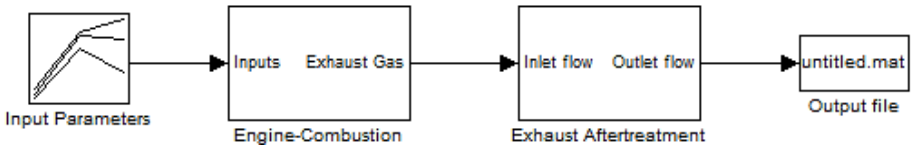

Figure 6.12: Model-based co-simulation of engine combustion and exhaust aftertreatment in the environment of MATLAB Simulink

A single engine testing point at 2000RPM and 199Nm was set to run through the co-simulation system to show that the framework functions satisfactory. The engine model runs on a predefined number of cycles (10 for this case) until it reaches steady state and then one additional engine cycle follows with the Kinetics SRM code engaged on inlet valves closing timing. At the end of the combustion process (opening of the exhaust valves) the Kinetics SRM provides the engine-out emissions concentrations to the exhaust aftertreatment model.

Because Axisuite requires the inputs for the aftertreatment system in a certain way, with the emissions concentrations in a fixed order, a Matlab script was written that reads the Kinetics SRM emissions and copies those values to their corresponding column. The emissions from Kinetics SRM are the sum of a single engine cycle at 2000RPM hence a 60 ms equivalent simulation total time needed to be set in the Axisuite aftertreatment model before exporting the model to Simulink. With the simulation time set the aftertreatment model collects the emissions concentrations from the Kinetics SRM output file to model the efficiency of the catalytic converter.

Finally, a Matlab script reads the outputs of the different simulation stages and writes a brief case summary starting with the control inputs of the engine, the performance output of the engine model, the combustion emissions total and the efficiency of the catalyst. The results from the co-simulation run matches the modelling outputs from the standalone simulation of the 3 software packages. Overall the co-simulation framework was successful, with a total

simulation time of 53 minutes running on a 16GB memory computer with 3.4GHz single-core processor.

6.5 Chapter Summary

The chapter starts by going through the development and calibration processes for the engine performance model in GT-SUITE. Next, the design process for the exhaust aftertreatment model in Axisuite was given. Moreover, the combustion and emissions code was coupled within the engine model and converted into a Simulink black-box model. Following, the exhaust aftertreatment model was also transferred into Simulink and linked with the rest of the system forming the multi-physics co-simulation framework. A single testing point was able to run successfully through the model-based framework proving that such a co-simulation scheme is possible.

7 Discussion

7.1 Overview

The main aim of this research is to develop a model-based multi-physics co-simulation framework of engine, combustion-formed emissions and exhaust aftertreatment. The framework validated through a case study based on a modern GDI V8 engine, has the potential of improving the conventional engine modelling approach of simulating each part of the engine system individually. Moreover, it was a necessity from the project's sponsor, that specific pre-selected commercial software packages are used for this research; GT-SUITE for engine modelling, Kinetics SRM suite for emissions predictions and Axisuite for exhaust aftertreatment analysis. The models will have to be connected, as indicated, using the MATLAB Simulink environment. A drawback of commercial software is that it does not always meet the specific goals of interest and this might reduce the validity of the actual solution. Additionally, getting solutions to a problem requires the input of a professional service firm, which may imply postponing work. For the case of Kinetics SRM engine suite 13 different versions of the software were co-developed through the analysis of this research. Following is a critical review of the strategy taken to conduct this research, including the key developments of the multi-physics modelling system.

7.2 Calibration and Validation of the Stochastic-Based GDI Combustion Model

This research demonstrated the effectiveness of having the Kinetics SRM tool to improve the limitations of the conventional single-cylinder and concept engine methods commonly used in practice. For this reason, a V8 modern GDI engine was available for experimental measurements. The main steps consisted of developing a stochastic-based combustion model, and validating it by direct comparison with experimental data. The development process of the model involved the analysis of the simulation results obtained through sensitivity studies on the number of stochastic particles, as well as the internal parameters of the heat transfer and turbulent mixing sub-models.

The analysis of the number of stochastic particles that are dividing the computational space of the cylinder, showed an almost linear increase of the

time needed for each simulation run, but with a noticeable jump in completion time after the 30 particles. However, when examining to find the best trade-off between simulation time and emissions prediction accuracy, the 25-stochastic particles setup was found to be the optimal setting for the combustion model and it was adopted for the rest of the research.

Furthermore, a stochastic heat transfer constant of 1000 was found to give better simulation results with faster completion time compared to the common 2000 value. When the exchange factor of the stochastic heat transfer was tested at low settings it was noted that it was interacting with the soot sub-model causing it to fail and hence the model was unable to predict any particulate matter. As with before, an optimal accuracy/time value was assigned, at 0.2.

Moving to the parameters of the turbulent mixing sub-model, the mechanical-to-scalar timescale ratio can be ignored in future investigations since it had almost no effect on the simulation outputs. But the turbulent mixing timescale largely affecting the concentrations of hydrocarbons, carbon monoxide and particulates number, was reaching the optimum balance of computational effort and calculated emissions at a timescale of 0.005 seconds, much shorter than the recommended 0.2 seconds.

Nevertheless, a major drawback of the combustion model is the fact that it can only simulate direct injection events after the closing of the intake valves. With a typical GDI engine injecting fuel directly into the cylinder during the intake stroke, the software capability is limited and cannot directly investigate the influence of direct injection events on the combustion characteristics and emissions formation. At the current stage of the simulation package, the best solution was the combination of an equivalence fuel air ratio factor that assumes fully mixed stoichiometric mixture, along with the application of a modified in-cylinder pressure mass fraction burned-based profile. Regardless of not including the fuel injection sub-model into the calculations, the simulation is running more than two times faster compared to a typical model that includes direct fuel injection. This not only enhances the model’s running

time, but it also progressing the model one step closer to real-time simulations.

7.2.1 Integration of Detailed Chemistry-Based Code into 1D Engine Model

Once calibrated the GT-SUITE engine model was able to provide very accurate predictions about the engine performance and in general it is offering a great deal of information about the engine system. After the Kinetics SRM combustion model was validated, it was implemented into GT-SUITE via a user-friendly template that links the engine model with the chemical kinetics module of the stochastic-based combustion tool. It was observed through the release of different versions of the Kinetics SRM, that the chemistry solver of the software has compatibility issues when coupled with the same version of GT-SUITE. This is an internal programming matter of the kinetics SRM suite that the user has no access to it.

Furthermore, an essential limitation of the GT-SUITE was found to be the termination of the multi-processor simulation capability when an external cylinder model, like the Kinetics SRM combustion template, is used. With the combustion model taking around 85% out of the total co-simulation time, the feature of splitting the computational effort on many processor units will be a major achievement and it will advance the system to even reach real-time simulation capabilities.

7.2.2 Formation of Coupled Model-Based Co-Simulation Framework

With the current versions of the software packages successfully linked together through MATLAB Simulink, the system has proven that a global system that covers the engine, emissions and exhaust aftertreatment is possible. However, similar with GT-SUITE coupled with an external combustion object, the standalone simulation of Axisuite has also the disadvantage of not having the feature of engaging more than one processor core to deal with the calculations. The problem of heavy computational effort was significantly increased when the Axisuite exhaust aftertreatment model was converted into S-Function blocks in MATLAB Simulink. The objects representing the components of the catalyst were offering the user very limited

access, therefore any attempt to reduce the complexity of the system was denied.

By combining the restricted access to edit the internal settings of each region of the system, with the multi-physics framework limitation to operate on a single processor unit, the result is an impractical modelling tool. Even though simplifications are made to the system, still the simulation completion time for each run is still too computational costly. At this stage of the research the most feasible solution to this problem is the use of multi-dimensional look-up tables instead of the actual 1D and stochastic models. For instance, a standalone simulation set can be executed in the Kinetics SRM model running on a multi-core machine. The simulation setup will include the calibration settings derived from the parameterization study for optimum emissions prediction accuracy at the lowest possible simulation time. The simulation outputs will then be used to form a high-resolution combustion map, which can replace the combustion model and reduce the simulation time to a great extent. The same procedure can be utilised for the standalone Axisuite simulation, but with the main difference of running the simulation on only one processor.

7.2.3 System Reduction Procedure

Although the different domain parts of the system were proven to be compatible and a preliminary simulation run was successful, it was noticeable that the simulation time needed to complete each engine case increased dramatically compared to the sum of time required to run the models in standalone simulation. Some of the several possibilities that could be causing the system to run slowly are the complex MATALB S-functions which are called at each time step and the time step size itself. With a smaller time step the system is able to capture important events during the simulation, conversely, a step size that is too small will produce more output points than necessary and slow down the simulation. The simulation speed could also be affected if the model is very complex, involving a lot of model referencing and subsystems.

The system reduction process is mostly oriented at achieving the key objective of speeding up the co-simulation time. The heaviest subsystem in

terms of computational effort was identified to be the Kinetics SRM code working within GT-SUITE. Hence, the combustion process computational time reduction is achieved by reducing the number of Kinetics SRM-active cylinders from 8 down to just one cylinder in the GT-SUITE/Kinetics SRM coupled model. In this way all the computations are solved for cylinder no.1 without significantly losing simulation accuracy. Furthermore, the 1D engine performance model may achieve shorter simulation times by combining the pipes and flow splits to form bigger and simpler volumes, thus allowing the system to take bigger time steps. Yet this process will require for the engine model to be re-calibrated for prediction accuracy. Correct heat transfers coefficients and the geometric variations of the model should change accordingly, but maintaining the quality of the model.

Still, most of the subsystems of the overall Simulink framework cannot be reduced furthermore or altered at all due to the limited function block characteristics. However, the reduction of the simulation completed time can be achieved by simplifying the model-based framework by means of replacing the computational heavy parts of the system with look-up tables, thus not compromising the system's prediction capability. For instance, a standalone simulation of Kinetics SRM can be executed for the full operating conditions of the engine under investigation and therefore produced an emissions concentrations look-up table to be used within the Simulink framework.

8 Conclusions and Future Work

8.1 Conclusions

The main conclusions of the work presented in this thesis can be summarised as follows:

- The parameterisation study for the internal parameters of the combustion model enabled faster simulation runs with higher prediction accuracy for engine-out emissions.
- Considering the results attained from applying the new settings of the parameters, the combustion model proved that can deliver high quality CO and CO2 emissions predictions and produce good trends for all the emission pollutants.
- Development and application of a novel model-based multi-physics co-simulation framework that covers aspects like engine power, fuel consumption, exhaust emissions, and aftertreatment performance for a GDI V8 engine
- It was demonstrated that coupling different modelling software together is possible via an integration platform based on MATLAB Simulink environment, however modifying specific sub-models proved to be currently inaccessible.
- The model-based framework allows new calibration studies to be performed which enables optimisation algorithms and control development
- There is still a need to develop a simulation platform which offers transient engine cycle capability and flexibility

8.2 Future work

Some future research improvements of the implemented model-based multi-physics co-simulation framework are listed as following:

- Further development and study of the combustion model by considering other approaches which are focused on the direct injection events taken into consideration in the simulation

- Additional work is needed to address the computational efficiency of the co-simulation framework by applying model reduction techniques, for which ensuring the quality of the system is preserved

References

[1] A. Martyr and M. Plint, Engine testing: Theory and Practice, 3rd ed., Elsevier: Technology & Engineering, 2012.

[2] Y. Rosefort, A. Wiartalla, H. Kwee and S. Pischinger, “Exhaust aftertreatment integrated, DOE-based calibration,” SAE International 2012-01-1303, 2012.

[3] G. Merker, Simulating Combustion Simulation of Combustion and Pollutant Formation for Engine Development, Berlin: Heidelberg: Springer - Verlag, 2006.

[4] G. D'Errico, G. Ferrari and A. Onovati, “Modelling the pollutant emission from a SI engine,” *SAE Paper,* no. 2002-01-0006, 2002.

[5] J. Appel, H. Bockhorn and M. Frenklach, “Kinetic modeling of soot formation with detailed chemistry and physics,” *Combustion and Flame,* vol. 121, no. 1-2, pp. 122-136, 2000.

[6] R. D. Reitz, “Princeton,” 27 June 2012. [Online]. Available: http://www.princeton.edu/cefrc/Files/2012%20Lecture%20Notes/Reitz/Princeton-CEFRC1.pdf. [Accessed 1 December 2013].

[7] A. Bhave, J. Ehteridge, A. Smaillbone and S. COble, “Optimisation of injection strategy, combustion characteristics and emissions for IC engines using advanced simulation technologies,” *SAE Technical Paper,* no. 2011-26-0080, 2011.

[8] A. Smallbone, A. Coble, A. Bhave and S. Mosbach, “Implementing detailed chemistry and in cylinder tratification into 0/1D IC engine cycle simulation tools,” *SAE Technical Paper,* no. 2011-01-0849, 2011.

[9] J. Etheridge, S. Mosbash, M. Kraft and H. Wu, “A detailed chemistry multi cycle simulation of a gasoline fueled HCCI engine operated with NVO,” *SAE International,* vol. 2, no. 1, pp. 13-27, 2009.

[10] S. Kubo, M. S. Celnik, A. Raj and K. O. Kim, “Towards a detailed soot model for internal combustion engines,” *Combustion and Flame,* vol. 156, no. 6, pp. 1156-1165, 2009.

[11] L. Cao, H. Su, S. Mosbach and M. Kraft, “Studing the influence of direct injection on PCCI combustion and emissions at engine idle condition using two dimensional CFD and Stochastic reactor model,” *SAE Technical Paper,* no. 2008-01-0021, 2008.

[12] F. Mauss, M. Kraft, H. Su, S. Mosbach and J. X. Wang, “Dual injection HCCI engine simulation using a stochastic reactor model,”

International Journal of Engine Research, vol. 8, no. 1, pp. 41-50, 2007.

[13] G. C. Koltsakis, C. K. Dardiotis, Z. C. Samaras, M. Frey, G. Wenninger, B. Krutzsch and O. A. Haralampous, “Model-based Optimization of Catalyst Zoning in Diesel Particulate Filters,” SAE, 2008.

[14] G. Koltsakis, S. Skarlis, T. Nastos, D. Karamitros, C. Vogt and S. Sakashita, “Model based optimization of advanced SCR substrates,” *International Journal of Automotive Engineering,* vol. 6, no. 2, pp. 45-52, 20015.

[15] A. Pedlow, G. McCullough, A. Coguet and K. Hansen, “Optimization of Kinetic Parameters for an Aftertreatment Catalyst,” SAE International, 2014.

[16] C. KinYip, O. Andrzej, K. Volkov and O. Duran, “Comparison of Engine Simulation Software for Development of Control System,” *Modelling and Simulation in Engineering,* vol. 2013, p. 21, 2013.

[17] Gamma Technologies, *GT-SUITE engine performance application manual,* Gamma Technologies Inc, 2012.

[18] CMCL Innovations, “CMCL Innovations,” 2015. [Online]. Available: http://www.cmclinnovations.com/. [Accessed August 2015].

[19] Exothermia, “Exothermia,” Exothermia S.A, 2015. [Online]. Available: http://exothermia.com/. [Accessed 2015].

[20] Mathworks, “Mathworks,” The MathWorks, Inc., 2015. [Online]. Available: http://uk.mathworks.com/. [Accessed 2015].

[21] S. Mosbach, H. Su, M. Kraft, A. Bhave, F. Mauss and Z. Wang, “Dual injection HCCI engine simulation using a stochastic reactor model,” *International Journal of Engine Research,* vol. 8, no. 1, pp. 41-50, 2007.

[22] H. Su, A. Vikhansky, S. Mosbach, M. Kraft, B. A, T. Kobayashi and F. Mauss, “A computational study of an HCCI engine with direct injection during gas exchange,” *Combustion and Flame,* vol. 147, no. 1-2, pp. 118-132, 2006.

[23] A. Bhave, M. Balthasar, M. Kraft and F. Mauss, “Analysis of a natural gas fueleed homogeneous charge compression ignition engine with exhaust gas recirculation using a stochastic reactor model,” *International journal of engine research,* vol. 5, no. 1, pp. 93-104, 2004.

[24] S. Mosbach, M. Kraft, A. Bhave, F. Mauss, J. Mack and R. Dibble, “Simulating a homogeneous charge compression ignition engine fuelled with a DEE/EtOH blend,” SAE Paper, 2006.

[25] A. Aldawood, S. Mosbach and M. Kraft, “HCCI combustion phasing transient control by hydrogen-rich gas,” SAE, 2009.

[26] S. Mosbach, A. M. Aldawood and M. Kraft, “Real-time evaluation of a detailed chemistry HCCI engine model using a tabulation technique,” *Combustion Sciense and Technology,* vol. 156, no. 6, pp. 1156-1165, 2008.

[27] S. Mosbach, M. Celnik, A. Raj, M. Kraft, H. Zhang, S. Kubo and K. Kim, “Towards a detailed soot model for internal combustion engines,” *Combustion and flame,* vol. 156, no. 6, pp. 1156-1165, 2010.

[28] R. Aaron, A. Smallbone and A. Bhave, “Implementing detailed chemistry and in-cylinder stratification into 0/1-D IC engine cycle simulation tools,” SAE international, 2011.

[29] K. Frojd, C. Perlman, A. Tuner and F. Mauss, “Lund Combution Engineering,” 2011 2011. [Online]. Available: http://www.loge.se/pdf/FINAL_1D%20Engine%20Modeling%20with%20Detailed%20Reaction%20Kinetics-SFFlameDays2011.pdf. [Accessed October 2013].

[30] CARB, “California Air Resources Board History,” November 2010. [Online]. Available: http://www.arb.ca.gov/knowzone/history.htm. [Accessed August 2013].

[31] CARB, “California 3900 Air Resources Board,” January 2010. [Online]. Available: http://www.ebudget.ca.gov/2013-14/StateAgencyBudgets/3890/3900/department.html. [Accessed August 2013].

[32] EPA, “U.S. Environmental Protection Agency,” 2013. [Online]. Available: http://www.epa.gov. [Accessed 10 August 2013].

[33] EEA, “European Environment Agency,” 2013. [Online]. Available: http://www.eea.europa.eu. [Accessed 10 August 2013].

[34] Xinhua, “China Daily,” 7 7 2004. [Online]. Available: http://www.chinadaily.com.cn. [Accessed 20 11 2012].

[35] SIAM, “Society of Indian Automobile Manufacturers,” 2001. [Online]. Available: www.siamindia.com. [Accessed August 2012].

[36] ADIT, “Australian Department of Infrastracture and Transport,” 2013. [Online]. Available: https://www.infrastructure.gov.au/roads/environment/emission/index.aspx. [Accessed August 2013].

[37] Yamaguchi and K. Jack, World Cars 1979, Herald Books, 1979.

[38] M. P. Walsh, “Carlines,” 2004. [Online]. Available: www.walshcarlines.com. [Accessed November 2012].

[39] J. Corporation, “Facts and Info 2001: A Guide to Japan's Auto Industry,” in *JAN Corporation 2001*, Tokyo, 2001.

[40] JAMA, “Japan Automobile Manufacturers Association, Inc,” Feb 2016. [Online]. Available: http://www.jama-english.jp/publications/MVS2015.pdf. [Accessed Feb 2016].

[41] M. o. t. Environment, “Motor Vehicle Exhaust Emission Standards,” Ministry of the Environment Government of Japan, 2015. [Online]. Available: http://www.env.go.jp/en/air/aq/mv/standards_table.html. [Accessed 2015].

[42] WHO, “Air Quality Guidelines for Particulate Matter, Ozone, Nitrogen Dioxide and Sulfur Dioxide Global Update,” World Health Organization, Copenhagen, 2005.

[43] B. Giechaskiel and G. Martini, “Review on engine exhaust sub-23 nm particles,” Joint Research Centre, Luxembourg, 2014.

[44] H. Seong, S. Choi and K. Lee, “Examination of nanoparticles from gasoline direct injection engines using transmission electron microscopy,” *International Journal of Automotive Technology,* vol. 15, no. 2, pp. 175-181, 2014.

[45] EEA, “European Environmental Agency,” 20 November 2010. [Online]. Available: www.eea.europa.eu. [Accessed 30 11 2012].

[46] EC, “Implementing and amending regulation No 715/2007 of the European Parliament and of the council on type-approval of motor vehicles with respect to emissions from light passenger vehicles and on access to vehicle repair and maintenance information,” *Official Journal of the European Union,* no. 199, pp. 1-135, 2008.

[47] A. Mamakos, “Feasibility of introducing particulate filters on gasoline direct injection vehicles,” Publications Office of the European Union, Luxembourg, 2011.

[48] EPA, “US Environmental Protection Agency,” 18 December 2012. [Online]. Available: http://www.epa.gov/otaq/standards/. [Accessed 1 December 2013].

[49] J. Erjavec, Automotive Technology: A Systems Approach: A Systems Approach, 5th ed., Delmar Cengage Learning, 2009.

[50] K. Jyotindra, Dynamometer: Theory and Application to Engine Testing, Xlibris Corporation , 2012.

[51] G. Karl-Heinrich and E. K. Antonsson, Springer Handbook of Mechanical Engineering: Volume 10, Springer, 2009.

[52] D. Gruden and W. Berg, Traffic and Environment: Volume 3, Springer, 2003.

[53] K. Brundell-Freij and E. Ericsson, “Influence of street characteristics, driver category and car performance on urban driving patterns,” *Transportation Research Part D: Transport and Environment,* vol. 10, no. 3, pp. 213-229, 2005.

[54] MOE, “Japan Ministry of the Environment,” 2013. [Online]. Available: http://www.env.go.jp/en/air/. [Accessed 10 August 2013].

[55] T. J. Barlow, S. Latham, I. S. McCrae and P. G. Boulter, “Department for Transport UK,” June 2009. [Online]. Available: https://www.gov.uk/government/uploads/system/uploads/attachment_data/file/4247/ppr-354.pdf. [Accessed September 2013].

[56] R. Shinko, “Japan External Trade Organization,” March 2008. [Online]. Available: http://www.jetro.go.jp/ttppoas/special/env_rep2_english/surveyreport.pdf. [Accessed September 2013].

[57] EEA, “European Union Emission inventory report 1990-2008,” *EEA Technical,* no. No 7/2010, 2010b.

[58] EC, “Regulation No. 443/2009 of the European Parliament and of the Council of 2009 setting emmission performance standards for new passenger cars,” *Official Journal of the European Union ,* no. 140, pp. 1-15, 2009b.

[59] UNECE, “WORLDWIDE HARMONIZED MOTORCYCLE EMISSIONS CERTIFICATION PROCEDURE,” 2004.

[60] UNECE, “United Nations Economic Commision for Europe,” 2013. [Online]. Available: http://www.unece.org/trans/main/welcwp29.html. [Accessed September 2013].

[61] JRC, “European Commission JRC,” September 2011. [Online]. Available: http://publications.jrc.ec.europa.eu/repository/bitstream/111111111/22907/2/reqno_jrc66031_lbna24921enn.pdf. [Accessed September 2013].

[62] ECJ, “European Commision,” 2011. [Online]. Available: http://ec.europa.eu/clima/policies/transport/vehicles/docs/2011_pems_jrc_62639_en.pdf. [Accessed September 2013].

[63] J. B. Heywood, Internal Combustion Engine Fundamentals, New York: McGraw-Hill, 1988.

[64] Waulis, “Waulis,” Waulis Motors Ltd, 2015. [Online]. Available: http://waulis.com/. [Accessed August 2015].

[65] Hilite, “Hilite International,” Hilite International Inc, 2010. [Online]. Available: http://www.hilite.com/. [Accessed August 2015].

[66] M. Hitomi, J. Sasaki, K. Hatamura and Y. Yano, “Mechanism of Improving Fuel Efficiency by Miller Cycle and Its Future Prospect,” SAE Technical Paper, 1995.

[67] C. Wang, R. Daniel and H. Xu, “Research of the Atkinson Cycle in the Spark Ignition Engine,” SAE Technical Paper, 2012.

[68] S. Taniguchi, K. Yoshida and Y. Tsukasaki, “Feasibility Study of Ethanol Applications to A Direct Injection Gasoline Engine,” SAE Technical Paper, 2007.

[69] J. M. Atkins and C. R. Koch, “A well-to-wheel comparison of several powertrain technologies,” SAE Paper, Detroit, 2003.

[70] J. Kirwan, M. Shost, G. Roth and J. Zizelman, “3-Cylinder Turbocharged Gasoline Direct Injection: A High Value Solution for Low CO2 and NOx Emissions,” *SAE Int. J. Engines,* vol. 3, no. 1, pp. 355-371, 2010.

[71] W. Bandel, “The turbocharged GDI engine: boosted synergies for high fuel economy plus ultra-low emission,” SAE, Detroit, 2006.

[72] N. Fraser and H. Blaxill, “Engine downsizing and the application of gasoline direct injection to a high specific output turbocharged engine,” in *Fuel economy and engine downsizing seminar proceedings*, 2004.

[73] FEV, “FEV GmbH,” October 2009. [Online]. Available: http://www.fev.com/fileadmin/user_upload/Media/EngineeringServices/PassengerCarGasolineEngines/159_TecInfo_FEV_GT2-Reducing_CO2_of_Engines_by_2_stage_Turbo_charging.pdf. [Accessed August 2015].

[74] N. Cavina, A. Borelli, L. Calogero and R. Cevolani, “Turbocharger Control-Oriented Modeling: Twin-Entry Turbine Issues and Possible Solutions,” *SAE Int. J. Engines,* vol. 8, no. 5, pp. 2120-2132, 2015.

[75] J. Theis, U. Gobel, M. Kogel and T. Kreuzer, “Phenomenological Studies on the Storage and Regeneration Process of NOx Storage Catalysts for Gasoline Lean Burn Applications,” SAE Technical Paper, 2002.

[76] S. Philipp, R. Hoyer, F. Adam and S. Eckhoff, “Exhaust Gas Aftertreatment for Lean Gasoline Direct Injection Engines - Potential for Future Applications,” SAE Technical Paper, 2013.

[77] P. Venkataramana, “Homogeneous charge compression ignition engine,” *International Journal of Engineering Research & Technology,* vol. 2, no. 2, pp. 2278-0181, 2013.

[78] A. K. Singh and M. K. Paswan, “Homogeneous Charge Compression Ignition Engine,” *International Journal of Mechanical Engineering and Robotics Research,* vol. 3, no. 1, pp. 204-215, 2014.

[79] F. Zhao, M. Lai and D. Harrington, Automotive spark-ignited direct injection gasoline engines, Oxford: Pergamon, 2000.

[80] L. Araneo, A. Coghe, G. Brunello and R. Dondé, “Effects of Fuel Temperature and Ambient Pressure on a GDI Swirled Injector Spray,” SAE Technical Paper, 2000.

[81] H. Edtmayer, S. Schmidt, S. Leiber and T. Schabetsberger, “Design of a Tumble-Orientated Intake Port Layout for a Gasoline Combustion Process Used in Power Sport Application,” SAE Technical Paper, 2011.

[82] G. Hoffmann, B. Befrui, A. Berndorfer, W. F. Piock and D. L. Varble, “Fuel System Pressure Increase for Enhanced Performance of GDi Multi-Hole Injection Systems,” *SAE Int. J. Engines,* vol. 7, no. 1, 2014.

[83] B. Befrui, G. Corbinelli, M. D'Onofrio and D. Varble, “GDI Multi-Hole Injector Internal Flow and Spray Analysis,” SAE Technical Paper 2011-01-1211, 2011.

[84] M. Lindstrom, “Injector Nozzle Hole Parameters and their Influence on Real DI Diesel Performance,” Royal Institute of Technology, Stockholm, 2009.

[85] EIA, “Energy Information Administration US,” 2011. [Online]. Available: http://www.eia.gov/petroleum/. [Accessed 10 August 2013].

[86] G. Pollack, Water has three phases – gas, liquid, and solid, Washington: University of Washington, 2011.

[87] W. M. Haynes, Handbook of chemistry and physics, 91 ed., Boca Raton: CRC Press, 2010.

[88] R. Stone, Introduction to internal combustion engines, 3rd ed., London: MacMillan, 1999.

[89] A. Hillier, Fundamentals of motor vehicle technology, Oxford: Nelson Thornes, 2004.

[90] P. Eastwood, Critical topic in exhaust gas after treatment, Ford Motor Company, 2000.

[91] M. Cha-Lee, P. Simsoo, K. Hang-Sang, M. Kyoungdoug and C. Myung-Sik, “Experimental investigation of the effect of thin-wall substrates and spark timing retard on total hydrocarbon emissions during cold start,” Loughborough, 2004.

[92] R. Bosch, Gasoline Engine Management, 3rd edition ed., BOSCH Gmbh, 2006.

[93] A. J. Hubbard, “Hazardous air pollution emission potential from a wood fired furnance,” *Combustion science and technology,* vol. 108, pp. 297-309, 1995.

[94] A. V. Bridgewater, “Advances in Thermochemical biomass conversion,” Blackie and professional publishers, London, 1994.

[95] A. M. Kanury, “Combustion characteristics of biomass fuels,” *Combustion science and technology,* vol. 97, pp. 461-491, 1994.

[96] P. Smith and W. Cheng, “Massachusetts Institute of Technology,” March 2013. [Online]. Available: http://web.mit.edu/2.61/www/Lecture%20notes/Lec.%2007%20mixture%20preparation+gdi.pdf. [Accessed August 2013].

[97] D. Kittelson and M. Kraft, “Particle formation and models in internal combustion engines,” Cambridge Centre for Computational Chemical Engineering, 2014.

[98] D. Lihui, H. Weiqiang, L. Xingyu and W. Yuesen, “Comparative Study on Particles Formation in a Diesel Engine When Lubricating Oil Involved in Fuel Combustion,” *Journal of Chemistry,* vol. 2015, p. 7, 2015.

[99] M. Erwin, The Peterson automotive troubleshooting and repair manual, Grosset & Dunlap, 1975.

[100] H. Ebner and A. Jaschek, “The Importance of Blow-By Measurements, Measuring Equipment Required and Implementation,” *SAE Technical Paper,* no. 981081 , 1998.

[101] J. Hussain, K. Palaniradja and N. Algumirthi, “Effect of Exhaust Gas Recirculation (EGR) on Performance and Emission characteristics of a Three Cylinder Direct Injection Compression Ignition Engine,” *Alexandria Engineering Journal,* vol. 51, no. 4, pp. 241-247, 2012.

[102] R. Gukelberger, T. Alger, B. Mangold and J. Boehler, “Effects of EGR Dilution and Fuels on Spark Plug Temperatures in Gasoline Engines,” *SAE World Congress and Exhibition,* no. 2013-01-1632, 2013.

[103] Csere and Csaba, “10 Best Engineering Breakthroughs,” *Car and Drive,* p. 33, 1 1 1988.

[104] R. Goldsmith, Passenger car exhaust emissions, Mechanical Incorporated Engineer, 1990.

[105] Y. A. Cengel and M. A. Boles, Thermodynamics An engineering approach, 5th ed., Boston: McGraw-Hill, 2006.

[106] R. Brandt, Y. Wang and J. Grizzle, “Dynamic Modeling of a Three Way Catalyst for SI Engine Exhaust Emission Control,” *IEEE Transactions on Control Systems Technology,* vol. 8, no. 5, pp. 767-776, 2000.

[107] N. Guillen-Hurtado, V. Rico-Perez, A. Garcia-Garcia, D. Lozano-Castello and A. Bueno-Lopez, “Three-way catalysts: Past, present and future,” Department of Inorganic Chemistry. University of Alicante. (Spain), Alicante, 2012.

[108] R. J. Farrauto and R. M. Heck, “Catalytic converters: state of the art and perspectives,” Catal, 1999, pp. 351-360.

[109] V. Ganesan, Internal combustion engines, 2nd ed., McGraw Hill, 2004.

[110] S. P. Bharat and D. P. Kuldeep, “A Review paper on Catalytic Converter for Automotive Exhaust Emission,” *International Journal of Applied Engineering Research,* vol. 11, no. 11, p. 5, 2012.

[111] Y. Kiyota and K. Tsuji, “Development of Diesel Trap Oxidizer System,” *SAE,* no. 860294, 1986.

[112] B. Graskow , D. Kittelson, I. Abdul-Khalek and M. Ahmadi, “Characterization of exhaust particulate emissions from a spark ignition engine,” *SAE Technical paper,* no. 980528, 1998.

[113] A. Q. Ashton, Advances in Environment Research and Application, Atlanta: ScholarlyEditions, 2013.

[114] J. Johnson, S. Bagley, L. Gratz and D. Leddy, “A review of diesel particulate control technology and emissions effects,” *SAE Technical Paper,* no. 940233, 1992.

[115] T. D. Durnin, J. M. Norbeck and D. R. Cocker, “Particulate matter mass measurement and physical characterization,” University of California Riverside, California, 2004.

[116] M. Ogris, P. Hollere, P. Kapus and G. Fraidl, “Reduction of particulate number emission of GDI engines by application,” 2010.

[117] C. Saito, T. Nakatani, Y. Miyairi, K. Yuuki, M. Makino, H. Kurachi, W. Heuss, T. Kuki, Y. Furuta, P. Kattouah and C. D. Vogt, “New particulate filter concept to reduce particule number emissions,” *SAE Technical,* no. 2011-01-0814, 2011.

[118] R. Konieczny, R. Brueck and N. Zaldua-Moreno, “The challenge of future and particulate reduction,” 2010.

[119] M. Masoudi, “Pressure drop of segmented diesel particulate filters,” *SAE Journal ,* no. 2005-01-0971, 2005.

[120] G. C. Koltsakis, D. N. Katsaounis, Z. C. Samaras, S. Saberi, A. Boehm and D. Naumann, “Filtration and Regeneration Performance of a

Catalyzed Metal Foam Particulate Filter," *SAE Paper,* no. 2006-01-1524, 2006.

[121] D. Pinturaud, A. Charlet and C. Caillol, "Experimental study of DPF loading and incomplete regeneration," *SAE journal,* no. 2007-24-0094, 2007.

[122] G. P. Merker, C. Schwarz and R. Teichmann, Combustion engines development, New York: Springer, 2012.

[123] G. Stiesch, Modeling engine spray and combustion processes, Berlin: Springer, 2010.

[124] F. Ekstrom and J. Somhorst, "Multidisciplinary Simulation Model for the Balancing of Powertrain Combustion, Control and Components for Optimal Fuel Consumption, Emissions, Cost and Performance for a Diesel Engine Powered Passenger Car," SAE Technical Paper, 2012.

[125] P. P. J. van den Bosch and A. C. van der Klauw, Modeling, Identification and Simulation of Dynamical Systems, Boca Raton: CRC Press, 1994.

[126] I. Arsie, C. Pianese and G. Rizzo, "Identification of Emission Models in a Spark Ignition Engine for Control Application," in *5th IEEE Mediterranean Conference on Control Systems* , Paphos, 1997.

[127] R. Isermann, Engine modeling and control: modelling and electronic management of internal combustion engines, London: Springer, 2014.

[128] Y. Shi, G. Hai-Wen and D. R. Rolf, Computational optimization of internal combustion engines, London: Springer-Verlag, 2011.

[129] M. Chiodi , An Innovative 3D-CFD-Approach towards Virtual Development of Internal Combustion Engines, Kraftfahrzeugtechnik, 2011.

[130] A. I. Khuri and J. A. Cornell, Response Surfaces: Designs and Analyses, New York: Marcel Dekker, Inc., 1996.

[131] R. H. Myers, D. C. Montgomery and C. M. Anderson-Cook, Response Surface Methodology: Process and Product Optimization Using Designed Experiments, New Jersey: John Wiley & Sons, Inc., 2009.

[132] T. Srikanth and V. Kamala, "A real coded genetic algorithm for optimization of cutting parameters in turning," *International Journal of Computer Science and Network Technology,* vol. 8, no. 6, pp. 189-193, 2008.

[133] G. Wang and Z. Dong, "Adaptive response surface method - A global optimization scheme for approximation-based design problems," *Engineering Optimization,* vol. 33, no. 6, pp. 707-733, 2001.

[134] N. Zangeneh, A. Azizian, L. Lye and R. Popescu, “Application of response surface methodology in numerical geotechnical analysis,” in *55th Canadian Society of Geotechnical Conference*, Ontario, 2002.

[135] J. L. McClelland, D. E. Rumelhart and G. E. Hinton, “The appeal of parallel distributed processing,” *Parallel Distributed Processing: Explorations in the Microstructure of Cognition - Foundations,* vol. 1, pp. 3-44, 19986.

[136] G. F. Luger and W. A. Stubblefield, Artificial Intelligence: Structures and Strategies for Complex Problem Solving, Redwood City, California: Benjamin/Cumming Publishing, 1993.

[137] J. M. Zurada, Introduction to Artificial Neural Systems, West Group, 1992.

[138] Y. Sekmen, M. Golcu, P. Erduranli and Y. Pancar, “Prediction of perfomance and smoke emission using artificial neural network in diesel engine,” *Mathematical and computational application,* vol. 11, no. 3, pp. 205-214, 2006.

[139] N. Gholamhassan, G. Barat, Y. Talal and R. Hadi, “Combustion Analysis of a CI Engine Performance using Waste Cooking Biodiesel Fuel with an Artificial NeuralNetwork Aid,” *American Journal of Applied Sciences,* vol. 4, no. 10, pp. 756-764, 2007.

[140] B. Ghobadian, H. Rahimi, A. M. Nikbakht, G. Najafi and T. F. Yusaf, “Performance and emission characteristics of diesel engine and petrol-driven engine by ANN,” in *International Conference on Computer Systems and Technologies*, 2009.

[141] Y. H. Zweiri, “Diesel engine indicated torque estimation based on artificial neural networks,” *International journal of intelligent technology,* vol. 2, no. 2, pp. 233-239, 2006.

[142] B. Wu, F. Zoran, M. K. Denise, L. Gregory and J. P. Michael, “Using artificial neural networks for representing air flow rate through a 2.4 litter VVT engine,” in *Powertrain & Fluid systems Conference and Exhibition*, Florida, 2004.

[143] V. Gisca, A. Mereacre and M. Pisarenco, “Utilization of Neural Networks for Observing the Internal Combustion Engine’s Function,” in *7th International Conference on Development and Application Systems*, Suceava, 2004.

[144] P. N. Blumberg, G. A. Lavoie and R. J. Tabaczynski, Phenomenological models for reciprocating internal combustion engines, Ford, Research, 1978, 1979.

[145] J. N. Mattavi, E. G. Groff, Lienesch, F. A. Matekunas and R. N. Noyes, “Engine Improvements through combustion modelling,” *Combustion modelling in reciprocating engines,* 1980.

[146] J. B. Heywood, “Engine combustion modelling - An overview,” *Combustion modeling in reciprocating engines,* 1980.

[147] D. Foster, “An Overview of Zero-Dimensional Thermodynamic Models for IC Engine Data Analysis,” SAE, 1985.

[148] J. Ramos, “Comparisons between thermodynamic and one-dimensional combustion models of spark-ignition engines,” *Applied Mathematical Modelling,* vol. 10, no. 6, pp. 409-422, 1986.

[149] E. A. Guggenheim, Thermodynamics: An Advanced Treatment for Chemists and Physicists, 7th ed., Amsterdam: Elsevier Science Publishing Co Inc, 1985.

[150] X. H. Liu, S. Gharahbaghi and S. Richardson, “Modelling of HCCI Engines: Comparison of Single-zone, Multi-zone and Test Data,” *SAE International,* no. 2005-05-11, 2005.

[151] S. M. Aceves, J. R. Smith, C. K. Westbrook and W. J. Pitz, “Compression ratio effect on methane HCCI combustion,” *Journal of Engineering for Gas Turbine and Power,* vol. 121, pp. 569-574, 1999.

[152] J. E. Dec, “A computational study of the effects of low fuel loading and EGR on heat release rates and combustion limits in HCCI engines,” SAE, 2002.

[153] I.-P. Chang and L. Guan-Yu, “Design of the SI engine air-fuel ratio controller,” 2007.

[154] W. J. Annand, “A New Computation Model of Combustion in the Spark-Ignition Engine,” *Proceedings of the Institution of Mechanical Engineers,* vol. 119, pp. 119-126, 1971.

[155] N. C. Blizard and J. C. Keck, Experimental and theoretical investigation of turbulent burning model for internal combustion engines, No 740191 ed., SAE Paper, 1974.

[156] F. J. Zeleznik, “Combustion modeling in internal combustion engines,” *Comb. Sci. Tech.,* vol. 59, 1976.

[157] R. J. Tabaczynski, C. R. Ferguson and K. Radhkarishan, A turbulent entrainment model for spark ignition engine combustion, No. 770647 ed., SAE Paper, 1977.

[158] S. D. Hires, R. J. Tabaczynski and J. M. Novak, The prediction of ignition delay and combustion intervals for a homogeneous charge, spark ignition engine, No. 780232 ed., SAE Paper, 1978.

[159] H. Hiraki and J. M. Rife, Performance and NOx model of a direct injection stratified charge engine, No. 800050 ed., SAE Paper, 1980.

[160] N. P. Komninos and C. D. Rakopoulos, “Modeling HCCI combustion of biofuels: A review,” *Renewable and Sustainable Energy Reviews,* vol. 16, no. 3, pp. 1588-1610, 2012.

[161] J. I. Ramos, Internal Combustion Engine Modelling, Washington: Taylor & Francis Inc, 1989.

[162] A. Agarwal, Z. S. Filipi and D. M. Baker, Assessment of single- and two-zone turbulence formulations for quasi-dimensional modeling of spark-ignition engine combustion, Volume 136, Issue 1-6 ed., Combustion Science and Technology, 1998.

[163] S. Verhelst and C. Sheppard, “Multi-zone thermodynamic modelling of spark-ignition engine combustion–an overview,” *Energy Conversion and Management,* vol. 50, no. 5, pp. 1326-1335, 2009.

[164] J. R. Serrano, F. J. Arnau, P. Piqueras, A. Onorati and G. Montenegro, “1D gas dynamic modelling of mass conservation in engine duct systems with thermal contact discontinuities,” *Elsevier,* vol. 49, no. 1078–1088, p. 11, 2009.

[165] T. Cerri, A. Onorati and E. Mattarelli, “1D Engine Simulation of a Small HSDI Diesel Engine Applying a Predictive Combustion Model,” ASME, 2008.

[166] F. Furno and R. Gonard, “Diesel Injection-System Simulation: Added Value of the Energy Conservation Equation,” *SAE International,* no. 2011-01-0389, 2011.

[167] J. F. Helgaker and T. Ytrehus, “Coupling between Continuity/Momentum and Energy Equation in 1D Gas Flow,” *2nd Trondheim Gas Technology Conference,* vol. 26, pp. 82-89, 2012.

[168] G. R. Fowles and G. L. Cassiday, Analytical Mechanics, Brooks, 2005.

[169] F. Kreith, R. M. Manglik, M. S. Bohn and S. Tiwari, Principles of Heat Transfer, Cengage Learning, Inc, 2009.

[170] M. D. Rosello, J. R. Serrano, X. Margot and J. M. Arnau, “Analytic numerical approach to flow calculation in intake and exhaust systems of internal combustion engines,” *Mathematical and Computer Modelling,* vol. 36, pp. 33-45, 2002.

[171] R. J. Pearson and D. E. Winterbone, “Calculation of one-dimensional unsteady flow in internal combustion engine. How long should it take?,” 1996.

[172] C. Chryssakis, J. Bohbot and M. Miche, “Simulation of a 4-Cylinder Turbocharged Gasoline Direct Injection Engine Using a Direct Temporal Coupling Between a 1D Simulation Software and a 3D Combustion Code,” *SAE International,* p. 11, 2006.

[173] D. E. Winterbone and R. J. Pearson, Design techniques for engine manifolds, London: Professional engineering puplishing, 1990.

[174] G. P. Blair, “Design and simulation of four stroke engines,” *SAE R-186,* no. ISBN 0-7680-0440-3, 1999.

[175] M. Badami, F. Millo and G. Giaffreda, “Experimental and computational analysis of a high performance four stroke motorcycle engine equipped with a variable geometry exhaust system,” *SAE Paper,* no. 2002-01-001, 2002.

[176] J. Galindo, J. M. Lujan, J. R. Serrano, V. Dolz and S. Guilain, Design of an exhaust manifold to improve transient performance of a high speed turbocharged diesel engine, vol. 28 ed., Experimental thermal and fluid science, 2004.

[177] O. Vitek, J. Macek and M. Polasek, “New approach to turbocharger optimization using 1D simulation tools,” *SAE Paper,* no. 2006-01-0438, 2006 .

[178] M. Baratta, E. Spessa and P. Mairone, “Numerical Investigation of Turbolag Reduction In HD CNG Engines by means of exhaust valve variable actuation and spark timing control,” *KSAE International journal of automotive technology,* vol. Vol. 11, 2010.

[179] C. Hirsch , Numerical Computation of Internal and External Flows: The Fundamentals of Computational Fluid Dynamics, 2 ed., Butterworth-Heinemann, 2007.

[180] X. Liu and M. Chen, “CFD Analysis for Cooling Water Cavity of a Four-Cylinder Gasoline Engine,” *Advanced Materials Research,* vol. 940, pp. 184-187, 2014.

[181] J. Pan, R. Nigro and E. Matsuo, “3-D Modeling of Heat Transfer in Diesel Engine Piston Cooling Galleries,” SAE, 2005.

[182] N. Watanabe, K. Masahiko and Y. Nobuyuki, “An 1D-3D Integrating Numerical Simulation for Engine Cooling Problem,” *SAE International,* no. 2006-01-1603, 2006.

[183] W. Nessim and F. Zhang, “A simulation study of an advanced thermal management system for heavy duty diesel engines,” in *International conference on mechanical engineering and material science*, 2012.

[184] B. Minovski and L. Lofdahl, “Study of Software Integration for Transient Simulation of Future Cooling System for Heavy Truck Application,” SAE, 2014.

[185] H. Hassan, “Integration of 1D and 3D simulationsof engine cooling system,” in *International Symposium on Distributed Computing and Applications to Business, Engineering and Science*, 2011.

[186] J. Wendt, Computational Fluid Dynamics: An Introduction, Springer Science & Business Media, 2013.

[187] P. Wesseling, Principles of computational fluid dynamics, Heidelberg: Springer-Verlag, 2001.

[188] H. K. Versteeg and W. Malalasekera, An Introduction to Computational Fluid Dynamics: The Finite Volume Method, Pearson Prentice Hall, 2007.

[189] K. B. Vinodh, N. Sivagaminathan and N. Gopalakrishan, “Air flow and charge motion study of engine intake port,” in *37th National and 4th International Conference on Fluid Mechanics and Fluid Power*, 2010.

[190] H. Ogawa, Y. Matsui, S. Kimura and J. Kawashima, “Three-dimensional computation of in-cylinder flow and combustion characteristics in diesel engines — Effect of wall impingement models of fuel droplet behavior on combustion characteristics,” *JSAE Review,* vol. 18, no. 2, pp. 95-99, 1997.

[191] R. Reitz, N. Ayoub, M. Gonzalez and R. Hessel, “Improvements in 3-D Modeling of Diesel Engine Intake Flow and Combustion,” SAE, 1992.

[192] G. Sucharitha and A. Kumaraswamy, “Analysis on Three Dimensional Flow of direct injection diesel engine for different piston configuration using CFD,” *Indian Journal Science and Technology,* vol. 6, 2013.

[193] C. D. Rakopoulos, G. Kosmadakis and E. Pariotis, “Investigation of piston bowl geometry and speed effects in a motored HSDI diesel engine using a CFD against a quasi-dimensional model,” *Energy Conversion and management,* vol. 51, no. 3, pp. 470-484, 2010.

[194] B. Somerville, S. MacGregor, S. Charlton and B. Nasseri, “A study of air motion in an IDI passenger car diesel engine,” in *IMechE Experimental & Predictive Methods in Engine Research & Development*, 1993.

[195] A. Gharahghani, S. Mirsalim and S. Jazayeri, “Numerical Investigation of Flow Field and Combustion in a Dual Fuel Diesel Engine,” SAE, 2010.

[196] S. Henriot, J. Bohbot, A. Kleemann, O. Laget and B. Reveille, “CFD aided development of gasoline engines,” International multidimensional engine modeling user's group meeting, Malmaison, 2005.

[197] V. Knop and E. Essayem, “Comparison of PFI and DI Operation in a Downsized Gasoline Engine,” SAE, 2013.

[198] M. Chiodi, A. Perrone, P. Roberti and M. Bargende, “3D-CFD Virtual Engine Test Bench of a 1.6 Liter Turbo-Charged GDI-Race-Engine with Focus on Fuel Injection,” SAE, 2013.

[199] T. Wallner, “Optimization of Direct Injection Hydrogen Combustion Engine Performance, Efficiency and Emission,” *Proceedings of the Institution of Mechanical Engineers,* vol. 227, pp. 99-109, 2012.

[200] H. Barths, H. Pitsch and N. Peters, “3D simulation of Di diesel combustion and pollutatn formation using a two component reference fuel,” *Oil and Gas science and technology,* vol. 54, no. 2, 1999.

[201] B. P. Vanzieleghem, C. A. Chryssaki, R. O. Grover, H. G. Sick and D. N. Assanis, “Modeling of gasoline direct injection mixture formation using KIVA-3V,” University of Michigan, 2004.

[202] C. H. Lee and R. D. Reitz, “A comparative study on CFD simulation of spray penetration between gas jet and standard KIVA-3V spray model over a wide range of ambient gas densities,” *Journal of Mechanical Science and Technology,* vol. 26, no. 12, pp. 4017-4025, 2012.

[203] T. M. Belal, M. Marzouk and M. M. Osman, “Investigating Diesel Engine Performance and Emissions Using CFD,” *Energy and Power Engineering,* vol. 5, pp. 171-180, 2013.

[204] J. Quio, J. C. Dent and C. P. Garner, “Diesel engine modelling under steady state and transient conditions using a transpute based concurrent computer,” *SAE Paper,* no. 922226, 1992 .

[205] R. J. Tabaczynski, “Turbulent Flows in Reciprocating Internal Combustion Engines,” in *Internal Combustion Engineering: Science & Technology*, Springer, 1990, pp. 243-285.

[206] P. A. Durbin and B. A. Pettersson, Statistical Theory and Modeling for Turbulent Flows, 2 ed., John Wiley and Sons, 2011.

[207] R. Schiestel, Modeling and Simulation of Turbulent Flows, John Wiley & Sons, 2010.

[208] C. L. Berselli, I. Traian and W. J. Layton, Mathematics of Large Eddy Simulation of Turbulent Flows, Springer, 2005.

[209] D. C. Wilcox, Turbulence modeling for CFD, D C W Industries, 2006.

[210] J. Smits, “Modeling of a fluid flow in an internal combustion engine,” Eindhoven University of Technology, Eindhoven, 2006.

[211] E. Doran and D. Cook, “Large Eddy Simulation (LES) of Gas Exchange in IC Engines,” 2012.

[212] L. Yongfeng , P. Pucheng and L. Yong, “Numerical simulation of direct injection gasoline engine model,” Wuhan, 2011.

[213] S. B. Pope, Turbulent Flows, Cambridge : Cambridge University Press, 2000.

[214] D. C. Haworth and T. H. E, “Probability density function approach for multidimensional turbulent flow calculations with application to in-cylinder flows in reciprocating engines,” *AIAA,* vol. 29, no. 2, 1990.

[215] D. C. Haworth and S. B. Pope, “Transported probability density function methods for reynolds-averaged and large-eddy simulations,” *Turbulent Combustion Modeling,* vol. 95, pp. 119-142, 2011.

[216] C. Dopazo and E. E. O'Brien, “An approach to the autoignition of a turbulent mixture,” *Acta Astronautica,* vol. 1, pp. 1968-1975, 1974.

[217] H. M. Taylor and S. Karlin, An introduction to stochastic modeling, 3rd ed., San Diego: Academic Press, 1998.

[218] M. Morgalla, “Engine simulations using a stochastic reactor model,” Brandenburgische Technische Universitat, 2011.

[219] S. B. Pope, “The relationship between the propability approach and particle models for reaction in homogeneous turbulence,” *Combustion Flame,* vol. 35, pp. 41-45, 1979.

[220] A. Stuart and K. Ord, Kendall's Advanced Theory of Statistics, 6th ed., London: Edward Arnold, 1998.

[221] B. Challen and R. Baranescu, “Diesel engine reference book,” in *SAE International*, 1999.

[222] A. Smallbone, A. Bhave and M. Hillman, “Virtual performance and emissions mapping for diesel engine design optmization,” *SAE International,* no. 2013-01-0308, p. 23, 2013.

[223] A. Coble, A. Smallbone, A. Bhave, S. Mosbach and M. Kraft, “Implementing detailed chemistry and In-cylinder stratification into 0/1D IC engine cycle simulation tools,” SAE technical paper, 2011.

[224] C. Benjamin, R. Roff and C. Rutland, “Performance of an OpenMP parallel flow solver for engine CFD simulations,” *SAE Congress,* 2012.

[225] A. Montanaro, L. Alloca and D. Ettorne, “Experimental characterization of high pressure impinging sprays for CFD modelling of GDI engines,” *SAE International,* no. 2011-01-0685, pp. 747-763, 2011.

[226] J. Bonbot, V. Knop, O. Laget and C. Angelberger, “High performance 3D CFD codes for complex piston engine applications,” *SAE Congress,* 2010.

[227] N. Gillet, J. Bonbot and A. Benkenida, “IFP-C 3D: an unstructured parallel solver for reactive compressible gas flow with spray,” *Oil and Gas technology,* vol. 64, pp. 309-335, 2009.

[228] L. Cao, H. Zhao and X. Jiang, “Investigation into controlled auto-ignition combustion in a GDI engine with single and split fuel injections,” *SAE Technical Paper,* no. 2007-01-0211, 2007.

[229] R. Kaiser, C. Hinterberger and M. Olesen, “3D simulation of soot loading and regeneration of diesel particulate filter systems,” *SAE Technical Paper,* no. 2007-01-1143, 2007.

[230] W. Waidmann, A. Boemer and M. Braun, “Adjustment and verification of model parameters for diesel injection CFD simulation,” *SAE Techincal Paper,* no. 2006-01-0241, 2006.

[231] H. Lehtiniemi, F. Mauss, I. Magnusson and M. Balthasar, “Modeling diesel engine combustion with detailed chemistry using a progress variable approach. 2005-01-3855,” in *SAE*, 2005.

[232] H. Lehtiniemi, Y. Zhang, R. Rawat and F. Mauss, “Efficient 3D CFD combustion modeling with transient flamelet models. 2008-01-0957,” in *SAE*, 2008.

[233] R. Steiner, C. Bauer, C. Kruger, F. Otto and U. Maas, “3D simulation of DI diesel combustion applying a progress variable approach accounting for complex chemistry. 2004-01-0106,” in *SAE*, 2004.

[234] L. Cao, A. Bhave, H. Su, S. Mosbach, M. Kraft, A. Dris and R. McDavd, “Influence of injection timing and piston bowl geometry on PCCI combustion and emissions,” *SAE Int J Engines,* vol. 2, pp. 1019-1033, 2009.

[235] A. Smallbone, W. Liu, C. Law, X. You and H. Wang, “Experimental and modeling study of laminar flame speed and non-premixed counterflow ignition of h-heptane,” *Proceedings of the combustion institute,* vol. 32, no. 1, pp. 1245-1252, 2009.

[236] J. Andrae, T. Brink and G. Kalghatgi, “HCCI experiments with toluene reference fuels modelled by a semidetailed chemical kinetics mechanism,” *Combustion and Flame,* vol. 155, no. 4, pp. 696-712, 2008.

[237] H. Gurran, P. Gaffuri, W. Pitz and C. Westbrook, “A comprehensive modeling study of iso-octane,” *Combustion and flame,* vol. 155, no. 4, pp. 253-280, 2008.

[238] K. Kostecka, A. Rabah and C. Palmer, “Gc/ms analysis of the aromatic composition of gasoline,” *Journal of chemical education,* vol. 72, no. 9, pp. 853-, 1995.

[239] W. Pitz and C. Mueller, “Recent progress in the development of diesel surrogates fuels,” *Progress in energy and combustion science,* vol. 37, no. 3, pp. 330-350, 2011.

[240] F. Battin-Leclerc, “Detailed chemical kinetic models for the low-temperature combustion of hydrocarbons with application to gasoline and diesel fuel surrogates,” *Progress in Energy and Combustion Science,* vol. 34, no. 4, pp. 440-498, 2008.

[241] T. Lu and C. Law, “Toward accommodating realistic fuel chemistry in large-scale computations,” *Progress in energy and combustion science,* vol. 35, no. 2, pp. 192-215, 2009.

[242] M. Kraft, P. Maigaard, F. Mauss, M. Christensen and B. Johansson, “Investigation of combustion emissions in a homogeneous charge compression injection engine,” *Proceedings of the combustion institute,* vol. 28, pp. 1195-1201, 2000.

[243] A. Prodan and R. Prodan, “Stochastic simulation and modelling,” Iuliu Hatieganu University, 2014.

[244] J. Etheridge, S. Mosbach, M. Kraft, H. Wu and N. Collings, “Investigating cycle to cycle variations in an SI engine through experiments and a new computational model,” University of Cambridge, Cambridge, 2008.

[245] B. Huang, E. Hu, Z. Huang, J. Zheng, B. Liu and D. Jiang, “Cycle-by-cycle variations in a spark ignition engine fueled with natural gas–hydrogen blends combined with EGR,” *International Journal of Hydrogen Energy,* vol. 34, no. 19, pp. 8405-8414, 2009.

[246] S. B. Han, “Cycle-to-cycle variations under cylinder-pressure-based combustion analysis in spark ignition engines,” *KSME International Journal,* vol. 14, no. 10, pp. 1151-1158, 2000.

[247] E. Abdi, A. Burluka, T. Hattrell, K. Liu, C. Sheppard, J. Neumeister and N. Crundwell, “Study of cyclic variation in an SI engine using quasi-dimensional combustion model,” SAE, 2007.

[248] J. Serras, P. Aleiferis, D. Richardson and S. Wallace, “Mixture preparation and combustion variability in a spray guided DISI engine,” SAE, 2007.

[249] A. Brown, C. Stone and P. Beckwith, “Cycle by cycle variations in spark ignition engine combustion - modelling of flame kernel displacements as a cause of cycle by cycle variations,” SAE, 1996.

[250] H. Daneshyar and P. Hill, “The structure of small scale turbulence and its effect on combustion in spark ignition engines,” *Prog Energy Combust,* vol. 13, pp. 47-73, 1987.

[251] S. B. Han and Y. J. Chung, “A Study on the Effect of Operating Conditions for the Stability at Idle,” *KSME International Journal,* vol. 12, no. 4, pp. 694-700, 1998.

[252] H. Shen, P. C. Hinze and J. B. Heywood, “A Study of Cycle-to-Cycle Variations in SI Engines Using a Modified Quasi-Dimensional Model,” SAE, 1996.

[253] J. A. Gatowski, J. B. Heywood and C. DeLaplace, “Flame Photographs in a SparkIgnition Engine,” *Combustion and flame,* vol. 56, pp. 71-81, 1984.

[254] B. Johansson, “Cycle to cycle variations in SI engines - the effects of fluid flow and gas composition in the vicinity of the spark plug on early combustion,” SAE, 1996.

[255] K. Aydin, “Effect of engine parameters on cyclic variations in spark ignition engines,” in *6th International Advanced Technologies Symposium*, Adana, 2011.

[256] J. Bohbot, C. Chryssakis and M. Miche, “Simulation of a 4-Cylinder Turbocharged Gasoline Direct Injection Engine Using a Direct Temporal Coupling Between a 1D Simulation Software and a 3D Combustion Code,” *SAE International,* no. 2006-01-3263, p. 11, 2006.

[257] CMCL Innovations, “Kinetics & SRM engine suite user manual v8.2.15,” CMCL Innovations, Cambridge, 2015.

[258] N. Morgan, A. Smallbone, A. Bhave, M. Kraft, R. Cracknell and G. Kalghatgi, “Mapping surrogate gasoline compositions into RON/MON space,” *Combustion and flame,* vol. 157, pp. 1122-1131, 2010.

[259] J. Etheridge, S. Mosbach, M. Kraft and H. Wu, “A detailed chemistry simulation of the SI-HCCI transtition,” University of Cambridge, Cambridge, 2010.

[260] A. Bhave, M. Kraft, A. Oakley and H. Zhao, “Evaluating EGR-AFR operating range of a HCCI engine,” SAE, 2005.

[261] IMechE, Internal Combustion Engines: Performance, Fuel Economy and Emissions, Oxford: Chandos Publishing, 2009.

[262] U. A. Galip, P. Huei and M. Cakmakci, Automotive Control Systems, Cambridge: Cambridge University Press, 2012.

[263] S. Nabi, M. Balike, J. Allen and K. Rzemien, “An overview of hardware-in-the-loop testing systems at visteon,” SAE Paper, Warrendale, 2004.

[264] N. Shidore and M. Pasquier, “Interdependence of system control and component sizing for a hydrogen fueled hybrid vehicle,” SAE Paper, Warrendale, 2005.

[265] O. Philipp, M. Buhl, S. Diehl and M. Huber, “Engine ECU Function Development Using Software-in-the-Loop Methodology,” SAE Technical Papers, 2005.

[266] X. Zhang and C. Mi, Vehicle Power Management: Modeling, Control and Optimization, London: Springer, 2011.

[267] B. Lumpp, M. Tanimou, M. McMackin and E. Bouillon, “Desktop Simulation and Calibration of Diesel Engine ECU Software using Software-in-the-Loop Methodology,” SAE International, ., 2014.

[268] X. Dingyu and C. YangQuan, System simulation techniques with matlab and simulink, John Wiley & Sons, 2013.

[269] A. R. Plummer, “Model-in-the-Loop Testing,” *Journal of Systems and Control Engineering,* vol. 220, no. 3, pp. 183-199, 2006.

[270] T. Huayin, R. Burke, S. Akehurst, C. Brace and L. Smith, “Behaviours of a GDI Gasoline Engine during Start,” SAE Technical Paper 2014-01-1374, 2014.

[271] B. Chen, Y. Wu, H. Tsai and B. Chen, “Development of Engine Model Using Modulization Method for EMS Verification through MIL and HIL,” SAE Technical Paper 2014-01-1097, 2014.

[272] R. Rask and M. Sellnau, “Simulation-Based Engine Calibration,” *SAE International,* no. 2004-01-1264, p. 14, 2004.

[273] E. A. Elrady and L. Gan, DoE - design of experiments : methods and applications in engine development, Munich: sv corporate media, 2005.

[274] S. A. Gothekar, K. C. Vora, G. R. Mutha, N. H. Walke and N. V. Marathe, “Design of Experiments: A Systems Approach to Engine Optimization for Lower Emissions,” *SAE Technical Paper,* no. 2007-01-17, 2007.

[275] R. Kamel and M. Shaikh, Statistical design of experiments with engineering applications, Boca Raton: Taylor & Francis, 2005.

[276] Mathworks, “Mathworks,” 2012. [Online]. Available: http://www.mathworks.co.uk/products/datasheets/pdf/model-based-calibration-toolbox.pdf. [Accessed December 2013].

[277] R. L. Gorsuch, Factor analysis, 2nd ed., Hillsdale: Lawrence Erlbaum, 1983.

[278] J. Antony, Design of experiments for engineers and scientists, Oxford: Butterworth-Heinemann, 2003.

[279] G. E. Box, J. S. Hunter and W. G. Hunter, Statistics for Experiments: Design, Innovation and Discovery, 2nd ed., Wiley, 2005.

[280] R. Mukerjee and C. F. Wu, A modern theory of factorial designs, New York: Springer, 2006.

[281] J. C. Wu and M. S. Hamada, Experiments: Planning, Analysis and Optimization, 2nd ed., New York: Wiley & Sons, 2009.

[282] J. Lawson, Design and Analysis of Experiments with SAS, CRC Press, 2010.

[283] L. Eriksson, E. Johansson and N. Kettaneh-Wold, Design of Experiments: Principles and Applications, 3rd ed., Umea: Umetrics, 2008.

[284] M. Cavazzuti , Design of Experiments, Springer, 2013.

[285] F. Buekenhout and M. Parker, “The number of nets of the regular convex polytopes in dimension <= 4,” *600-Cell,* vol. 186, pp. 69-94, 1998.

[286] D. C. Montgomery, Design and Analysis of Experiments, John Wiley & Sons, 2005.

[287] E. W. Weisstein, “Wolfram Mathworld,” December 2013. [Online]. Available: http://mathworld.wolfram.com/CompleteGraph.html. [Accessed December 2013].

[288] K. R. Shah and K. Bikas, Theory of Optimal Designs, New York: Springer, 1989.

[289] P. F. Martijn and W. Weng-Kee, Applied Optimal Designs, London: Wiley, 2005.

[290] F. Pukelsheim, Optimal Design of Experiments, SIAM, 2006.

[291] E. Johannsson, N. Kettaneh-Wold, C. Wilkstrom, S. Wold and L. Eriksson, Design of experiments, Schweden: Umetrics AB Umea, 2000.

[292] D. R. Cox and N. Reid, The Theory of the Design of Experiments, Florida: Chapman and Hall, 2000.

[293] E. L. Melnick and B. S. Ever, Encyclopedia of Quantitative Risk Analysis and Assessment, Wiley, 2008.

[294] L. Kuipers and H. Niederreiter , Uniform Distribution of Sequences, New York: Dover Publications Inc, 2006.

[295] Openturns, “Openturns,” 2013. [Online]. Available: http://doc.openturns.org/openturns-latest/html/ReferenceGuide/cid4.xhtml. [Accessed 2013].

[296] K. Hinkelmann and O. Kempthorne, Design and Analysis of Experiments, Introduction to Experimental Design, New Jersey: Wiley, 2008.

[297] S. N. Deming and S. L. Morgan, Experimental Design: A Chemometric Approach, 2nd ed., Amsterdam: ELSEVIER, 1993.

[298] JMP, “JMP Statistical Discovery,” December 2013. [Online]. Available: http://www.jmp.com/support/help/The_Simplex_Lattice_Design.shtml. [Accessed December 2013].

[299] L. Pronzato and W. G. MÄuller, “Design of computer experiments: space flling and beyond,” April 2011. [Online]. Available: http://hal.archives-ouvertes.fr/docs/00/68/58/76/PDF/Stat_Comp-V2.pdf. [Accessed November 2013].

[300] A. Dean, M. Morris, J. Stufken and D. Bingham, Handbook of Design and Analysis of Experiments, New York: CRC Press, 2015.

[301] E. Hendricks and S. C. Sorenson, “Mean value modelling of spark ignition engines,” SAE Technical Papers, 1990.

[302] KIVA, “LANL KIVA,” 2014. [Online]. Available: http://www.lanl.gov/orgs/tt/pdf/techs/kiva.pdf. [Accessed December 2014].

[303] A. Fire, “AVL Fire,” AVL LIST GmbH, 2015. [Online]. Available: https://www.avl.com/fire2. [Accessed February 2015].

[304] R. Design, “Reaction Design chemkin,” Reaction Design, 2014. [Online]. Available: http://www.reactiondesign.com/products/chemkin/. [Accessed December 2014].

[305] CMCL Innovations, Kinetics & SRM Engine Suite User Manual v8.2.9, Cambridge: CMCL Innovations, 2014.

[306] D. R. Croft and D. G. Lilley, Heat Transfer Calculations Using Finite Difference Equations, London : Applied Science Publishers Ltd, 1977.

[307] A. Gogan, B. Sunden, A. Lehtiniemi and F. Mauss, “Stochastic model for the investigation of the influence of turbulent mixing on engine knock,” *SAE Paper,* no. No 2004-01-2999, 2004.

[308] W. H. Press, S. A. Teukolsky, W. T. Vetterling and B. P. Flannery, Numerical recipes in C++, Cambridge: Cambridge University Press, 2002.

[309] H. Hiroyasu, T. Kadota and M. Arai, “Development and use of a spray combustion modeling to predict diesel engine efficiency and pollutant

emissions combustion modeling," *Bulletin of the JSME,* vol. 26, no. 214, 1983.

[310] C. Graham and D. Talay, Stochastic Simulation and Monte Carlo Methods: Mathematical Foundations of Stochastic Simulation, Springer, 2013.

[311] S. Pope, "PDF methods for turbulent reactive flows," *Prog energy combustion science,* vol. 11, pp. 119-192, 1985.

[312] G. Technologies, "GT-SUITE Engine Performance Application Manual v7.5," Gamma Technologies Inc, Westmont, 2014.

[313] T. Morel and R. Keribar, "A Model for Predicting Spatially and Time Resolved Convective Heat Transfer in Bowl-in-Piston Combustion Chambers," SAE Technical Paper 850204, 1985.

[314] Exothermia, Axisuite User Guide Version 2015A, Thessaloniki: Exothermia, 2015.

[315] D. N. Tsinoglou, G. C. Koltsakis, D. K. Missirlis and K. J. Yakinthos, "Transient modeling of flow distribution in automotive catalytic converters," *Applied Mathematical Modeling,* vol. 28, pp. 775-794, 2004.

[316] F. M. White, Fluid Mechanics, McGraw-Hill, 2003.

[317] VDI-Waermeatlas, VDI-Waermeatlas, Dusseldorf: VDI-Verlag , 1992.

[318] H. Santos and M. Costa, "The relative importance of external and internal transport phenomena in three way catalysts," *International journal of heat and mass transfer,* vol. 51, no. 5-6, pp. 1409-1422, 2008.

[319] P. V. Danckwerts, "Continuous Flow Systems Distribution of Residence Times," *Chemical Engineering Science,* vol. 2, no. 1, pp. 1-13, 1953.

[320] N. Wakao and J. M. Smith, "Diffusion in catalyst pellets," *Chemical Engineering Science,* vol. 17, no. 825-834, p. 825, 1962.

[321] JLR North America LLC, "NP10-V8JLR: AJ133 5.0-Liter DFI V8 Engine," Jaguar Land Rover North America LLC, 2009.

[322] H. C. Michaels and B. K. Fulper, "Nitrous oxide emission factors for mobile sources," in *AWMA emissions inventory*, LA, 1998.

[323] G. Enzo, F. Gustavo and R. Palmaccio, "Numerical analyses of EGR techniques in a turbocharged sprak-ignition engine," *Applied thermal engineering journal,* vol. 39, pp. 95-104, 2012.

[324] J. N. Vianna, A. Reis and A. B. Oliveira, “Reduction of pollutants emissions on SI engines,” *Journal of the Braz. Soc. of Mech. Sci. & Eng.,* vol. XXVII, no. 3, pp. 217-222, 2005.

[325] C. Daniel, “One-at-a-Time Plans,”,” *Journal of the American Statistical Association,* vol. 68, no. 342, 1973.

[326] V. Czitrom, “One-Factor-at-a-Time versus Designed Experiments,” *The American Statistician,* vol. Vol 53, no. 2, 1999.

[327] E. George, Statistics for Engineers: An Introduction to Design, Data Analysis, and Model Building, New Jersey: John Wiley & Sons, 2005.

[328] G. E. Box and N. Draper, Response Surfaces, Mixtures, and Ridge Analyses, Wiley, 1987.

[329] H. Smith, Applied Regression Analysis, John Wiley, 1998.

[330] Gamma Technologies, GT-Power user's manual version 7.3, Westmont: Gamma Technologies Inc, 2014.

[331] G. N. Pontikakis and A. M. Stamatelos, “Identification of catalytic converter kinetic model using a genetic algorithm approach,” *Journal of Automobile Engineering,* vol. 218, no. 12, pp. 1455-1472, 2004.

[332] S. Soares and J. R. Sodre, “Effects of atmoshperic temperature and pressure on the performance of a vehicle,” *Proc Instn. Mech. Engrs,* vol. 216, no. 6, pp. 473-477, 2002.

[333] S. Mosbach, A. Aldawood and M. Kraft, “Real time evaluation of a detailed chemistry HCCI engine model using a tabulation technique,” *Combustion science and technology,* vol. 180, pp. 1263-1277, 2008.

[334] Ricardo, *Ricardo Wave user's manual,* Ricardo Inc, 2009.

[335] Lotus, *Lotus Engineering Software user's manual,* Lotus Group plc, 2011.

[336] A. Boost, “AVL Boost,” 2015. [Online]. Available: https://www.avl.com/simulation-tools1/. [Accessed February 2015].

[337] M. E. Kassaby and M. A. Nemit, “Studying the effect of compression ratio on an engine fueled with waste oil produced biodiesel/diesel fuel,” *Alexandria Engineering Journal,* vol. 52, no. 1, pp. 1-11, 2013.

[338] O. Laguitton, C. Crua, T. Cowell, M. R. Heikal and M. R. Gold, “The effect of compresison ratio on exhaust emissions from a PCCI diesel engine,” *Energy Conversion & Management,* vol. 48, no. 11, pp. 2918-2924, 2007.

[339] C. Johanson, Auto Engine Performance and Driveability, Goodheart-Willcox Co Inc, 2004.

[340] R. Manimaran, N. Alagumiurthi, K. Palaniradja and J. Hussain, “Effect of Exhaust Gas Recirculation on Performance and Emission of a Compression Ignition Engine with Staged Combustion,” *International Journal of Energy Engineering,* vol. 2, no. 6, pp. 285-292, 2012.

[341] C. K. Ndiema, “The combustion characteristics of the Kenyan Biomass Stove,” Department of Fuel and Energy, University of Leeds, Leeds, 1992.

[342] K. E. Voss, J. K. Lampert, R. J. Farrauto, G. W. Rice, A. Punke and R. Krohn, “Catalytic Oxidation of Diesel Particulates with Base Metal Oxides,” *Catalysis and Automotive Pollution Control,* vol. 96, pp. 499-515, 1995.

[343] A. J. Martyr and M. A. Plint, Engine Testing: The Design, Building, Modification and Use of Powertrain Test Facilities, Butterworth-Heinemann, 2012.

[344] K. Popovici and J. Pieter, Real-Time Simulation Technologies: Principles, Methodologies, and Applications, CRC Press, 2012.

[345] J. Ledolter and A. J. Swersey, Experimental Design with Applications in Marketing and Service Operations, Stanford University Press, 2007.

[346] H. Langouet, L. Metivier, D. Sinoquet and T. Quang-Huy, “International Conference on Engineering Optimization,” Rio de Janeiro, 2008.

[347] M. Hafner, “Steps towards an optimization of the dynamic emission behavior,” Pisa, 2001.

[348] B. Christian and C. Jermann, Global Optimization and Constraint Satisfaction, XII ed., Springer Berlin Heidelberg, 2003.

[349] C. Tindle, “Mathworks Automotive Conference,” Michigan, 2007.

[350] L. Guzzella and A. Amstutz, “Control of diesel engines,” *IEEE Control Systems,* vol. 18, pp. 53-71, 1998.

[351] H. Hoschschwarzer, “Automatische Motor-parameter optmierung,” Tu Graz, 1990.

[352] R. T. Marler and J. S. Arora, “Survey ofmulti-objective optimization methods for engineering,” *StructMultidiscOptim,* vol. 26, pp. 369-365, 2004.

[353] A. Carlos and C. Coello, “A short tutorial on evolutionary multiobjective optimization,” Mexico, 2001.

[354] S. Singiresu, Engineering optimization theory and practice, 4th ed., Chichester: John Wiley & Sons, 2009.

[355] S. S. Rao, T. S. Pan and V. B. Venkayya, “Optimal placement of actuators in actively controlled structures using genetic algorithms,” *AIAA Journal,* vol. 29, no. 6, pp. 942-943, 1991.

[356] C. Coello, G. B. Lamont and V. D. Veldhuizen, Evolutionary algorithms for solving multi-objective problems, 2nd ed., New York: Springer, 2007.

[357] E. Zitzler, M. Laumanns and S. Bleuler, “A tutorial on evolutionary multiobjectve optimization,” Swiis Federal Institute of Technology, Zurich, 2011.

Appendix

Model-Based Catalyst Design Optimisation

A parametric analysis was performed with the aim of identifying the optimal physical design of the catalytic converter. The analysis is based on the current aftertreatment model of the AJ133 engine and it focuses on minimising the total emissions concentrations of the engine running under NEDC conditions. A one-stage test plan with 4 factors was designed in MATLAB MBC toolbox to statistically study the relationship between the catalyst's design parameters and the engine-out emissions. Minimum and maximum values of the factors were based on ±50% of the standard catalyst setup. The test plan is based on a space filling Latin hypercube experimental design. In general, space-filling designs are used when there is little or no information about the underlying effects of factors on responses. The Latin hypercube type is selected to randomly generate the points. A number of 100 testing points is selected and distributed as evenly as possible around the operating space, thanks to the space-filling design setup.

Factors	Responses
Substrate length [m]	Carbon monoxide [ppm]
Substrate diameter [m]	Carbon dioxide [ppm]
Substrate thickness [m]	Total hydrocarbons [ppm]
Cell density [cpsi]	Nitrogen oxides [ppm]

Table A.1: Responses and factors of the model-based catalyst design

The simulation was completed for 100 different setups and the total emissions concentrations of each setup was imported into the MBC toolbox to statistically analyse the design. Several response model were compared and finally a radial basis function Gaussian was fitted as the best model based on the evaluation of the observations number, response surface, PRESS RMSE, parameters number and residuals position. Finally, after fitting the model, surface plots of the responses were used to analyse the data. It can be seen from the results that with the increase of the catalyst area, length and surface volume the conversion efficiency of the system is increased, hence less total pollutants concentrations at the exhaust tail-pipe. **Error! Reference source n**

ot found. shows the 4 factors at their highest level generating the global optimal settings for minimising the emissions in the exhaust aftertreatment system. However, it must be noted that packaging constraints and development cost are not taken into consideration in this analysis.

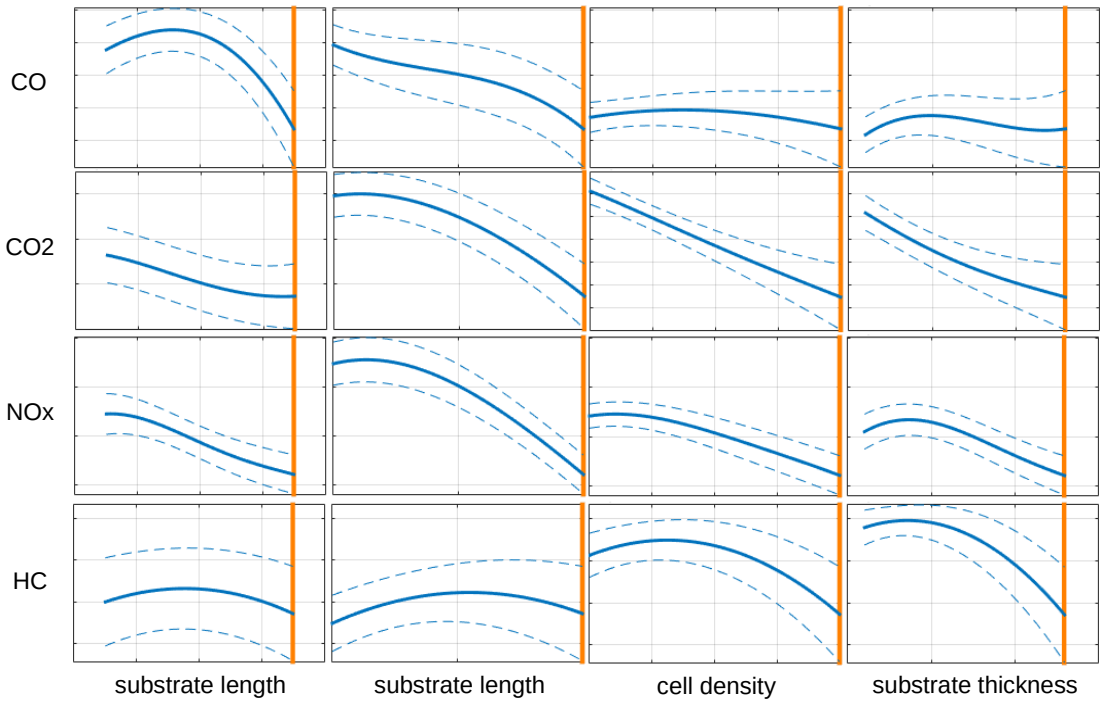

Figure A.2: Cross-section surface view of the responses